Data-driven stochastic reliability assessment of the US electricity grid under large penetration of variable renewable energy resources

Submitted in partial fulfillment of the requirements for

the degree of

Doctor of Philosophy

in

Civil and Environmental Engineering

Reshmi Ghosh

B.Tech Civil Engineering, University of Mumbai
M.S. Civil & Environmental Engineering, Carnegie Mellon University
M.S. Engineering & Public Policy, Carnegie Mellon University

Carnegie Mellon University
Pittsburgh, PA
October, 2021

Acknowledgements

This research was possible through the generous contribution of FCT Portugal (Project Reference (FCT): CMIP-ERI/TIC/0045/2014), Carnegie Mellon's Carnegie Institute of Technology Dean's Fellowship and Civil and Environmental Engineering department at CMU. I also want to acknowledge the support of University of Michigan's Asset Laboratory and Professor Michael Craig who provided the necessary resources and access to Great Lakes High Performance Computing Cluster, without which the analysis presented in all projects would have been incomplete.

I want to thank Scott, for helping me from the beginning of my journey at CMU, for being a friend to lift me up when I was down, and for cracking the best jokes in between serious advisor-advisee meetings. His expertise in economics and passion for the use of data-driven methods inspired my goals and encouraged me to pursue a Ph.D. You were, are, and will always be my favorite! I also want to thank Professor Constantine Samaras for sharing his expertise and guiding me to refine my research work. He also made sure that everything that I wanted was always available to me. In between his busy work schedule, he stayed up late to ensure my documents were proof-read and my presentations were polished. I also want to extend my most sincere gratitude to Professor Michael Craig for promoting my efforts and supporting my research. His knowledge and experience in the domain of energy-systems reliability inspired the work presented in this dissertation. Finally, I want thank and acknowledge the guidance of my committee members Professor Mitchell Small and Professor Matteo Pozzi for their support during my Ph.D. milestones. My journey to CMU was shaped by the guidance of a couple of close friends, and I will be forever indebted to each one of them and cannot thank them enough. Finally, a special note of gratitude to my parents who always encouraged me to pursue my dreams and made me the person I am today. Thank you, all!

Contents

Abstract **1**

1 Introduction **5**

1.1 Changes in power system reliability by including renewable energy generators 5

1.2 Importance of multidecadal high frequency temperature-driven demand data 7

1.3 Inter-annual variability impacts on renewable energy reliability for long-term systems planning 9

1.4 Research overview 11

1.5 Dissertation Structure 12

2 Stochastic Effective Load Carrying Capability (ELCC) values for the case of New York with varying levels of offshore wind energy penetration **15**

2.1 Introduction 16

2.2 Methods 21

2.2.1 Data 21

2.2.2 Wind profiles 22

2.2.3 Solar profile 23

2.2.4 Effective Load Carrying Capability Method 24

2.2.5 Scenario Development 25

2.3 Results 28

2.3.1 Spatial heterogeneity of ELCCs for all VREs 28

2.3.2 Analysis of additional VRE generators over base fleet scenarios 30

2.3.3 Comparison of ELCC estimates under 2030 base fleet scenarios against Current fleet scenario 32

2.4 Discussions 33

3 Analysis of electricity demand response to multidecadal interannual variability of temperature using machine learning methods to better support technological and policy developments for the power systems of the US 37

3.1 Abstract 38

3.2 Keywords 38

3.3 Introduction 39

3.4 Methods 45

3.4.1 Area of study 45

3.4.2 Data 46

3.4.3 Data Cleaning and Pre-processing 47

3.4.4 Model Selection 48

3.4.5 Model validation 50

3.5 Results 51

3.5.1 Model performance 51

3.5.2 Peak demand changes in reconstructed data 56

3.5.3 Change in Load Factor 62

3.6 Discussion 63

4 Multidecadal assessment of reliability contributions from renewable energy sources under deep uncertainty for ISNE, ERCOT, and CA-ISO leveraging temperature response of hourly load 67

4.1 Abstract 68

4.2 Introduction 68

4.3 Methods 72

4.3.1 Area of study 73

4.3.2 Data Sources 74

4.3.3 Wind profiles 75

4.3.4 Solar profile 76

4.3.5 Effective Load Carrying Capability Method 76

4.3.6 Base Generator Fleet and Storage Fleet 78
4.3.7 Total Interchange 78
4.3.8 Metrics 79
4.4 Results 80
4.4.1 Change in absolute reliability benefits of VRE generators 81
4.4.2 Variability of reliability contributions in Independent System Operator of New England (ISO-NE) 83
4.4.3 Variability of reliability contributions in California Independent System Operator (CA-ISO) 84
4.4.4 Variability of reliability contributions in Electricity Reliability Council of Texas (ERCOT) 86
4.4.5 Comparison across generators 89
4.4.6 Validating the change in reliability benefits 90
4.5 Discussions and Future Work 94

5 Conclusions and Future Work **97**
5.1 Summary 98
5.2 Policy Implications 102
5.3 Future Work 103
5.4 Data Contributions and Code 104

Appendix A: Appendix supporting Chapter 2 **105**
A.1 Forced Outage Rates 105
A.2 ELCC Maps 106

Appendix B: Appendix supporting Chapter 3 **123**
B.1 Balancing Authority acronyms 123
B.2 Model Validation 126
B.3 Top 20 demand hours for all Balancing Authorities 127

Appendix C: Appendix supporting Chapter 4 **133**
C.1 ELCC Maps for ISO-NE, CAISO, and ERCOT 133

References **186**

List of Figures

2.1 Distribution of ELCC value of VRE generators over current fleet (Scenario CS in section 4.3.6). 29

2.2 Box plot distribution of ELCC for solar, onshore wind, and offshore wind generators added to five scenarios described in section 4.3.6 for the NY-ISO region using multiple nameplate capacities. 30

2.3 Distribution of ELCC values for solar, onshore wind turbine, and offshore wind turbine generators of nameplate capacities 50MW - 500MW for all four scenarios relative to the Current Scenario of generator fleet from EIA 860, 2019 described in section 4.3.6. Note, only three nameplate capacities have been represented here as larger capacities have relatively low relevance in understanding subtle nuances in variation of ELCC values since the ELCC values for VRE generators decrease with increasing capacity. 32

3.1 Map of the US delineating boundaries of major Balancing Authorities 46

3.2 Final architecture of the LSTM model after experimenting with several hyper-parameters and testing their performance against validation set. We propose a stacked-LSTM model with 2 layers, and dropout regularization with probability of 0.2. 50

3.3 Examples of balancing Authorities showing asymmetrical Temperature-demand relationship, which implies that factors other than temperature significantly influence hourly electricity consumption in these regions. 55

3.4 Hourly temperature-load relationship of Midcontient Independent System Operator and Electricity Reliability Council of Texas 57

3.5 Hourly reconstructed demand values exceeding 99th percentile of hourly observed demand between 2015 - 2019 for each year of reconstruction (1980 -2014) segregated by months (colored) for the largest BAs of the US. 59

3.6 Auto-correlated hourly temperatures corresponding to the 20 largest reconstructed demand values in Figure 3.5, segregated by months (colored) for the largest BAs of the US. 60

3.7 Heatmap representing coefficient of variation values for the top twenty reconstructed temperature-driven demand proxies for balancing authorities in the US. Amongst the top 10 largest BAs, we find the greatest year-to-year variability occurring in ERCOT, followed by CA-ISO, TVA, SOCO, and DUK. 61

3.8 Distribution of annual load factors between 1980 - 2019 for all BAs considered in this study. Tennessee Valley Authority (TVA) has the largest interquartile range among the top 10 largest BAs, indicating large difference in year-to-year change in annual load factors. While, Midcontinent Independent System Operator (MISO) and Electricity Reliability Council of Texas (ERCOT) have moderate interquartile ranges, rest of the top 10 large BAs show very small changes in load factors 62

4.1 Geographical diversity of ELCCs of a new 100-MW onshore wind generator included to the existing base fleet in the area governed by ISO-New England. Gridded cell (41.0 N, -70.625 W) is Cape Cod, a small peninsular region in the state of Massachusetts. This shows the largest reliability contribution across all 40 years. 84

4.2 The impact of IAV of weather variables on ELCC values for a 100-MW VRE generator in ISO-NE. The onshore wind ELCCs (CV_{ov} = 113.84%, CV_{50} = 53.76%, and CV_{99} = 38.84%) showed largest variability across the 40-year timeline followed by offshore wind (CV_{ov} = 54.11%, CV_{50} = 40.19%, and CV_{99} = 28.61%). Conversely, variability in solar ELCCs (CV_{ov} = 19.93%, CV_{50} = 16.22%, and CV_{99} = 12.85%) was found to be significantly small. Offshore wind generators will provide the largest reliability contributions for ISO-NE when compared against other VREs. 85

4.3 The impact of interannual variability of weather variables on ELCC values for a 100MW VRE generator, added to the 2019 base fleet of CA-ISO. The onshore wind ELCCs (CV_{ov} = 99.48%, CV_{50} = 38.89%, and CV_{99} = 16.30%) showed largest variability across the 40-year timeline followed by offshore wind (CV_{ov} = 68.51%, CV_{50} = 53%, and CV_{99} = 16.84%). Conversely, variability in solar ELCCs (CV_{ov} = 37.34%, CV_{50} = 25.46%, and CV_{99} = 13.63%) was found to be significantly small. 87

4.4 Impact of interannual variability of weather variables on ELCC values for a 100MW VRE generator, added to the 2019 base fleet of ERCOT across all 40 years of study. The onshore wind ELCCs (CV_{ov} = 94.85%, CV_{50} = 45.38%, and CV_{99} = 29.05%) showed largest variability across the 40-year timeline followed by offshore wind (CV_{ov} = 72.08%, CV_{50} = 50.46%, and CV_{99} = 27.61%). In contrast, variability in solar ELCCs (CV_{ov} = 16.29%, CV_{50} = 8.5%, and CV_{99} = 7.78%) was found to be considerably small. 88

4.5 Spatial heterogeneity of solar and offshore wind ELCC values for the three BAs in 2019. The geographical footprint of ISO-NE is considerably smaller in size 43% of CA-ISO footprint and 26% of ERCOT footprint, leading to a narrower spread of capacity contribution values for all generator types across all 40 years. 90

4.6 Shift in interquartile range of ELCC values for 100MW VRE generators across all 4 years of available hourly observed demand in ERCOT. We find the difference in CV of ELCCs while using reconstructed demand against observed demand for onshore wind ($CV_{ov_{diff}}$ = -24.92%, $CV_{50_{diff}}$ = -1.72%, $CV_{99_{diff}}$ = 16.76%), solar ($CV_{ov_{diff}}$ = 4.44%, $CV_{50_{diff}}$ = 8.66%, $CV_{99_{diff}}$ = -0.8%), and offshore wind generator ($CV_{ov_{diff}}$ = -32.74%, $CV_{50_{diff}}$ = -17.266%, $CV_{99_{diff}}$ = -5.77%). The capacity contributions from a 100MW are marginally underestimated even in this case. Significantly large changes in (CV_{ov} for onshore and offshore wind in ERCOT indicates shift in optimal geographical area for reliability contributions in wind generators. The shift in overall, 50th percentile, and 99th percentile values is greatest for the case of offshore wind generator in ERCOT. 92

4.7 Shift in interquartile range of ELCC values for 100MW VRE generators across all 4 years of available hourly observed demand in CA-ISO. We find the difference in CV of ELCCs while using reconstructed demand against observed demand for onshore wind ($CV_{ov_{diff}}$ = -8.2%, $CV_{50_{diff}}$ = -13.52%, $CV_{99_{diff}}$ = -15.78%), solar ($CV_{ov_{diff}}$ = -2.1%, $CV_{50_{diff}}$ = -7.77%, $CV_{99_{diff}}$ = -24.57%), and offshore wind generator ($CV_{ov_{diff}}$ = -0.01%, $CV_{50_{diff}}$ = -3.57%, $CV_{99_{diff}}$ = -15.64%). Negative changes for all three VRE generators indicate that using reconstructed demand, the capacity contributions from a 100MW are marginally underestimated, but not significantly. The shift in overall, 50th percentile, and 99th percentile values is greatest for the case of solar generator in CA-ISO. 93

4.8 Shift in interquartile range of ELCC values for 100MW VRE generators across all 4 years of available hourly observed demand in ISO-NE.We find the difference in CV of ELCCs while using reconstructed demand against observed demand for onshore wind ($CV_{ov_{diff}}$ = -16.01%, $CV_{50_{diff}}$ = -0.58%, $CV_{99_{diff}}$ = -14.28%), solar ($CV_{ov_{diff}}$ = -23.29%, $CV_{50_{diff}}$ = -15.72%, $CV_{99_{diff}}$ = -29.99%), and offshore wind generator ($CV_{ov_{diff}}$ = -9.78%, $CV_{50_{diff}}$ = -5.53%, $CV_{99_{diff}}$ = -0.05%). Although the difference in CV seems moderate, difference between median ELCC for offshore wind generator is very high (19.0% vs. 39% for the case using reconstructed demand vs. observed demand, respectively). This indicates for the case of ISO-NE, the underestimated peak demand from reconstruction efforts in chapter 2, significantly undermines the reliability contributions from offshore wind generators. 93

A.1 Geographical distribution of ELCC values for solar generators over the current base fleet (Reference Case) 108

A.2 Geographical distribution of ELCC values for offshore wind generators over the current base fleet (Reference Case). 109

A.3 Geographical distribution of ELCC values for onshore wind generators over the current base fleet (Reference Case). 110

A.4 Geographical distribution of ELCC values for solar generators over a base fleet representing High Offshore scenario 111

A.5 Geographical distribution of ELCC values for offshore wind generators over a base fleet representing High Offshore scenario 112
A.6 Geographical distribution of ELCC values for onshore wind generators over a base fleet representing High Offshore scenario 113
A.7 Geographical distribution of ELCC values for solar generators over a base fleet representing High Onshore scenario 114
A.8 Geographical distribution of ELCC values for offshore wind generators over a base fleet representing High Onshore scenario 115
A.9 Geographical distribution of ELCC values for onshore wind generators over a base fleet representing High Onshore scenario 116
A.10 Geographical distribution of ELCC values for solar generators over a base fleet representing the High Solar scenario. 117
A.11 Geographical distribution of ELCC values for offshore wind generators over a base fleet representing the High Solar scenario. 118
A.12 Geographical distribution of ELCC values for onshore wind generators over a base fleet representing the High Solar scenario. 119
A.13 Geographical distribution of ELCC values for solar generators over a base fleet representing the High Natural Gas scenario. 120
A.14 Geographical distribution of ELCC values for offshore wind generators over a base fleet representing the High Natural Gas scenario. 121
A.15 Geographical distribution of ELCC values for onshore wind generators over a base fleet representing the High Natural Gas scenario. 122

B.1 Hourly temperature values corresponding to the reconstructed top 20 demand hours between 1980 - 2019 segregated by months (colored) for BAs of the US. 129
B.2 Hourly demand values corresponding to the reconstructed top 20 demand hours between 1980 - 2019 segregated by months (colored) for BAs of the US. 130
B.3 Hourly top 20 demand hours between 1980 - 2019 for Balancing Authorities (in alphabetical order) of the US. 131
B.4 Hourly top 20 demand hours between 1980 - 2019 of Balancing Authorities of the US.132

C.1 Geographical distribution of ELCC values between 1980 -1985 for a new 100-MW offshore wind generator added to the existing base fleet from 2019 of IS0-New England. 134
C.2 Geographical distribution of ELCC values between 1986 -1991 for a new 100-MW offshore wind generator added to the existing base fleet from 2019 of IS0-New England. 135
C.3 Geographical distribution of ELCC values between 1992 -1997 for a new 100-MW offshore wind generator added to the existing base fleet from 2019 of IS0-New England. 136
C.4 Geographical distribution of ELCC values between 1998 - 2003 for a new 100-MW offshore wind generator added to the existing base fleet from 2019 of IS0-New England. 137
C.5 Geographical distribution of ELCC values between 2004 - 2009 for a new 100-MW offshore wind generator added to the existing base fleet from 2019 of IS0-New England. 138
C.6 Geographical distribution of ELCC values between 1980 -1985 for a new 100-MW onshore wind generator added to the existing base fleet from 2019 of IS0-New England. 139
C.7 Geographical distribution of ELCC values between 1986 -1991 for a new 100-MW onshore wind generator added to the existing base fleet from 2019 of IS0-New England. 140
C.8 Geographical distribution of ELCC values between 1992 -1997 for a new 100-MW onshore wind generator added to the existing base fleet from 2019 of IS0-New England. 141
C.9 Geographical distribution of ELCC values between 1998 - 2003 for a new 100-MW onshore wind generator added to the existing base fleet from 2019 of IS0-New England. 142
C.10 ELCC values between 2004-2009 for a new 100-MW onshore wind generator added to the existing base fleet of IS0-New England. 143
C.11 ELCC values between 2010 - 2014 for a new 100-MW onshore wind generator added to the existing base fleet from 2019 of ISNE. 144
C.12 Geographical distribution of ELCC values between 2016 - 2019 for a new 100-MW onshore wind generator added to the existing base fleet from 2019 of IS0-New England. 145
C.13 Geographical distribution of ELCC values between 1980 -1985 for a new 100-MW offshore wind generator added to the existing base fleet from 2019 of IS0-New England. 146
C.14 Geographical distribution of ELCC values between 1986 -1991 for a new 100-MW offshore wind generator added to the existing base fleet from 2019 of IS0-New England. 147
C.15 Geographical distribution of ELCC values between 1992 -1997 for a new 100-MW offshore wind generator added to the existing base fleet from 2019 of IS0-New England. 148

C.16 Geographical distribution of ELCC values between 1998 - 2003 for a new 100-MW offshore wind generator added to the existing base fleet from 2019 of IS0-New England. 149

C.17 Geographical distribution of ELCC values between 2004 - 2009 for a new 100-MW offshore wind generator added to the existing base fleet from 2019 of IS0-New England. 150

C.18 Geographical distribution of ELCC values between 2010 - 2014 for a new 100-MW offshore wind generator added to the existing base fleet from 2019 of IS0-New England. 151

C.19 Geographical distribution of ELCC values between 2016 - 2019 for a new 100-MW offshore wind generator added to the existing base fleet from 2019 of IS0-New England. 152

C.20 Geographical distribution of ELCC values between 1980 -1985 for a new 100-MW solar generator added to the existing base fleet from 2019 of CAISO. 153

C.21 Geographical distribution of ELCC values between 1986 -1991 for a new 100-MW solar generator added to the existing base fleet from 2019 of California Independent System Operator. 154

C.22 Geographical distribution of ELCCs for a new 100-MW solar generator added to the existing base fleet of California Independent System Operator between 1992 -1997. . 155

C.23 Geographical distribution of ELCCs for a new 100-MW solar generator added to the existing base fleet of California Independent System Operator between 1998 - 2003. . 156

C.24 Geographical distribution of ELCCs for a new 100-MW solar generator added to the existing base fleet of California Independent System Operator between 2004 - 2009. . 157

C.25 Geographical distribution of ELCCs for a new 100-MW solar generator added to the existing base fleet of California Independent System Operator between 2010 - 2015. . 158

C.26 Geographical distribution of ELCCs for a new 100-MW solar generator added to the existing base fleet of California Independent System Operator between 2016 - 2019. . 159

C.27 Geographical distribution of ELCCs for a new 100-MW onshore wind generator added to the existing base fleet of California Independent System Operator between 1980-1985. 160

C.28 Geographical distribution of ELCCs for a new 100-MW onshore wind generator added to the existing base fleet of California Independent System Operator between 1986 -1991. 161

C.29 Geographical distribution of ELCCs for a new 100-MW onshore wind generator added to the existing base fleet of California Independent System Operator between 1992 -1997. 162

C.30 Geographical distribution of ELCCs for a new 100-MW onshore wind generator added to the existing base fleet of California Independent System Operator between 1998 - 2003. 163

C.31 Geographical distribution of ELCCs for a new 100-MW solar generator added to the existing base fleet of California Independent System Operator between 2004 - 2009. . 164

C.32 Geographical distribution of ELCCs for a new 100-MW onshore wind generator added to the existing base fleet of California Independent System Operator between 2010 - 2015. 165

C.33 Geographical distribution of ELCCs for a new 100-MW onshore generator added to the existing base fleet of California Independent System Operator between 2015 - 2019. 166

C.34 Geographical distribution of ELCCs for a new 100-MW offshore wind generator added to the existing base fleet of California Independent System Operator between 1980 -1985. 167

C.35 Geographical distribution of ELCCs for a new 100-MW offshore wind generator added to the existing base fleet of California Independent System Operator between 1986 -1991. 168

C.36 Geographical distribution of ELCCs for a new 100-MW offshore wind generator added to the existing base fleet of California Independent System Operator between 1992 - 1997. 169

C.37 Geographical distribution of ELCCs for a new 100-MW offshore wind generator added to the existing base fleet of California Independent System Operator between 1998 - 2003. 170

C.38 Geographical distribution of ELCCs for a new 100-MW offshore wind generator added to the existing base fleet of California Independent System Operator between 2004 - 2009. 171

C.39 Geographical distribution of ELCCs for a new 100-MW offshore wind generator added to the existing base fleet of California Independent System Operator between 2010-2015. 172

C.40 Geographical distribution of ELCCs for a new 100-MW offshore wind generator added to the existing base fleet of California Independent System Operator between 2016-2019. 173

C.41 Geographical distribution of ELCC values between 1980 -1985 for a new 100-MW solar generator added to the existing base fleet from 2019 of California Independent System Operator. 174

C.42 Geographical distribution of ELCC values between 1986 -1991 for a new 100-MW solar generator added to the existing base fleet from 2019 of ERCOT. 175

C.43 Geographical distribution of ELCCs for a new 100-MW solar generator added to the existing base fleet of California Independent System Operator between 1992 -1997. . 176

C.44 Geographical distribution of ELCCs for a new 100-MW solar generator added to the existing base fleet of California Independent System Operator between 1998 - 2003. . 177

C.45 Geographical distribution of ELCCs for a new 100-MW solar generator added to the existing base fleet of California Independent System Operator between 2004 - 2009. . 178

C.46 Geographical distribution of ELCCs for a new 100-MW solar generator added to the existing base fleet of ERCOT between 2010 - 2015. 179

C.47 Geographical distribution of ELCCs for a new 100-MW solar generator added to the existing base fleet of ERCOT between 2016 - 2019. 180

C.48 Geographical distribution of ELCCs for a new 100-MW onshore wind generator added to the existing base fleet of ERCOT between 1980-1985. 181

C.49 Geographical distribution of ELCCs for a new 100-MW onshore wind generator added to the existing base fleet of ERCOT between 1986 -1991. 182

C.50 Geographical distribution of ELCCs for a new 100-MW onshore wind generator added to the existing base fleet of ERCOT between 1992 -1997. 183

C.51 Geographical distribution of ELCCs for a new 100-MW onshore wind generator added to the existing base fleet of ERCOT between 1998 - 2003. 184

C.52 Variability of ELCCs between 2004 - 2009 for a new 100-MW onshore wind generator added to the existing base fleet of ERCOT. 185

List of Tables

2.1 Parameters for solar generation in NREL System Advisor Model (SAM) 23

2.2 Summary table of capacities of each type of generator in each of the base fleet scenarios described in section 4.3.6. Capacity of generators such as Nuclear (5.70GW), Hydroelectric Pumped Storage (4.7GW), Flywheels (0.06GW), Landfill Gas (0.12GW), Municipal Solid Waste (0.3GW), and Petroleum Liquids (3.9GW) are aggregated under 'Others' and are held constant for all scenarios after planned retirements were removed. All values are in GWs. 27

3.1 Results from the validation process for LSTM and PLR models by splitting trainable data in 80:20 ratio (train vs. validation set) with their optimal hyper-parameter setting for each BA. Note, during the model selection process, multiple hyper-parameter changes were made to derive the most optimal set, but the table shows only the best results obtained. 52

3.2 Balancing Authorities ranked in descending order of maximum hourly consumption in the period between 2015 - 2019 (observed data) 55

4.1 Parameters for solar generation in SAM; same as Chapter 2 76

4.2 Statistical measures describing the range of year-to-year changes in absolute ELCC values for each generator within the entire footprint of the three Balancing Authorities across the 40-year study period (1980 - 2019). Note, ELCC values are in % points and are always integers, but some upper bounds are float type in nature because we subset onshore or offshore area grid cells whose count result in odd numbers, leading to float values. 82

A.1 Table describing the temperature dependent FORs for six conventional generator types, where CC refers to combined cycle, NG is the simple gas cylce, DS refers to diesel based generators, HS is hydroelectric pumped storage, NU is nuclear, and ST refers to steam turbines. 106

B.1 Balancing Authorities in the US; their full names and their corresponding acronyms that is used in main paper 124

B.2 Optimal Hyper-parameters chosen for the LSTM model architecture 127

Abstract

The impacts of climate change will exacerbate humanitarian crises at a global level, and there is an urgent need to eliminate greenhouse gas (GHG) emissions from the power system infrastructure. While deploying clean energy resources in the current grid will help in decarbonization, variable and uncertain availability of solar and wind resources will introduce additional challenges in the operation of a grid. Thus to achieve a reliable clean electricity transition it is important to think about how renewable energy resources can be increased in the grid while minimizing potential challenges. This dissertation begins by examining the reliability contribution of incorporation of large solar photovoltaic (PV), onshore wind, and offshore wind generators for the case of New York Independent System Operator (NYISO) using a method called Effective Load Carrying Capability (ELCC). ELCC quantifies the reliability benefit of adding generators with certain nameplate capacity on top of the existing base fleet of generators. We define five different future scenarios to account for potential pathways in energy transition of the base fleet through 2030. In these future scenarios, we then add the generator of interest to assess its contribution to the grid and repeat the process for multiple nameplate capacities for offshore wind, onshore wind, and solar power across the entire footprint of New York. We conclude that, from a reliability perspective choosing offshore wind generators irrespective of size (capacity) is more worthwhile as compared to onshore wind farms for serving high demand periods as median capacity contributions (ELCC values) of offshore is 20 times greater than solar generators. Furthermore, analyses using our scenarios indicate that addition of solar generators in a base fleet with abundance of onshore and offshore wind generators contributes towards increasing system reliability and vice-versa. Thus, the diversification of future base fleet is necessary to meet demand shortfalls effectively.

Next, we reconstruct proxies of temperature-driven hourly electricity demand data to investigate the response of electricity demand to the variability of temperature over multiple decades to understand the change in peak load. Investments in power system capacity expansion projects are based on understanding of accurate, region-specific peak demand requirements. Balancing Authorities of the US report hourly demand records only from 2015. This constrains the scope of analysis to understand change in demand only to five or six years. Electricity use is strongly influenced by temperature and as the grid is designed to handle maximum load days, which tend to be the hottest days in many areas, the increasing intensity of extreme heat days will require additional investments in peak generation capacity, transmission, or storage. Along with changing demand, the scope to analyze the generating capacity gap after adding variable solar and wind resources is also limited, as demand data corresponding to hourly solar radiation and wind speed records are unavailable. Thus, there is a need to reconstruct demand data based on observed historical temperature, rather than forecast demand based on simulated future temperature records from climate change models. We attempt to fit various advanced machine learning models to understand the best choice for reconstruction based on performance on the validation set. We conclude that a "one-model fits all" approach as suggested in existing literature performs poorly. We also find that within the largest balancing authorities, ranked in the order of size and maximum demand consumption, Tennessee Valley Authority, Midcontinent Independent System Operator, and Electricity Reliability Council of Texas are most sensitive to temperature changes with the coefficient of variation of 20 largest demand hours (representative of peak demand) ranging between 15 - 19%.

In Chapter 4, we underscore the need for assessing grid reliability while accounting for long-term inter-annual variability in supply as well as demand side. We enlist the limitations of chapter 2 result because of unavailability of long-term consistent demand records. Thus, we propose to conduct reliability analysis of three different Balancing Authorities, that is ISO-NE, CA-ISO, and ERCOT to account for spatial heterogeneity which influences temperature, and also use hourly reconstructed demand proxies from Chapter 3 in conjunction with synchronous solar, onshore wind, and offshore wind capacity factors over four decades. We find that ELCC values for offshore wind generators vary significantly across years and has a coefficient of variation value that is 3 times larger than the coefficient of variation value of ELCCs from solar generators over 40 years between 1980 - 2019.

We conclude that because offshore wind ELCC contributions are significantly large in east and west coast, ISO-NE and CA-ISO should include more offshore wind irrespective of large variability. Whereas ERCOT witnessed the largest capacity contributions from solar generators, which is also less sensitive to interannual variability effects of weather variables. Thus, it is worthwhile to provide capital subsidies for solar generators in Texas.

Chapter 1

Introduction

1.1 Changes in power system reliability by including renewable energy generators

Renewable energy resources like onshore wind, offshore wind, and solar energy are increasingly being used as the primary tools to reduce greenhouse gas (GHG) emissions as a part of the large decarbonization effort for power systems. These technologies are diffusing into the existing grid at an unprecedented rate all around the world (IEA, 2020). Even the U.S. is set to experience tremendous growth in renewable energy, especially offshore wind power, with the goal to make the power system cleaner and carbon-pollution free (*AEO* 2021). In 2020, U.S. solar energy capacity had increased by 25%, and wind capacity increased by 48.3%, that is, an additional 9.8 GW and 14.3 GW of new generator capacity, respectively (EIA, 2021). The U.S. Department of Energy's (DOE) Annual Energy Outlook 2021 (*AEO* 2021) expects that electricity generation mixes across the U.S. will change rapidly, with renewable energy being the fastest-growing source through 2050 due to competitive capital costs and federal tax credits.

Although renewable energy resources are growing faster than other dispatchable sources of energy, the uncertainty associated with their hourly availability introduces integration challenges. Assessing the reliability of solar and wind generators as they become integrated in the future, while considering

multiple future grid transition scenarios is of particular importance as it will guide the planning process of power systems (Martinot, 2016; Bistline et al., 2020). Power system reliability is defined as the ability to meet demand at all times even during times of unplanned outages (NREL, 2016). Many studies exist around the assessment of power system reliability, but to comprehensively assess the value of adding solar, onshore wind, and offshore wind generators, appropriate methods need to be used to account for the natural variability of solar and wind resources along with related storage and outage issues in the future grid (Castro and Ferreira, 2001; Ibanez and Milligan, 2014). The analysis of capacity contributions of power systems has largely been deterministic in nature even though solar and wind energy resources have variable distributions. There is a need to analyze future reliability of power systems stochastically. Hence, instead of a deterministic approach, a probabilistic way of thinking about the time-series distribution of renewable energy resources is required to assess reliability (Keane et al., 2010; Castro and Ferreira, 2001; Bromley-Dulfano, Florez, and M. T. Craig, 2021).

Established methods for assessing the reliability of adding large solar and wind generators to the power system have used the metric known as "Capacity Credit". Capacity credit (also known as the capacity value) of a solar or wind generator is the indicator of capacity contributions. There are two distinct methods for quantifying capacity credit of any generator: chronological and probabilistic. The chronological method of capacity credit quantification leverages a specific time period (such as high risk peak load hours) to quantify the contribution of wind and solar generators towards meeting demand. On the other hand, the probabilistic method accounts for variability of solar and wind resources, along with transmission and generator outages. Hence, the probabilistic method is more appropriate for our study. Effective Load Carrying Capability (or ELCC) is known to be an important metric for quantifying the capacity credit of a generator added to the existing base fleet (Beiter et al., 2020; Boccard, 2009; Ibanez and Milligan, 2014. Broadly, ELCC measures the amount of generating capacity (in MW) of a conventional generator that can be replaced by a specific renewable energy generator without compromising system reliability (Garrido, 2019).

Although ELCC is an important metric to comprehensively characterize several uncertainties and produce accurate reliability contributions from any variable renewable energy (VRE) generator of interest, studies using ELCC as a criterion have been fairly limited. This may be due to the complex

modeling and computing requirements, as well as lack of granular data sources required for a hourly reliability assessment. The literature around the use of ELCC and even the quantification of reliability contributions for renewable generators to the US grid generally has been fairly restricted to a single energy source assessment under constrained scenarios.

Moreover, no studies exist describing comprehensive reliability contributions from offshore wind farms in the US. Assessing the contribution of these offshore wind generators in the east coast states under multiple energy transition pathways is critical because by 2030 the state of New York will complete the development of 3 GW of offshore wind capacity (*AWEA fact sheet* 2019) and is planning to expand it to 9 GW by 2040. Moreover, states like Massachusetts, Connecticut, and Rhode Island will add 8 GW of offshore wind generating capacity by 2035(New England, 2019).

Thus, there is a need to evaluate the capacity contributions of adding new generators to the existing base fleet for multiple scenarios representing 2030 by leveraging a probabilistic approach, while focusing on integrating a new clean energy source – offshore wind, which has been ignored in existing literature surrounding probabilistic reliability assessment.

1.2 Importance of multidecadal high frequency temperature-driven demand data

Reliability assessment of renewable energy generators is not only dependent upon supply side variability, but is also affected by demand side variability. Electricity demand is influenced by the variability of temperature (Thornton, Hoskins, and Scaife, 2016; H. C. Bloomfield et al., 2016; Auffhammer, Baylis, and Hausman, 2017). The degree of variability differs between different time scales. Hourly electricity demand is affected by human behavior. Currently, hourly demand data from all Balancing Authorities (BAs) of the U.S. is only reported between July 2015 - mid 2020 (Tyler H. Ruggles and Farnham, 2020), effectively forcing any reliability-based study to develop assumptions about trends in historical hourly demand time series. This imposes limits on reliability assessment studies, constraining them to a couple of years, or requires researchers to make very broad generalizations about fixed hourly demand over multiple years or decades. Such assumptions

can lead to inaccurate reliability assessments and unrevealed system risks.

Existing studies have used linear regression models (H. C. Bloomfield et al., 2016; Hannah C. Bloomfield, D. J. Brayshaw, and Charlton-Perez, 2020; Bloomfield et al., 2018; Thornton, Hoskins, and Scaife, 2016; Auffhammer, Baylis, and Hausman, 2017; Fonseca et al., 2019; Kumler et al., 2019) to estimate hourly demand based on hourly air temperature, Heating and Cooling Degree Days (HDD & CDD), and some form of categorical variables (fixed effects). H. C. Bloomfield et al., 2016 develops 36 years (1980 -2015) of mutually consistent demand and wind power reconstructions using historical temperature and wind speed records from the NASA MERRA database (*MERRA-2* 2020), but uses a simple linear regression model to estimate the trends in hourly demand for over three decades. In a related study, Coker et al., 2020 used reanalysis data to reconstruct electricity demand between 1976 - 2016 using linear regression models to understand the temperature driven uncertainty in the capacity market of Great Britain. All of these studies leveraging hourly and daily aggregated temperature data from reanalysis and climate models, respectively, have utilized multiple linear regression models. The relationship between temperature and demand is non-linear in nature (Hor, Watson, and Majithia, 2005; De Felice, Alessandri, and Catalano, 2015; Valor, Meneu, and Caselles, 2001), but all existing studies attempting to reconstruct hourly demand data, by trying to fit a linear regression model (sometimes even with the use of splines) to estimate the functional relationship between hourly load and temperature. This undermines the actual non-linear relationship. There is a need to test robust deep learning models against traditional linear regression models to successfully capture the relationship between non-linear variables (here load and temperature), and also prove that these data-driven methods actually have the ability to perform well with large datasets.

Once the best method for reconstruction of weather-driven hourly demand proxies has been established, these proxies can be used to truly understand the complexity of integrating high offshore wind, onshore wind, and solar in the power system by analyzing the change in peak demand hours over a multidecadal time frame. But there are several shortcomings to these regression methods when applied to multidecadal time-frames, which undermines the trends in hourly demand peaks that are driven by temperature. Thus, appropriate data-driven methods need to be employed to closely model the dependency of demand on surface temperature and reconstruct hourly load data.

Existing studies have constructed the de-trended electricity demand in various parts of the world, but the basis of these analyses has been for short time periods (2-5 years) with broad datasets, often measuring the aggregated effects on a daily basis. Hence, to answer the questions around demand variability under the influence of changing temperature, first, there is a need to systematically study the relationship between hourly and load and temperature within contiguous US. Then robust regression-based reconstruction processes should be applied to develop hourly temperature-driven electricity demand proxies by leveraging historical temperature records from the NASA MERRA reanalysis dataset to successfully avoid any simulation-driven uncertainty from climate change models. Moreover, for an inclusive analysis, this process of reconstructing demand proxies should be repeated against all Balancing Authorities of the US to demand and temperature for four decades to account for spatial heterogeneity, system design, and electricity consumption patterns.

1.3 Inter-annual variability impacts on renewable energy reliability for long-term systems planning

Capacity expansion plans for power systems using renewable energy generators are often created to serve customers reliably over multiple decades. These plans, if not carefully devised, could lead to future system failures and power outages (Ahmad, 2021) and an increase in associated social and economic costs (Bryce et al., 2018). A renewable-intensive grid is highly dependent on atmospheric variables and their characteristics. The availability of resources contributing towards the generation of renewable energy, like solar irradiance, onshore wind, and offshore wind vary from one location to another. These resources do not only vary spatially, but also temporally on multiple time scales. As atmospheric processes change Hannah Bloomfield, D. Brayshaw, and Charlton-Perez, 2020, renewable energy resources will implicitly become more variable, which will then directly affect the operation of power systems that are reliant on utility-scale solar energy or wind energy farms. Thus, to successfully plan a robust clean electric grid, the reliability benefits from investing in wind and solar power should be studied for a longer time frame.

Established literature quantifies year-to-year variation (Interannual Variability or IAV) in atmo-

spheric variables like solar irradiance (Davy and Troccoli, 2012; Fedorov, 2019) and wind speed (Pryor, Shepherd, and Barthelmie, 2018; McVicar et al., 2012; Zeng et al., 2019; Jung, Taubert, and Schindler, 2019). Challenges for operating a grid with highly intermittent solar and wind energy resources is not solely based on supply-side variability, but also temperature response of demand. Studies of the effect on power systems due to temperature changes also have gained some recognition (Ruijven, De Cian, and Wing, 2019; Yalew et al., 2020; Maia-Silva, Kumar, and Nateghi, 2020). But, the assessment of weather influencing electricity demand and clean energy resources over multiple decades, and its effect on power system reliability, or the grid's ability to meet demand at all times have only started gaining some momentum (Collins et al., 2018; Bryce et al., 2018), although still limited to a handful of papers.

Several studies including Zeyringer et al., 2018; Coker et al., 2020; H. C. Bloomfield et al., 2016; Bloomfield et al., 2018; Collins et al., 2018 have conducted some form of reliability assessment for power systems in Europe under high renewable energy penetration scenarios using retrospective supply and demand side data for several decades. These studies have underscored the need of a multi-decade reliability assessment perspective for building robust energy markets, power systems and also for transporting electricity. But, equivalent reliability assessments for North America have been limited. Related studies in the context of US either focus on relatively smaller time scales (Kumler et al., 2019), or account for only supply side impacts due to interannual variability of atmospheric variables, while ignoring demand side changes (Shaner et al., 2018; Rinaldi et al., 2021).

To truly analyze the change in reliability contributions from including new renewable energy generators to existing base fleet, the variability in solar and wind energy needs to be considered in tandem with the response of hourly demand due to temperature changes over multiple decades. It is also imperative to jointly consider impacts due to temperature-driven forced outages on the power output from existing generators. A high-frequency analysis of effective capacity value addition from new solar, onshore wind, and offshore wind generators towards meeting excess demand, while considering combined interactions of power output from existing generators along with demand changes in a probabilistic fashion, has been missing from the energy systems literature for the US.

1.4 Research overview

Our proposed research contributes to the understanding of system reliability given two increasingly important trends: increasing renewable penetrations and inter-annual variability impacts on weather variables (solar, wind, temperature - which affects demand).

This thesis has three main research objectives, which are analyzed and addressed in Chapter 2, Chapter 3, and Chapter 4. We specifically want to answer the questions around the following objectives:

- Understand the reliability contributions from adding new renewable energy generators under different energy transition scenarios for 2030 for the US east coast (Chapter 2)
    1. What is the contribution of offshore wind farms towards future grid reliability during periods of higher demand under multiple energy transition pathways?
    2. How do the reliability contributions from offshore wind farms in New York compare to other renewable energy generators like utility scale solar PV and onshore wind farms for same and different nameplate capacities?
- Characterize the response of variability of temperature on demand for the contiguous US by reconstructing hourly proxies of weather-dependent temperature and analyze peak demand changes (Chapter 3)
    1. What has been the effect of the long-term interannual variability of temperature on the electricity demand for different Balancing Authorities of the US?
    2. What is the distribution of 20 largest demand hours for large Balancing Authorities?
    3. Which Balancing Authorities are most sensitive to temperature changes?
- Examine the change in reliability contributions from new solar PV, onshore wind, and offshore wind generators over a multidecadal time frame due to interannual variability impacts of temperature and other atmospheric variables contributing to clean energy production

1. What is the effect of inter-annual variability of solar and wind resources over a multidecadal time scale on the grid reliability of Independent System Operator of New England (ISO-NE), Electricity Reliability Council of Texas (ERCOT), and California Independent System Operator(CAISO), while contributing towards meeting peak demand as a response function of interannual variability of temperature?

2. How sensitive are ELCC estimates when observed demand is used instead of weather-driven hourly demand proxies? Are the trends in variation of reliability contributions broadly captured while using demand proxies?

1.5 Dissertation Structure

This dissertation document contains three research chapters, addressing the research objectives outlined above. Initial analysis from chapter 3 was accepted as a paper in this year's International Conference of Machine Learning (ICML'21), and was also presented as a poster. We are currently in the process of preparing all chapters for submission to peer-reviewed journals.

We begin by quantifying the reliability contributions to meet annual unmet demand hours by including more offshore wind generators in the US east coast in Chapter 2. This chapter comprehensively tests the reliability benefits of offshore wind generators across multiple energy transition pathways representative of the 2030 base fleet. Furthermore, we also compare the relative capacity contributions from offshore wind farms against solar and onshore wind generators of similar nameplate capacities.

In Chapter 3, we present a detailed analysis of reconstruction methods of temperature-driven demand proxies for 40 years (1980 - 2019), and analyze them to determine which Balancing Authorities will likely face more challenges due to variable temperature, and will thus need careful planning to make the infrastructure more resilient while being able to reliably deliver electricity.

In Chapter 4, we investigate the plausible changes in reliability from solar and wind generators for three systematically and geographically different Balancing Authorities using multidecadal hourly

solar irradiance, and wind speed data along with synchronous weather-driven temperature proxies developed in Chapter 3. This study is aimed at helping policymakers develop an understanding of the necessary comprehensive multidecadal reliability studies for planning robust power system expansion using renewable energy technologies. And lastly, Chapter 5 presents a summary and describes the overall conclusions and research contributions from the previous studies that are included in this dissertation.

Chapter 2

Stochastic Effective Load Carrying Capability (ELCC) values for the case of New York with varying levels of offshore wind energy penetration

Abstract

Several US states are trying to mitigate climate change impacts by including more renewable energy in their power systems. This process is further aided by the falling prices of solar and wind energy. One technology that will play a critical role in this decarbonization process is offshore wind energy. Many offshore wind farms are being planned from Maine to Maryland in the waters off of the Atlantic coast, and are expected to be fully commissioned by 2030. But as stakeholders involved in planning the decarbonization pathways are determining ways to integrate these generators in the existing grid smoothly, the question of system adequacy or ability to meet demand at all times, arises. This paper explores the contribution of new renewable energy generators in multiple future scenarios that represent the likely transitions we will witness by 2030, using a metric called Effective Load Carrying Capability (ELCC). ELCC measures how much additional load can be satisfied by the inclusion of a new generator. We define multiple energy transition scenarios for 2030 using a case study of the New York Independent System Operator (NY-ISO) and determine ELCC values for offshore wind turbines to compare them with onshore wind turbines and solar photovoltaics (PVs). Our results show that offshore wind generators will meet hourly demand shortfalls across all scenarios by providing 20 times more contribution than onshore wind and solar PV generators, with the maximum contribution in the case of a system with very large natural gas capacity, followed by a system with large solar power penetration. Overall, larger median offshore wind ELCC values indicate greater reliability against electricity shortages as compared to solar PVs and onshore wind farms even after considering spatial heterogeneity of wind resource availability. These results from our scenario-based analyses will help stakeholders make informed decisions to choose optimal renewable energy pathways while making the grid less carbon-intensive.

2.1 Introduction

With the impending threat of climate change and a revolution in renewable energy research and development, efforts are being focused on developing and optimizing how clean energy resources can be added to the existing grid without compromising its reliability. Along with solar energy,

and onshore wind energy, there is a recent push towards developing more wind farms in oceans, i.e., offshore wind energy, to harness the consistently available larger wind speeds than the land-based wind farms. The addition of offshore wind farms into the grid will also help diversify the energy portfolio and increase grid resiliency.

East coast states in the US are aggressively seeking bids to develop large offshore wind farms. For example, New York has already committed to developing 3 GW of offshore wind by 2030 (*AWEA fact sheet* 2019) and 9 GW by 2040, which is a 50%, and 350% increase respectively, of the current installed wind capacity of about 2 GW. Additionally, NY-ISO also expects to integrate 6 GW of solar power by 2040 (Operator, 2019). Other east coast states like Massachusetts, Connecticut, and Rhode Island are planning to add 8 GW of generating capacity from offshore wind farms in the next decade to the Independent System Operator of New England (ISO-NE) (New England, 2019). By 2035 most of these east coast states aim to meet 40% of electricity generation using renewable energy (as per their Renewable Portfolio Standards or RPS). Currently, these states are starting out with small RPS goals for offshore wind carve outs – like Maryland which aims to achieve 10% electricity generation from offshore wind by 2025, and is expected to amplify the offshore wind generation even further by 2030 (M.Cleveland, 2020)

Many studies have examined offshore wind energy resource and economic potential in different contexts. Dvorak et al., 2013 analyzed the temporal availability of strong offshore wind resources (i.e., gross capacity factor $> 45\%$) and compared this availability to the duration of peak demand periods between 2006-2010. They concluded that the best US locations to generate electricity during peak demand are the offshore areas along Maine to Maryland. Kempton et al., 2007 examined the potential offshore wind resources in the Mid-Atlantic Bight Area (MAB) of the US to satisfy electricity demand in coastal states from Massachusetts to North Carolina. A study by Lawrence Berkeley National Lab (Mills, Millstein, et al., 2018) leveraged the Locational Marginal Prices (LMPs) for years between 2007 -2016 and found that the price of offshore wind energy varies significantly in the range of \$40/MWh to \$110/MWh, and is highest along the shore of New York, Massachusetts, Rhode Island, and Connecticut. Notably, as indicated by the literature, the potential of developing offshore wind generators is enormous in the east coast of the US and is also cost-competitive with other conventional and renewable sources of energy.

But, in the US, offshore wind farms are still in the development phase, and we can only expect the large (> 1GW) offshore wind farms to become operational after 2025. As the federal agencies and stakeholders strategize plans to smoothly integrate offshore wind in the existing grid, it is crucial to analyze the value of introducing a new generator. This can be accomplished by critically assessing the addition of offshore wind energy generators and the positive changes brought about in the reliability of the power system with existing solar and onshore wind plants. The recent example of rolling blackouts by CAISO (CAISO, 2020) as it struggled to meet electricity demand under an ongoing heatwave underscored the need for reliability analyses. But along with the need for diversification, it is important to analyze the value of adding offshore wind generators due to its large CAPEX (capital expenditure) costs compared to other renewable energy counterparts (solar and onshore wind).

Prior studies assessing power system reliability under large scale renewable energy penetration have used the metric of 'capacity credit' (also known as capacity value) to characterize the impacts of a new generator in the system. Capacity credit for a generator (expressed in MW) is defined as the amount of conventional generating capacity that the generator of interest can replace without compromising the system's overall reliability, that is, the ability to meet demand at all times (Garrido, 2019). Thus, capacity credit is the contribution that a given generator makes to overall system adequacy (Ensslin et al., 2008). There are two methods of calculating capacity credit – chronological and probabilistic. The probabilistic method is considered most effective in accounting for solar and wind variability in addition to transmission and generator outages as joint distributions. Chronological ELCC method inherently uses a definite time period (such as peak demand hours) to quantify the contribution of solar and wind generation towards meeting demand. Thus, it fails to consider interactions of large renewable energy penetration and 'peak net demand'. Effective Load Carrying Capability (ELCC) is regarded as a robust metric to determine the capacity credit of a power system (Boccard, 2009; Beiter et al., 2020; Ibanez and Milligan, 2014). ELCC is the magnitude of the additional load that a power system can supply with the particular generator of interest without a net change in reliability (Milligan and Porter, 2008).

ELCC method has been used to determine the robustness of adding new renewable energy generators and their contribution to meet demand (Keane et al., 2010; Ibanez and Milligan, 2014;

Bothwell and Pavlak, 2015; Kumler et al., 2019; Zhao, U.-J. Oh, and Choi, 2019; Mills and Rodriguez, 2020; U. Oh et al., 2018). Examples of applying the ELCC method to solar and onshore wind studies include Perez et al., 2006 which uses demand data from 39 utilities to calculate the ELCC in the years 2002-2003. It also examines the capacity value of installing solar PV cells in different orientations that capture varying solar irradiance levels. In Denholm et al., 2020, the authors determined the capacity value of adding utility-scale battery stored energy to satisfy demand in FRCC and NY-ISO using the ELCC method and found that the contribution of solar PV with 4-hour storage units at a 10% grid penetration rate can support peak demand. Furthermore, Perez et al., 2006 calculated the ELCC of adding solar PV cells in a fleet for the reference year 2006 using satellite observations for irradiance and static historical demand data from then-recent years 2002 and 2003 to analyze the relationship between penetration levels and geometrical configuration of the PV. Furthermore, an NREL study (Keane et al., 2010) looked at assessing the Irish power system by calculating the value of adding onshore wind energy generators to meet demand given a target reliability level and evaluated the reliability by considering wind power as a negative load. They concluded that between 1999-2008, the capacity value of adding wind generators varied by 35% for the Irish Power system.

Even though ELCC is a powerful tool to understand the contribution of individual generators to meet demand shortfall, it has been used within a limited scope. The existing studies are either very outdated to help draw out insights for future grid planning or analyze the effect of integrating a singular technology into the existing grid. To address these concerns, a comprehensive scenario-based approach is used towards understanding the potential pathways in which energy systems could evolve and then assess the ELCC of adding three different renewable energy generators to multiple these base generator fleet scenarios.

Additionally, unlike conventional sources, and reliability studies based on solar and onshore wind energy, the ELCC method has been rarely used to capture the value of adding these offshore wind generators. The handful of studies that used ELCC for assessing the reliability of offshore wind in the US includes a recent NREL study (Beiter et al., 2020). The authors used NREL's WIND toolkit data and demand data from Independent System Operators (ISOs) in the northeast region of the US to calculate ELCC for varying levels of offshore wind penetration (0, 2, and 7 GW) in

the year 2024, and determined the capacity credit or capacity value of adding these new generators to the existing base fleet. They concluded that the value of adding offshore wind generators (at 7 GW penetration level in New York Independent System Operator or NY-ISO) to the entire base fleet was in the range of 14.5 % - 28.3 % to meet 100 peak hours of electricity demand.

However, all these studies focus on historic data describing old base fleet, or evaluate the ELCC of a singular energy source. Furthermore, the study also did not consider the evolving dynamics of the grid due to retirements and the addition of new generators, or even temperature dependent forced outage rates (FORs) of the conventional generators. They solely based their analysis on onshore wind and solar energy as the Variable Renewable Energy sources (VREs) and a single study based on offshore wind for a reference year of 2024. However, considerable uncertainty about reliability surrounds broad decarbonization decisions about generating assets as we try to understand the implications of introducing these VRE generators in the future grid. Through our study, we propose to numerically quantify the contribution of offshore wind farms, onshore wind farms, and utility-scale solar PVs towards 2030 grid reliability during periods of higher demand. We also want to fill the above identified research gap by determining the optimal choice between all the renewable energy sources mentioned above by comparing the offshore wind turbine generators with other renewable energy sources across different nameplate capacities and multiple energy transition scenarios.

As New York state is expected to include 17GW of offshore wind by 2030, our research quantifies the ELCC of VRE generators to be added across multiple scenarios of future generating base fleet for the case of NY-ISO balancing authority region. These scenarios are developed by using data from the NY-ISO interconnection queue and EIA Form 860 generator status, as we aim to measure the grid's reliability under different decarbonization pathways. We construct multiple scenarios of solar and wind energy penetration (both onshore and offshore wind) and establish a direct relationship between the value of including additional VRE generators and the variability of renewable energy resources on an hourly basis.

2.2 Methods

To assess the reliability contribution of offshore wind energy generators in the future for the NY-ISO region, we calculate the ELCC of adding a range of these generators and compare their contribution to scenarios where we add solar and onshore wind farms across New York. We first present how we calculate ELCC, then discuss how we develop scenarios for future generator base fleets. These diverse base fleets allow us to represent multiple energy transition pathways which could be realized by 2030. We focus our analysis on offshore wind generators because this technology is mostly still in the planning stage for the US. The US has no offshore wind farm in operation except for the relatively small 30MW offshore wind farm at Block Island (*Block Island Wind Farm* 2021).

2.2.1 Data

Generally, ELCC methods used in the existing literature (Keane et al., 2010; Bothwell and Pavlak, 2015) have leveraged some form of an observed meteorological dataset. However, we plan to derive results from a continuous and comprehensive dataset, without having to do any imputations to account for missing values. Hence, we chose to use a reanalysis dataset. As the name suggests, reanalysis data is the "re-analyzed" version of observed weather variable data generated using forecasting and data analysis methods (Keeley, 2021; *Reanalysis Data* n.d.). Reanalysis datasets are created to develop consistent records of the observed states, which otherwise have many gaps due to the method in which data is collected and stored (Keeley, 2021; *Reanalysis Data* n.d.). The NASA MERRA (Modern-Era Retrospective Analysis for Research and Applications)(*MERRA-2* 2020) data is a collection of robust reanalysis datasets for multiple climatological variables over an extensive period. Variables like wind speed (both eastern and northward component) at 2m, 10m, and 50m above the sea level, specific humidity, surface incoming shortwave flux, pressure, and temperature at 2m were collected from the MERRA database for the years 2015-2019. This period is of particular interest because of the concurrent availability of publicly available cleaned hourly electricity demand data for the balancing authority governing the state of New York, NY-ISO.

The first step towards calculating the ELCC of a given renewable energy generator is to extract

the atmospheric variables from the MERRA database and convert them to their corresponding energy generation output using the NREL "System Advisor Model" or SAM (Blair et al., 2014). Researchers at NREL have designed SAM to facilitate the decision-making process for renewable energy systems by providing a platform to convert resources like solar irradiance and wind speed to their corresponding energy output, i.e., solar and wind energy (*System Advisor Model* 2020). The process of conversion of weather resources to energy variables is:

- The first step is to use the extracted MERRA weather data as input in SAM to simulate hourly AC generation from solar and wind resources for a particular year, location, and generator design (plant nameplate capacity and type as onshore and offshore wind farms use different turbines).
- The AC generation profiles are then normalized to derive the corresponding hourly capacity factors (CFs).
- Lastly, for the VRE generator of interest, whose effectiveness we want to quantify by determining the ELCC, its nameplate capacity is multiplied by the capacity factor derived in step 2 to derive the generator's hourly AC power.

Based on the VRE of interest, additional parameters are specified in SAM. These parameters are described below under each generator type.

2.2.2 Wind profiles

For wind power profiles, a power law in SAM is used to extrapolate wind speeds to a typical turbine hub height. The estimated wind speed is then categorized under different onshore wind turbine classes as suggested in IEC 61400 (*IEC 61400* 2021), and power is quantified using SAM. For offshore wind, a particular wind turbine from the SAM database is used – the Senvion 6.2 MW turbine. We chose Senvion from the pool of available offshore wind turbines in the SAM database because it best represents the current scenario of the only operable offshore wind (Block Island Wind Farm) in the US.

Equation (2.1) represents the Power Law:

$$v_2 = v_1 * (h_2/h_1)^{\alpha} \tag{2.1}$$

Where v_2 is the wind speed at height h_2, v_1 is the wind speed at height h_1, and α is the wind shear constant which depends on the terrain (whether land or water, mountainous or flat land), and also varies by turbine height, season, and wind speed. As a hueristic, 1/7 is often used when all factors influencing the wind shear constant value are unavailable.

2.2.3 Solar profile

To simulate power generated by solar PVs, the Direct Normal Irradiance (DNI) and Diffuse Horizontal Irradiance (DHI) are determined using the Direct Insolation Simulation Code (DISC) model developed by (Maxwell, 1987; W. Holmgren et al., 2021; W. F. Holmgren, Hansen, and Mikofski, 2018). DNI is the amount of solar radiation received per unit area by any surface that is always held normal to direct sun's rays. At the same time, DHI is the amount of radiation received per unit area by any surface not directly in the sun's path but by scattered molecules and particles in the atmosphere. The SAM model then uses these two factors as inputs to quantify solar power.

Table 4.1 enlists other factors that was chosen for the conversion of solar irradiance to power in SAM.

Generator Parameter	Value
Nameplate Capacity	1MW
Azimuth	180°
Axis Type	Fixed @ Latitude Angle
DC:AC Ratio	1.1
Inverter Efficiency	96%

Table 2.1: Parameters for solar generation in NREL System Advisor Model (SAM)

2.2.4 Effective Load Carrying Capability Method

To quantify the ELCC of any generator, we first start by calculating the system reliability of the base fleet against the demand profile and use the Loss of Load Hours (LOLH) value to define reliability. LOLH is defined as the sum of hours on an annual basis when the load in a system exceeds the available capacity. NERC deems a fleet to be reliable only if it has a LOLH value of 2.4/year NERC, 2019, which means that in a year, the system is only allowed to have a demand shortfall for 2.4 hours cumulative or one outage day in 10 years. The steps towards quantifying ELCC of any generator are enlisted below:

1. First, we collect required data inputs for the system of interest, which includes generator location, nameplate capacity, FORs, and MERRA reanalysis data for hourly solar and wind profiles.

2. Next, we calculate the system's original reliability (in terms of LOLH), and compare it against the target reliability value of 2.4 LOLH/year.

3. If the system is under-reliable, i.e., the system LOLH value >2.4/year, thermal generators of 50MW is incrementally added to adjust the fleet composition until the base reliability matches our target reliability. If the system is over-reliable, i.e., the fleet LOLH <2.4/year, then the ELCC calculator changes the fleet composition by eliminating older thermal generators from the fleet. Older thermal generators are eliminated to compensate for systems with overbuilt capacity that generates invalid ELCC estimates.

4. Lastly, we include the renewable generator of choice with storage, and determine the system's new reliability (LOLH value), and then incrementally add a constant load until the system with the added generator achieves the target reliability.

The ELCC of the generator is the amount of additional load which was added for adjusting the system reliability after including the VRE generator of interest to match the target reliability of 2.4 LOLH/year. The ELCC value represents the ability of the generator included on top of the base fleet to serve additional demand. For example, if we add a 100 MW offshore wind generator on top

of any of the base fleet scenarios described below in section 4.3.6, and find the ELCC as 30%, it would mean that 30 MW of the offshore wind generator will be the effective contribution to meet any demand shortfall. By definition, ELCC values have units of power, but we report them as a percentage of the added generator's nameplate capacity. For example, we report a 25 MW ELCC for a 100 MW wind generator as 25%.

We repeat this process of quantifying the reliability of an additional VRE generator over a base fleet for each grid cell using a dimension of 50x60 km within the state of New York and its adjacent offshore area to account for spatial heterogeneity in wind and solar resources.

2.2.5 Scenario Development

Offshore wind farms in the US are in various stages of the project process, with many still being planned. Several offshore wind farms are expected to be fully operational by 2030. Hence, to represent a range of future base fleet of generators over which additional offshore wind farms could be added, we developed and tested multiple scenarios. Together, all these scenarios capture various pathways that the NY-ISO grid could evolve.

We first extract the details of base generator fleet from the EIA Form 860 which reports the type, nameplate capacity, and location (latitude and longitude) of all current generators within a state. We included all planned retirements as stated in the EIA 860 form, and we included planned generators from interconnection queue data. While interconnection queue records only report the county and do not report the specific coordinates of the planned generator (since they haven't been constructed), we assumed the centroid of the county to represent the generator location. This was used to determine the temperature dependent FORs for conventional generators, and also determine the hourly solar and wind availability for renewable generators. Additionally, to construct these scenarios, we analyzed several state renewable energy mandates, federal regulations, and RPS). Moreover, the interconnection queue data indicated considerable additions of large solar PVs, onshore wind, offshore wind generators and some natural gas generators. But, there were no significant planned capacity additions for Nuclear, Flywheels, Hydroelectric Pumped Storage, Landfill Gas, Municipal Solid Waste, Biomass, and Petroleum plants. Thus, the nameplate capacity

(minus any planned retirements) of these fuel sources was held constant for all scenarios described below. It was also assumed that all coal power plants retire and the future grid of NY-ISO is coal-plant free. Each scenario under consideration is described below.

1. **Current Scenario (CS):** This scenario represents the current fleet of the existing generators in the EIA 860 2019 database. No new generators from the interconnection queue are added in this scenario. Hence, it can be representative of the case where none of the planned generators from the interconnection queue are commissioned by 2030, and coal power plants are still functioning.

2. **High Offshore Wind Scenario (HOF):** This is a scenario for 2030 where new generators from the interconnection queue are added to satisfy the current Renewable Portfolio Standards (RPS) set by the state of New York. In this case, we ensure that the RPS mandates for solar energy, onshore wind energy, and offshore wind energy are met along with including additional offshore wind farms, i.e., making 100% of offshore wind capacity (17GW) in the interconnection queue operable. This scenario represents the case where along with meeting state renewable energy RPS, all offshore wind farms in the queue are actually commissioned by 2030. We also retire all coal power plants, along with very old natural gas steam turbines, and natural gas combined cycle plants (16GW of natural gas retired). This scenario leads to a base fleet system where the total available generating capacity is 52GW The base fleet also includes existing 4.6GW of Hydroelectric, 5.7GW of Nuclear, and 3.8GW of Petroleum based power plants.

3. **High Onshore Wind Scenario (HON):** This is a high onshore wind penetration scenario, where everything remains the same as the HOF Scenario, but 100% of onshore wind capacity in the interconnection queue, that will be commissioned by 2030 is approved and offshore wind capacity is reduced to meet 2030 RPS standards. Hence, we add 5.90GW of new onshore wind turbines to NY-ISO and reduce offshore wind capacity to 4.028GW (to ensure onshore wind is larger in capacity as well as meet the offshore RPS standard), while solar capacity remains same as HOF (6 GW).

4. **High Solar Scenario (HS):** This is a high solar scenario, where everything remains the

same as the HOF Scenario case, but 100% of solar capacity in the interconnection queue is approved and both onshore wind and offshore wind capacity is reduced to meet 2030 RPS standards. Thus, we add 9.45GW of solar capacity to the base fleet system which includes 5.34GW of onshore wind capacity and 4.028GW of offshore wind capacity.

5. **High Natural Gas Scenario (HNG):** This is a high natural gas use scenario, where everything remains the same as the Reference case and only some natural gas plants retire, while meeting 2030 RPS standards.

Table 2.2: Summary table of capacities of each type of generator in each of the base fleet scenarios described in section 4.3.6. Capacity of generators such as Nuclear (5.70GW), Hydroelectric Pumped Storage (4.7GW), Flywheels (0.06GW), Landfill Gas (0.12GW), Municipal Solid Waste (0.3GW), and Petroleum Liquids (3.9GW) are aggregated under 'Others' and are held constant for all scenarios after planned retirements were removed. All values are in GWs.

Generator Capacity	**Scenario CS**	**Scenario HOF**	**Scenario HON**	**Scenario HS**	**Scenario HNG**
Offshore wind	0	17.09	4.02	4.02	4.02
Onshore wind	1.99	3.35	5.91	3.35	3.35
Natural Gas	25.8	12.7	12.7	12.7	25.8
Coal	1.4	0	0	0	0
Solar	0.48	6.0	6.0	9.45	6.0
Others (held constant)	14.78	14.78	14.78	14.78	14.78
Total (GW)	**45.7**	**53.92**	**43.41**	**44.3**	**53.95**

By 2030, three types of generators will be added to the base fleet in the NY-ISO region, that is, offshore wind turbine, onshore wind turbine, and solar PV. While using the scenarios in the ELCC calculator, we ensured that we determine reasonable capacity of new renewable energy generators mentioned above (step 4 in section 4.3.5) that will be added to the system. We used minimum, maximum, and average values of nameplate capacity of these planned generators from the NY-ISO interconnection queue data to estimate the size (nameplate capacity) of generators for which we want to quantify its ELCC value. Additionally, to understand the relative contribution of each type of renewable energy generator to the New York grid by 2030, we compare generators of the same nameplate capacity.

2.3 Results

The observed peak load in 2019 in the NY-ISO region was 30.4GW. We found that, although for all scenarios the base fleet nameplate capacity is greater than the plausible peak demand (a base generator fleet is always planned for capacity that is greater than projected load to be functional during unexpected demand surges), some scenarios are more 'under-reliable' as compared to others. As explained in section 4.3.6, generator fleets are under-reliable when they have a LOLH value of greater than 2.4, which means that for more than 2.4 hours in a year, the fleet capacity is unable to meet hourly demand. The implications of system LOLH being > 2.4/year is that even though the total available nameplate capacity of the base fleet is greater than the demand, the system is under-reliable. This is because at certain hours the actual generating capacity, due to FORs, and variance in CFs of renewable energy generators was lower than demand. This is why a ELCC based high-frequency hourly analysis is important to understand the actual contribution of any generator to system reliability.

2.3.1 Spatial heterogeneity of ELCCs for all VREs

To quantify ELCC for each possible location within the NY-ISO region, we repeatedly ran the ELCC model for each grid cell within New York state. Through this process, we quantified a range of possible ELCC values to account for spatial and temporal variability in the availability of wind (onshore and offshore) and solar resources, which influences CFs through each hour of 2019 (as shown in Figure 2.1). The ELCC values are reported as percentages and can be interpreted as the fraction of the nameplate capacity of the VRE added that will be effective towards serving additional demand.

Geographically, the onshore and offshore wind ELCC values for all scenarios vary between 0 - 43% and 0 - 64%, respectively, whereas for solar, the ELCC values are modest and have smaller variability in regards to spatial distribution, ranging from 0% to 12%. The difference between 25th and 75th percentile (colored box) of wind ELCCs is considerably larger as compared to the solar ELCC range because wind resources have a relatively larger spatial heterogeneity and wind CFs are

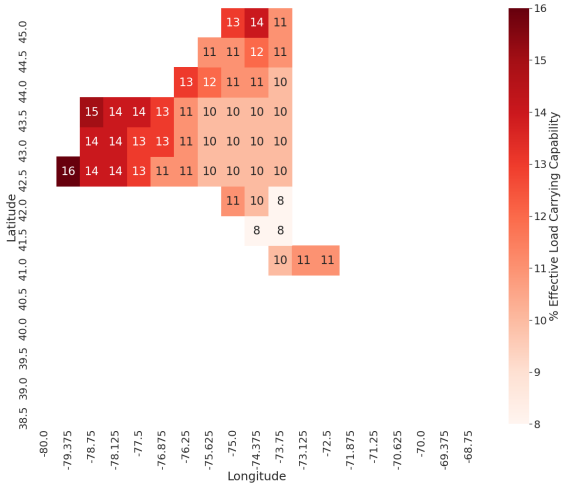

(a) 50MW solar generator

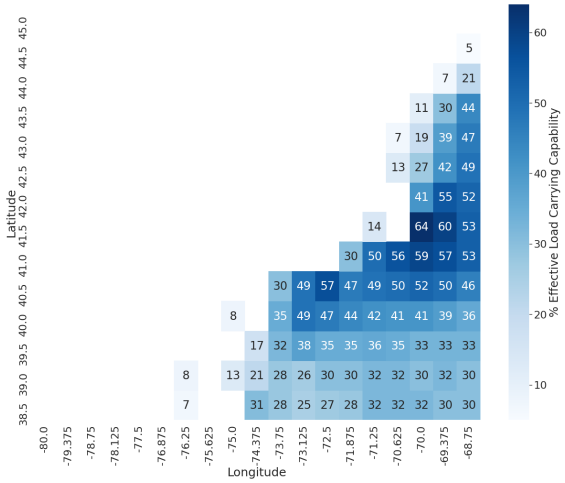

(b) 50MW offshore wind generator

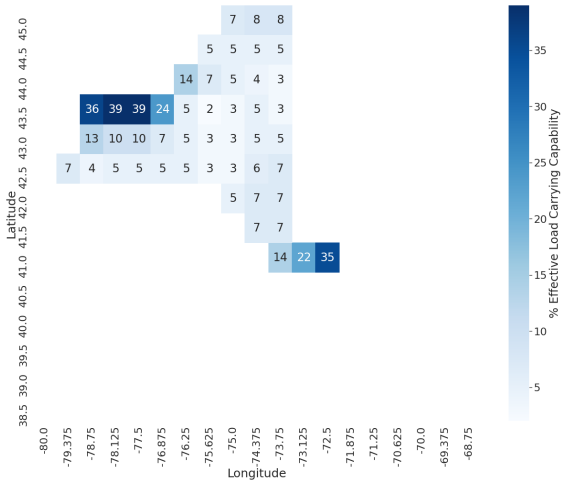

(c) 50MW onshore wind generator

Figure 2.1: Distribution of ELCC value of VRE generators over current fleet (Scenario CS in section 4.3.6).

not limited to only hours with sunshine. The narrow distribution of solar ELCCs indicated by its smaller box plots hint towards the nearly uniform distribution of solar irradiance across mainland New York.

Broadly, the difference in ELCC values across space can be directly attributed to the change in capacity factors across grid cells for both solar and wind resources. In the offshore area surrounding the New York state, the wind capacity factors become larger as we go up north towards the north-eastern states (coast of Massachusetts, New Hampshire, Maine). They also increase across the longitude, that is, going further away from the coast. Whereas, median solar capacity factors across mainland of New York state remains fairly constant and deviates only by small amounts. Any large change in solar ELCC values across New York is driven by the time correspondence of large capacity factor available in some grid cells during certain hours of the day to the unmet demand hours.

2.3.2 Analysis of additional VRE generators over base fleet scenarios

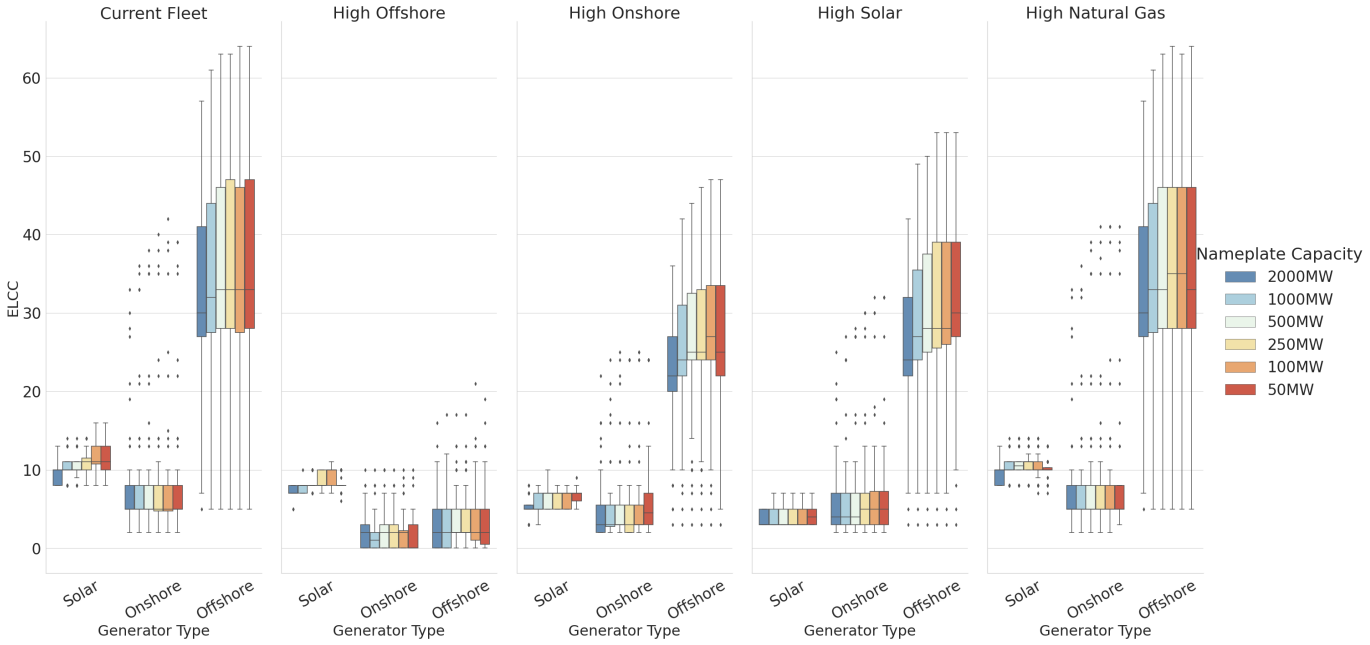

Figure 2.2: Box plot distribution of ELCC for solar, onshore wind, and offshore wind generators added to five scenarios described in section 4.3.6 for the NY-ISO region using multiple nameplate capacities.

Focusing on the effective contribution of adding VRE generators over the base fleet scenarios (described in 4.3.6), Figure 2.2 shows that the range of solar ELCC values is limited to a maximum value of 12% across all five scenarios, and its median ELCC is significantly lower (approximately 20 times) than the median ELCC of offshore wind generators. We can attribute the lower range to the small CFs of solar PVs, limited availability of solar radiation, and coincidence in availability of intense offshore wind speeds with the demand shortfalls. CFs for solar power are > 0 only during day-time hours, whereas offshore wind CFs are greater than 0 for almost all hours in a day. the standard deviation of solar ELCC values range between 1 and 2 , which means they remain similar. That is why the range of ELCC values of solar generators is significantly small as compared to its wind counterpart.

Conversely, as represented in Figure 2.2, median onshore ELCCs range between 3% to 8% and median offshore ELCCs vary between 3% to 34%. Moreover, comparing the median ELCC value for offshore and onshore wind generators, across each nameplate capacity (50 to 2000MW), we find that the contribution of offshore wind generators to meet demand shortfall is at least 6 times greater than onshore wind turbines in every scenario that is defined in section 4.3.6. In fact, the median ELCC value for offshore wind is always larger than onshore wind turbines and solar PVs. We attribute this finding to two key characteristics of offshore wind farms:

1. The availability of offshore wind through all hours in a day, which is coincident with demand peaks, and

2. The hub height and larger rotor diameter of the turbines placed offshore which helps in accessing better wind resources as compared to their land-based counterparts. Over mainland NY, maximum nameplate capacity of the turbines used (in accordance to IEC standards) was 1.5MW, whereas in offshore areas we have used the 6.2MW Senvion turbine.

Furthermore, when comparing each type of generator against itself, we see that as the nameplate capacity increases from 50MW to 2000MW, the ELCC values decrease. This is because the system becomes over reliable for certain hours when the best renewable energy resources are available but cannot meet electricity shortfalls in other hours. Hence, the marginal contribution from smaller

VRE generators is more significant than bigger VRE generators. Therefore, the maximum contribution towards meeting excess demand is by any generator of size 50MW or 100MW (depending on the scenario). But this conclusion is based on our assumption of fixed demand across all scenarios in 2030. However, in reality, the hourly demand can increase or decrease by 2030 in NY-ISO depending on the actual realization of the electrification process in various sectors and the inclusion of stringent energy efficiency measures, eventually leading to different demand shortfalls on an hourly basis (hence different LOLH).

2.3.3 Comparison of ELCC estimates under 2030 base fleet scenarios against Current fleet scenario

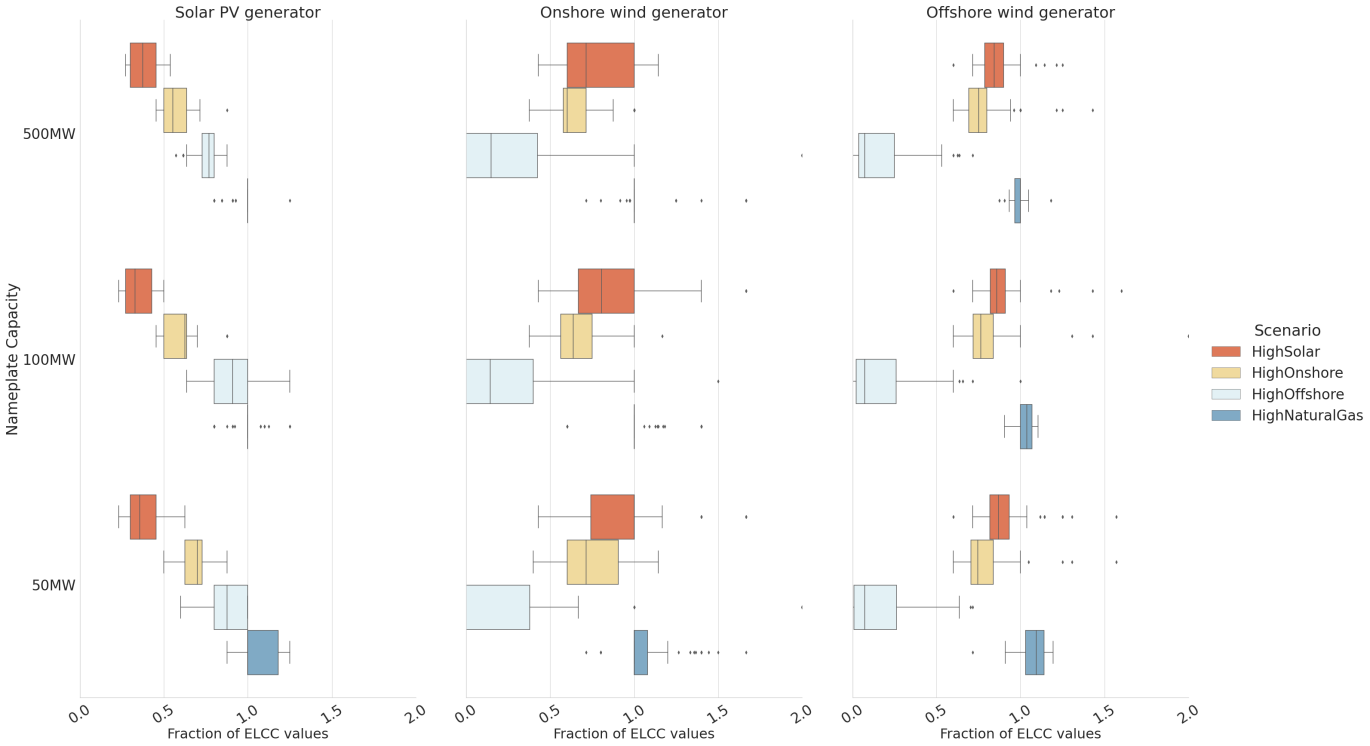

Figure 2.3: Distribution of ELCC values for solar, onshore wind turbine, and offshore wind turbine generators of nameplate capacities 50MW - 500MW for all four scenarios relative to the Current Scenario of generator fleet from EIA 860, 2019 described in section 4.3.6. Note, only three nameplate capacities have been represented here as larger capacities have relatively low relevance in understanding subtle nuances in variation of ELCC values since the ELCC values for VRE generators decrease with increasing capacity.

We compare the relative increase or decrease in ELCC values for each VRE generator type under

2030 base fleet scenarios relative to the Current Scenario from 2019. The results derived through this comparison will help stakeholders to think strategically about planning a diversified grid portfolio in the future capable of handling unexpected outages. Figure 2.3 shows that the distribution of ELCC values changes as base fleet changes under different considerations of 2030 energy transition scenarios (described in 4.3.6). The fractional values of ELCC (denoted by position of box plot as we are considering ELCC ratio of each scenario relative to the current generator fleet) for all three VRE generators is largest in the 'High Natural Gas' scenario. However, the High Natural Gas scenario was very similar to current fleet (Current Scenario in 4.3.6) with similar Natural Gas capacity, which justified the median (50th percentile) ELCC value of High Natural Gas scenario close to 1.

Moreover, comparing other fractional ELCC values for each scenario and generator type, we can conclude that solar and wind (both onshore and offshore) generators are complementary to each other. The 50th percentile of ELCC values for onshore and offshore wind generators across all nameplate capacities, is greater in High Solar scenario by 15% to 34% points against High Onshore and High Offshore scenario. We attribute the larger reliability contributions of wind generators to unmet demand during evening hours in a High Solar scenario, when solar generators become unavailable and excess demand is satisfied by offshore and onshore wind turbines. Similarly, 50th percentile of relative ELCC for solar generators are greater in High Offshore (light blue) and High Onshore (wheat) scenarios as the electricity shortfall not met by offshore and onshore wind resources in daytime hours are met by solar PVs. Thus, maintaining the diversity in base fleet composition against the VRE generator which is being added over it will be helpful in boosting the ELCC values and ensuring system reliability at a higher level than the cumulative reliability provided by a single VRE resource added in excess to the system.

2.4 Discussions

To understand the reliability value of adding large offshore wind energy farms to the grid, we conducted a comprehensive analysis of the NY-ISO grid by constructing multiple base fleet scenarios representative of 2030 grid transitions. We found that on average the median ELCCs of offshore

wind generators was 200% larger when compared against onshore wind and solar PV generators across all 2030 scenarios. But both onshore and offshore wind generators contributing to NY-ISO showed greater variability in ELCCs than solar generators due to the spatial heterogeneity in availability of wind resources. Gridded points which indicated large hourly offshore and onshore wind CFs also resulted in larger ELCC values in every scenario. Thus, there is a strong correlation between wind ELCCs and CFs. On the other hand, solar ELCCs showed a narrow distribution with the standard deviation varying between 1 to 3 around the mean solar ELCC.

Additionally, the large ELCCs of offshore wind in all five scenarios suggest that offshore wind farm development in the Atlantic coast of the US will lead to greatest reliability benefits by 2030 compared to onshore wind and solar PV, and thus there is significant value in adding more offshore wind in the grid. But there are several important considerations that needs to be accounted for while integrating this resource. First, as indicated in the Results section 2.3.1, wind ELCCs have a larger distribution ranging between 5-64% for offshore, and 3-42% for onshore depending on the largest available wind capacity factor. This indicates the relative location of offshore and onshore wind farms will determine their reliability contribution towards system adequacy as we consider fixed FORs for VREs. On the other hand, solar ELCCs are agnostic to spatial distribution of radiation as the solar irradiance value (and consequently CFs) have nearly similar magnitude over the entire state of New York.

Second, in addition to spatial variability, we quantified the sensitivity of ELCCs across four different scenarios and for the nameplate capacity of the added VRE over each base fleet scenario. The change in composition of base fleet across the four scenarios representing 2030 grid mix indicated the largest effect on the ELCC values varying the median ELCC of solar PV between -50% to +10% relative to the median solar ELCC in current fleet. Similarly, for onshore wind the median ELCC value varied in the range of -50% to 0% between all four scenarios relative to current fleet, and -95% to +6.25% for offshore ELCCs. The largest reduction of offshore wind ELCCs was noted in High Offshore scenario. We attribute the significant reduction of offshore wind ELCCs to the already saturated base fleet with offshore wind farms in HOF scenario, which produces hourly electricity with greater coincidence leaving demand shortfalls unmet when these wind farms are incapable of producing electricity. This is in tandem to the case of adding more solar generators to the HS

scenario. As all solar generators generate electricity at the same time, the fleet with additional solar generator is able to prevent day-time demand shortages, but becomes less reliable during evenings, when demand peaks in certain areas of a late afternoon peaking system, especially in summers. Thus, a diversified portfolio of generators helps in enhancing the contribution of individual VREs to meet system adequacy.

Third, when we tested the sensitivity of the ELCC values of all three VRE generator against increasing nameplate capacities and found that as nameplate capacity increases from 50MW to 2000MW, the ELCC values for all three VRE generators, solar PVs, onshore wind farms, and offshore wind farms decrease. But the reduction is ELCC values against increase in generator capacity is not uniform, and does not follow a singular trend. The change is caused due to the same reason stated above, i.e., saturating the grid with a single source of renewable energy implies generating excess electricity at certain hours when best resources are available, while enlarging the capacity gap in other hours when the resource is unable to generate adequate electricity.

But our analysis has several limitations, introduced due to the choice of technology associated with the VRE generators. Wind turbine specifications that have been used in our study are limited to a hub height of 90m and a rotor diameter of 140m. Any further change in turbine specifications will change the wind CFs in both onshore and offshore areas, thus changing the wind ELCC values. As planning agents seek to utilize state-of-the-art turbines in some planned offshore wind farms, the ELCC value of offshore wind in New York could become more significant. Additionally, our analysis considered PV panels of fixed axis type for solar generators, but axis-tracking solar PVs will contribute more towards system reliability. This is because the latter type will reorient itself with solar irradiance and contribute more towards generating electricity. Another critical aspect of planning decisions related to VREs is its dependency on capital costs or CAPEX. Future work could expand upon this analysis and derive the ratio of CAPEX against ELCC, i.e., $/ELCC value of each renewable energy generator, to understand the trade-offs of incorporating large VREs, which increase system reliability against their costs.

Additionally, there could be a significant effect on the ELCC values as more electric vehicles are included in the system and the load curve changes due to charging patterns. Moreover, electricity

demand is also subjected to large variability due to its dependence on temperature, which is poorly captured by the hourly records for a single year. Thus, as climate change impacts global air temperature variation, future reliability analysis should capture demand variability over a longer time frame to understand the difference in contributions by the solar and wind generators.

Despite all the caveats listed above, our ELCC modeling framework will help stakeholders develop efficient renewable energy integration strategies while successfully transitioning away from conventional sources of energy and preventing risks related to system inadequacy. Our results indicate that integrating more offshore wind in the future grid will prove beneficial under all circumstances and make the grid resilient to disruptions due to variability in the availability of wind and solar resources. The results also suggest that in order to develop a robust grid, it is helpful to include more offshore renewable energy generators while ensuring diversity of generator fleet. Solar power and offshore wind power complement each other as they have significant contributions towards meeting excess load at different times. As stakeholders discuss sustainable pathways for the decarbonization of the US power system and tackle climate change, comprehensive studies that combine various risks associated with grid reliability will help decision-makers carefully assess challenges with system adequacy.

Chapter 3

Analysis of electricity demand response to multidecadal interannual variability of temperature using machine learning methods to better support technological and policy developments for the power systems of the US

3.1 Abstract

Long-term planning of a robust power system requires the understanding of changing demand patterns. However, electricity demand is highly weather-sensitive and has inherent variability separate from intensifying effects due to climate change. Thus, the supply side variation from renewable resources, juxtaposed with variability in demand, will introduce additional challenges in the power system planning process. Unfortunately, understanding the influence of long-term (multiple decades) temperature variability on demand is not possible as long-term hourly electricity demand records are unavailable. This paper informs power system infrastructure planning by assessing the effects of hourly temperature variability and its impact on the demand in different Balancing Authorities (BAs) of the US, by reconstructing demand records using machine and deep learning-based regression models for four decades. We find that within the top 10 largest balancing authorities, ranked in the order of maximum demand, Tennessee Valley Authority, Midcontinent Independent System Operator, and Electricity Reliability Council of Texas are most sensitive to temperature changes with the coefficient of variation of 20 largest demand hours ranging between 15 - 19%.

3.2 Keywords

BA: Balancing Authority

LSTM: Long Short Term Memory

PLR: Piecewise Linear Regression

MISO: Midcontinent Independent System Operator, Inc.

NY-ISO: New York Independent System Operator ISO-NE: ISO New England

PJM: PJM Interconnection, LLC

ERCOT: Electric Reliability Council of Texas, Inc.

TVA: Tennessee Valley Authority

CA-ISO: California Independent System Operator

SWPP: Southwest Power Pool

3.3 Introduction

As federal and state policies mandate integrating higher levels of variable low-carbon energy resources into the existing grid, these mandates will open up new avenues to tackle the global issue of climate change (Hostick et al., 2012). Thus, to create a more sustainable grid, issues around energy and climate security must be considered in tandem, rather than separately, as one will influence the other. For systematic grid planning, it is important to develop policies and frameworks that ensure that the power system has enough capacity to meet electricity demand at all times using solar and wind resources. But, the addition of renewable energy resources in the grid will introduce additional variability and uncertainty due to their natural dependency on atmospheric processes. Moreover, electricity demand also depends on various factors including socio-economic variables, market design, technology advancements, and weather (Kumar et al., 2020). In fact, the seasonality of temperature is a key driver of variable demand (Coker et al., 2020). Hence, along with ensuring supply-side security to generate enough power, it has become increasingly necessary to assess the demand-side variability to understand power system reliability in a granular way.

Electricity demand is highly weather-sensitive and exhibits cyclicity. During the summer months, electricity demand peaks in the afternoon as businesses and households utilize significant energy for cooling requirements. Whereas in winter months, the peak of electricity consumption occurs in the evening. Similarly, within each day, depending on human behavior and temperature, electricity consumption changes by the hour but remains more or less similar across days, as human behavior is reasonably stable (Hodge, 2020). Furthermore, within a week consumers have different schedule during weekdays against weekends as commercial offices are closed, which influences demand patterns during different days of the week. Hence, the electricity demand shows a cyclic pattern across daily, weekly, and seasonal timescales. Most importantly, it is critical to understand the influence of weather on above mentioned electricity demand patterns at hourly resolution because it influences the actual decision to dispatch resources in a power system (Fonseca et al., 2019).

Peak demand as a response to temperature shows variation, i.e., the peak demand in summer is not representative of the peak electricity demand in the winter months, both in magnitude as well as timing due to difference in human consumption pattern. Additionally, variability in weather (air temperature) has a compounding effect on the cyclic nature of electricity demand. As temperature increases, electricity demand can be expected to increase to meet cooling needs, and thus change the nature of peak load (Maia-Silva, Kumar, and Nateghi, 2020; Yalew et al., 2020). In regions with high electrified heating, low temperatures also increase demand (Bessec and Fouquau, 2008). This change is further exacerbated as the earth continues to warm, and thus daily, weekly, and seasonal patterns in electricity demand will be altered due to the additional temperature gradients introduced by climate change. By assessing the spatial and long-term temporal variability of temperature over the mainland US, we can differentiate the effects of natural variability and climate change-related effects on temperature over electricity demand, especially because the effects due to the former are lesser-known to researchers.

Hourly demand data across multiple decades is useful to determine reliability of renewable energy systems i.e., if sufficient solar and wind resources are available during high load periods. In addition to using long time series of load data to capture the complexities involved with planning a cleaner grid, it is also extremely useful to understand the subtle changes in electricity demand as a response function of change in economy, as it is rapidly electrified (sectors like residential, transportation, and commercial sectors increasingly use more electricity). Unfortunately, hourly historical demand records spanning multiple decades is missing from the Balancing Authorities (BA) database, although spatially aggregated country-wide historical demand records available. A BA is an organization in the US responsible for maintaining electricity balance within its area of operation, and there are a total of 66 BAs governing different regions of the US. Differences in sectoral coverage of these BAs account for difference in energy policy and regulations, weather variation as well as consumption patterns. Thus, there is a need to conduct analysis of variation in demand at BA level rather than at a national scale.

Databases reporting hourly weather variables like solar irradiance and wind speed have massive historical records spanning multiple decades, especially 'Reanalysis' datasets. A reanalysis dataset, as the name suggests, is the reanalyzed version of weather data, generated using data analysis

methods to develop consistent records of the observed conditions, which otherwise has gaps due to techniques in which data is collected and stored. It is a robust collection of past observations of hourly wind and solar profiles for every region around the world gridded at a specific scale depending on the source. These datasets can be utilized to construct hourly wind and solar energy capacities to determine effective reliability contributions to a grid. But to compare the reliability contributions of these solar and wind generators against the demand, hourly historical records of electricity demand spanning across multiple decades is required, which is missing from the database maintained by all the BAs of the US. In Chapter 2, the ELCC analysis was constrained to five years between 2016-2019 because of lack of consistent hourly demand data. Additionally, data from publicly available climate models (Bukovsky and Mearns, 2020) either lack spatial granularity or temporal granularity, or both, unless customized using downscaling techniques (requires large and expensive compute resources). This creates a need to reconstruct granular demand data with a focus to understand how inter annual variability of temperature has been affecting the electricity demand on an hourly basis.

Despite the rich literature in understanding the response of electricity demand to changes in temperature, granular level assessment of hourly demand variability for the case of the contiguous US has not been attempted. But in the European context, several use cases of reconstructed electricity demand have appeared in literature, including but not limited to practices to analyze sensitivity of power systems to meteorological changes, uncertainty in electricity market, identification of Targeted Circulation Types (Thornton, Hoskins, and Scaife, 2016; H. C. Bloomfield et al., 2016; Hannah C. Bloomfield, D. J. Brayshaw, and Charlton-Perez, 2020; Coker et al., 2020). These studies have been particularly important for reconstructing past load using statistical methods to comprehensively characterize the impact of climate change, and variability of meteorological resources on the reliability of European power system with high wind penetration.

In one study, H. C. Bloomfield et al., 2016 used reanalysis data to understand the true climate sensitivity of Great Britain's power system, which is dominated by wind energy, by re-constructing 36 years of mutually consistent aggregated demand data (using Multiple-Linear Regression analysis with fixed effects to account for exogenous variables). This data was used to determine the residual (unmet) demand by differencing the available wind capacity in the system over the 36

year timeline to determine how much load was required to serve with conventional generators. In an extended study, Bloomfield et al., 2018 conducted a similar analysis with Generalized Additive Models (GAMs) for the power system of Great Britain to understand the effect of inter-annual variability (IAV) of temperature on total annual energy curtailment, and peak residual load. Additionally, reconstructions of electricity load has also been Hannah C. Bloomfield, D. J. Brayshaw, and Charlton-Perez, 2020 reconstructed electricity demand data (with heating and cooling degree days as additional predictors to the original model described in H. C. Bloomfield et al., 2016) for each country in the European subcontinent, to identify a new set of Targeted Circulation Types (TCTs). Moreover, Hannah Bloomfield, D. Brayshaw, and Charlton-Perez, 2020 also released the back-forecasted hourly electricity demand data publicly (developed using ERA5) as an attempt to enable researchers to understand country-level variability of solar and wind power resources in conjunction with demand.

Coker et al., 2020 used a reanalysis dataset to reconstruct electricity data between 1979-2016 using linear regression models, and used the reconstructed data to understand the uncertainty in capacity market of Great Britain. Thornton, Hoskins, and Scaife, 2016 reconstructed 38 years of electricity demand and 16 years of natural gas demand to explicitly model the relationship between demand and temperature on an annual, seasonal, and monthly basis to identify the weather dependencies for the case of the UK. To make the analysis robust, they removed any non-temperature driven demand variability and purely regressed demand on temperature to check for climate related variability. The authors found strong negative correlation between temperature and demand as well as temperature and gas supply, and also identified that this correlation inflated during winter.

Although simple regression methods which have been widely adopted in the studies above would help in predicting the weather dependent electricity demand changes, conventional linear/multivariate linear regression methods lack the ability to generalize due to their limited ability to model non-linear relationships as well as to work with larger dataset. The non-linear relationship between temperature and load has been widely discussed in the existing literature (Hor, Watson, and Majithia, 2005; De Felice, Alessandri, and Catalano, 2015; Valor, Meneu, and Caselles, 2001). It is thus imperative to ensure the model architecture adopted for predicting temperature dependent demand changes has the capability to generalize to any region which shows significant temperature

in with minimal adjustments.

For the U.S. mainland, multiple studies have focused on assessing the long term IAV of wind speeds(Krakauer and D. S. Cohan, 2017; X. Li et al., 2010; Pryor, Shepherd, and Barthelmie, 2018), and solar radiation, i.e., variability in renewable energy resources independent of their connection to demand, but none in conjunction with long-term electricity demand. Other US based studies (Shaner et al., 2018; Rinaldi et al., 2021) attempted to quantify the capacity gap in solar/wind energy during high demand spells over multiple decades (approximately 30 years) and used demand data from a representative year due to lack of historical demand records. Shaner et al., 2018 looked at analyzing 36 years of global hourly weather data between 1980 – 2015 to quantify variability of solar and wind resources as a function of time and location and estimate the gaps with electricity demand data. Here they used a single year (2015) of hourly electricity demand data, in absence of historical records and replicated it 36 times to compare against available solar and wind capacity.Rinaldi et al., 2021 also used hourly demand data from a single year (2018) to compare against available wind and solar power resources over 39 years for California and WECC Interconnect to find the gap in available resources and load. Even though these papers delineates representations of how IAV in renewable energy resources will affect grid planning, it fails to consider the variability in demand that will be induced due to temperature. Replicating a representative year's demand data for the length of period of study due to the unavailability of consistent hourly load data fails to capture the uncertainty in grid reliability as a response of variability in demand over multiple decades.

Moreover, a few studies also discussed the use of Piecewise Linear Regression (PLR) to forecast future demand using temperature from climate models and fixed effects (accounting for socio-economic factors) (Carreño et al., 2020; Fonseca et al., 2019). They model the future variability of wind and solar resources synchronously with future demand, and capture future variability in temperature induced by climate change. Fonseca et al., 2019 in particular forecasted electricity demand between 2055-2065 and 2089-2099 using temperature derived from climate models and assessed the impact of wind and solar power variability for the Tennessee Valley Association. These papers serve as a good example to develop insights about methods to forecast demand in the US, but the use of climate models for temperature records in place of reanalysis/observed temperature data

fail to account for the response of demand on IAV of temperature. Additionally, the climate data used was downscaled statistically, whereas publicly available climate models (such as NARCAAP and NA-CORDEX) require computational and time expensive refinements to derive hourly values of atmospheric variables, making the process to become more cumbersome.

In a related study, Auffhammer, Baylis, and Hausman, 2017 constructed a dataset of aggregated daily demand values of temperature response function to understand the change in load patterns in the future under the effect of climate change. The study used linear regression models, which inflates the sum of squared errors due to linearity assumption while modeling the relationship between temperature and demand. Temperature and demand follow a 'curved' relationship and can be best approximated using non-linear regression methods. Additionally, the study implicitly incorporated uncertainty from climate models which biases the daily constructed demand estimates.

To conclude, existing studies based on Europe have used regression based reconstruction techniques to create long time-series of historical demand data records, to ultimately understand the deep variability being induced in a grid due to inclusion of wind and solar resources along with changing demand, but the same has not been attempted for the US. To our best knowledge there does not exist any paper that has attempted to reconstruct electricity demand or even assess the hourly interannual variability of temperature over multiple decades and its effect on observed electricity demand data. Additionally, the methods applied to reconstruct demand in all existing papers (multiple linear regression) could be easily replaced by a PLR model and more sophisticated deep learning methods like Long Short Term Memory (LSTM) model. LSTM based neural networks are considered robust formulations to work with long multi-variate time series data. They are known to increase generalizability and accuracy of predictions by reducing model bias (Hochreiter and Schmidhuber, 1997).

Until now, the existing body of literature in the US has primarily focused on modeling the temperature response of aggregated electricity demand distribution over a few years by leveraging daily or monthly aggregated load values. Thus, to fill this research gap, in this paper we propose to quantify the change in electricity demand, especially hourly and seasonal peak load due to weather variation at a granular(hourly) level. Moreover, we use a multidecadal time frame to successfully capture

the load response under long-term interannual temperature variability for the contiguous US and thus identify the change in variance and mean of peak demand for the largest demand hours. Identifying these changing demand patterns is imperative to construct a robust power system. It will help planning agents to determine capacity gaps in a heavy renewable system and create reliable resource reserves for continuous electricity supply. Using historical observed hourly temperature records in place of projected climate change-based temperature estimates at a dis-aggregated time scale will make our estimations more robust. In all, this paper analyzes the uncertainty imbibed in the weather-sensitive portion of electricity demand by reconstructing four decades of temperature-driven hourly demand proxies, which will aid in identifying which BAs in the US have been the most sensitive interannual variability of temperature in the past. Thus, it will help stakeholders identify and strategize plans to make these systems more robust, as climate change will make air temperature more variable, eventually making electricity demand uncertain and increasing costs to operate a grid (Bryce et al., 2018). Moreover, it will also support planning agents to reduce the burden of economic and social costs due to outages influenced by climate-sensitive portions of electricity demand under extreme temperatures.

3.4 Methods

3.4.1 Area of study

Within the contiguous US, we chose to focus on assessing the weather sensitivity of electricity demand at the BA level (Figure 3.1) rather than state or national level because a BA is responsible for maintaining the reliability of regional power systems for commercial purposes. A specific BA is responsible for maintaining the balance of electricity supply and demand for a state or a group of states. Moreover, there is a need to reconstruct the hourly demand proxies for all BAs individually to account for spatial heterogeneity that influences temperature as well as complex electricity demand patterns and their end consumers. Furthermore, since this is a regression based problem with the predictor space containing thousands of records, we aim to control for compute time and space to ensure resourcefulness by proposing models that are computationally efficient yet

sophisticated to recognize the complexity in relationship between load and weather.

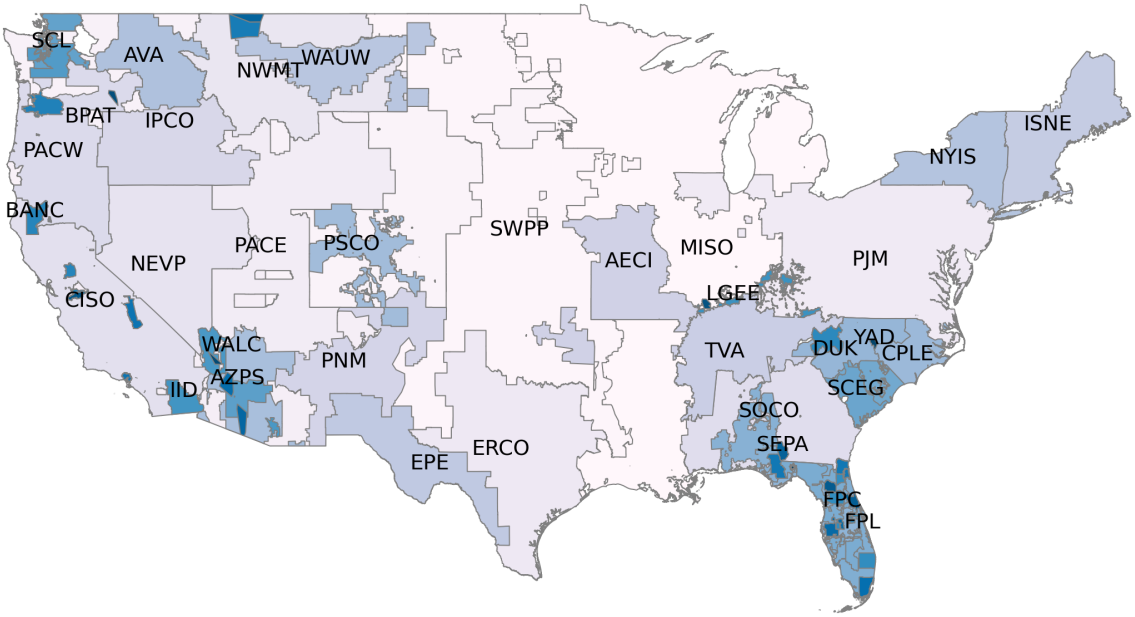

Figure 3.1: Map of the US delineating boundaries of major Balancing Authorities

3.4.2 Data

To simulate the effect of weather on electricity demand, our models while training used all of available publicly reported high-frequency hourly demand records (reported in MW per hour) from each BA between mid 2015-2019 (Tyler H. Ruggles and Farnham, 2020) with hourly temperature instances from NASA MERRA reanalysis dataset (Bosilovich, Lucchesi, and Suarez, 2015). The full names of all balancing authorities is available in the Supplementary Information section (Table B.1). Reanalysis data is generated using data analysis methods to develop consistent records of the observed conditions, which otherwise has gaps due to techniques in which data is collected and stored. To account for unobserved factors affecting the electricity demand, we feature-engineered fixed effect coefficients for each hour of the day, different days of the week, different months, and annual long term trends (as used in Fonseca et al., 2019). This enabled our models to control for changes in load due to socio-economic factors and human behavior. We use statsmodels, scikit-learn , and PyTorch to implement our models in python programming language, and since PyTorch does not have the required capability to work with data other than float and integer values, the

categorical variables were encoded in their respective sine and cosine formulation and used as predictors. Additionally, in the LSTM, the hourly electricity demand is based on a fixed-length sequence of hourly inputs (described in Section 3.4.4).

Even while assessing the impact of IAV of temperature variation on spatially and temporally differentiated hourly electricity demand data, we used observed hourly temperature records between 1980 - 2019 from the MERRA reanalaysis database as opposed to future temperature records from climate models, as we wanted to prevent the leakage of additional bias from uncertainty in Global/Regional Climate Models. Moreover, climate change models only report robust daily and monthly aggregated weather variables, and necessitates further downscaling process to extract hourly variables from these aggregated versions. Our aim in this study was to assess the influence of observed temperature dependent variability on electricity demand over multiple decades on an hourly basis to support planning agents in analyzing capacity gaps in power systems and also help in identifying the systems (BAs) that historically have been at most risk to variability in air temperature. Thus, we use available historical temperature records to train our models, and also for deriving the temperature-driven demand proxies.

3.4.3 Data Cleaning and Pre-processing

From the BA database for hourly electricity demand, any entity in the state of Alaska as well as in Canada were removed to make the dataset representative of contiguous US. Furthermore, data from *HIFLD Control Areas* n.d. was used to determine the coordinates of the largest population center in each BA, and the specific coordinates were used to extract corresponding hourly temperature data from MERRA. We implicitly assume homogeneous weather conditions within the entire geographical footprint of each BA, and thus use a single coordinate from the MERRA gridded data to extract hourly temperature for each year between 1980 - 2019 for training and reconstruction of demand proxies. The temperature records in MERRA are reported in Kelvin scale. Thus, we appropriately treated the data to scale the temperature records to °Celsius scale.

Additionally, the preliminary values of hourly electricity demand were considerably larger than its hourly temperature counterpart, as well as the sine and cosine encodings of the fixed effects

variables. This necessitated normalization of the dependent and predictor variables in a minimum-maximum format (Kramer, 2016 function 'MinMaxScaler'), to ensure that the model fit doesn't bias itself towards large values of any predictor (Mohsin, Hamdan, and Bakar, 2013).

3.4.4 Model Selection

We first mathematically formulate the relationship between dependent variable (hourly electricity demand) and the predictors (hourly temperature and the exogenous variables describing the fixed effects) by fitting multiple machine and deep learning based models that are generalizable to all BAs. We narrow down to two structurally different models to understand the impact of temperature change on electricity demand, a variant of linear regression model for greater interpretability of predictors, i.e., the multi-variate Piecewise Linear Regression or PLR (as suggested in H. C. Bloomfield et al., 2016; Carreño et al., 2020; Fonseca et al., 2019). PLR is an enhanced version of linear regression, which has the capability to model different trends in different subsets of the data. This model determines the relationship between the response variable, and predictors for different ranges of input variables. That is, in different sub-regions of the predictor space may contain distinct linear relationships. PLR is also known as segmented linear regression, as it fits different linear formulations to different segments of the input variable. But, a Piecewise Linear Regression follows the same assumptions as Linear Regression models, and thus, it may fail generalize in the case of large dataset, as used in this study.

To overcome these shortcomings, we extend existing methods proposed in literature to include a second model which is capable of recognizing sequential inputs to capture long-term dependencies in predictor space and has the ability to to capture the underlying relationship between predictors and the dependent variable even for very large datasets. An existing deep learning model capable of performing the above mentioned functionalities is the Long Short Term Memory (LSTM) network. LSTM have been documented to perform significantly better than other machine learning methods due to their ability of capturing non-linear relationships and flexibility of working with significantly large datasets while accounting for long-term dependencies between the dependent and of the input variables. LSTM algorithm (Hochreiter and Schmidhuber, 1997) is the upgraded

version of the classic Recurrent Neural Networks, applied to many time series based analysis for its ability to efficiently model sequential data. Each LSTM layer contains several LSTM units (which depends on the length of sequence of inputs being fed into the network), and each unit contains a framework called as - 'gating mechanism' (Sorkun, İNCEL, and Paoli, 2020) which helps to deal with vanishing and exploding gradients efficiently during back-propagation of training process. This gating mechanism consists of an input gate, output gate, and forget gate, which ultimately feeds into a cell state ($C_{h,t}$). The cell state $C_{h,t}$ learns how much information needs to be retained from previous time steps and what information should be passed on to the next time step (t) and hidden layer (h). In Figure 3.2, we describe the proposed LSTM architecture used for training the model. The structure of this neural network was arrived at after validating the performance of the best set of hyper-parameters (explained in Appenix A.2, Section B.2). As LSTM structure expects sequences of input, either of fixed or variable length, the optimal length of input variables is also treated as a hyper-parameter. For the case of time series based regression of temperature response of hourly demand data, a fixed sequence length is more appropriate. We selected 24 as the fixed sequence length (after multiple experiments with values between 12-36 against validation) to denote that a reconstructed proxy of temperature-driven hourly electricity demand value depends on input records in the past 24 hours. The sequence length parameter is an empirical choice that researchers need to make based on domain knowledge, but can also be considered as a hyper-parameter. Hence, the dependent(hourly demand) variable at any time t can be described as a function of fixed sequences (of length 24) of temperature and corresponding fixed effect (FE) as shown in Equation (3.1)

$$demand_t = f(temperature_{t_{-23}..t}, FE_{t_{-23}...t})$$

(3.1)

The LSTM network in Figure 3.2 has two initial inputs, that is the cell state ($C_{t,h}$ and hidden state ($h_{t,h}$). These are initialized with zeros. The cell state and the hidden state are parts of every LSTM

unit, which helps the unit to ascertain how much information from previous time step should be remembered, and what information should be passed on to the next time step (Hochreiter and Schmidhuber, 1997). While both cell state ($C_{t,h}$) and hidden state ($h_{t,h}$) are responsible for storing necessary information to be passed on to future time steps, $C_{t,h}$ is an attribute of long-term memory capability, that stores information of not necessarily immediate previous time steps. While $h_{t,h}$ is the memory capability that passes information from immediate previous events and overwrites at every step.

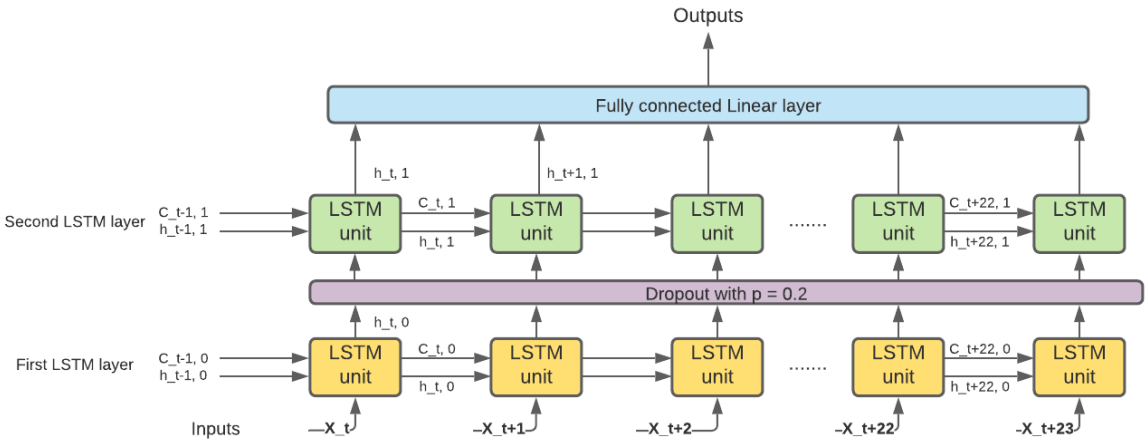

Figure 3.2: Final architecture of the LSTM model after experimenting with several hyper-parameters and testing their performance against validation set. We propose a stacked-LSTM model with 2 layers, and dropout regularization with probability of 0.2.

3.4.5 Model validation

A critical component of the model selection process is the model validation, which helped us determine the best performing model and appropriate hyper-parameters to use. We used a combination of scale dependent and percentage error metrics to validate our models against observed data from all BAs of the US, located in geographically diverse regions to account for diverse weather regimes, complex electricity consumption patterns, and end use sectors (results from validation process included in Appendix 5.4, Table 4.1). The three criteria used to measure model performance were:

1. Root Mean Squared Error (RMSE): The RMSE is an absolute measure, that squares the

deviation from the mean, to prevent the positive and negative deviations from cancelling each other. This is a scale dependent criteria, and is formulated as:

$$RMSE = \sqrt{\frac{1}{n}\Sigma_{i=1}^{n}\left(y_j - \hat{y_j}\right)^2}$$

where y_j is the observed variable and $\hat{y_j}$ is the estimated form of the dependent variable

2. Adjusted coefficient of determination (R^2) The adjusted R^2 value indicates how much variation in the dependent variable can be explained by the predictors in the model.

3. Mean Absolute Percentage Error (MAPE): The MAPE is a percentage based error metric which measures the relative forecasting error from regression models in % points.

$$MAPE = (\frac{1}{n})\sum_{i=1}^{n}\left|\frac{y_j - \hat{y_j}}{y_j}\right|$$

where y_j is the observed variable and $\hat{y_j}$ is the estimated form of the dependent variable

These evaluation metrics individually are widely used to evaluate regression models. We use a combination of three different criteria to ensure a comprehensive validation process while choosing between the LSTM and PLR model.

3.5 Results

3.5.1 Model performance

Before reconstructing the hourly demand data to analyze the effect of long-term temperature variability on electricity demand, we extensively tested our models to determine the optimal hyperparameters, and choose the best model for further analysis. We found that the LSTM model performed significantly better than the PLR model for all three evaluation criteria across all the BAs (Table 3.1).The Root Mean Squared Error (RMSE) values of the reconstructed demand estimates from validation set using the LSTM model for all BAs was relative lower than the RMSE

values from the PLR model. This was also true for coefficient of determination values for estimates derived using both models. The LSTM model resulted in significantly large R^2 values for all BAs than the PLR model, indicating that the formulation of predictors in LSTM model could explain significantly large variance in the dependent variable (hourly demand) as compared to PLR model. We attribute the optimal performance of LSTM model to the ease at which deep learning models capture complex relationships between dependent variable and associated predictors, in this case, hourly electricity demand and hourly temperature plus cyclic time variables capturing human behavior. Along with learning complex non-linear relationships between dependent variable and predictors, LSTM models can account for long-sequential inputs without necessarily treating any auto-correlation related effects and are known to produce reliable results for tasks related to multivariate time series analysis (Waheeb and Ghazali, 2020; Z. Chen et al., 2021).

Table 3.1 shows the validation process results for both models against three criteria, that is, RMSE, MAPE, and R^2 with their optimal hyper-parameter setting for each BA.

Table 3.1: Results from the validation process for LSTM and PLR models by splitting trainable data in 80:20 ratio (train vs. validation set) with their optimal hyper-parameter setting for each BA. Note, during the model selection process, multiple hyper-parameter changes were made to derive the most optimal set, but the table shows only the best results obtained.

BA	$Demand_{max}$	$RMSE_{LSTM}$	R^2_{LSTM}	$MAPE_{LSTM}$	$RMSE_{PLR}$	R^2_{PLR}	$MAPE_{PLR}$
AEC	1211	98.273	46.91%	12.65%	222.25	negative	46.80%
AECI	5279	505.47	18.04%	16.06%	484.09	negative	21.30%
AVA	2376	145.74	70.28%	8.26%	169.26	46.80%	11.12%
AZPS	7558	376.21	85.14%	7.66%	462.62	70.70%	9.51%
BANC	4763	227.19	74.44%	7.17%	233.24	68.05%	7.73%
BPAT	10943	606.50	55.77%	6.82%	642.25	44.66%	8.12%
CHPD	591	175.54	negative	74.76%	1363106	negative	100659%
CA-ISO	49899	2720.84	67.89%	8.05%	2809.90	51.60%	7.63%
CPLE	14416	1055.42	57.55%	11.46%	1077.93	9.61%	13.24%
CPLW	1182	82.19	52.41%	10.48%	84.08	negative	12.52%
DOPD	397	27.84	53.20%	11.84%	113211	negative	22238%
DUK	21608	1541.07	59.71%	9.95%	1639.58	20.98%	12.44%

EPE	1985	89.06	86.41%	7.02%	109.59	76.06%	9.08%
ERCOT	74533	4496.45	75.12%	9.09%	5540	50.72%	12.76%
FMPP	3677	219.76	79.90%	11.80%	255.38	71.75%	9.17%
FPC	12443	781.16	76.19%	9.92%	828.77	69.58%	10.73%
FPL	24991	1425.00	83.18%	7.75%	1401.05	82.52%	7.85%
GCPD	858	80.60	negative	11.57%	75.855	negative	13.42%
GVL	452	25.71	80.07%	8.45%	28.52	75.56%	10.39%
HST	115	7.91	75.75%	9.99%	7.85	74.90%	10.73%
IID	1081	103.92	49.27%	16.92%	121.173	48.22%	26.74%
IPCO	3700	236.59	65.00%	9.74%	233.45	53.90%	10.29%
ISO-NE	25763	1524.35	65.62%	7.69%	2019.52	negative	36.25%
JEA	3080	206.95	67.61%	10.29%	220.24	51.11%	10.47%
LDPW	7059	468.76	61.23%	9.38%	470.741	29.77%	8.61%
LGEE	6920	500.92	60.00%	9.58%	540.391	8.90%	10.94%
MISO	119733	5618.12	79.20%	5.68%	5916.84	62.42%	6.24%
NEVP	8603	379.53	83.21%	5.84%	490.29	73.29%	9.11%
NSB	108	7.48	72.09%	11.48%	7.89	64.39%	12.83%
NWMT	1961	127.32	31.38%	7.66%	120.56	24.48%	8.44%
NY-ISO	32076	1663.55	75.92%	7.66%	1838.33	55.88%	7.97%
PACE	8907	479.90	65.43%	9.89%	382.40	61.57%	5.10%
PACW	4037	354.08	45.45%	12.26%	359.96	negative	15.48%
PGE	4023	241.42	66.15%	7.48%	236.26	55.07%	7.79%
PJM	152890	9338.01	63.54%	7.81%	9940.74	19.87%	8.98%
PNM	2608	124.36	78.60%	6.27%	138.47	55.83%	6.08%
PSCO	9640	625.73	48.68%	7.11%	454.11	35.39%	7.65%
PSEI	5504	314.05	74.05%	6.86%	364.89	55.70%	8.52%
SC	5117	366.59	65.82%	9.60%	410.58	6.90%	10.51%
SCEG	4807	266.23	77.98%	7.25%	310.44	57.63%	8.97%
SCL	1870	84.21	80.68%	5.74%	96.75	71.80%	6.48%

SOCO	45745	3007.49	68.83%	8.83%	3934.04	17.78%	13.91%
SRP	7243	368.00	85.01%	7.83%	438.80	77.04%	10.37%
SWPP	51524	3131.18	53.87%	7.82%	3647.36	32.39%	10.60%
TAL	621	41.84	69.50%	9.75%	42.20	58.35%	10.94%
TEC	4413	292.25	73.16%	9.13%	293.19	71.30%	9.38%
TEPC	3664	232.64	50.29%	13.44%	237.67	59.99%	10.73%
TIDC	653	36.95	74.45%	8.69%	40.36	66.63%	10.63%
TPWR	998	51.31	76.15%	6.84%	63.66	54.95%	8.77%
TVA	32511	2423.53	53.55%	10.46%	2630.08	5.22%	13.10%
WACM	4433	242.72	40.39%	6.55%	221.77	38.58%	6.03%
WALC	1919	130.80	38.12%	9.47%	149.12	33.90%	12.45%
WAUW	168	12.96	15.98%	11.17%	11.74	14.36%	11.81%

Although the LSTM model performed optimally to reconstruct the hourly trends in electricity demand based on weather variability for most BAs, a handful of BAs located in the Northwestern region of the US, in the state of Washington, and a few BAs in the state of Florida, showed no discernible temperature-demand relationship. Figure 1 represents some of these BAs which had no defined relationship correlating air temperature and hourly demand. These BAs also had R^2 value less than 50%, which implied that significant amount of variance in dependent variable could not be explained by our choice of predictor set.

For example, the Public Utility District No. 1 of Chelan County (BA acronym: CHPD), Public Utility District No. 2 of Grant County, Washington (BA acronym: GCPD), etc. showed R^2 values in the range of 2-10% during the validation process, even after considerable hyper-parameter tuning and changes in model architecture of the LSTM network. This indicated that BAs which showed significant asymmetry in the temperature-demand relationship have other dominant factors affecting the hourly load. For all analyses, we took care to eliminate any BA that did not show a relatively smooth temperature-load relationship.

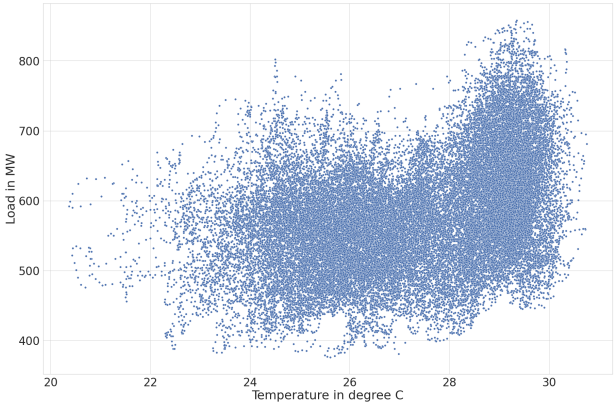

(a) Public Utility of Grant County, Washington (GCPD)

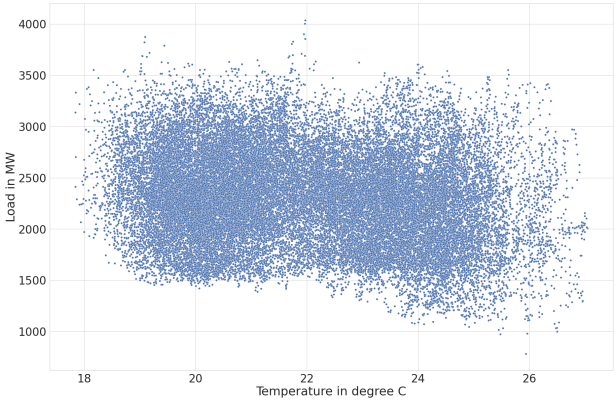

(b) Pacific Cooperation West (PACW)

Figure 3.3: Examples of balancing Authorities showing asymmetrical Temperature-demand relationship, which implies that factors other than temperature significantly influence hourly electricity consumption in these regions.

Table 3.2: Balancing Authorities ranked in descending order of maximum hourly consumption in the period between 2015 - 2019 (observed data)

BA	Maximum hourly demand in MW	R^2_{LSTM} validation
PJM Interconnection, LLC (PJM)	152890	63.54%
Midcontinent Independent System Operator, Inc. (MISO)	119733	79.20%
Electric Reliability Council of Texas, Inc. (ERCOT)	74533	75.12%
Southwest Power Pool (SWPP)	51524	53.87%
California Independent System Operator (CA-ISO)	49899	69.89%
Southern Company Services, Inc. - Trans (SOCO)	45745	68.33%
Tennessee Valley Authority (TVA)	32511	66.38%
New York Independent System Operator (NY-ISO)	32076	75.92%
ISO New England (ISO-NE)	25763	65.62%
Florida Power & Light Co. (FPL)	24991	83.18%
Duke Energy Carolinas (DUK)	21608	59.71%

3.5.2 Peak demand changes in reconstructed data

Inter annual weather variability significantly influences two components of electricity demand. First, sub-daily or hourly variation in temperature influences change in peak and shoulder loads, and second, IAV of temperature across multiple decades modulates variation in median electricity demand. Peak load assessment is critical in designing a system capable of handling unexpected demand surges, and creating contingency reserves.

We start by comparing the 20 largest peak temperature-driven demand hour proxies between 2015 - 2019 to the twenty largest peak hourly observed demand for the same time period. We find that the temperature-driven demand proxies estimated by both the LSTM and PLR models underestimate the range of demand outliers (or anomalous demand hours). This is because regression based methods are robust at capturing the general trend of data-distribution of dependent variable around the average values, but fails to understand the trend of outliers and more importantly the predictor set used for isolating the temperature dependency of electricity demand is only able to explain up to 85% of the variance in dependent variable (as per our R^2 validation results). Among PLR and LSTM, LSTM model was still substantially better than PLR model to recognize the outliers hourly demand records. But,to make the comparison of 20 largest demand records homogeneous and identify the most sensitive BA, we compare the reconstructed proxies of temperature-driven hourly demand created for 2015 - 2019 to proxies in our test set for 1980 - 2014, instead of comparing 20 largest observed demand hours to reconstructed proxies from 1980 - 2014. Thus, we reconstructed load data for the entire range of available weather data, i.e., 1980 - 2019, using the LSTM model to create a consistent dataset of the weather-sensitive portion of hourly demand.

Figure 3.5 shows the top 20 demand hours for each year of reconstructed demand as a response to temperature function for the eight largest balancing authorities (Table 4.1), and Figure 3.6 presents the corresponding auto-correlated 24 temperature values that were used to estimate the top twenty demand hours in each of the eight BAs. We show the auto-correlated temperature rather than corresponding hourly incident temperature for each of the top demand values in Figure 3.5 because the LSTM model leveraged sequential input. At any n^{th} hour the estimated electricity demand was quantified using n - 24 length of predictors. Moreover, we analyze the variability of twenty

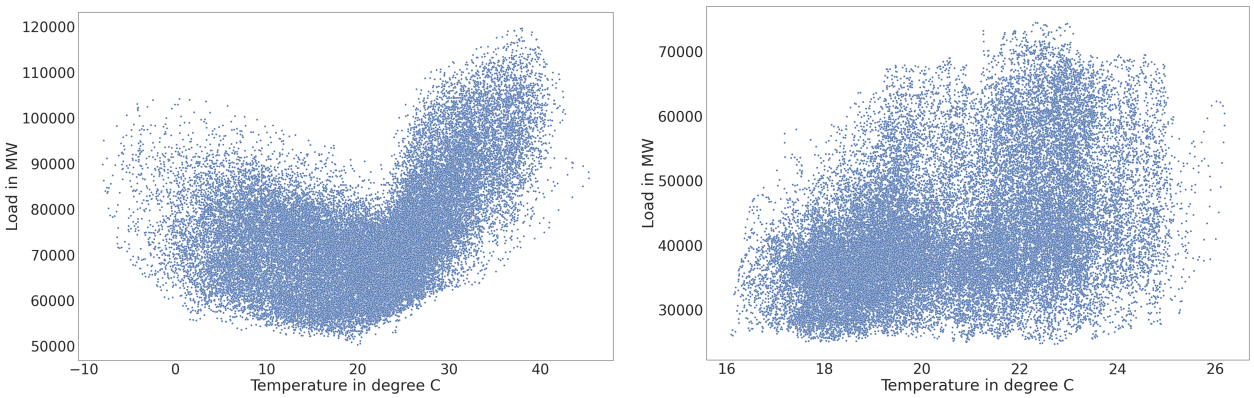

(a) MISO (b) ERCOT

Figure 3.4: Hourly temperature-load relationship of Midcontient Independent System Operator and Electricity Reliability Council of Texas

largest demand hours in each year of reconstruction because annual peaks in power system drives the capacity planning process as it quantifies peak demand across a wider horizon in comparison to daily peaks (Auffhammer, Baylis, and Hausman, 2017).

Overall, for the case of both summer and winter peaking systems, the extent variation of demand hours is driven by extreme temperatures. To corroborate this hypothesis, we compare the distribution of top twenty reconstructed demand hours and the associated temperatures which estimated it (Figure 3.6). We find that all large BAs show a positive correlation biggest demand hours and temperature, except for ERCOT, which shows negative non-linear correlation. The right tail of the temperature-load curve (Figure 3.4 a) indicates a high-degree of positive correlation between higher temperatures leading to higher demand, which the model failed to recognize only for ERCOT. We attribute this behavior to a noisy temperature-demand relationship for the case of ERCOT, as shown in Figure 3.4 (b), which both the LSTM model and Piecewise Linear Regression model failed to recognize.

We use coefficient of variation (CV) to compare the deviation of 20 largest demand values over the reconstruction timeline to account for difference in magnitude of electricity consumption in each BA. CV is the normalized form of standard deviation and is estimated as the ratio of the standard deviation of variable of interest in a given period to its average value. Comparing the deviation of 20 largest demand hours within each BA and across all years, we find that largest variability across

all years is observed in Southern Company Services Inc. (SOCO) with CV varying between 18% - 20%. However, SOCO presents significant variability of 20 largest demand records only in 2005 and 2011 corresponding to hotter days in June, August and September (Figure 3.6). Tennessee Valley Authority (TVA) with coefficient of variation of about 17%. The largest variability in peak demand hours are not consistent for TVA, as the reconstructed demand proxies indicates a large dispersion of top 20 demand hours only for 1980 through 1984.

Figure 3.5 also indicated that Midcontient independent System Operator (MISO), and California Independent System Operator (CA-ISO) for every year of proxy demand reconstruction, also showed inconsistent deviation of 20 largest demand values, and resulted in a coefficient of variation value of 17% and 16% respectively. This was followed by Southwest Power Pool (SWPP) with a coefficient of variation value of 15% (Figure 3.7). In contrast, among the 10 largest balancing authorities ranked in the order of largest hourly power consumption, PJM Interconnection and New York System Operator (NY-ISO) present lower coefficient of variation of 8% and 9% respectively implying smaller changes in peak demand requirements over year under the influence of changing temperature changes.

Similarly, we also analyzed the spread of 20 largest temperature-driven demand proxies for all the BAs (plots of 20 largest demand included in Appendix A.2, Figures B.1, B.2, B.3, and B.4) of the US after removing any BA which showed R^2 values $<=$ 50%. BAs in the south-western region like Arizona Public Service Company (AZPS) and Nevada Power Company (NEVP), and BAs in southern states of the US, like City of Tallahassee (TAL), Duke Energy Florida, Inc. (FPC) show very large spread of 20 largest demand hours across 1980 - 2019, leading to coefficient of variation value of about 28%. Several smaller sized balancing authorities like the Salt River Project Agricultural Improvement and Power District (SRP; located in the state of Arizona), Utilities Commission of New Smyrna Beach (NSB; located in the state of Florida), Turlock Irrigation District (TIDC; located in the state of California) also indicated significantly large coefficient of variation values of 30%, 29%, and 27% respectively. Comparing these to their corresponding temperature values (Figure 3.6), we find that for all above BAs summer time temperature in months between May - September influence the 20 largest demand hours.

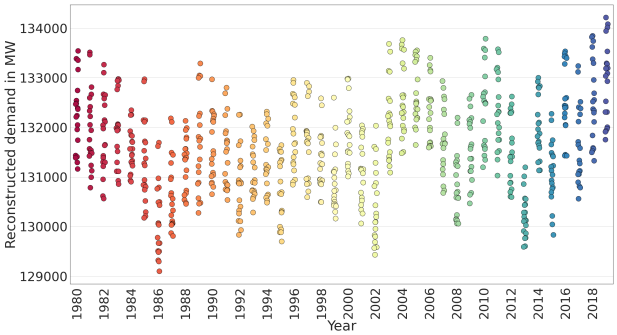

(a) PJM Interconnection, LLC (PJM)

(b) Midcontinent ISO (MISO)

(c) Electric Reliability Council of Texas (ERCOT)

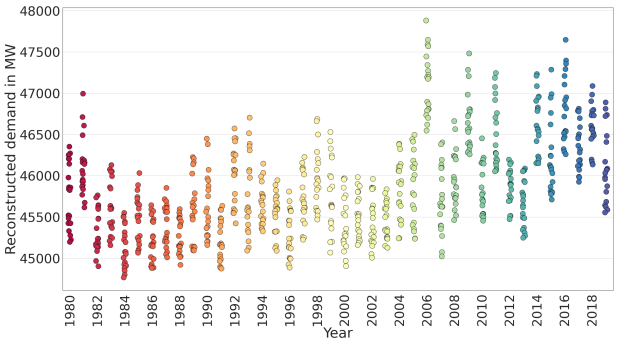

(d) Southwest Power Pool (SWPP)

(e) California Independent System Operator (CISO)

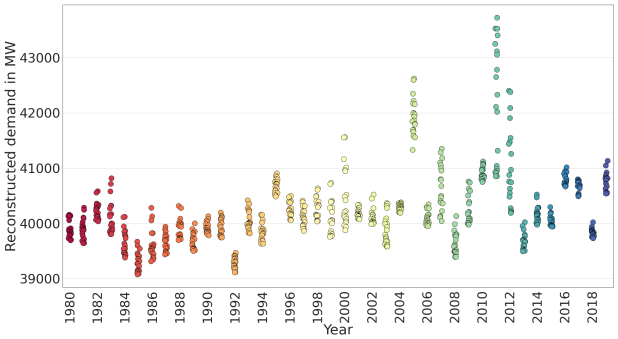

(f) Southern Company Services, Inc. (SOCO)

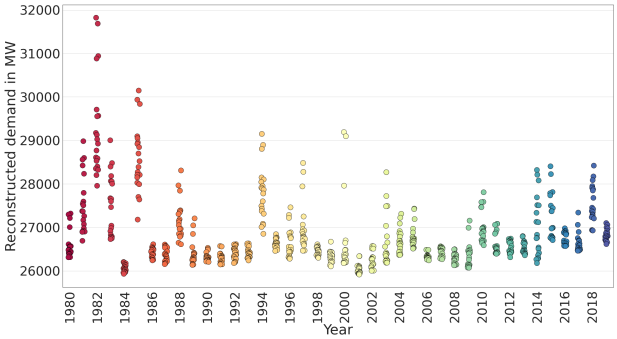

(g) Tennessee Valley Authority (TVA)

(h) New York Independent System Operator (NYISO)

Figure 3.5: Hourly reconstructed demand values exceeding 99th percentile of hourly observed demand between 2015 - 2019 for each year of reconstruction (1980 -2014) segregated by months (colored) for the largest BAs of the US.

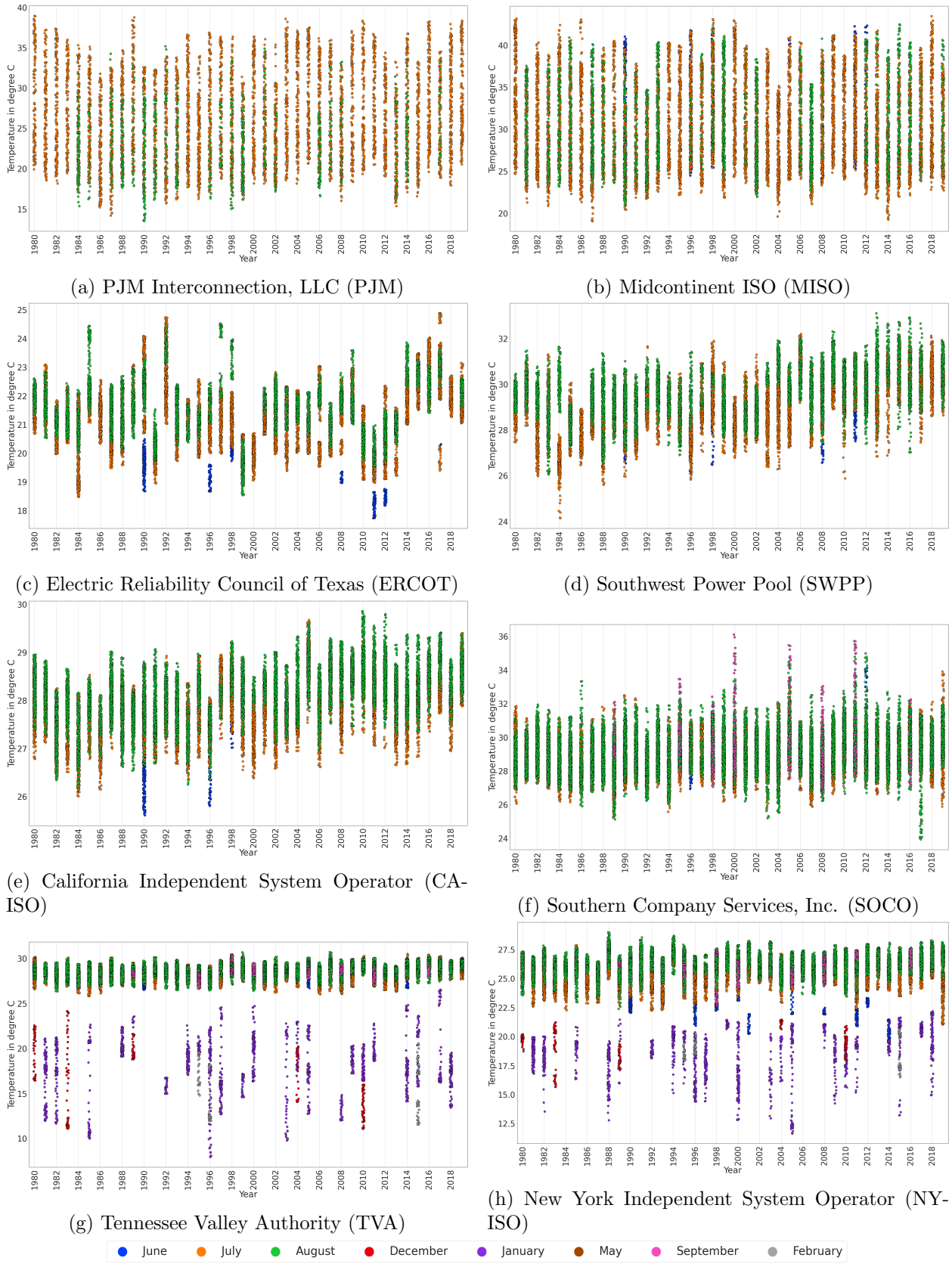

(a) PJM Interconnection, LLC (PJM)

(b) Midcontinent ISO (MISO)

(c) Electric Reliability Council of Texas (ERCOT)

(d) Southwest Power Pool (SWPP)

(e) California Independent System Operator (CAISO)

(f) Southern Company Services, Inc. (SOCO)

(g) Tennessee Valley Authority (TVA)

(h) New York Independent System Operator (NYISO)

Figure 3.6: Auto-correlated hourly temperatures corresponding to the 20 largest reconstructed demand values in Figure 3.5, segregated by months (colored) for the largest BAs of the US.

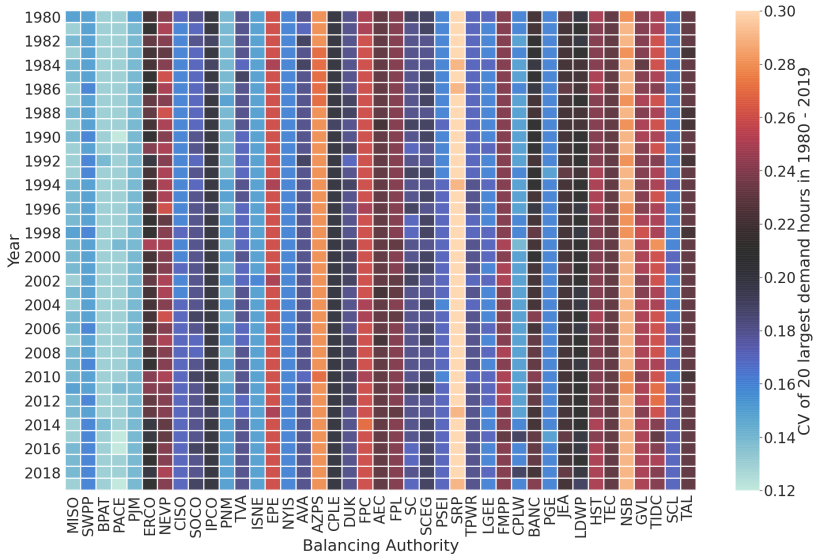

Figure 3.7: Heatmap representing coefficient of variation values for the top twenty reconstructed temperature-driven demand proxies for balancing authorities in the US. Amongst the top 10 largest BAs, we find the greatest year-to-year variability occurring in ERCOT, followed by CA-ISO, TVA, SOCO, and DUK.

Conversely, for the case of TVA, NY-ISO, and also Independent System Operator of New England (ISO-NE), colder days in December, January and March significantly drives the largest demand, as shown in Figure 3.6. For these systems, the right and left tail of the temperature-load curve drives peak demand, and thus if climate change amplifies the inter-annual variability in both and summer winter months, these BAs will become more vulnerable to system outages.

In all, the BAs like SOCO, TVA, MISO, CA-ISO, SWPP, etc., which show large deviations of 20 large demand hours, and thus, these balancing authorities will be at a higher risk to variability in hourly weather patterns. Smaller sized BAs with large CV are also at risk, but the problem is more pronounced in larger BAs because these entities serve geographically diverse areas, with different socio-economic status, and also different energy policies. In particular, greater risk of weather variability will introduce additional challenges in managing CA-ISO and MISO because of its very large solar and wind energy footprint.

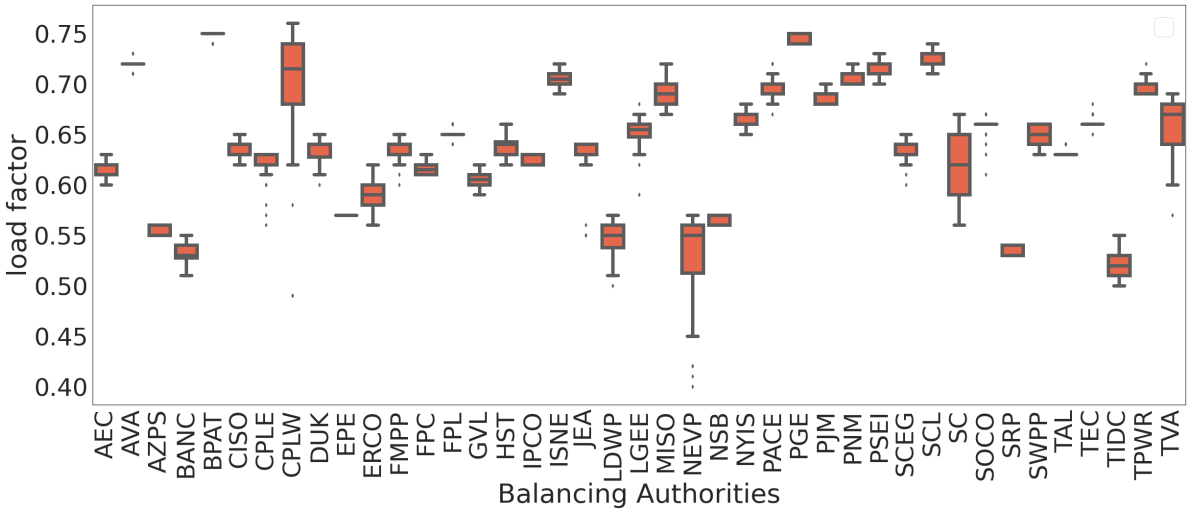

Figure 3.8: Distribution of annual load factors between 1980 - 2019 for all BAs considered in this study. Tennessee Valley Authority (TVA) has the largest interquartile range among the top 10 largest BAs, indicating large difference in year-to-year change in annual load factors. While, Midcontinent Independent System Operator (MISO) and Electricity Reliability Council of Texas (ERCOT) have moderate interquartile ranges, rest of the top 10 large BAs show very small changes in load factors

3.5.3 Change in Load Factor

Load factor is defined as the ratio of average demand over a specific period to the peak demand in that period. Load factors are used to measure the change in electricity consumption over time. Large load factors indicate that the mean electricity demand is similar to peak hourly demand, and the system capacity built for generation is being utilized efficiently. Smaller load factors indicate that peak demand in the system are very large as compared to average demand and are limited to certain hours of the time frame under consideration. We analyze the change in annual load factors between 40 years of our study. The distribution of annual load factors across 1980 - 2019 are represented as box plots for all BAs in Figure 3.8.

Larger interquartile ranges in box plots shown in Figure 3.8 implies large changes in annual load factors indicating that the temperature-driven demand peaks are large for certain years versus other in comparison to average temperature-driven demand. This implies that in BAs like TVA, MISO, and ERCOT with change in temperature, the consumption and eventually utilization of generating capacity will differ significantly between years. With large changes in peaks and mean consumption

due to temperature, deploying strategies such as Demand Response and Peak shaving will become increasingly difficult.

In contrast, for moderately sized BAs, like NEVP and SC, the distribution of year-to year change in load factor is even larger implying that the consumption of electricity in these BAs differ significantly from peak demand across the 40 years being studied. Even though, NEVP and SC govern smaller regions, grid management with the integration of Electric Vehicles (which is considered as variable load) in the future will likely be disruptive as these BAs already indicate variable peak demand requirements due to temperature changes.

3.6 Discussion

In this paper, we utilize high frequency hourly weather data from MERRA and observed demand from all BAs of the US, coupled with human behavior based fixed effects to reconstruct a dataset that represents the climate-sensitive portion of hourly load for four decades between. Reliance on climate models implicitly imbibes uncertainty in the analysis and also requires costly downscaling process which limits the use of climate model for large scale country-wide analysis. Thus, we base our analysis on historical temperature records to conduct a fine-scaled quantification of change in peak and median electricity demand patterns due to natural variability of temperature across contiguous US. Since we use present-day (2015 -2019) hourly demand to train our models, we implicitly include the representation of modern-day energy efficiency measures, technologies, and consumption patterns in our modeling efforts.

Through the modeling process, we demonstrate the efficacy of machine and deep learning models to quantify the sensitivity of electricity demand due to weather variability (natural variability of temperature from historical records) by generating reconstructions of high-intensity hourly demand data. We showed that modern neural network based LSTM models outperform traditional machine learning method of multi-variate linear regression as used in existing studies (Auffhammer, Baylis, and Hausman, 2017; Bloomfield et al., 2018; Hannah C. Bloomfield, D. J. Brayshaw, and Charlton-Perez, 2020; Fonseca et al., 2019). Additionally, we also show that, due to differences in geography

and time, it is recommended to train and validate data-driven models for each BA.

Our initial validation process included a comparison of reconstructed peak temperature-driven hourly demand proxies between mid 2015 - 2019 to the corresponding 20 largest observed demand peaks data for each Balancing Authority. We found that both, LSTM and Piecewise Linear Regression models significantly underestimates the demand anomalies or the peak demand outliers in each year of validation. While, existing patterns in outliers from 20 largest temperature-driven demand proxies of some BAs (like AZPS, TVA, NEVP, etc.) were captured accurately, in other balancing authorities the LSTM model performed marginally to capture outliers. This can be attributed to the noisy data points in temperature-load relationship which introduces bias in our estimates.

Overall, we find that 18% of all BAs (total 66) do not indicate a smooth temperature-load curve, which implies that additional socio-economic factors and changes in demographics affect electricity consumption patterns. Examples of such BAs include the Associated Electric Cooperative, Inc. (AECI) in the midwest; Public Utility District No. 1 of Chelan County (CHPD), PUD No. 1 of Douglas County (DOPD), Public Utility District No. 2 of Grant County, Washington (GCPD) in the pacific northwest; Western Area Power Administration - Rocky Mountain Region (WACM), Western Area Power Administration - Rocky Mountain Region (WALC), and Western Area Power Administration - Upper Great Plains West (WAUW) and a few others. We eliminated these BAs before performing further analysis as they also showed very small R^2 values during the validation process.

While analyzing annual peak demand changes in large BAs it was found that almost all large BAs react to summer-time temperatures except for the case of TVA, NY-ISO, and ISO-NE. We further also explored changes in 20 largest temperature-driven demand proxies between years, and within each year of reconstruction (1980 - 2019). BAs like MISO and SWPP showed indicated significant CV of the 20 largest demand proxies, 13% and 16% respectively. Even though the coefficient of variation values are less than 20% for large BAs, even small CV values implies bigger risks. This is because BAs like MISO, PJM, ERCOT, SWPP, govern states with cumulative large energy consumption and even small changes in temperature-driven demand variability can stress the grid infrastructure. This is more concerning for the case of MISO which governs states like Iowa, North

Dakota, South Dakota and others, which largely rely on wind energy (also intermittent in nature). Future amplifications in natural variability of temperature due to climate change induced effects would make the capacity gaps wider for hours during the day when wind production is limited. Furthermore, calibrating the impact on moderately sized BAs we found that, demand variability is more prominent in SOCO, followed by TVA and CA-ISO. All three systems are summer peaking, and like MISO, managing CA-ISO will be increasingly harder with more changes climate sensitive portion of electricity demand as CA-ISO is heavily dependent on solar power production.

Several caveats pertain to our analysis. First, while reconstructing hourly demand data for each BA, we used the coordinates of the largest population center under the governing BA of interest to extract matching hourly temperature data. For example, we chose the location of Nashville for the Tennessee Valley Authority (TVA) to train the models and reconstruct the hourly demand data. This implicitly biases our model towards a single weather zone in a BA, and estimates demand according to that weather zone. But in reality, a BA may have several weather zones, and a handful of large BAs (like ERCOT and ISO-NE) also report zonal electricity demand. Future work could use temperature from multiple weather zones to scale and reconstruct electricity demand for the BAs which report zonal electricity consumption.

From the validation experiments, we found that the use of LSTM model for reconstructing temperature-driven demand proxies resulted in fairly robust estimates for large BAs. While, for the case of small and mid-sized BAs like PACW, WAUW, WALC, WACM, CHPD, GCPD, NWMT, IID, DOPD, AEC, AECI, etc. both models failed to characterize the change in hourly demand due to temperature changes leading to R^2 values of less than 50% implying the predictor space could not capture most of the variance in dependent variable. This indicates that further validation experiments are required with a larger subset of weather-related predictors which includes Heating and Cooling degree days (Tyler H Ruggles and Caldeira, 2022) and humidity (Fonseca et al., 2019).

Second, since we aimed to reconstruct multidecadal hourly demand values rather than estimating aggregated values of daily or monthly load without biasing our estimates by including simulations from climate change models, we used historical temperature data. This also helped in isolating the effects of natural variability of temperature against climate change induced variability due to

anthropogenic forcings. But, should there be a case where robust hourly air temperature records from downscaled climate models are available, the proposed LSTM model architecture can be used to determine the sensitivity of hourly electricity demand under the impact of different trajectories of climate change.

We ignore any factor other than temperature to model the effects of weather on electricity demand, assuming extreme air temperature drives the large peak demand requirements in the US power system. Future analysis could integrate the impact of air humidity on electricity demand to determine if BAs in different regions of the US resulted in lower/higher reconstructed hourly demand values. M. Craig et al., 2021 found that the impact of humidity on electricity demand in states of Mississippi and Alabama (BAs governing these states are TVA, AEC, and SOCO) is more pronounced as compared to southeastern states. The results from a BA level study which includes humidity would likely show qualitatively similar results to the ones we discuss in this paper as the model predictors might explain significant variance in the BAs which were filtered out.

Despite these limitations, our results offer insights into the impact of natural variability of weather on the BAs of the US. They are particularly useful in delineating the weather sensitive BAs based on historical reference hourly temperature and identify which BAs would face additional challenges while integrating intermittent renewable energy resources like solar and wind energy. Understanding weather-driven variability is crucial to build a power system that enables a high-degree of reliability contribution towards meeting excess demand at all times.

Additionally, we also use robust deep learning based to generate dataset spanning across 40 years of the climate-sensitive portion of electricity demand. This dataset will help energy planners and researchers to understand inter-annual variability based reliability changes in the existing grid, and thus help them consolidate plans for BAs which requires the most attention. These set of vulnerable BAs already show serious response to natural variability of temperature. Hence, the vulnerability will be further magnified under future climate change related impacts. Accounting for both natural weather variability and climate changes impacts separately in long-term planning process will help manage investment errors and highlight effective strategies for climate change adaption and mitigation.

Chapter 4

Multidecadal assessment of reliability contributions from renewable energy sources under deep uncertainty for ISNE, ERCOT, and CA-ISO leveraging temperature response of hourly load

4.1 Abstract

Balancing Authorities (BAs) in the US are analyzing appropriate strategies to increase renewable energy capacity in their respective systems, due to the rapidly falling prices of wind and solar technologies and evolving policies mandating or encouraging more clean energy sources for power production. But long-term power systems planning studies involving decisions related to capacity expansion, transmission, and storage, often lead to infrastructure development for multiple decades. Investment decisions in the present will affect future grid planning processes, and thus it is important to create plans that account for uncertainty in power production as well as change in demand, especially the variability in capacity contributions induced due to changing weather conditions. In this chapter, we assessed the reliability contributions from solar, onshore wind, and offshore wind generators for three large BAs, and found that for the BA governing Texas, Electricity Reliability Council of Texas (ERCOT), solar generators provide large reliability across all 40 years as compared to onshore and offshore wind generators, and is significantly less sensitive to changing weather. This is because ERCOT already has substantial contributions from onshore wind farms and our ELCC results from Chapter 2, proved the need for diversification of generators. On the other hand, offshore wind farms will provide greater reliability contributions in ISO-New England (ISO-NE) and California Independent System Operator (CA-ISO), but offshore wind capacity factors is very sensitive to inter-annual variability impacts of wind speed, with its effective reliability contribution value changing by approximately 40% between 1980 -2019 for both cases.

4.2 Introduction

The North American Electricity Reliability Corporation (NERC) (Council, 2020) concluded in their recent long term reliability assessment study for 2021 - 2030 that there is an increased risk associated with large penetration of solar and wind power resources for large Balancing Authorities (BAs) which includes most parts of Western Interconnect, ERCOT (Electricity Reliability Council of Texas), PJM, and MISO (Mid-west Independent System Operator). While these BAs are known to already have large dependency on renewable energy resources (ERCOT relies on approximately

20% onshore wind generation), BAs governing large population centers like Boston (ISO-NE) and major cities in California (CA-ISO) may experience reliability challenges as more wind and solar power is added into the grid.

Stakeholders involved in the grid planning process conduct system reliability assessments while considering uncertainties to ensure the continuous reliability of electricity supplies. But these reliability assessments are largely based on available hourly demand and weather data, and are thus constrained to a small time-frame which is not sufficient to account for variability in the resource supply (solar radiation and wind speeds) as well as uncertainty in hourly load. The process of robust long-term planning of a grid system requires accounting for changes in electricity consumption while determining the optimal size of generators to be added to the system. Thus, there is a growing need to understand reliability of power systems over a longer time scale while taking into account the impact of interannual variability (IAV) of temperature on demand as well as interannual variability of resources like solar and wind. Hence, along with assessing variable supply of solar and wind power (from both onshore and offshore counterparts), we need to assess reliability in conjunction with demand as a response function of changing temperature.

However, the hourly electricity demand data needed for conducting long-term analyses of reliability for a grid is unavailable. Currently, the Balancing Authorities of the US report hourly demand data on public platforms only for the past five years, that is, hourly demand requirements between July 2015 - October 2020 (Tyler H. Ruggles and Farnham, 2020). Any annual reliability assessments based on this dataset will be constrained to an effective time scale between 2016 to 2020. Previously, in Chapter 3, we investigated appropriate methods to reconstruct proxies of temperature-driven hourly demand data using regression methods. Our proposed method of using deep learning models resulted in relatively robust multidecadal- estimations of hourly demand as compared to previously attempted methods in the literature. We also explored the difference in year to year variation pf 20 largest demand hours, and determined which Balancing Authorities showed significant sensitivity on demand-side due to historical weather changes. This was done to aid planning agents in the process of building reliable power systems.

Thus, to effectively plan a grid with new generators (both conventional and renewable energy-

based) of varying nameplate capacity, it is imperative to understand the requirements of the grid over the long term while taking into account seasonality of demand and supply.

Wu et al., 2018 studied the variability in resources which contributes to the generation of renewable energy, and found that terrestrial near surface wind speed for North America and Central Asia decreased with a linear trend of -0.11 ms^{-1} per decade, with second most significant decreases have occurred in parts of Europe, East Asia, and South Asia with mean linear trend of -0.08 $ms^{-}1$ per decade. Zeng et al., 2019 found that large decadal-scale variations of near-surface wind are determined by internal-decadal ocean-atmosphere oscillations. They also estimated that for the case of the contiguous US, variability in wind speed has aided in growing wind power production. Over the last few decades, the change in mean annual wind speed in North America has changed the potential of wind energy generation by $\pm$ 2% . These changes in near surface wind speed can alter the available high intensity wind resources for wind power production and thus perturb the reliability estimates reliant on which long-term power system infrastructure are planned.

Researchers, stakeholders involved with the energy industry, and utility company managers have always been interested in understanding the impact of change in weather variables on reliability contributions from power systems. But the body of literature specifically trying to understand the effect of interannual variability in solar irradiance, wind speed, and temperature on long-term power system planning and analysis have only started to grow. Auffhammer, Baylis, and Hausman, 2017 in their study cited the need to understand the impact of long-term temperature changes on peak summer demand across the state of California to strategize capital investments in energy infrastructure. Maia-Silva, Kumar, and Nateghi, 2020 and Yalew et al., 2020 also underscore the need to include temperature variability in long-term planning studies for the grid. Bryce et al., 2018 in their latest study highlighted the economic impact of ignoring interannual variability of solar power in Hawaii by analyzing records from 15 years. Moreover, studies by Hannah Bloomfield, D. Brayshaw, and Charlton-Perez, 2020; Bloomfield et al., 2018; Coker et al., 2020 focused on assessing the sensitivity of the European power system to weather variables have used back-forecasted electricity demand for multiple decades to assess the power system performance.

A handful of studies (Slusarewicz and Daniel S Cohan, 2018; Kumler et al., 2019) have attempted

to analyze the solar and wind power complementarity towards satisfying peak demands while considering their interannual variability over a relatively short time frame of less than ten years. Contrary to these studies based on the US power system setting, studies evaluating European power system reliability studies are increasingly accounting for multidecadal interannual variability (Thornton, Hoskins, and Scaife, 2016; Collins et al., 2018; Coker et al., 2020; Zeyringer et al., 2018), etc. In fact, Coker et al., 2020 underscored the necessity to account for supply and demand side interannual variability for successful energy market design in the UK. Collins et al., 2018 also used an economic model to optimize for power system reliability for the European subcontinent, i.e. meeting demand at an hourly resolution using existing base fleet generators, but this analysis doesn't capture the reliability benefits from new generators that maybe added to the base fleet in future.

Studies related to characterization of weather variables that impact grid planning remain constrained to a handful of papers. Although substantial progress has been made to understand how much solar or wind energy is available at a certain region over a specific period, a comprehensive analysis of variability of these variables over time and over geographical conditions and its impact on grid reliability in the context of contiguous US remains vague. Thus, this paper aims to help stakeholders involved in the grid planning process to think about reliability assessments from adding new solar and wind energy generators over a multidecadal time frame.

However, related studies for the case of the US either focus on smaller time scales Kumler et al., 2019 as explained above, or account for either supply side interannual variability of solar or wind and ignore demand side variation Shaner et al., 2018; Rinaldi et al., 2021. A comprehensive study assessing the reliability of the US grid while accounting for both IAV of renewable energy supply and demand over a multidecadal time-frame has been missing from the literature.

The definition of a reliability metric also varies among the existing studies. A complete analysis of weather-driven interannual variability impacts on power systems involves carefully incorporating variability in solar and wind capacity factors influencing new VREs for offshore and onshore locations separately, considering the combined interactions of temperature-driven demand variability and effects due to weather-driven forced outage rates on existing base fleet of conventional genera-

tors. The combined interactions from all factors can be probabilistically modeled to derive effective reliability contributions from the new solar and wind generators. A probabilistic analysis of reliability contributions from the addition of extra renewable energy generators can be completed using the Effective Load Carrying Capability (ELCC) metric as utilized in Bromley-Dulfano, Florez, and M. T. Craig, 2021; Keane et al., 2010; Madaeni, Sioshansi, and Denholm, 2012 and Chapter 2.

The goal of this project is to fill the research gap of accounting for variability while assessing reliability contribution from adding new renewable energy generators over a multi-decade time frame while also incorporating effects of electricity demand uncertainty. We thus propose to fill this gap by analyzing the effect interannual variability weather variables affecting both production and demand side of power system across multiple decades.

Thus, we aim to study the change in reliability contributions from new solar, onshore wind and offshore wind energy resources over a 40-year time scale for ISO-NE (Independent System Operator of New England), ERCOT (Electricity Reliability Council of Texas), and CA-ISO (California Independent System Operator) in a probabilistic fashion by trying to incorporate several sources of uncertainties.

4.3 Methods

In order to successfully answer the identified research gap, we use proxies of weather driven hourly demand reconstructed in Chapter 3 for the 1980 - 2019 timeline, for all three BAs, and derive the change in effective reliability contributions of adding new offshore wind, onshore wind, and solar generators into the grid. The aim of this study is to conduct a robust analysis to understand the change in capacity contributions of a system of diverse fleet of generators while taking into account the multidecadal interannual variability of weather variables while synchronously accounting for demand as a response function of interannual variability of temperature. To accurately isolate the effects of weather-related changes on the reliability contributions, we hold all other factors, such as the grid composition and electricity interchanges, constant from 2019.

For a comprehensive analysis, we also conduct a sensitivity analysis on our final variability measures

for the three BAs, by utilizing observed demand data between 2016 - 2019 (ignoring 2015, as BAs hourly demand only from 2nd July 2015, which is an inappropriate input to quantify annual target reliability), and comparing the newly derived reliability estimates against the ELCC estimates derived from using weather-driven demand proxies (reconstructed hourly demand; Chapter 3). Our goal here is two fold, that is, we aim to analyze the difference in overall median ELCC values in reconstructed demand and observed demand case, and also compare the difference in deviation of ELCC values from the mean in both cases. The former criteria would indicate if we are over/under estimating capacity contributions from the variable renewable energy generators (VREs) while using the proxies of demand data, whereas the latter criteria would indicate if our models capture the trend in variability of reliability contributions accurately.

To simulate the effect of weather on the reliability contributions from additional renewable energy generators included in the base fleet, our model uses multiple decades of high frequency hourly demand data and spatially differentiated temperature data for individual Balancing Authorities of interest.

4.3.1 Area of study

Our analysis focuses on three different Balancing Authorities, ISO-NE, CA-ISO, and ERCOT. Together these three BAs accounts for approximately 26% of the cumulative 2019 electricity consumption of the U.S. Moreover, these BAs are located in geographically diverse locations, which makes the study comprehensive to understand the impact of ignoring long-term effect of weather variability across multiple spatially heterogeneous locations, in temperature response of demand patterns on the grid reliability.

We choose these three balancing authorities for in this paper over other Independent System Operators because ISO-NE, ERCOT, and CA-ISO are geographically and systematically diverse. While ISO-NE governs multiple states (Massachusetts, Connecticut, Rhode Island, Vermont, New Hampshire, & Maine), ERCOT and CA-ISO individually serve the states of Texas and California respectively. Additionally, the geographical diversity in these three choices ensures that we account for spatial heterogeneity of temperature which will influence demand, as well as renewable energy

mandates which is largely dependent on the political sentiment in each region.

4.3.2 Data Sources

Existing studies (Keane et al., 2010; Bothwell and Pavlak, 2015) for determining reliability using the ELCC metric have used datasets containing observed meteorological values. However, as indicated in Chapter 2, we leverage the NASA MERRA reanalysis dataset (*MERRA-2* 2020) as it is free from any missing values, and thus eliminates the need for imputations (which otherwise introduces another layer of uncertainty in quantifying stochastic reliability contributions from renewable energy generators). Reanalysis datasets are created to develop consistent records of the observed states, which otherwise have many gaps due to the method in which data is collected and stored (Keeley, 2021; *Reanalysis Data* n.d.). The NASA MERRA (Modern-Era Retrospective Analysis for Research and Applications)(*MERRA-2* 2020) data reports multiple climatological variables over an extensive period. Variables like wind speed (both eastern and northward component) at 2m, 10m, and 50m above the sea level, specific humidity, surface incoming shortwave flux, pressure, and temperature at 2m were extracted from the MERRA database for the years 1980 - 2019. We choose the four decades between 1980 - 2019 for our study to conduct a complete analysis leveraging all available data points, while using concurrent reconstructed hourly demand values, which are approximations or proxies of temperature driven hourly load.

After, we extract the atmospheric variables from the MERRA database have, we use a python script to call the NREL "System Advisor Model" (SAM) module (Blair et al., 2014) and convert the variables to their corresponding energy generation output. Researchers at NREL have designed SAM to facilitate the decision-making process for renewable energy systems by providing a platform to convert resources like solar irradiance and wind speed to their corresponding solar and wind energy output at specific locations (*System Advisor Model* 2020). The process of conversion of weather variables to corresponding energy outputs begins with extracting MERRA weather data to be fed as inputs in SAM and simulate hourly AC generation from solar and wind resources for a particular year, location, and generator design (plant nameplate capacity and type as onshore and offshore wind farms use different turbines). Next, the AC generation profiles are then normalized

to derive the corresponding hourly capacity factors (CFs). Lastly, for the renewable energy generator of interest, whose effectiveness we want to quantify by determining the ELCC, its nameplate capacity is multiplied by the capacity factor derived in step 2 to derive the generator's hourly AC power.

Based on the choice of generator, that is, either solar, onshore wind, or offshore wind, additional parameters are specified in SAM. These parameters are described below under each generator type.

4.3.3 Wind profiles

For wind power profiles, a power law in SAM is used to extrapolate wind speeds to a typical turbine hub height. The estimated wind speed is then categorized under different onshore wind turbine classes as suggested in IEC 61400 (*IEC 61400* 2021), and power is quantified using SAM. For offshore wind, a particular wind turbine from the SAM database is used – the Senvion 6.2 MW turbine. We chose Senvion from the pool of available offshore wind turbines in the SAM database because it best represents the current scenario of an operating offshore wind (Block Island Wind Farm) in the US.

Equation (4.1) represents the Power Law:

$$v_2 = v_1 * (h_2/h_1)^{\alpha} \tag{4.1}$$

Where v_2 is the wind speed at height h_2, v_1 is the wind speed at height h_1, and α is the wind shear constant which depends on the terrain (whether land or water, mountainous or flat land), and also varies by turbine height, season, and wind speed. As a hueristic, 1/7 is often used when all factors influencing the wind shear constant value are unavailable.

4.3.4 Solar profile

To simulate power generated by solar PVs, the Direct Normal Irradiance (DNI) and Diffuse Horizontal Irradiance (DHI) are determined using the Direct Insolation Simulation Code (DISC) model developed by (Maxwell, 1987; W. Holmgren et al., 2021; W. F. Holmgren, Hansen, and Mikofski, 2018). DNI is the amount of solar radiation received per unit area by any surface that is always held normal to direct sun's rays. At the same time, DHI is the amount of radiation received per unit area by any surface not directly in the sun's path but by scattered molecules and particles in the atmosphere. The SAM model then uses these two factors as inputs to quantify solar power.

In Table 4.1, we enlist some parameters that was chosen for the conversion of solar irradiance to solar power in SAM.

Table 4.1: Parameters for solar generation in SAM; same as Chapter 2

Generator Parameter	Value
Nameplate Capacity	1MW
Azimuth	180°
Axis Type	Fixed @ Latitude Angle
DC:AC Ratio	1.1
Inverter Efficiency	96%

4.3.5 Effective Load Carrying Capability Method

To quantify the ELCC of any generator, we follow the method used in Bromley-Dulfano, Florez, and M. T. Craig, 2021, and modify it to include necessary functionalities required for quantifying capacity contributions of offshore wind generators. For conducting an analysis, hinged on determining the ELCC of a renewable energy generator, first an appropriate metric to define the system reliability of the base fleet against the hourly load profile needs to be established. Similar to Bromley-Dulfano, Florez, and M. T. Craig, 2021, we use Loss of Load Hours (LOLH) metric to define system reliability. LOLH is defined as the sum of hours on an annual basis when the load in a system exceeds the available generating capacity. NERC defines system reliability as by LOLH value, and according to their standards a fleet is reliable if it has a LOLH value of 2.4/year NERC, 2019. It means means that annually, the system in consideration is only allowed to have demand

shortfall for 2.4 hours cumulative or one outage day in 10 years.

After the metric to define reliability has been established, for quantifying the ELCC of any generator, we first collect required data inputs for the system of interest, which includes generator location, nameplate capacity, FORs, and MERRA reanalysis data for hourly solar and wind profiles. Next, we calculate the system's original reliability (in terms of LOLH), and compare it against the target reliability value of 2.4 LOLH/year (as defined by NERC). If the system is under-reliable, i.e., the system LOLH value >2.4/year, thermal generators of 50MW is incrementally added to adjust the fleet composition until the base reliability matches our target reliability. Otherwise, if the system is over-reliable, i.e., the fleet LOLH <2.4/year, then the ELCC calculator changes the fleet composition by eliminating older thermal generators from the fleet. Older thermal generators are eliminated to compensate for systems with overbuilt capacity that generates invalid ELCC estimates. Lastly, we include the renewable generator of choice (in this paper a 100-MW solar, onshore wind, or offshore wind generator) with storage, and determine the system's new reliability (LOLH value), and then incrementally add a constant load until the system with the added generator achieves the target reliability. Note, while quantifying the system reliability, we also use a probabilistic method to account for outages (planned and unexpected) in the generating fleet. As described in Bromley-Dulfano, Florez, and M. T. Craig, 2021, we use temperature-dependent Forced Outage Rates (FORs), instead of fixed outage rates to capture the failure in resource adequacy from conventional and renewable energy generators comprehensively, and ultimately determine the LOLH of the fleet.

The ELCC of any generator is the amount of additional load which was added for adjusting the system reliability after including the solar, onshore wind, offshore wind generator to match the system target reliability of 2.4 LOLH/year. The ELCC value quantifies the ability of the new generator added to the base fleet to serve excess demand. By definition, ELCC values have units of power, but in the method prescribed in this paper, it is reported as a percentage of the added generator's nameplate capacity. For example, we report a 25-MW ELCC for a 100-MW wind generator as 25%.The ELCC values are always integers, as Bromley-Dulfano, Florez, and M. T. Craig, 2021 round off the excess load added/removed to match the system reliability with target reliability. This process of quantifying the reliability of an additional VRE generator over a base

fleet is repeated for each grid cell using a dimension of 50x60 km within the area governed by ISO-NE, CA-ISO, and ERCOT, and also the adjacent offshore area to account for spatial heterogeneity in solar, onshore, and offshore wind resources.

4.3.6 Base Generator Fleet and Storage Fleet

We determine the capacity of the base generator fleet for ISO-NE, CA-ISO, and ERCOT from the Form EIA-860 from the Energy Information Agency (U. EIA, 2015). To delineate the impact of interannual variability of renewable energy sources as well as air temperature, we use the active 2019 generator fleet composition in each BA across the time frame of analysis (1980 - 2019), so that the final ELCC quantification is representative of changes only in availability of wind and solar resources, and the temperature response of hourly demand.

The interconnection queue data indicated the addition of wind and solar generators in the capacity range of 50 - 1500-MW for ISO-NE, CA-ISO, and ERCOT. But in chapter 1 we found that with increasing capacity, ELCC contributions do not proportionally change, as large capacity of a single renewable energy resource does not benefit the power system, rather diversity does. Thus, while assessing the interannual variability impacts on the capacity contributions of solar, onshore wind, and offshore wind generators, we only use the case of new addition of 100-MW generators.

4.3.7 Total Interchange

The total interchange of hourly electricity demand for each of the three BAs in our case study was roughly 2% of of the hourly electricity demand. Thus, to better isolate the effect of interannual variability of weather variables on the reliability contributions from new VRE generator additions, we hold the total interchange exchanges from 2019 constant for all 40 years of study (1980 - 2019) for the case of all Balancing Authorities considered in this study.

4.3.8 Metrics

The method described in Section 4.3.5, quantifies ELCC values as % points of capacity contributions. If we are assessing how reliable a newly added 100-MW offshore wind farm will be towards meeting unmet hourly demand hours or demand shortfalls, and the estimated the ELCC value to be 30%, it means the new 100-MW onshore wind farm will only effectively contribute 30-MW capacity towards meeting demand shortfall. ELCC values always range between 0 to 100%, although 100% capacity contribution from VRE is unrealistic due to intermittent resource availability, and system down-time, which we factor in as outages.

Furthermore, we are interested in studying the characteristics of the VRE generators from each of the 40 annual years of capacity contribution profiles ($N_{years} = 40$; 1980 - 2019) for each balancing authority across its entire footprint. Selecting a single gridded cell to determine the interannual variability impacts on ELCC values of any VRE generator would explicitly ignore the impact of geographical diversity of wind and solar resources. As this analysis is aimed to help stakeholders and planning agents involved with power system capacity expansion planning process, to make informed decisions about renewable energy investments, it is important to understand which regions within a BA will contribute optimally to system reliability if a 100-MW VRE generator is constructed there. Hence, while quantifying the change in ELCCs we also measure the influence spatial heterogeneity in ELCC values for a specific generator within each BA by repeating the reliability calculations for each grid cell. Furthermore, for measuring the variability of reliability or ELCC values across all 40 years for each VRE generator type and each BA, we use the metric of Coefficient of Variation or CV.

$$CV = \frac{\sigma}{\mu} \tag{4.2}$$

CV (Equation (4.2)) is the normalized form of standard deviation, that is, it is the ratio of the standard deviation of the variable of interest in a specific period to the variable's mean value quantified over that same period. It helps in measuring the spread of the variable of interest around its mean. It is dimension and unit-less. Hence it is an appropriate metric to understand

the impact of interannual variability on the reliability contributions (ELCC values) of newly added VRE generators.

We use the Coefficient of Variation (CV) to understand the distribution of ELCC values around the mean ELCC across all 40 years, for a particular generator type and BA of interest. Large CV values indicate greater level of dispersion of ELCC values, which eventually translates to higher degree of uncertainty in reliability contributions from a particular VRE generator when used in a long-term power system infrastructure project. Conversely, smaller CV values assert robust capacity contribution from that generator.

4.4 Results

We analyze each BA separately to isolate the difference in geographic positioning, energy policy and regulations, as well as consumption patterns, and thus the results are split into five sections. The first section (Section 4.4.1) broadly describes the statistical measures of ELCC values for all three generators in each BA. The next three sections, Section 4.4.2, 4.4.3, and 4.4.4 analyzes the impact of weather IAV on production and demand side of power systems in ISO-NE, CA-ISO, and ERCOT respectively, by drawing out conclusions based off Coefficient of Variation or (CV_{inter}) in reliability contributions from solar and wind generators of 100-MW. The fourth section, Section 4.4.6, discusses how sensitive the reliability contributions are to hourly demand values, while holding all other variables such as total interchange, renewable energy contributions, base fleet composition, forced outage rates, etc., constant. This section shows how much weather IAV affects the power systems and the provides information to understand the significance of peak load hours in ELCC calculations, and how annual hourly risks (unmet demand hours) influences the reliability contributions in conjunction with change in weather variables.

We study the spread of reliability contribution from a 100-MW generator across the entire territory governed by ISO-NE, CA-ISO, and ERCOT. In Chapter 2, we showed wind generators, i.e, offshore wind and onshore wind generators are subjected to greater variation in ELCC values as wind capacity factor vary from one gridded location to another. Thus, a single CV estimate for ELCC

in this paper must be interpreted with caution, as the variability in capacity contributions from a generator implicitly captures geographical diversity of reliability contributions from wind and solar generators. To better isolate the geographical diversity in ELCC values, we also analyze the CV of median ELCCs (CV_{50}) and CV of 99th percentile of ELCCs (CV_{99}) for every case. We focus on studying the change in 50th and 99th percentile of ELCC values for all renewable energy generator types and BAs because the 50th percentile (median ELCC) indicates the most favorably occurring ELCC value across the entire region governed by a particular BA, and 99th percentile indicates the best or the optimal ELCC value for the generator of interest within the BA's footprint for a specific year. Large changes in the 99th percentile of ELCC value will help us understand the impact of changing climate on maximum reliability contributions from any VRE generator.

4.4.1 Change in absolute reliability benefits of VRE generators

In Table 4.2, we describe the range of year-to-year change in 25th percentile, median (50th percentile), 75th percentile, and max ELCC values for 1980 - 2019, obtained for new solar, onshore wind, and offshore wind generator of 100-MW added to the base fleet of each BA. Comparing the absolute maximum ELCC % points for ISO-NE, we can conclude that offshore wind generators will provide more capacity contributions than solar and onshore wind. Solar generators provide the least reliability benefits for the case of ISO-NE, and this can be attributed to relatively low intensity solar radiation in the US east coast leading to small solar capacity factors and better alignment of offshore resource availability to peak demand requirements, which makes offshore wind a favorable choice. The range of maximum ELCC values for each year between 1980 - 2019 for ISO-NE shows us a significant difference in onshore wind because contributions because of citing a hypothetical onshore wind generator Cape Cod, MA. This specific grid cell extends the range of ELCCs. In reality, Cape Cod being a small peninsular extension of Massachusetts into the Atlantic Ocean, can be considered an offshore region. But, analyzing the range of median (50th percentile) ELCC value across 1980 - 2019 for each generator from Table 4.2, it can be concluded that within the area governed by ISO-NE, the largest variability in absolute ELCC values is seen for the case of offshore wind generator (7 - 45%), followed by onshore wind (0 - 7%), and then solar (5 - 11%). If this grid cell describing Cape Cod is ignored, the range of maximum ELCC value from adding a

new onshore wind generator of 100-MW is limited to 2 - 8%.

Table 4.2: Statistical measures describing the range of year-to-year changes in absolute ELCC values for each generator within the entire footprint of the three Balancing Authorities across the 40-year study period (1980 - 2019). Note, ELCC values are in % points and are always integers, but some upper bounds are float type in nature because we subset onshore or offshore area grid cells whose count result in odd numbers, leading to float values.

Balancing Authority	**Generator**	**25th %**	**50th %**	**75th %**	**Max**
ISO-NE	Onshore	0 - 5	0 - 7	2 - 11	8 - 50
	Solar	5 - 10	5 - 11	7 - 11	7 - 13
	Offshore	5 - 32.5	7 - 45	9 - 45	11 - 57
CA-ISO	Onshore	0 - 8	3 - 18	10 - 31.25	35 - 77
	Solar	2 - 7	3 - 8	5 - 10	7 - 11
	Offshore	4 - 49	8 - 66	14 - 74	41 - 80
ERCOT	Onshore	0 - 10	2 - 12.5	5 - 21	13 - 53
	Solar	22 - 33	2 - 10	27 - 38	32 - 46
	Offshore	0 - 10	25 - 34.5	2 - 17	7 - 27

Similarly, for the case of CA-ISO, the range of 'Max' ELCC values for each generator indicates optimal reliability benefits can be extracted from offshore wind farms. Unlike ISO-NE, CA-ISO has significantly large (5x) solar capacity factors, but the CA-ISO base fleet from 2019 indicated that it is already saturated with several solar PV plants. As described in Chapter 2, Section 2.3.2, diversification of generator mix is of utmost necessity to reap the best reliability contributions from adding more renewable energy generators. Adding a new solar generator of 100-MW to the existing solar PV plants in the CA-ISO grid would mean generation from these solar PV plants occur during the same hours. Thus, demand shortfalls during other times of the day will be unmet. Conversely, offshore wind capacity factors are significantly large throughout all hour of the day, leading to coincident power production during unmet demand hours. But, like ISO-NE largest variability due to fluctuations in weather-variable is prominently visible for the reliability contributions from offshore wind generators.

In ERCOT, inclusion of a 100-MW solar generator leads to largest reliability benefits. The base fleet of ERCOT already has substantial share of wind power (U. EIA, 2015). Thus, adding more onshore or offshore wind generators to the base fleet leads to marginal capacity contributions to meet demand shortfalls, as all wind generators produce electricity concurrently when the intensity of wind resource is high. In contrast, solar generators have different power production profile throughout

the day, which makes it an favorable choice for meeting excess demand, when wind resources do not have adequate intensity to produce power. Thus, the range of median ELCC values across 1980 - 2019 for solar generators is about 5 times greater than onshore wind generators, and 10 times greater than offshore wind generators. The detailed maps of absolute ELCC values for all three generators in each balancing authority is available in Appendix B.3, Figures C.1 to C.52.

In order to numerically quantify the variability in ELCC values, we used Coefficient of Variation metric, and discuss the dispersion of ELCCs for all three VRE generators, across 1980 - 2019 for each balancing authority in Sections 4.4.2, 4.4.3 and 4.4.4.

4.4.2 Variability of reliability contributions in Independent System Operator of New England (ISO-NE)

Changing solar and wind resource availability across all 40 years of study, as well as temperature response of demand showed a pronounced impact on reliability contributions from the addition of new onshore wind turbines to the base fleet of ISO-NE. As discussed in section 4.4.1, Cape Cod, Massachusetts shown in Figure 4.1 as gridded cell 41.0 N, -70.625 W, showed the largest onshore wind farm capacity contribution. We attribute this to larger wind energy potential near the Atlantic coast.

The spread of ELCC values for a 100-MW onshore wind farm, solar, and offshore wind farm are shown in Figure 4.2 across all 40 years of studied data. These box plots represent the reliability contributions of adding the VRE generators listed above to the existing base fleet of generators from the year 2019 in ISO-NE. Comparing the trends of statistical measures of interannual variability impacts on reliability benefits of onshore wind generator of 100-MW for all 40 years, we find that the overall coefficient of variation of ELCC is $CV_{ov} = 113.9\%$, the change in median ELCC or CV_{50} is 53.8%, and CV_{99} is 38.8%. The difference in CV of overall, 50th percentile, and 99th percentile ELCC values indicates the importance of isolating the impact of spatial heterogeneity of ELCC values. CV of overall ELCC values captures the spread of the range of capacity contributions from a 100-MW onshore wind farm at each gridded location of the MERRA reanalysis dataset describing the ISO-NE, and thus the year-to-year variability is influenced by including Cape Cod. Removing

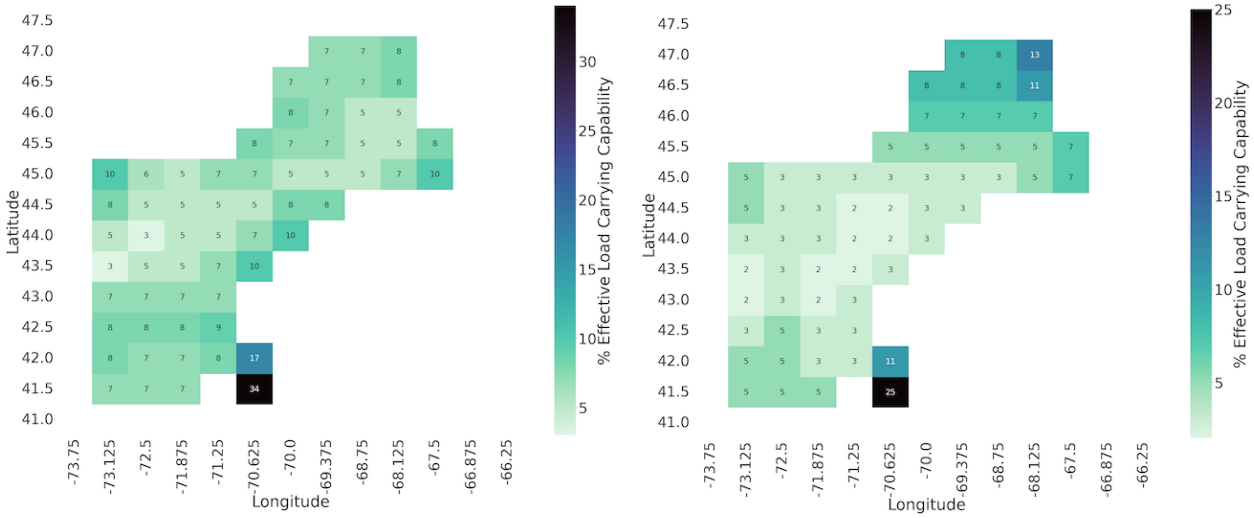

(a) Onshore wind ELCC values for 1980

(b) Onshore wind ELCC values for 2019

Figure 4.1: Geographical diversity of ELCCs of a new 100-MW onshore wind generator included to the existing base fleet in the area governed by ISO-New England. Gridded cell (41.0 N, -70.625 W) is Cape Cod, a small peninsular region in the state of Massachusetts. This shows the largest reliability contribution across all 40 years.

this grid cell lowers the CV_{ov} of onshore wind to 39.2%.

For 100MW solar generator within ISO-NE, there are modest changes in the capacity contributions over 40 years, as the CV_{50} and CV_{99} value is 16.23% and 12.85%, respectively. This means both 50th percentile (median) reliability contributions and 99th percentile reliability (largest) contributions remain moderately small over all years of study. Solar generators have smaller spatial heterogeneity than onshore wind farms, due to availability of similar solar capacity factors within the footprint of ISO-NE. Thus, for all 40 years of study (1980 - 2019), comparing all three VRE generators for the case of ISO-NE against each other from Figure 4.2, we conclude that, reliability benefits offshore wind generators will witness the largest variability.

4.4.3 Variability of reliability contributions in California Independent System Operator (CA-ISO)

In Figure 4.3, unlike the case of ISO-NE, we find that land based wind resources in CA-ISO have relatively larger reliability contributions towards meeting demand shortfalls than ISO-NE.This can be attributed to larger capacity factors of wind resources in California (Lopez et al., 2021). But,

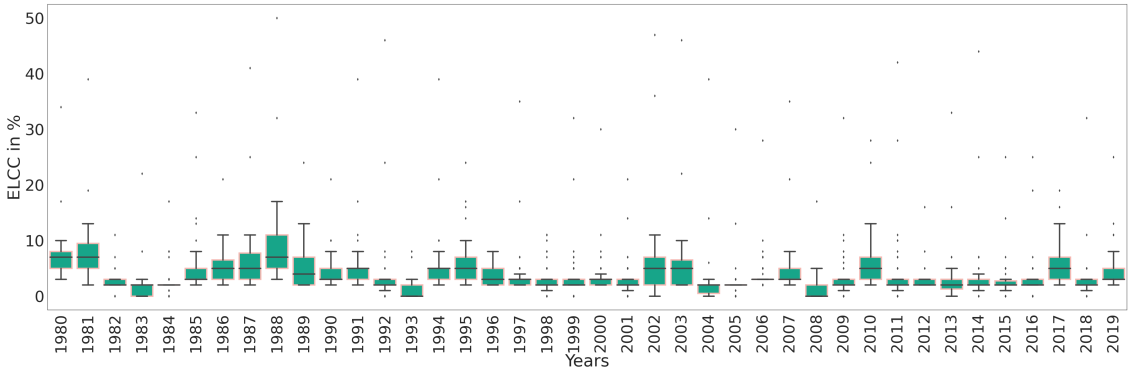

(a) capacity contributions of 100-MW onshore wind farm within the ISO-NE footprint

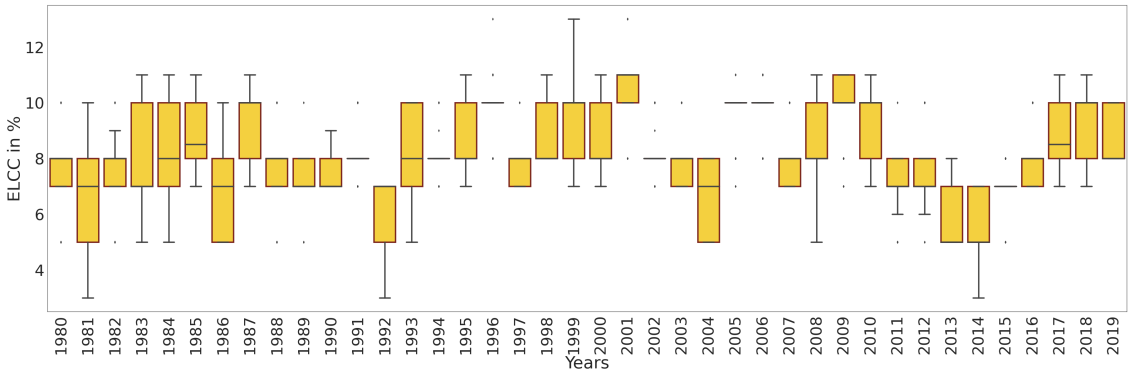

(b) capacity contributions of 100MW solar within the ISO-NE footprint

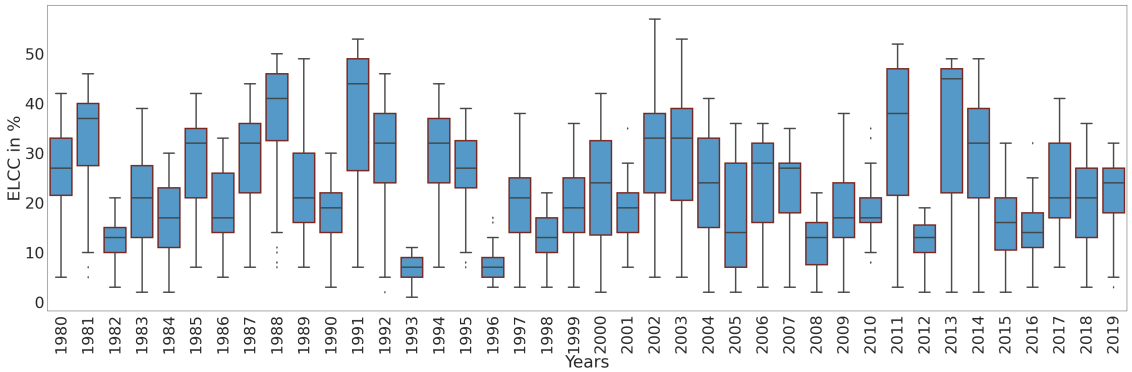

(c) capacity contributions of 100-MW offshore wind farm within the ISO-NE footprint

Figure 4.2: The impact of IAV of weather variables on ELCC values for a 100-MW VRE generator in ISO-NE. The onshore wind ELCCs (CV_{ov} = 113.84%, CV_{50} = 53.76%, and CV_{99} = 38.84%) showed largest variability across the 40-year timeline followed by offshore wind (CV_{ov} = 54.11%, CV_{50} = 40.19%, and CV_{99} = 28.61%). Conversely, variability in solar ELCCs (CV_{ov} = 19.93%, CV_{50} = 16.22%, and CV_{99} = 12.85%) was found to be significantly small. Offshore wind generators will provide the largest reliability contributions for ISO-NE when compared against other VREs.

within CA-ISO, characterizing the spread of onshore wind ELCC values across multiple years in the 40-year timeline against offshore wind ELCCs using the interquartile ranges (middle 50% ELCCs) we find robust capacity contributions from offshore generators. The median onshore ELCC value is approximately 3 times smaller than median offshore ELCC for all 40 years The 50th percentile of ELCC values for onshore wind vary between 8 - 19%, whereas for offshore wind generators, the median ELCC across all years vary between approximately 12 -76%. The change in optimal wind ELCC value that is CV_{99} of offshore wind and onshore wind is approximately same(16.30% vs. 16.84%) and significantly smaller than its corresponding CV_{50} values, implying that if offshore and onshore wind generators are optimally located within the footprint of CAISO, the effect of interannual variability of wind capacity factors on reliability contributions will be fairly small.

Solar generators, on the other hand, have a consolidated spread of reliability contributions and are less sensitive to year-to-year changes in solar capacity factors. Smaller reliability contributions from solar generators in CA-ISO can be attributed to the characteristics of its base fleet, which is already saturated with solar generators. Any further addition of solar generator results in marginal increase in system reliability (thus smaller ELCC values) as all solar PV plants will generate power during the same periods, leaving demand shortfalls at other hours unsatisfied. Hence, solar ELCC values have a maximum contribution of 12% across all years.

4.4.4 Variability of reliability contributions in Electricity Reliability Council of Texas (ERCOT)

In Section 4.4.1, it was found that a new 100-MW solar generator in ERCOT provide 5 times more median reliability benefits than onshore wind generator of the same nameplate capacity and offshore wind. The base fleet of ERCOT is saturated with wind generators, resulting in marginal reliability contributions from addition of any new wind generator (both onshore and offshore).

Figure 4.4 also indicated that the CV_{ov}, CV_{50}, and CV_{99} of ELCC values for the 100-MW solar generator varied by very small amounts, that is between 37.34%, 25.46%, and 13.63% respectively, indicating very small variability even with larger reliability contributions. Thus, we can confidently conclude the solar generators are less sensitive to changes in solar irradiance between the 40-year

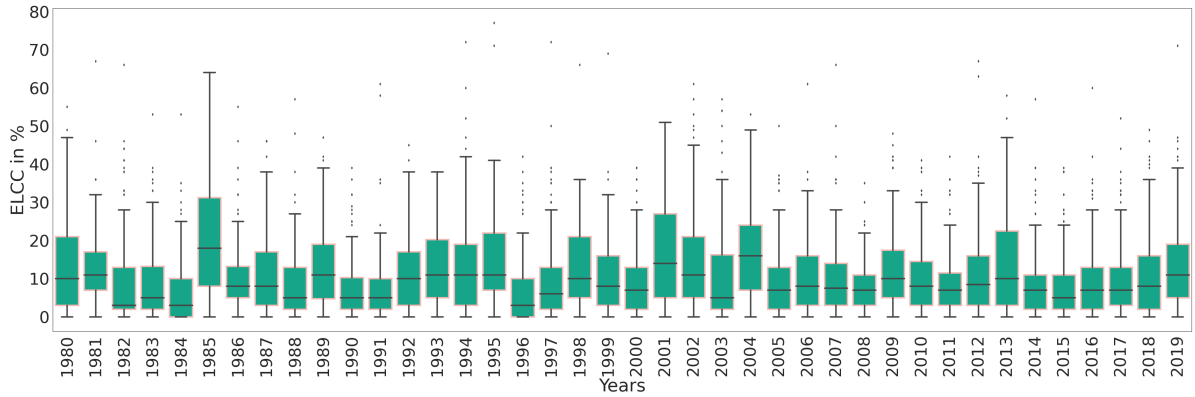

(a) capacity contributions of 100MW onshore wind farm within the CA-ISO footprint

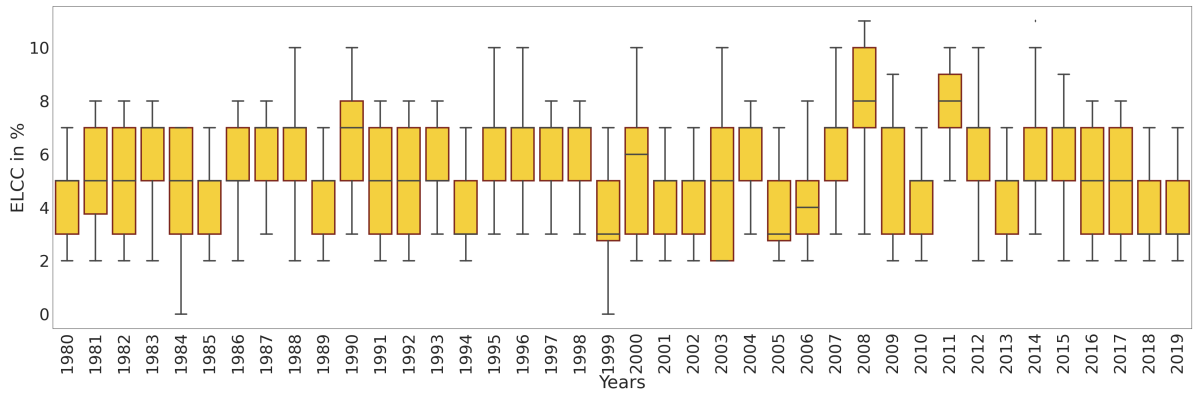

(b) capacity contributions of 100MW solar within the CA-ISO footprint

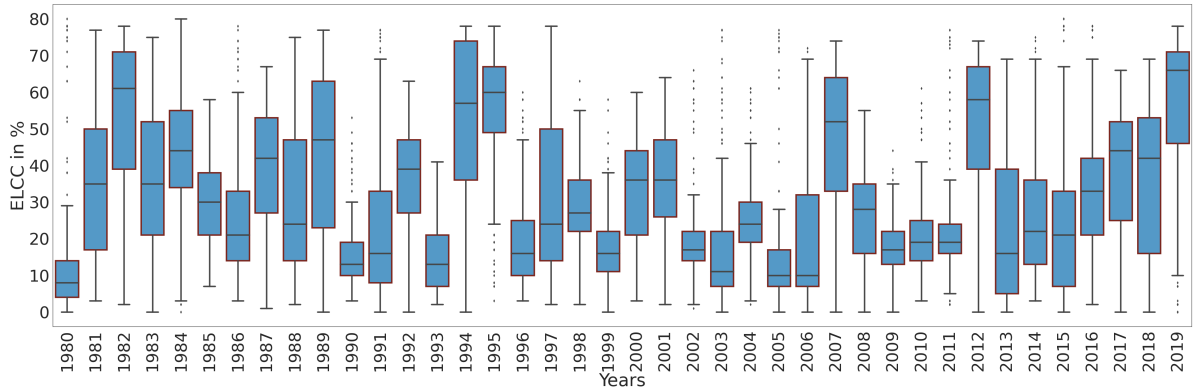

(c) capacity contributions of 100MW offshore wind farm within the CA-ISO footprint

Figure 4.3: The impact of interannual variability of weather variables on ELCC values for a 100MW VRE generator, added to the 2019 base fleet of CA-ISO. The onshore wind ELCCs ($CV_{ov} = 99.48\%$, $CV_{50} = 38.89\%$, and $CV_{99} = 16.30\%$) showed largest variability across the 40-year timeline followed by offshore wind ($CV_{ov} = 68.51\%$, $CV_{50} = 53\%$, and $CV_{99} = 16.84\%$). Conversely, variability in solar ELCCs ($CV_{ov} = 37.34\%$, $CV_{50} = 25.46\%$, and $CV_{99} = 13.63\%$) was found to be significantly small.

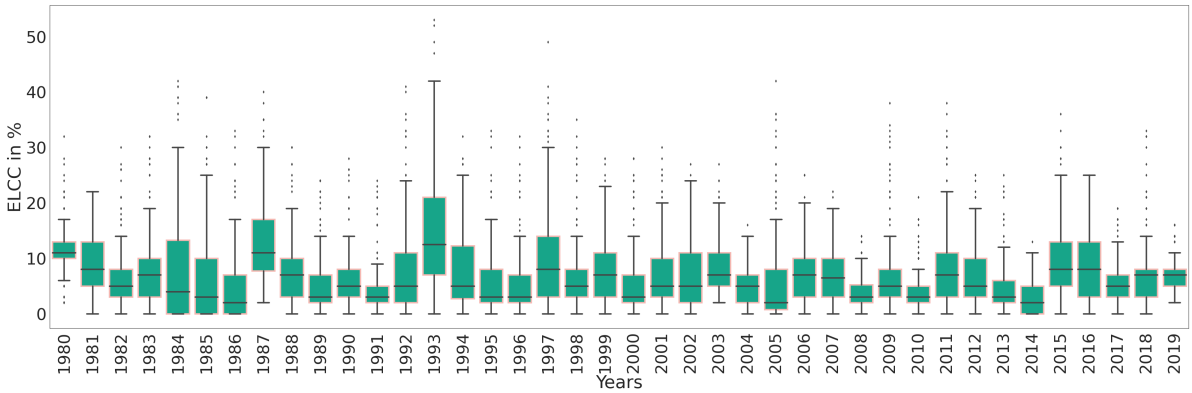

(a) capacity contributions of 100MW onshore wind farm at every gridded location within ERCOT

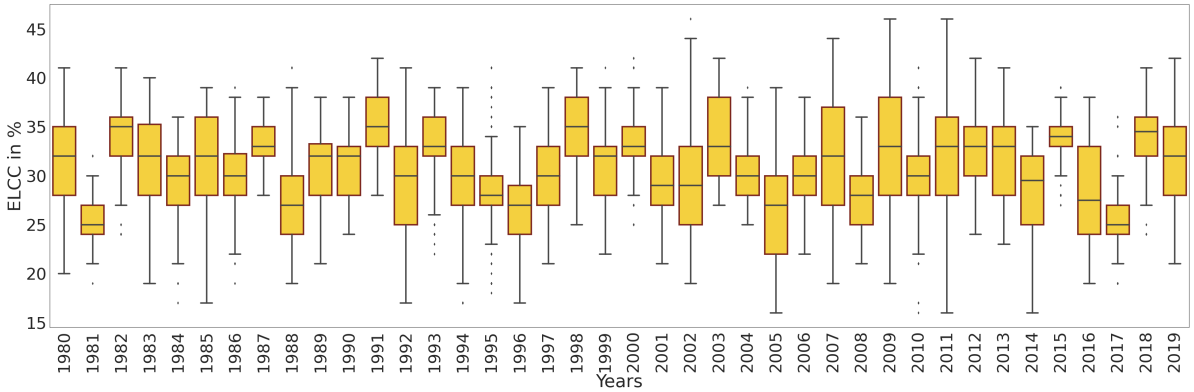

(b) capacity contributions of 100MW solar generator at every gridded location within ERCOT

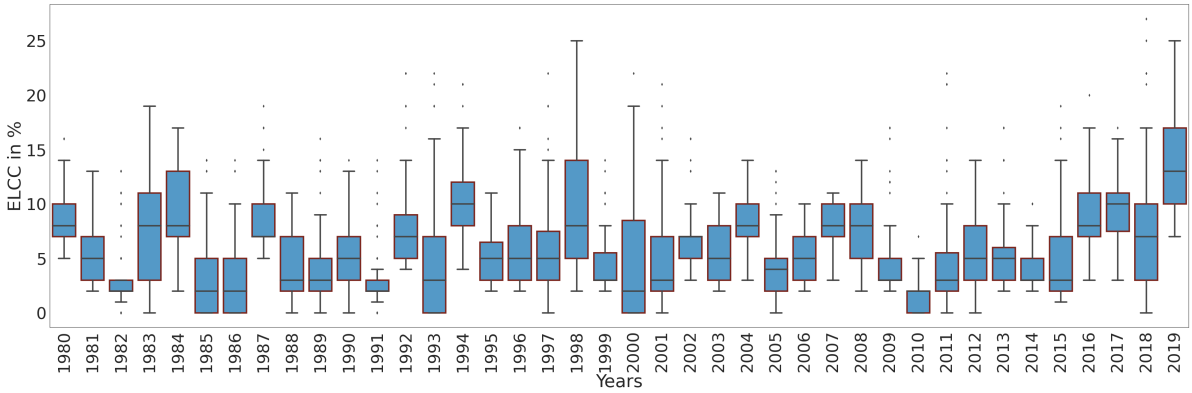

(c) capacity contributions of 100MW offshore wind farm at every gridded location within ERCOT

Figure 4.4: Impact of interannual variability of weather variables on ELCC values for a 100MW VRE generator, added to the 2019 base fleet of ERCOT across all 40 years of study. The onshore wind ELCCs (CV_{ov} = 94.85%, CV_{50} = 45.38%, and CV_{99} = 29.05%) showed largest variability across the 40-year timeline followed by offshore wind (CV_{ov} = 72.08%, CV_{50} = 50.46%, and CV_{99} = 27.61%). In contrast, variability in solar ELCCs (CV_{ov} = 16.29%, CV_{50} = 8.5%, and CV_{99} = 7.78%) was found to be considerably small.

time frame of our study, even when the capacity contribution is large.

Conversely, CV of ELCCs of 100MW onshore wind generators have comparatively large variability in ERCOT, leading to CV_{ov} value of 99.48%, CV_{50} value of 38.89%, and CV_{99} value of 16.30%. This is also true for change in year-to-year ELCC values for offshore wind generator in ERCOT which had CV values of 72.08%, 50.46%, and 27.61% for CV_{ov}, CV_{50}, and CV_{99}, respectively. Thus, offshore wind generators in ERCOT showed the largest change in reliability benefits across 1980 - 2019 with small capacity contributions, while solar generators had large contributions towards meeting demand shortfalls with a smaller degree of year-to-year variability.

4.4.5 Comparison across generators

In all three BAs (Figure 4.5), the solar generators indicated smallest changes in reliability contributions across all 40 years of study, even with varying magnitude of ELCCs. For ERCOT, the 50th percentile solar reliability contributions were largest as compared to onshore wind and offshore wind, whereas for ISO-NE and CA-ISO reliability contributions from solar generators to meet excess demand was smallest among other generators. This can be attributed to the difference in composition of base fleet. ERCOT base fleet is saturated with onshore wind generators, and the addition of any type of wind generator (onshore or offshore) leads to marginal reliability benefits, as all wind generators would generate electricity during same hours, leaving unmet demand shortfalls at other times of the day unattended. But, the 50th percentile solar ELCC value in all three BAs varied only 8.5% to 26%. In contrast, onshore wind and offshore wind generators showed very large variability with their median ELCC varying by a factor of greater than 50% (case of ISO-NE and CA-ISO).

Decomposing the ELCC values spatially. in Figure 4.5, the large spatial distribution of solar ELCC values in ERCOT can be attributed to the location and size Texas, which receives an abundance of solar irradiance leading to larger capacity as well. The size of the BAs being studied also plays an important role in determining the range of ELCC values as more geographically distinct reliability contributions from generators can be witnessed in BAs which are larger in size as compared to narrow ranges of ELCC values in each year for small BAs like ISO-NE. In fact, the geographical

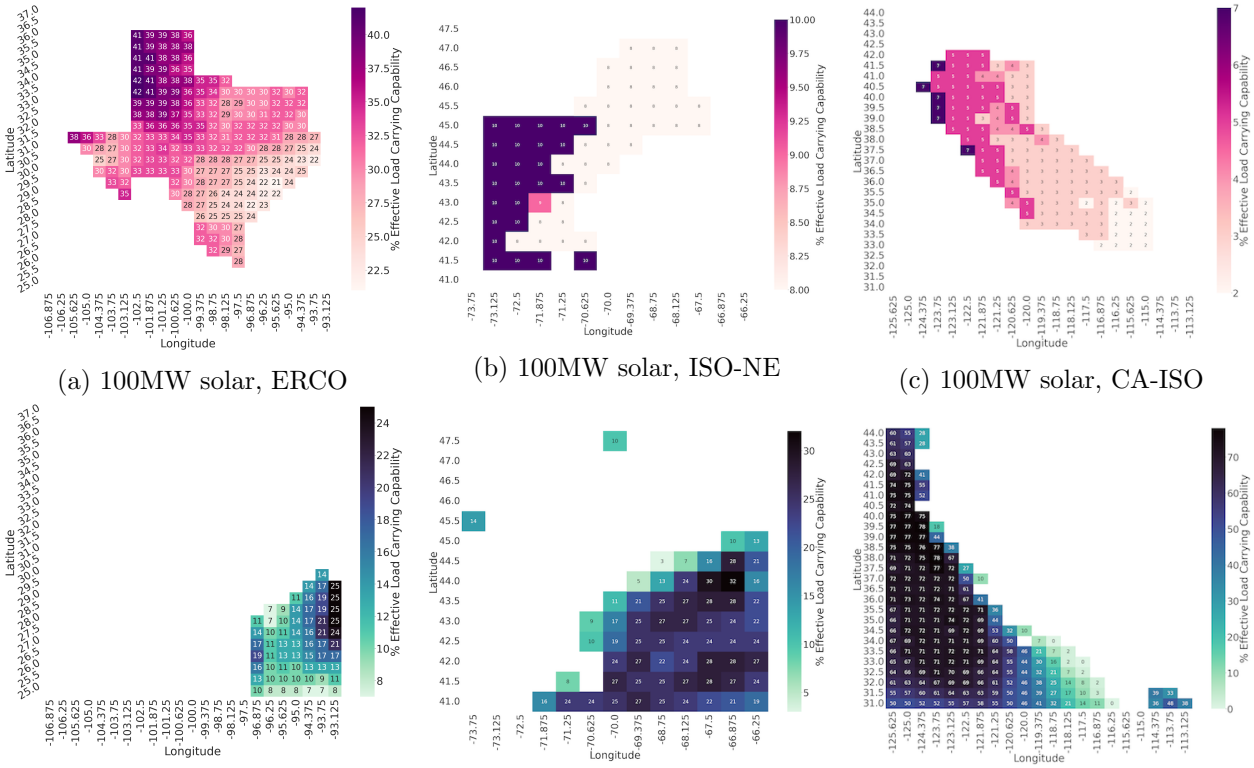

(a) 100MW solar, ERCO

(b) 100MW solar, ISO-NE

(c) 100MW solar, CA-ISO

(d) 100MW offshore wind, ERCOT

(e) 100MW offshore wind, ISO-NE

(f) 100MW offshore wind, CA-ISO

Figure 4.5: Spatial heterogeneity of solar and offshore wind ELCC values for the three BAs in 2019. The geographical footprint of ISO-NE is considerably smaller in size 43% of CA-ISO footprint and 26% of ERCOT footprint, leading to a narrower spread of capacity contribution values for all generator types across all 40 years.

footprint of ISO-NE is considerably smaller as compared to ERCOT and CA-ISO. Hence, while broadly comparing ELCCs across balancing authorities for a particular generator type, especially wind-based generators, care must be taken to understand the limitation on range of ELCC values for that generator due to differences in size of BAs, which affects the overall distribution of favorable wind and solar capacity factors.

4.4.6 Validating the change in reliability benefits

In this paper, we leveraged the reconstructed hourly demand proxies by our proposed neural network architecture (explained in Chapter 3). The neural network model even with robust performance against traditional multivariate linear regression model could accurately estimate significantly large

peak demand hours only for some years for our BAs. Since ELCC based reliability benefit calculations of any VRE generator hinges upon the use of peak load to quantify demand shortfalls and determine the generator's capacity contributions, any underestimations of peak load will shift the ELCC values for that generator. Thus, to check for the robustness of our ELCC estimates, we validate them using by cross-checking the ELCCs estimated using reconstructed demand proxies to the ELCCs quantified using observed hourly demand records. We conducted the validation process by quantifying the difference in coefficient of variation between reconstructed and observed demand case, and finding the difference in COV overall ELCC values ($CV_{ov_{diff}}$), COV of 50th percentile of ELCC values ($CV_{50_{diff}}$), and COV of 99th percentile ($CV_{99_{diff}}$) of ELCC values for each VRE generator within each BA. As observed hourly data for BAs are only available between mid 2015 - 2019, we use the timeline of 2016 - 2019 to validate our estimates. The magnitude of shift in overall, 50th percentile and 99th percentile of ELCC values from the reconstructed demand case indicates how robustness our estimates were. It is critical to note that, to isolate the impacts of demand value while all other inputs (including weather dependent capacity factors for solar and wind generators, base fleet, temperature dependent forced outage rates, and total interchange) are held constant.

In all, Figures 4.7, 4.8, and 4.6, indicate that for almost all cases being studied in this paper, the underestimations of peak demand hours in the reconstructed load profiles lead to undermining of reliability contributions from solar, offshore wind, and onshore wind generators. But, the general trends across the effective capacity contributions from different VRE generators for each BA remain the same. Figure 4.6b, validates our results from section 4.4.4, where we had shown that for the case of ERCOT, solar generators will have the largest reliability contributions across all forms of renewable energy generators (median solar ELCC values > median onshore and offshore ELCC values). This was also true for the case when we replaced reconstructed hourly demand inputs by observed demand values. In a similar comparison across different BAs for the case of using reconstructed demand vs. observed demand, we see that the broad trend of capacity contributions from specific VRE generators remain the same. For example, comparing Figure 4.8c and 4.7c, we find that larger offshore wind reliability contribution in CA-ISO when compared to ISO-NE remains true for both reconstructed demand case and observed demand case.

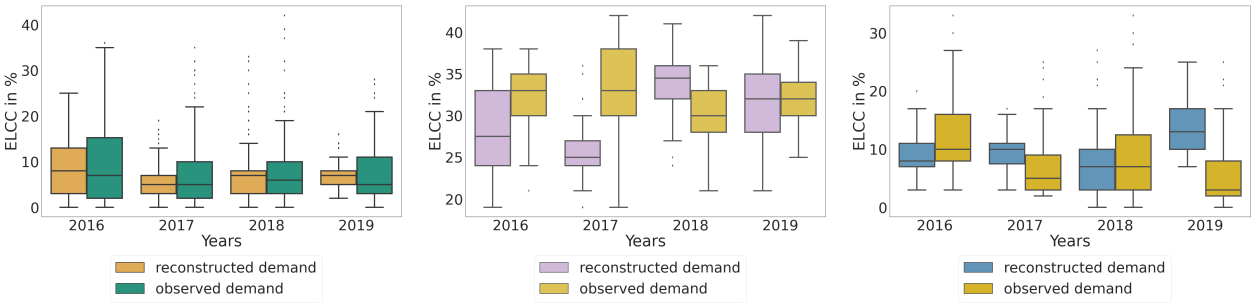

(a) 100MW onshore generator (b) 100MW solar generator (c) 100MW offshore generator

Figure 4.6: Shift in interquartile range of ELCC values for 100MW VRE generators across all 4 years of available hourly observed demand in ERCOT. We find the difference in CV of ELCCs while using reconstructed demand against observed demand for onshore wind ($CV_{ov_{diff}}$ = -24.92%, $CV_{50_{diff}}$ = -1.72%, $CV_{99_{diff}}$ = 16.76%), solar ($CV_{ov_{diff}}$ = 4.44%, $CV_{50_{diff}}$ = 8.66%, $CV_{99_{diff}}$ = -0.8%), and offshore wind generator ($CV_{ov_{diff}}$ = -32.74%, $CV_{50_{diff}}$ = -17.266%, $CV_{99_{diff}}$ = -5.77%). The capacity contributions from a 100MW are marginally underestimated even in this case. Significantly large changes in (CV_{ov} for onshore and offshore wind in ERCOT indicates shift in optimal geographical area for reliability contributions in wind generators. The shift in overall, 50th percentile, and 99th percentile values is greatest for the case of offshore wind generator in ERCOT.

Figure 4.7b indicates a higher degree of variability in ELCCs of solar generators when observed hourly demand is used in case of reconstructed hourly demand, with 50th percentile solar ELCC values being moderately similar to 50th percentile of onshore ELCC values. Moreover, solar generators in CA-ISO shows largest difference in CV of 99th percentile ELCC ($CV_{99_{diff}}$ = -24.57%) in comparison to offshore and onshore wind generators. This shows that, in CA-ISO with varying peak demand, optimal (best) capacity contributions from solar generator will be significantly affected. Across the 4-year timeline, change in CV of overall ELCC values and 50th percentile ELCCs is smallest for offshore wind generators ($CV_{ov_{diff}}$ = -0.01%), indicating harmonious effect of spatial heterogeneity of wind resources in both reconstructed and observed demand case, with small sensitivity towards peak demand changes ($CV_{99_{diff}}$ = -15.64%).

Figure 4.8c indicates substantial difference in offshore ELCCs derived using reconstructed demand data and observed demand data, for each year in 2016 to 2019. The median ELCCs for the observed case is about 2x times greater than in the reconstructed demand case. Solar ELCCs (Figure 4.8b) also show moderate differences in observed demand vs. reconstructed demand case. Although, comparing the difference in CV for overall, 50th percentile, and 99th percentile ELCC values for offshore wind generators, we find that the difference in CV is smallest among other generators.

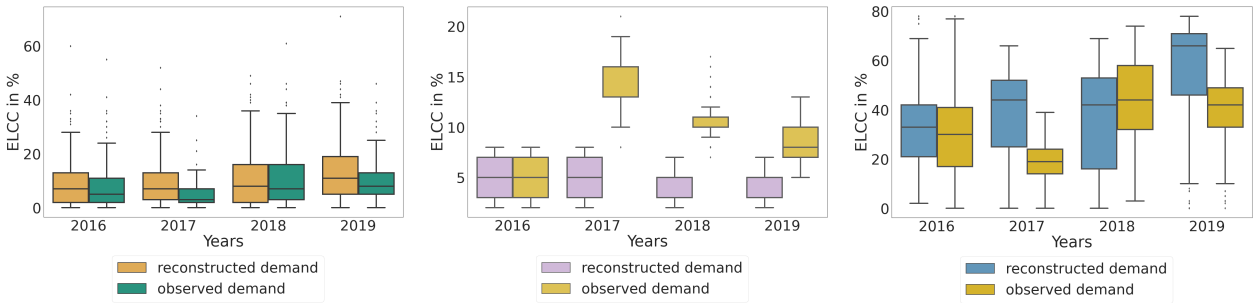

(a) 100MW onshore generator (b) 100MW solar generator (c) 100MW offshore generator

Figure 4.7: Shift in interquartile range of ELCC values for 100MW VRE generators across all 4 years of available hourly observed demand in CA-ISO. We find the difference in CV of ELCCs while using reconstructed demand against observed demand for onshore wind ($CV_{ov_{diff}}$ = -8.2%, $CV_{50_{diff}}$ = -13.52%, $CV_{99_{diff}}$ = -15.78%), solar ($CV_{ov_{diff}}$ = -2.1%, $CV_{50_{diff}}$ = -7.77%, $CV_{99_{diff}}$ = -24.57%), and offshore wind generator ($CV_{ov_{diff}}$ = -0.01%, $CV_{50_{diff}}$ = -3.57%, $CV_{99_{diff}}$ = -15.64%). Negative changes for all three VRE generators indicate that using reconstructed demand, the capacity contributions from a 100MW are marginally underestimated, but not significantly. The shift in overall, 50th percentile, and 99th percentile values is greatest for the case of solar generator in CA-ISO.

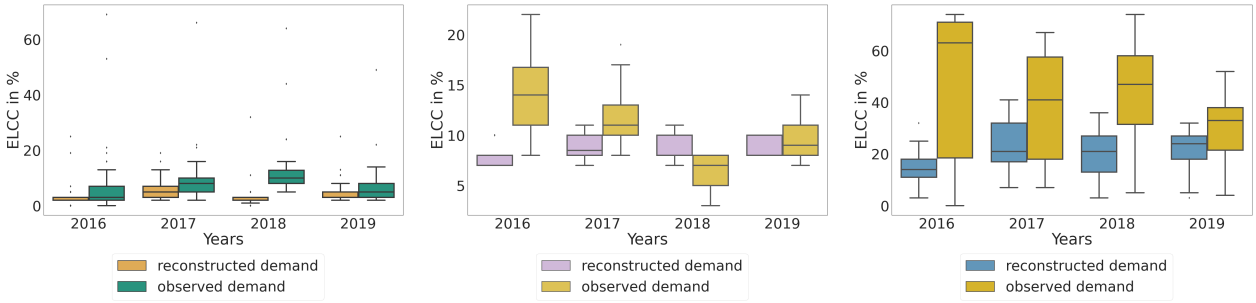

(a) 100MW onshore generator (b) 100MW solar generator (c) 100MW offshore generator

Figure 4.8: Shift in interquartile range of ELCC values for 100MW VRE generators across all 4 years of available hourly observed demand in ISO-NE.We find the difference in CV of ELCCs while using reconstructed demand against observed demand for onshore wind ($CV_{ov_{diff}}$ = -16.01%, $CV_{50_{diff}}$ = -0.58%, $CV_{99_{diff}}$ = -14.28%), solar ($CV_{ov_{diff}}$ = -23.29%, $CV_{50_{diff}}$ = -15.72%, $CV_{99_{diff}}$ = -29.99%), and offshore wind generator ($CV_{ov_{diff}}$ = -9.78%, $CV_{50_{diff}}$ = -5.53%, $CV_{99_{diff}}$ = -0.05%). Although the difference in CV seems moderate, difference between median ELCC for offshore wind generator is very high (19.0% vs. 39% for the case using reconstructed demand vs. observed demand, respectively). This indicates for the case of ISO-NE, the underestimated peak demand from reconstruction efforts in chapter 2, significantly undermines the reliability contributions from offshore wind generators.

The underestimation in peak demand hours in the reconstructed data may have led to suppressed quantification of capacity contributions, but the ELCC calculator still effectively captures the normalized trend of interannual variability impacts on the effective reliability contributions from offshore wind farms.

Overall, the interquartile range of ELCC estimates for all three type of VRE generators using reconstructed demand is in agreement with ELCC values quantified using observed demand, holding all other inputs and weather-related variables, i.e., the renewable energy capacity factors constant.

4.5 Discussions and Future Work

Our study underlines the need for integrating a perspective to analyze long-term reliability trends while strategizing electricity sector capacity expansion requirements, especially while adding large VRE generators. Changes in capacity contributions from any new solar or wind energy generator due to weather variability is imminent, and will be further exacerbated due to climate change. Thus, to mitigate any operational challenges in future, we need to combine long-term power system planning with variability in spatial and temporal representation of solar radiation, wind speed, and temperature variables. By combining weather-driven variability in the planning process, by appropriately approximating the supply and demand side changes for several decades, planning agents and researchers will be able to create a robust renewable energy driven grid system.

Our choice of using the probabilistic Effective Load Carrying Capability method, to determine the system reliability for each of the 40 years for multiple renewable energy sources, enables us to capture granular level hourly variability in wind and solar resources across different locations, whilst also accounting for temperature driven forced outage rates in the base fleet of conventional generators, total exchange/interchange of hourly electricity, and weather-driven demand changes. The key insight here for national policymakers attempting to understand ways to achieve long-term decarbonization pathway is that solar generators are significantly robust to inter-annual variability impacts in ISO-NE, CAISO, and ERCOT, but reliability contributions of solar generators is large only in the case of ERCOT. For other two BAs, offshore wind will provide significantly larger reliability contribution (this is in alignment with our findings from Chapter 1), but is subjected to larger inter-annual variability impacts.

But there are several pitfalls in our framework and modeling approach. First, in section 4.4.6, we showed that the reconstructed demand used in determining effective capacity contributions from

solar, onshore wind, and offshore wind generators are not perfect. Rather, they are approximations or proxies of weather-driven hourly demand. These proxies underestimate the actual peak demand requirements, leading to smaller number of hourly risks, and eventually lower ELCC values or reliability contributions from any VRE generators. To better estimate the effect of interannual variability on capacity contributions, a robust form of demand reconstructions considering weather zones (as described in chapter 2 discussions) is necessary. Moreover, the demand reconstructions were hinged on temperature response from a single gridded cell (largest population center in the BA of interest) which neglects the full range of possible temperature changes across the geographical footprint of a BA. Using reconstructions of robust weather-zone normalized hourly demand could potentially offset any bias introduced in our analysis.

Second, we estimate wind farm capacity contributions using a limited set of turbines described in *System Advisor Model* 2020. Specifically, the offshore reliability contributions is hinged on the characteristics (hub height, and turbine blade size) of a single Senvion 6.2MW turbine. As the research and development process is expanded to strategize ways to deploy larger offshore wind turbines, the ELCC values for these wind turbines will be different. Although re-estimating the ELCC values is possible using the methods proposed in this paper, with minimal changes to the python ELCC calculator.

Last, we only analyze the case of ISO-NE, CA-ISO, and ERCOT in this paper. But with enough computing resources, the same models and framework could be expanded to all BAs of the US, to comprehensively determine the change in reliability contributions of new solar and wind generators. A large-scale analysis of the entire contiguous US will help stakeholders make informed decisions about national energy security policies.

Moreover, our analysis fails to take into account detailed inter-regional electricity transfer from adjacent Independent System Operators to provide necessary exchanges and satisfy demand shortfalls because we held total interchange of electricity constant from 2019. This when addressed will further perturb the ELCC estimations especially for the case of CAISO, which is a part of the Western Interconnect. An improvement to this analysis could be based on predicting historical total interchange of electricity for all 40 years of study by using an auto-correlation based time

series model like ARIMA and also finding the dependency of electricity exchanges on temperature changes. Moreover, a detailed analysis considering economic factors may also indicate if it increasing dependency on interchanged electricity during times of highly unreliable renewable energy generation better than investing in storage and its associated inefficiencies.

Furthermore, we hold the base fleet of generators constant from 2019 and evaluate the change in reliability benefits from a single VRE generator added to the fleet. But in reality, over 40 years, multiple renewable energy generators could be added to the base fleet. To make the quantification of change in reliability benefits from addition of VRE generators more comprehensive, this study could be extended to include scenarios wherein VRE generators are added incrementally at regular intervals (after 10 years). This will also help stakeholders understand dynamic change in reliability benefits from adding multiple VRE generators and possibly diverse generators to the base fleet at different intervals in time.

In spite of all the listed caveats, this paper robustly captures the granular details of reliability contributions from offshore, onshore, and solar generators against impacts induced by changing weather variables.

Chapter 5

Conclusions and Future Work

5.1 Summary

Power system planning agents, researchers, and scholars are actively seeking ways to understand the challenges associated with integrating more renewable energy into the grid, while striving to maintain the system reliability. As anthropogenic activities continue to increase greenhouse gases (GHGs), the impacts from climate change on society and the environment will increase. As the world decarbonizes its electricity system, the variability and characteristics of atmospheric conditions such as temperature, solar radiation, and wind speed will make integration of solar, onshore wind energy, and offshore wind energy introduces new challenges.

The objective of this dissertation was to assess the reliability contributions from adding new variable renewable energy generators to the US grid, under various scenarios that comprehensively characterize multiple sources of uncertainty related to weather related interannual variability as well as regulations pertaining to energy transition pathways. Renewable energy sources like solar and wind energy are a critical tool to decarbonize the power system, and mitigate climate change impacts. But, due to their variability, complete reliance on using only these energy sources to access electricity at all hours of the day is challenging. Thus, there was a need to understand how old, carbon-intensive conventional generating capacity can be replaced by adding new clean sources of energy without compromising system reliability. This objective was achieved by analyzing the capacity contributions from solar, onshore wind, and offshore wind energy generators under different pathways to achieve increasing levels of decarbonization, reconstructing proxies of weather-driven changes in hourly demand for a multidecadal time frame to mitigate any limitations in reliability based studies due to lack of publicly available load records, and using these proxies of hourly demand (as a response to changing temperature) along with variable hourly wind speed, and solar radiation data to estimate probabilistic reliability contributions from the VREs across three large balancing authorities in the US.

Chapter 2 presented the characterization of variable renewable energy generators that will be added in the state of New York, and its adjacent offshore area. Multiple energy transition scenarios for the base generator fleet were developed by carefully considering the federal and state renewable energy integration targets as well as details from the Renewable Portfolio Standards (Megan Cleveland,

2021) to determine appropriate capacity expansion plans using renewable energy and natural gas resources for the next decade. We found that, broadly, based on the standards and state mandates, for New York, five different energy scenarios can plausibly characterize the range of futures. These were the Reference Case scenario representing business as usual grid composition in 2019, High Solar, High Onshore Wind, High Offshore Wind, and High Natural Gas scenarios illustrating changes in future grid composition in New York state. We then deployed the probabilistic 'Effective Load Carrying Capability' method to estimate the capacity contributions from including additional solar, onshore wind, and offshore wind generators of varying capacity levels (50 - 2000MW) to each of the base fleet scenarios described above, and found that across all scenarios, and generator capacity differences, offshore wind energy is the most reliable resource towards meeting excess demand requirements in the next decade. Even though ELCC values for offshore wind generators across all plausible energy transition scenarios have a significantly large distribution (5 - 64%), the median reliability benefits from adding offshore wind generators is 20x greater than solar generators of equivalent nameplate capacities.

While Chapter 2 presented a comprehensive representation of reliability benefits from adding more offshore wind energy into the grid of New York state (governed by the Independent System Operator of New York), the analysis was based on several assumptions. First, we held hourly demand from 2019 constant for all scenarios, but in the future, electricity demand consumption patterns will change due to population growth, energy policies, and climate change. These changes will modify peak demand, which in turn will vary hourly risks, ultimately affecting the ELCC values or capacity contributions from new generators. Second, while we accounted for total interchange or exchange of electricity between Balancing Authorities, we ignored the impacts from any transmission-related outages.

In Chapter 3, we underscored the need of multidecadal hourly demand data to accurately conduct power system reliability studies. Balancing authorities within the North American region (US & Canada) report hourly demand data only for the past five years, which limits accessibility to high-frequency hourly demand data required for conducting long-term reliability assessment of the grid. Broad assumptions are made to study multidecadal power system reliability, which introduces a higher-degree of uncertainty in the reliability estimates. Thus, to fill this research gap, in Chapter

3, we reconstructed 40 years of temperature-driven hourly demand proxies for a subset of Balancing Authorities (40 out of a total of 66) in the US. This reconstruction was achieved by using a robust deep learning model, which had the ability to learn long-term dependencies between sequential input, while being generalizable to create demand proxies for all BAs. The subset of Balancing Authorities were chosen after carefully checking the relationship between temperature and observed demand (also used for training) in each one. The 20 largest temperature-driven demand proxies in each year of reconstruction (between 1980 - 2019) enabled us to carefully examine and determine which Balancing Authorities were significantly susceptible to changes in weather. Among the largest Balancing Authorities, the Midcontinent Independent System Operator (MISO), Electricity Reliability Council of Texas, California Independent System Operator (CA-ISO), Southern Company Services, Inc. - Trans (SOCO), New York Independent System Operator (NY-ISO), and Independent System Operator of New England (ISO-NE), showed the largest variability in reconstructed temperature-driven demand proxies with coefficient of variation values of about 15% . Even though BAs of moderate and smaller sizes like the Arizona Public Service Company (AZPS), Nevada Power Company (NEVP), Salt River Project Agricultural Improvement and Power District (SRP), etc. showed greater variability in their 20 largest reconstructed demand records (coefficient of variation of about 30%) as compared to large sized BAs, the latter subset, including ERCOT and SOCO govern geographically diverse areas, and even small variations in peak demand requirements imply that the overall system is at greater risk to temperature changes. Thus, the scale of social impact due to power outages will be large in these BAs will be large.

However, validating the reconstructed temperature-driven hourly electricity demand proxies derived from the LSTM and Piecewise Linear Regression (PLR) models against the observed 20 largest peak demand for all Balancing Authorities (except for NEVP, AZPS, PJM, & NYISO) between 2015 - 2019, showed that both LSTM and PLR models underestimate the peak demand hours or the 'anomalous' demand requirements. We term the largest demand as anomalous as the underlying pattern in these demand outliers are not accurately captured by most machine and deep learning models leading to underestimated peak demand estimates. Comparatively the PLR model underestimates the proxies by a greater degree (500%) than the LSTM model. But the approximations of temperature-driven hourly demand in each BA is still useful to determine the relative sensitivity

to interannual variability of weather, and determine which Balancing Authorities require additional climate change resiliency strategies.

Finally, in Chapter 4, large uncertainties surrounding the availability of solar and wind resources in geographically diverse locations, and its impact on grid reliability under significant renewable energy penetration, was quantified for a multidecadal time frame. The variability in solar and wind energy was combined with synchronously changing variability in temperature-driven hourly demand, to estimate probabilistic capacity credit of newly added solar, onshore wind, and offshore wind generators in three systematically different Balancing Authorities. The probabilistic reliability assessment was based on determining the Effective Load Carrying Capability of the generator of interest. The change in ELCC values from the same generator across 40 years (1980 - 2019) was estimated using the coefficient of variation metric while holding other exogenous variables, such as the grid composition (or base fleet composition), total amount of electricity interchange, and size of generator constant across all years. Only weather-dependent variables, that is, the capacity factors from solar and wind generators of 100 MW, the temperature-driven demand proxies from Chapter 3, and temperature-driven forced outages varied between the years, which helped in isolating the weather-related impacts from technological and social impacts on reliability contributions.For the case of CA-ISO and ISO-NE offshore wind generators provided the greatest reliability benefits towards meeting excess demand (20x and 5x greater than solar and onshore wind resources), while for ERCOT region solar ELCC values were 9x greater than onshore wind and offshore wind generators. Overall, the study also indicated wind generators on an average will be impacted more (coefficient of variation of reliability benefits from offshore wind generators on average was 38%) by interannual variability impacts on supply and demand side than solar resources.

However, since this study was based on the proxied temperature-driven demand values, the median ELCC values for offshore wind generator in ISO-NE, and solar generators in CA-ISO and ISO-NE were somewhat underestimated when validated against ELCC values derived using observed data (Chapter 4, section 4.4.6). A detailed analysis around the use of normalized weather zone based temperature values to reconstruct the demand proxies may result in better estimates, as in Chapter 3, we had implicitly assumed homogeneous temperature across the entire footprint of a Balancing Authority, and used a single gridded cell to extract temperature.

5.2 Policy Implications

The results in this dissertation provide strong evidence for the need to assess the effective reliability benefits by including various types of renewable energy generators under multiple scenarios. Robust power system infrastructure should be built without comprising on system reliability while simultaneously managing the combined effects of temperature-driven hourly demand variability and renewable energy intermittency. Results from Chapter 2 indicated the need to include capacity expansion plans that encourage more offshore wind energy production in New York while cautioning policymakers to understand the necessity of grid diversification using different renewable energy generators. The inclusion of multiple reliable renewable energy generators on the grid helps to address social costs associated with power outages and aids economic development by creating more employment opportunities. Furthermore, even with large spatial heterogeneity in reliability estimates, the capacity contributions from offshore wind energy generators are dependent on the siting process. These generators will significantly increase system reliability under the energy transition pathway adopted through 2030.

Planning agents and policymakers require reliable information for system adequacy studies and the reconstructed electricity demand proxies in Chapter 3 satiates the need for appropriate data sources to study power systems comprehensively. Moreover, analysis of the reconstructed temperature-driven load proxies will help grid planners recognize which balancing authorities require additional support to mitigate impacts due to varying temperatures and help them strategize like Demand Response and Peak Shaving. Utility companies and grid managers could leverage the multidecadal hourly reconstructed demand proxies to study the effect of integrating variable generation such as solar and wind energy farms and electric vehicles to a grid that is already sensitive to temperature changes. This analysis can aid in making informed investment decisions to tackle climate change, as anthropogenic factors will make the temperature even more variable, leading to more fluctuations in peak demand requirements in certain balancing authorities.

Lastly, Chapter 4 implied that the direction of renewable energy integration should not be homogeneous. Different regions in the US are impacted differently due to interannual variability of solar radiation, wind speed and temperature-driven demand. While power systems in CA-ISO and

ISO-NE will greatly benefit from the inclusion of offshore wind energy, ERCOT should include more solar energy as it has a substantial number of wind energy generators. Overall, capacity contributions from solar PV plants is less likely to be impacted due to interannual variability of the solar irradiance, as compared to offshore wind. But reliability benefits from offshore wind generators on both the east and west coast even with large interannual variability impacts is very large. Thus, federal agencies could aid in the process of renewable energy integration by providing more subsidies to wind power projects on the east and west coast, and for solar power projects in Texas.

5.3 Future Work

Limitations with the study presented in this thesis can be dealt by further studying the following aspects:

1. The analysis from Chapter 2 can be improved to include demand records representative of year 2030. We held demand from 2019 to be constant to avoid incorporating uncertainty in demand records by forecasting them from 2019. As population grows, energy efficiency measures changes, and policies surrounding grid management are altered, the demand would change, leading to different peak loads and demand shortfalls, eventually changing the ELCC estimates of future solar, onshore wind, and offshore wind generators added to the base fleet of NY-ISO.

2. The reconstructed demand proxies in Chapter 3 were based on the broad assumption that temperature within BAs (both large and small) remain constant throughout the footprint of the balancing authority. This assumption may hold for BAs covering smaller regions within certain states, but for larger BAs like PJM, Midcontinent Independent System Operator (MISO), Independent System Operator of New England (ISO-NE), Southwest Power Pool (SWPP), etc., which governs multiple states and are spread across geographical areas covering hundreds of square miles, a single temperature value which drives changes in hourly demand is not appropriate. Weather-zone differentiated temperature records should be used to create reconstructed demand proxies rather than hinging on temperature records from a

single gridded cell representative of the largest population center in a BA.

3. Lastly, in Chapter 4, we assumed a constant base fleet of generators for all 40 years of analysis between 1980 - 2019, over which our renewable generator of interest was added. In a real world scenario, the addition of VRE generators will be dynamic as multiple renewable energy generators could be added incrementally in different points of time during the 40-year timeline. Thus, the analysis can be improved by including scenarios of base fleet of generators representative of future energy transition pathways to better understand dynamic change in reliability benefits from new renewable energy generators as base fleet composition also changes, while also including multiple renewable energy generators at different intervals.

5.4 Data Contributions and Code

We created 4 decades of temperature-driven hourly demand proxies from research conducted in Chapter 3 for 40 of 66 Balancing Authorities of the US. These 40 BAs showed a definite temperature-load relationship and the estimated demand proxies can be considered reliable. Moreover, the code used in Chapter 2, 3, and 4 is open source. All datasets that have been generated (reconstructed demand proxies from Chapter 3), along with detailed python scripts and corresponding Readme is available on https://github.com/reshmighosh/Data-driven-stochastic-reliability-benefit-analysis (Github).

Appendix A: Appendix supporting Chapter 2

A.1 Forced Outage Rates

Forced Outage Rate (FOR) is the probability that a dispatchable or conventional generator will not be operable and will be incapable of contributing towards fleet capacity due to equipment failure or unexpected maintenance. FORs are dependent on generator technology type, age, ambient temperature. The value of FORs for conventional generators are derived from Murphy, Sowell, and Apt, 2019. The temperature used in this paper is between -15°C to 35°C (inclusive) in increments of 5°C. To determine the FOR of each type of conventional generator incorporated from EIA 860, 2019 and interconnection queue, we us gridded hourly temperature from MERRA dataset and the generator technology. Broadly, Murphy, Sowell, and Apt, 2019 classifies the conventional generators in six different categories, i.e., combined cycle gas, simple cycle gas, diesel, hydroelectric pumped storage, nuclear, and steam turbine. After classifying the EIA 860 generator data into these categories, we first obtain the hourly temperature per generator location within the state of New York, and then assign the FOR dependent on technology and temperature to each generator whilst grouping the temperature values into the 5°C bins. Table A.1 describes the temperature dependent FORs used for conventional generator technologies.

On the other hand, renewable energy generators are also known to become inoperable at certain times of the year, but unlike conventional generators whose operation is highly influenced

Table A.1: Table describing the temperature dependent FORs for six conventional generator types, where CC refers to combined cycle, NG is the simple gas cylce, DS refers to diesel based generators, HS is hydroelectric pumped storage, NU is nuclear, and ST refers to steam turbines.

Temperature in °C	CC	NG	DS	HS	NU	ST
-15	14.9%	19.9%	21.2%	7%	1.9%	13.3%
-10	8.1%	9.9%	17.0%	4.3%	1.8%	11.2%
-5	4.8%	5.1%	13.7%	3.2%	1.7%	9.9%
0	3.3%	3.1%	11.6%	2.7%	1.8%	9.1%
5	2.7%	2.4%	10.6%	2.6%	1.8&	8.6%
10	2.5%	2.2%	10.2%	2.6%	1.9%	8.2%
15	2.8%	2.4%	10.4%	2.7%	2.1%	8.4%
20	3.5%	2.7%	13.6%	2.7%	2.7%	8.6%
25	3.5%	3.1%	13.5%	2.5%	3.7%	9.4%
30	4.1%	3.9%	14.3%	2.9%	6.6%	11.4%
35	7.2%	6.6%	17.5%	8.2%	12.4%	14.0%
Unconditional forced outage rates for all	3.3%	2.8%	10.9%	2.4%	2.6%	9.4%

by temperature, renewable energy generators face outages mostly due to unexpected maintenance requirements. Thus, we assign a fixed FOR of 5% to offshore wind, onshore wind, and solar PV generators.

A.2 ELCC Maps

For each gridded data point within the MERRA atmospheric dataset for the region governed by NY-ISO, we found the ELCC of adding future VRE generators on top of diversified base fleets (based on 2030 energy transition scenarios) and generated maps. These maps are helpful in recognizing the spatial pattern of ELCC values for different VRE generators (represented as a consolidated form of box plot distribution in the main paper). Below we show the distribution of ELCC values for all scenarios and for each nameplate capacity, in the order:

1. Current Scenario
2. High Offshore wind Scenario
3. High Onshore wind Scenario
4. High Solar Scenario

5. High Natural Gas scenario

The maps presented in Figure A.2 - Figure A.15 show the spatial distribution of ELCC values of new solar, offshore wind, and onshore wind generators under five scenarios representative of energy transition pathways through 2030. The spatial heterogeneity associated with ELCC values is driven by capacity factors of solar and wind resources. Areas surrounding the Great Lakes region have larger wind potential leading to significant reliability benefits from onshore wind generators. Similarly, some areas in the offshore area adjacent to New York have larger capacity factors leading to better ELCC values (64% In Reference Case) than others. Conversely, solar capacity factors are have more homogeneous spatial distribution but smaller capacity contributions. In all, it is generators with higher ELCC values but we greater spatial heterogeneity is preferred over generators with smaller ELCC values and more homogeneous distribution.

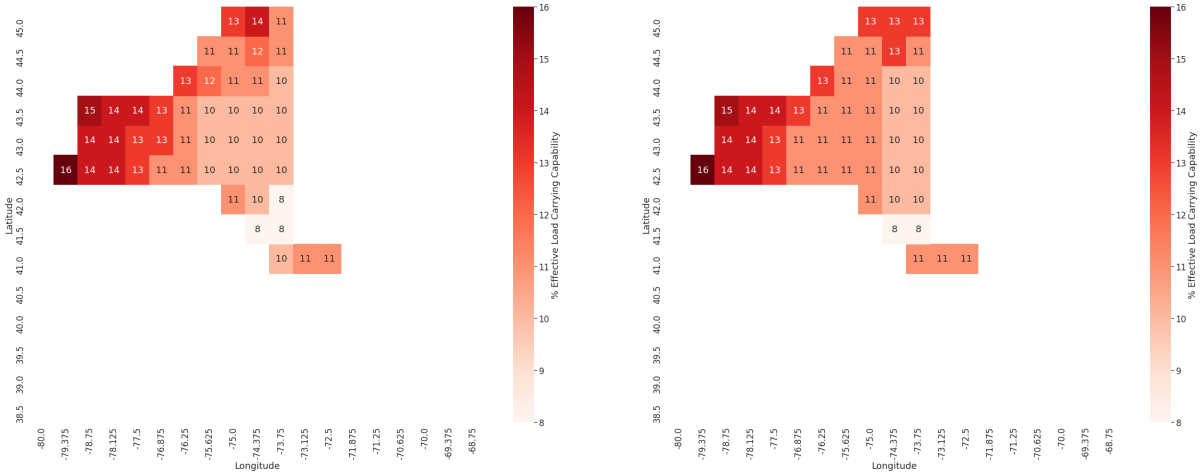

(a) 50MW solar PV generator

(b) 100MW solar PV generator

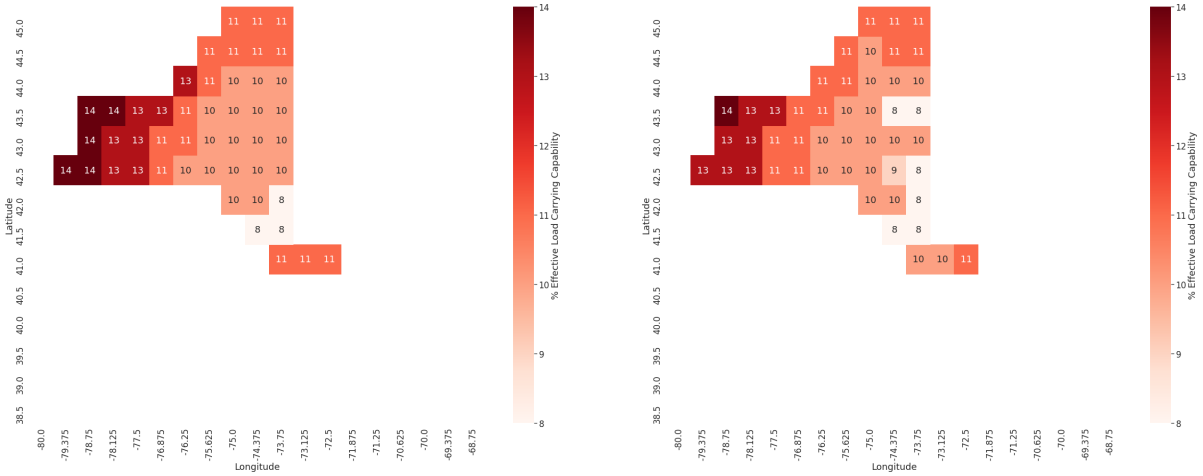

(c) 250MW solar PV generator

(d) 500MW solar PV generator

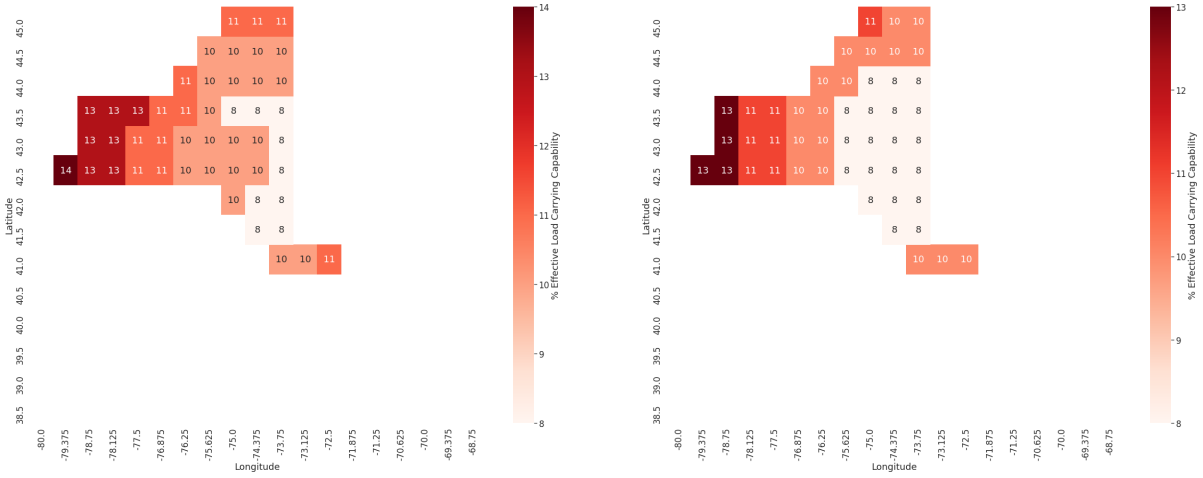

(e) 1000MW solar PV generator

(f) 2000MW solar PV generator

Figure A.1: Geographical distribution of ELCC values for solar generators over the current base fleet (Reference Case)

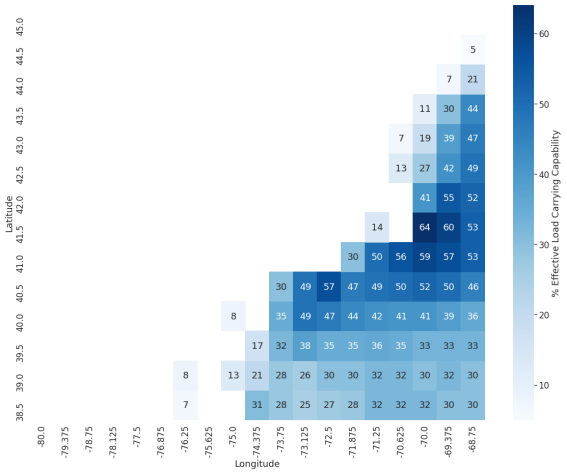

(a) 50MW offshore wind generator

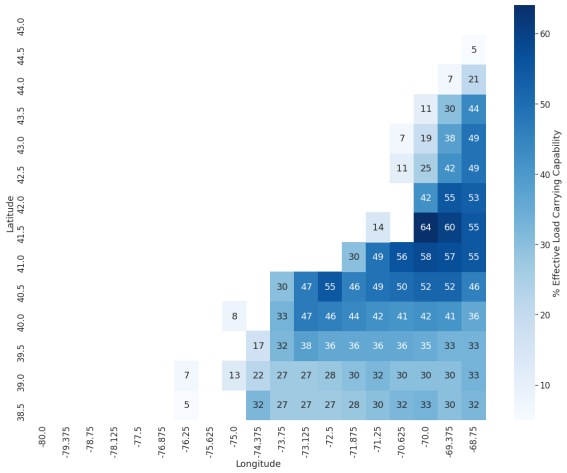

(b) 100MW offshore wind generator

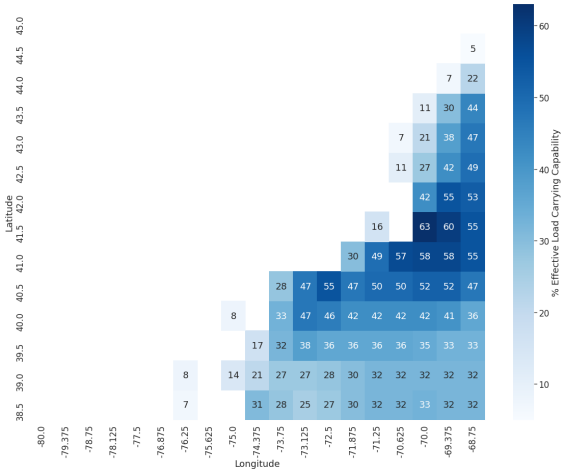

(c) 250MW offshore wind generator

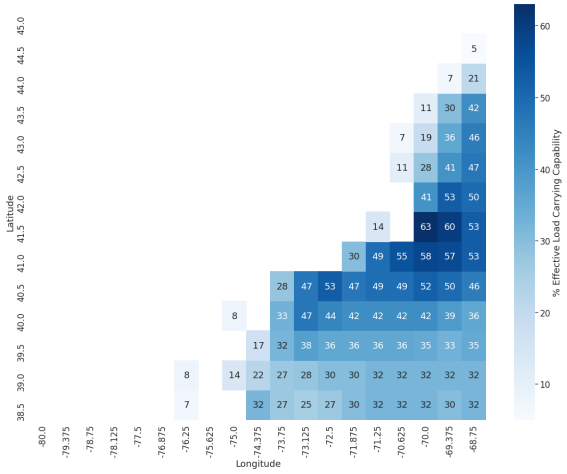

(d) 500MW offshore wind generator

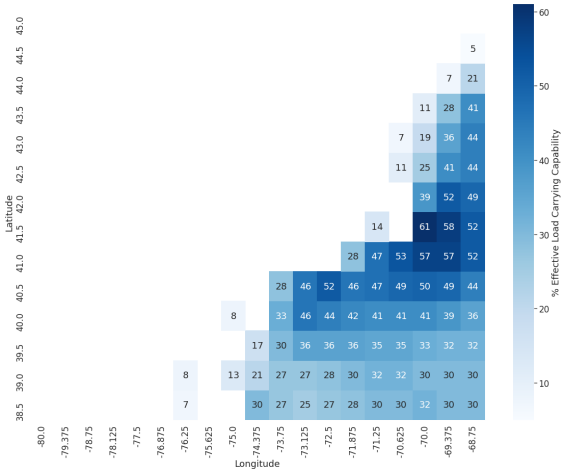

(e) 1000MW offshore wind generator

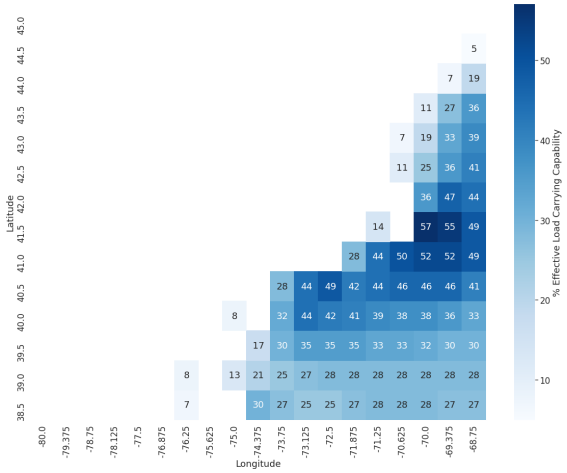

(f) 2000MW offshore wind generator

Figure A.2: Geographical distribution of ELCC values for offshore wind generators over the current base fleet (Reference Case).

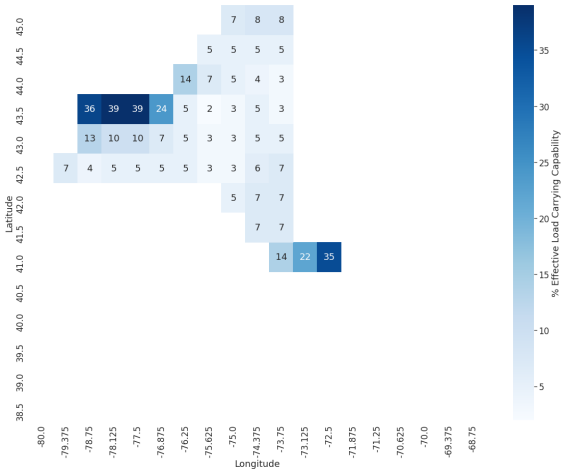

(a) 50MW onshore wind generator

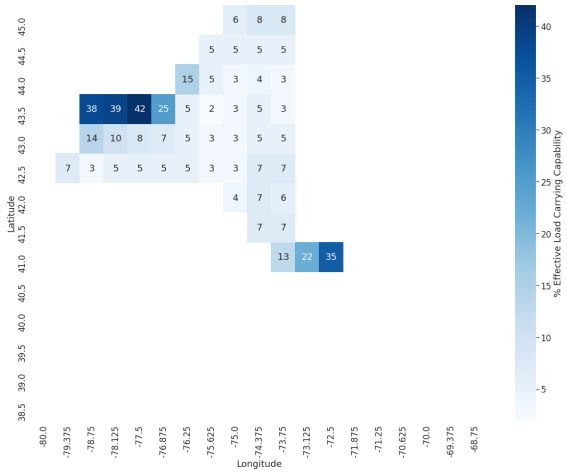

(b) 100MW onshore wind generator

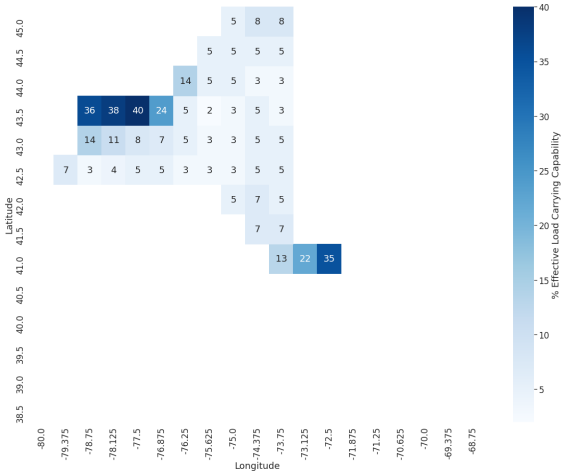

(c) 250MW onshore wind generator

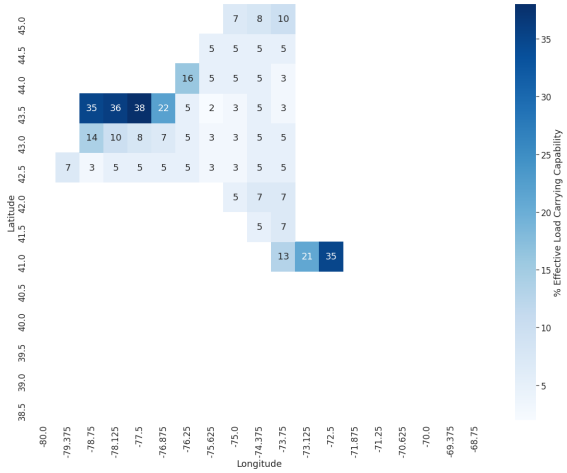

(d) 500MW onshore wind generator

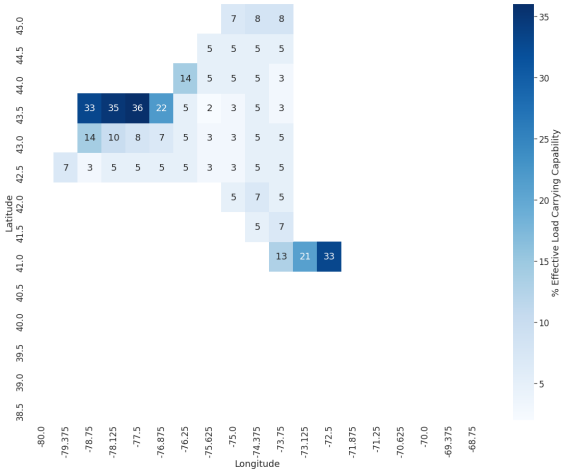

(e) 1000MW onshore wind generator

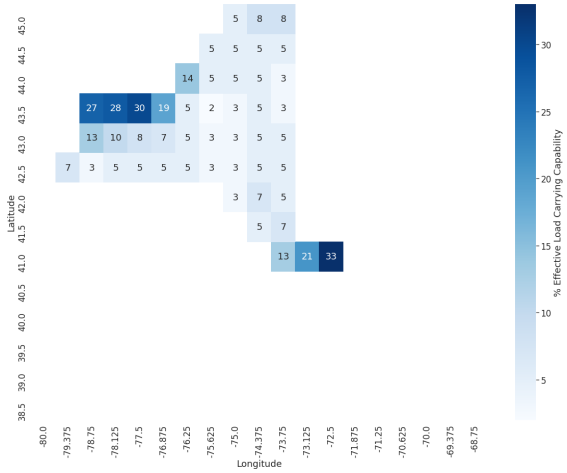

(f) 2000MW onshore wind generator

Figure A.3: Geographical distribution of ELCC values for onshore wind generators over the current base fleet (Reference Case).

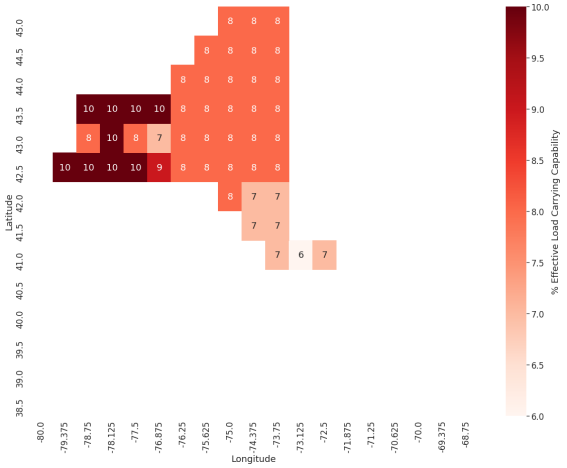

(a) 50MW solar PV generator

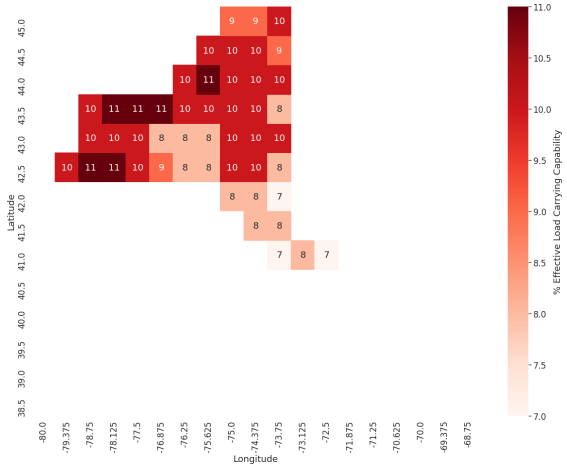

(b) 100MW solar PV generator

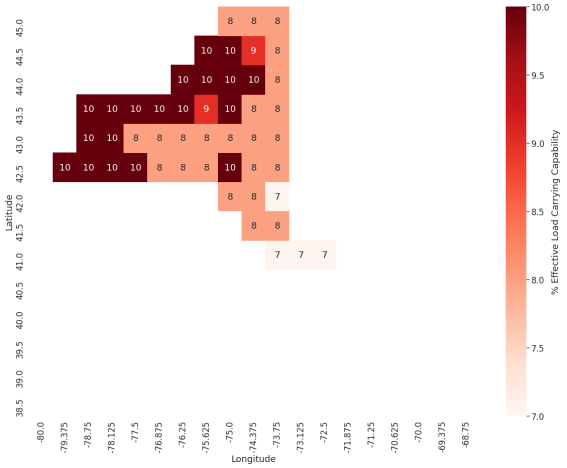

(c) 250MW solar PV generator

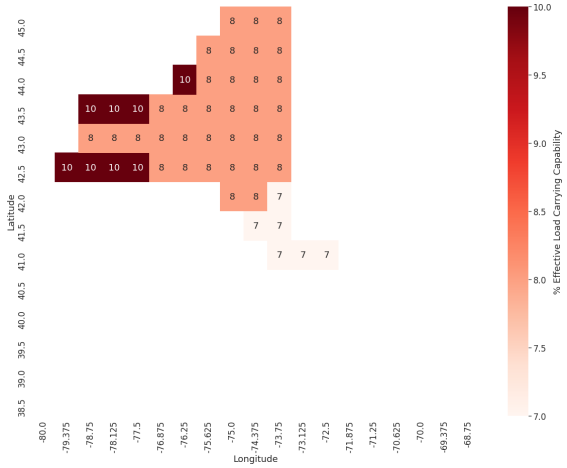

(d) 500MW solar PV generator

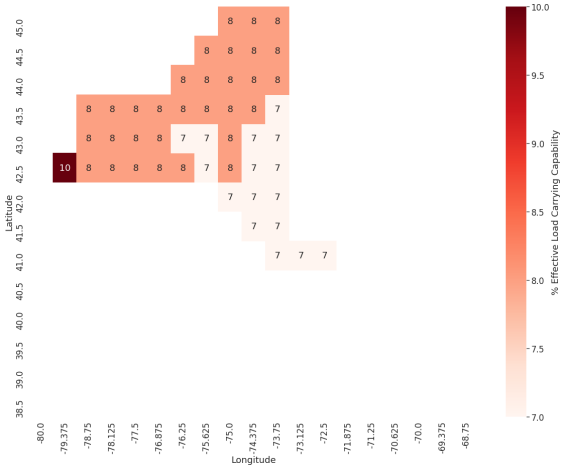

(e) 1000MW solar PV generator

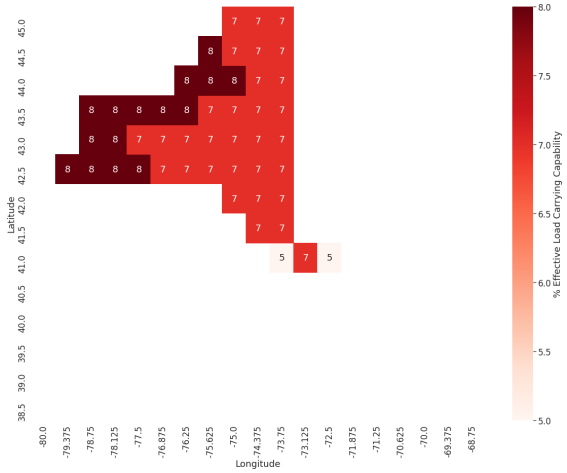

(f) 2000MW solar PV generator

Figure A.4: Geographical distribution of ELCC values for solar generators over a base fleet representing High Offshore scenario

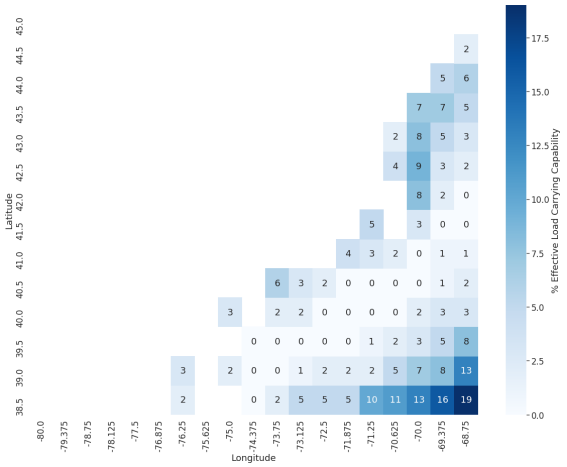

(a) 50MW offshore wind generator

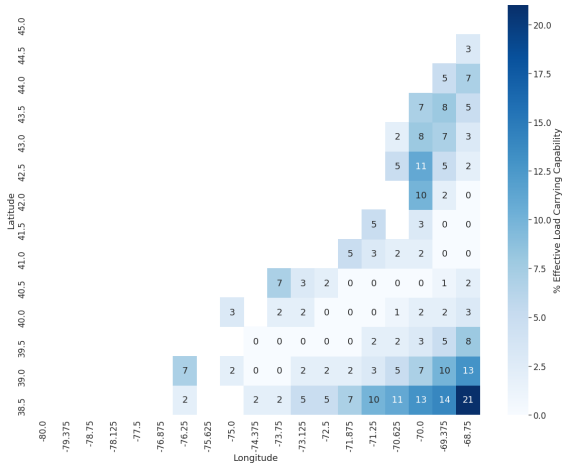

(b) 100MW offshore wind generator

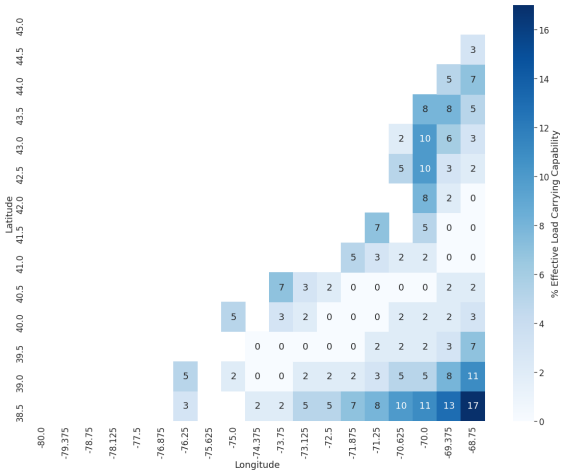

(c) 250MW offshore wind generator

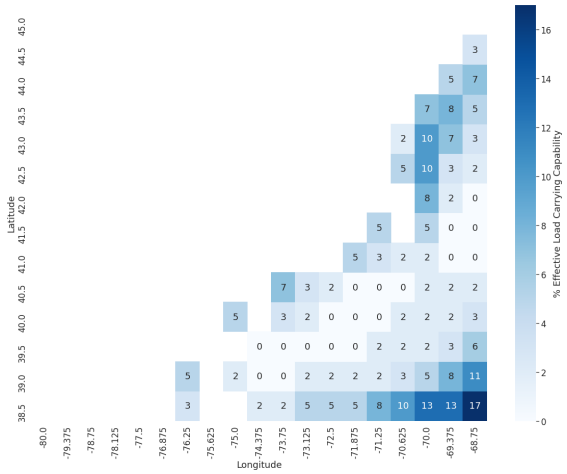

(d) 500MW offshore wind generator

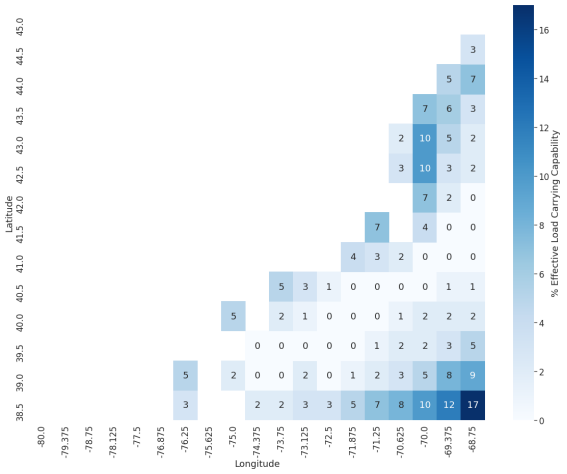

(e) 1000MW offshore wind generator

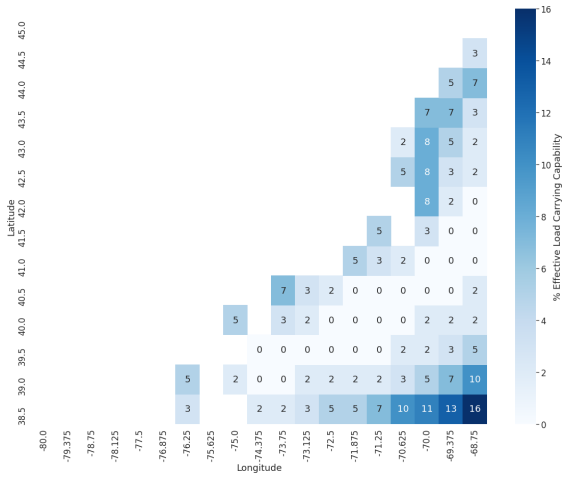

(f) 2000MW offshore wind generator

Figure A.5: Geographical distribution of ELCC values for offshore wind generators over a base fleet representing High Offshore scenario

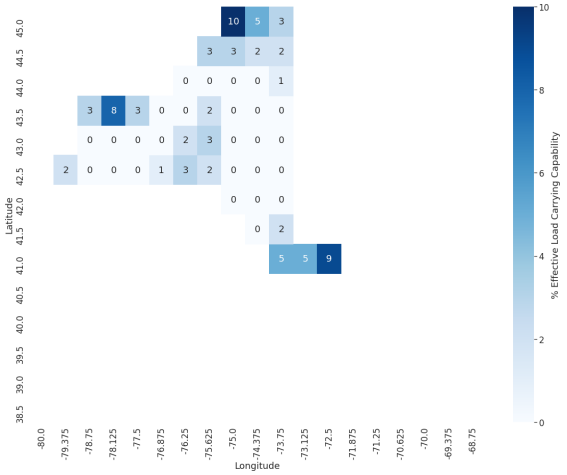

(a) 50MW onshore wind generator

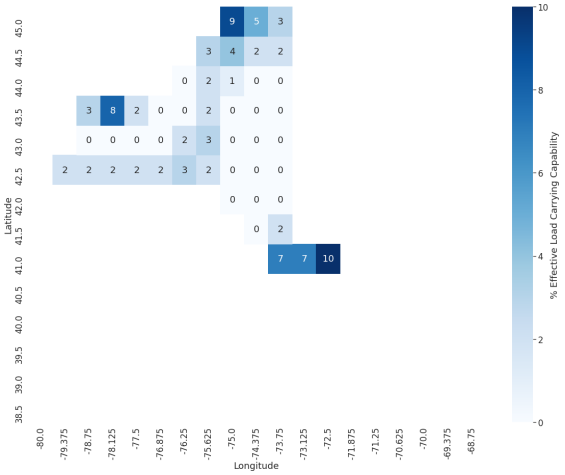

(b) 100MW onshore wind generator

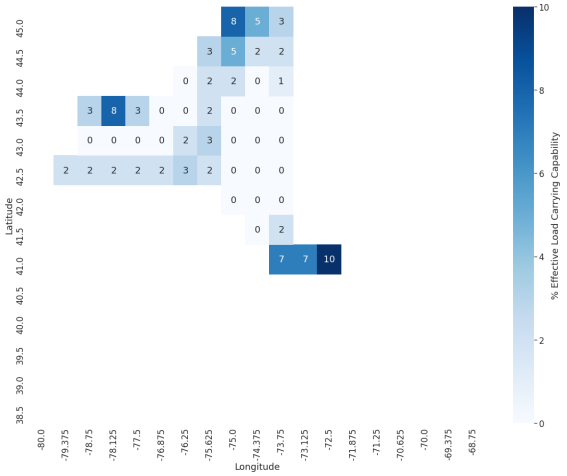

(c) 250MW onshore wind generator

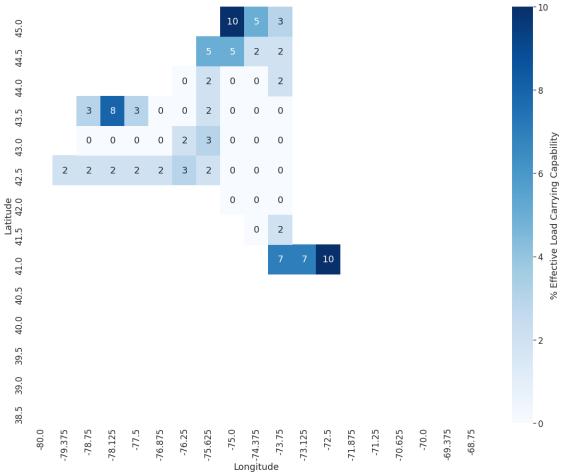

(d) 500MW onshore wind generator

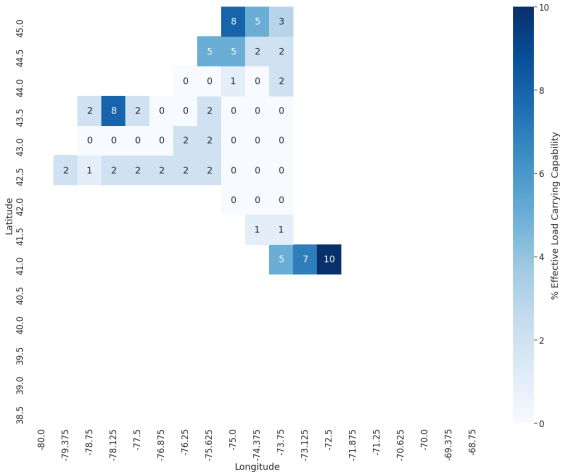

(e) 1000MW onshore wind generator

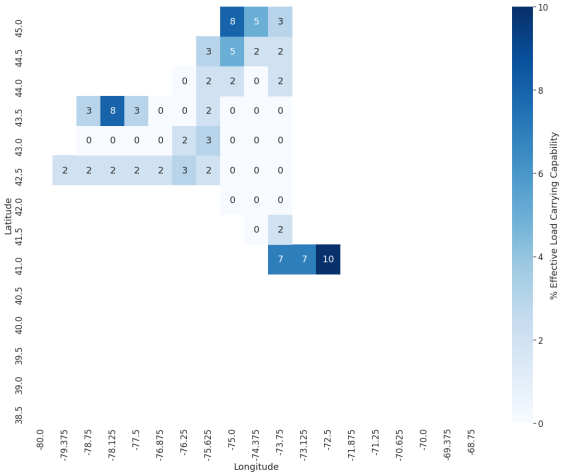

(f) 2000MW onshore wind generator

Figure A.6: Geographical distribution of ELCC values for onshore wind generators over a base fleet representing High Offshore scenario

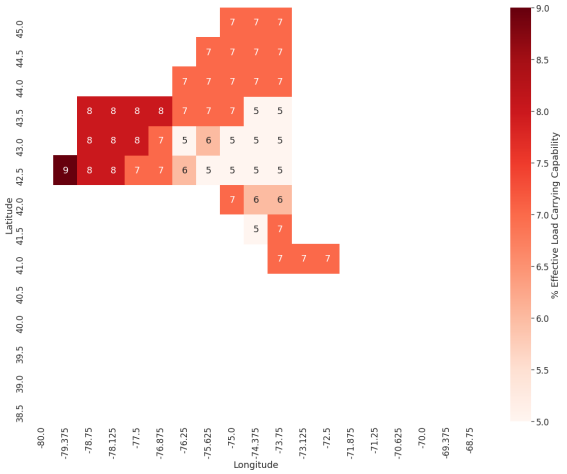

(a) 50MW solar PV generator

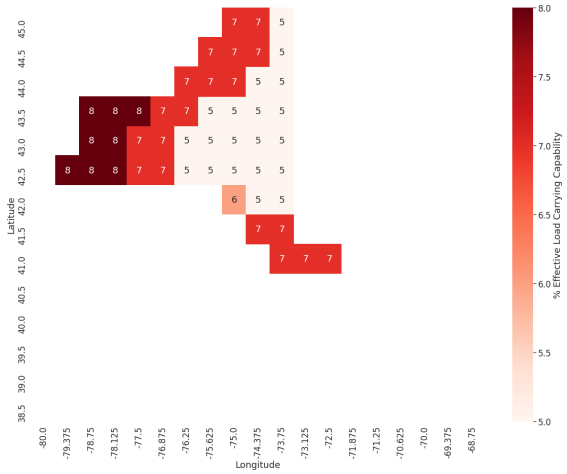

(b) 100MW solar PV generator

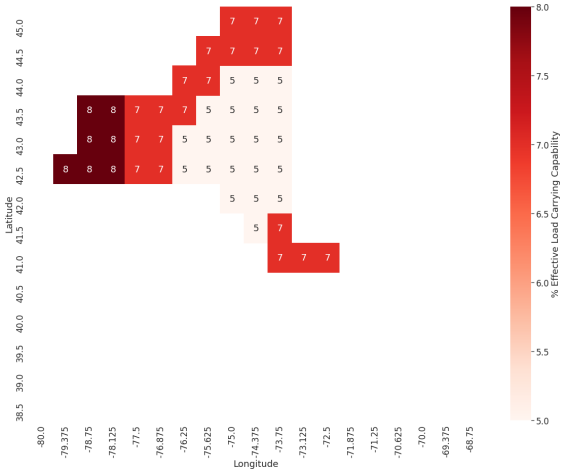

(c) 250MW solar PV generator

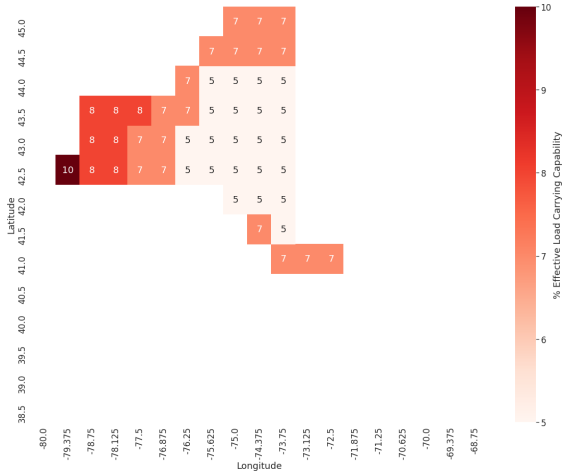

(d) 500MW solar PV generator

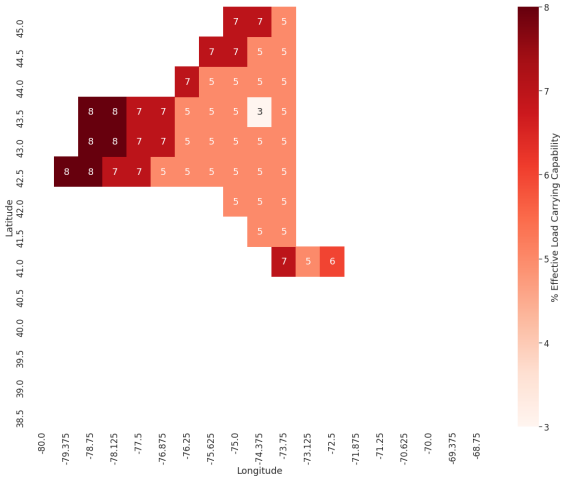

(e) 1000MW solar PV generator

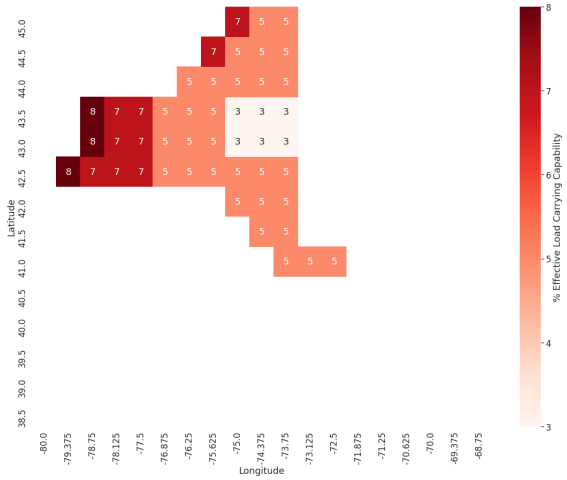

(f) 2000MW solar PV generator

Figure A.7: Geographical distribution of ELCC values for solar generators over a base fleet representing High Onshore scenario

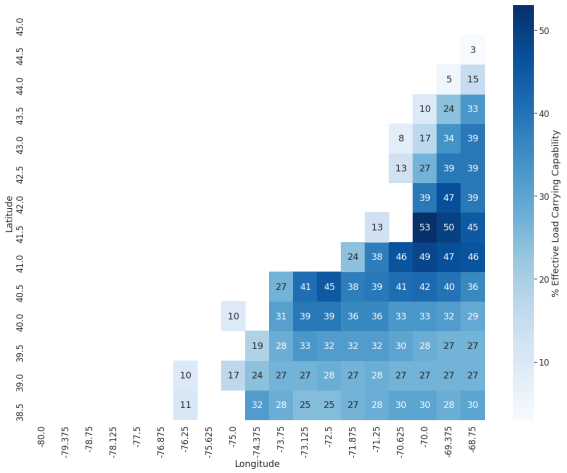

(a) 50MW offshore wind generator

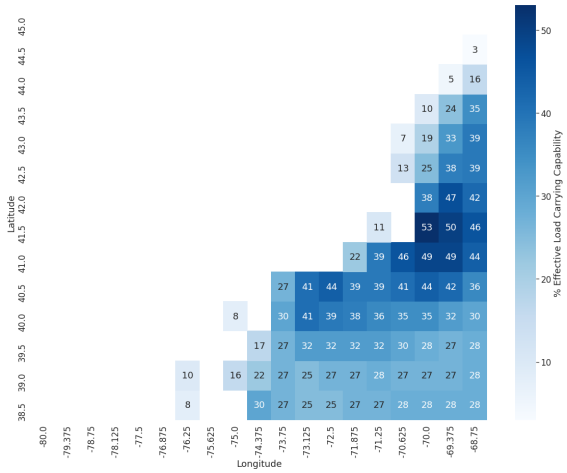

(b) 100MW offshore wind generator

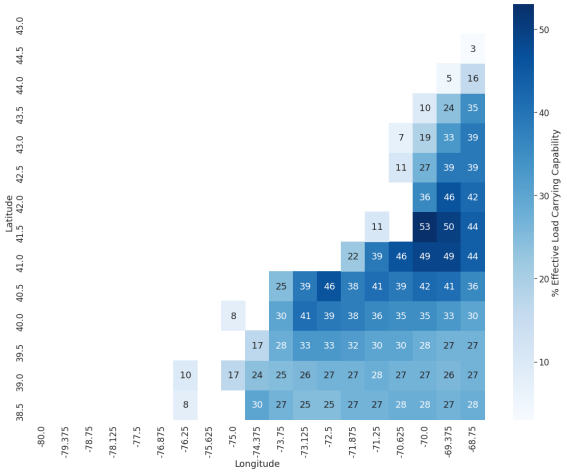

(c) 250MW offshore wind generator

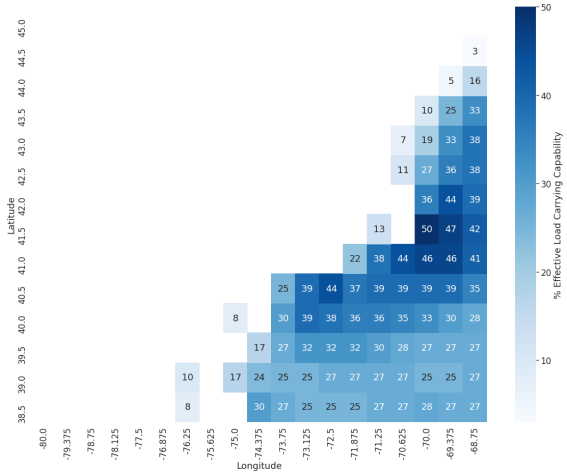

(d) 500MW offshore wind generator

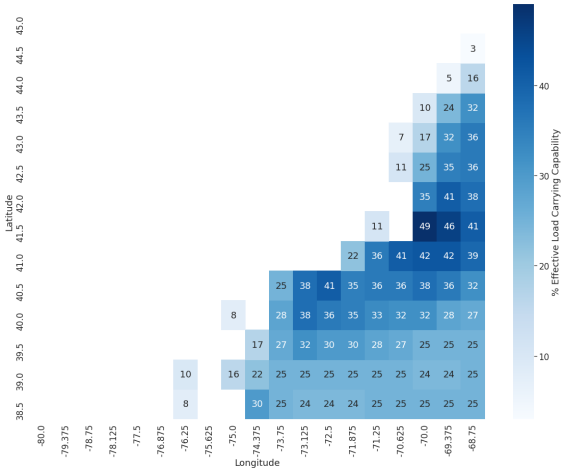

(e) 1000MW offshore wind generator

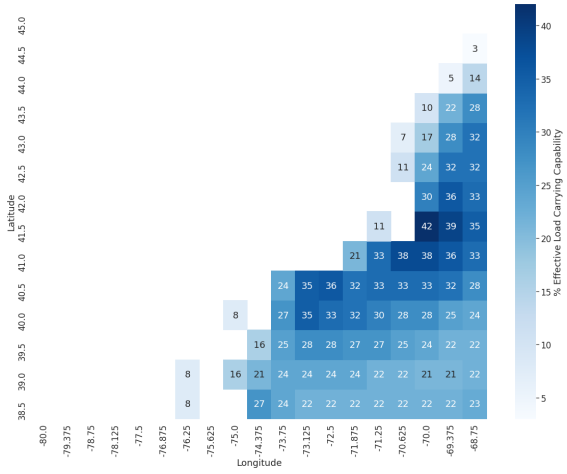

(f) 2000MW offshore wind generator

Figure A.8: Geographical distribution of ELCC values for offshore wind generators over a base fleet representing High Onshore scenario

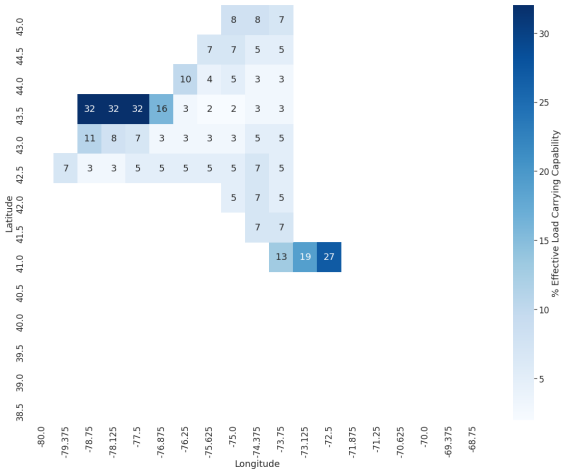

(a) 50MW onshore wind generator

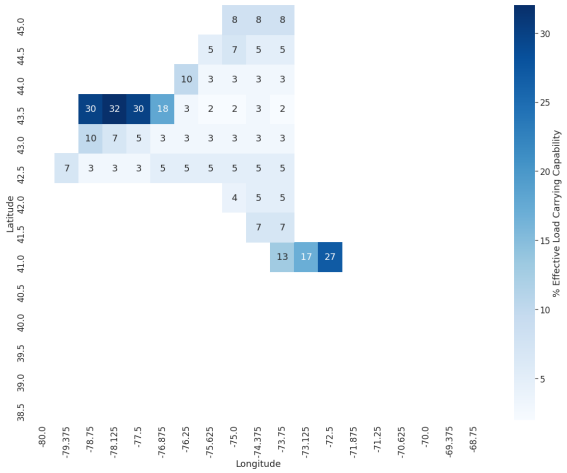

(b) 100MW onshore wind generator

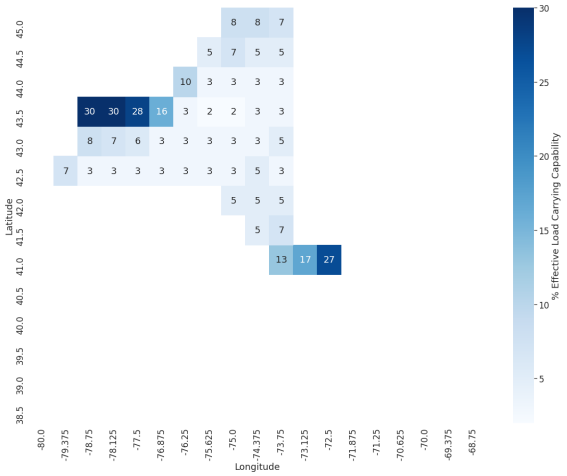

(c) 250MW onshore wind generator

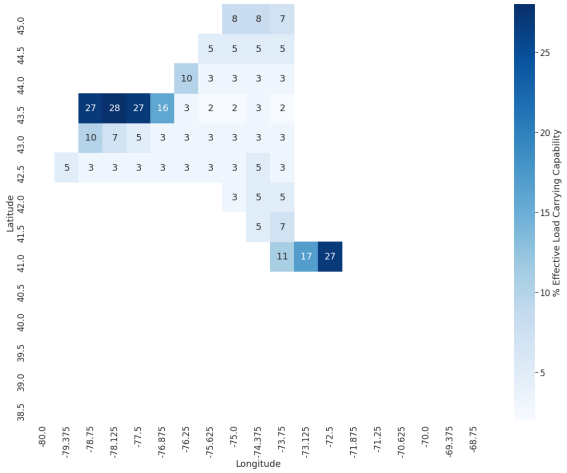

(d) 500MW onshore wind generator

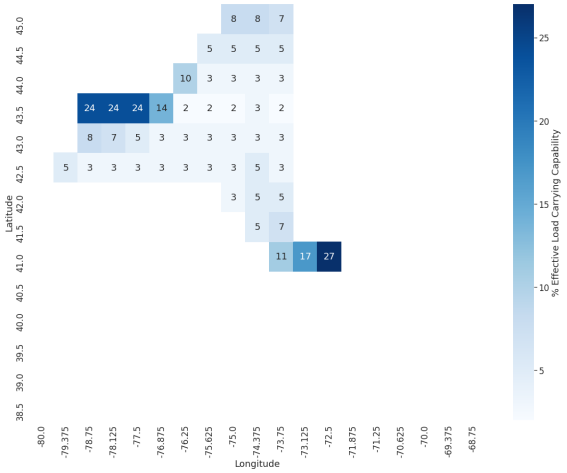

(e) 1000MW onshore wind generator

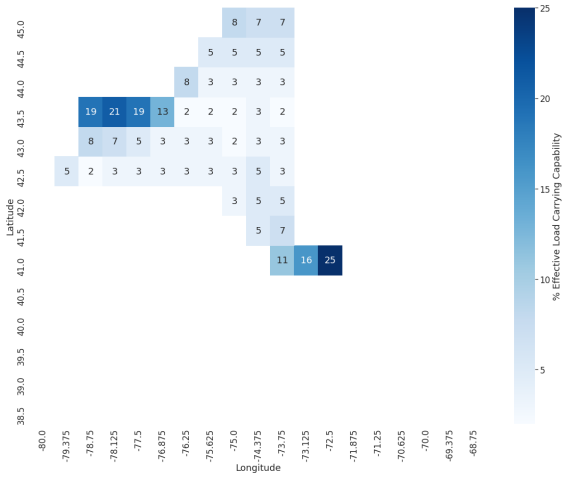

(f) 2000MW onshore wind generator

Figure A.9: Geographical distribution of ELCC values for onshore wind generators over a base fleet representing High Onshore scenario

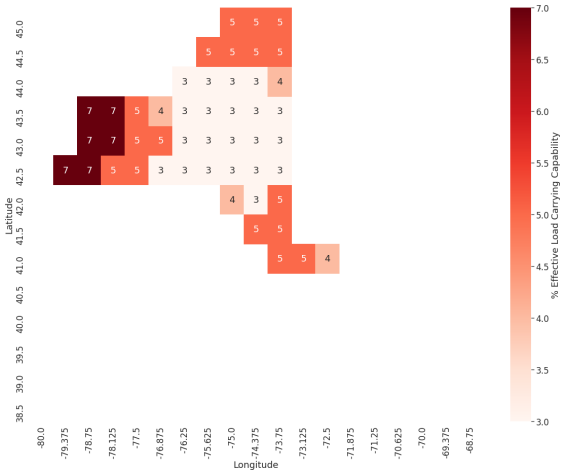

(a) 50MW solar PV generator

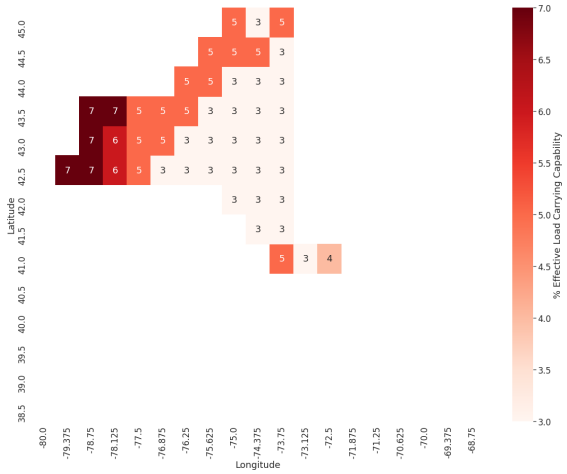

(b) 100MW solar PV generator

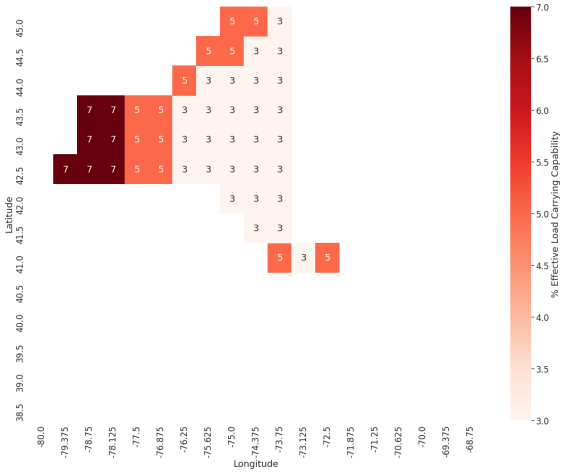

(c) 250MW solar PV generator

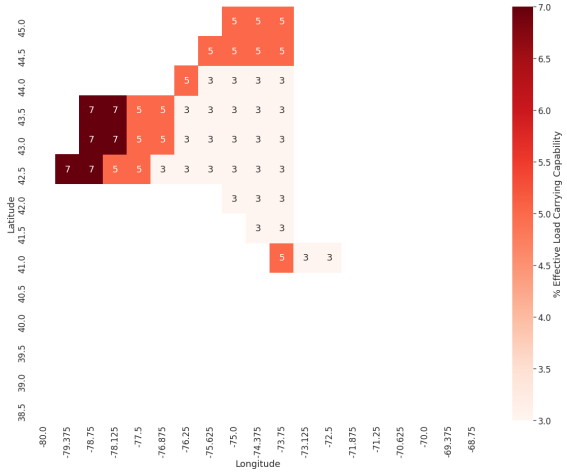

(d) 500MW solar PV generator

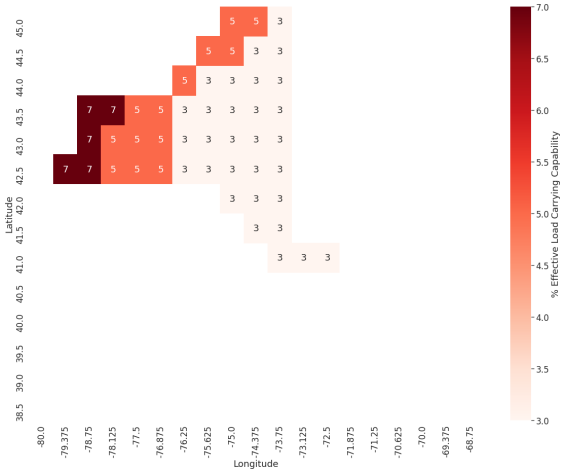

(e) 1000MW solar PV generator

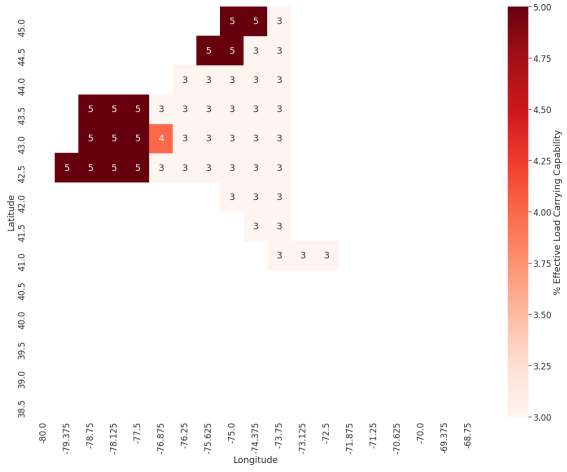

(f) 2000MW solar PV generator

Figure A.10: Geographical distribution of ELCC values for solar generators over a base fleet representing the High Solar scenario.

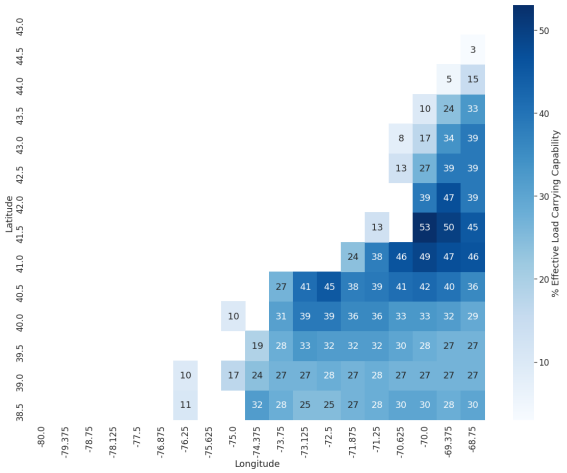

(a) 50MW offshore wind generator

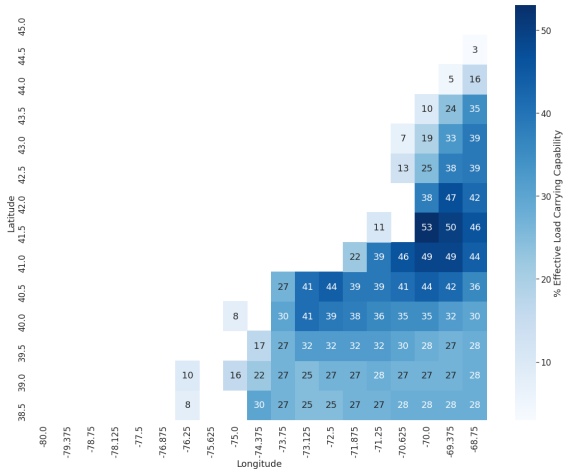

(b) 100MW offshore wind generator

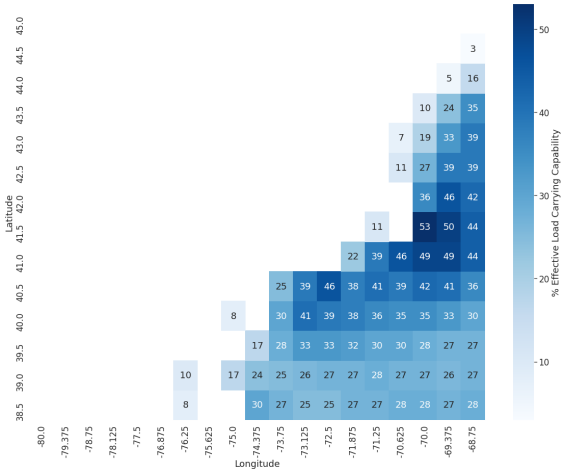

(c) 250MW offshore wind generator

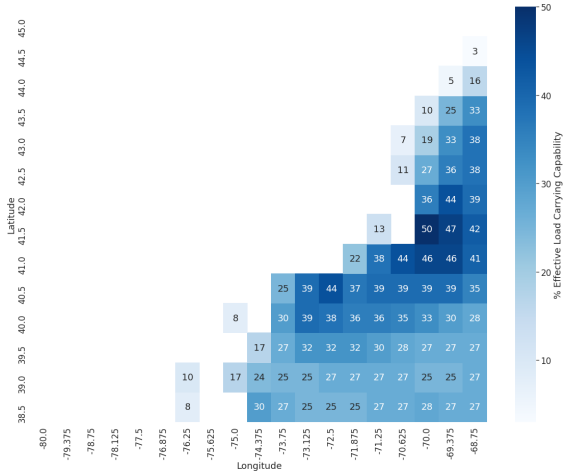

(d) 500MW offshore wind generator

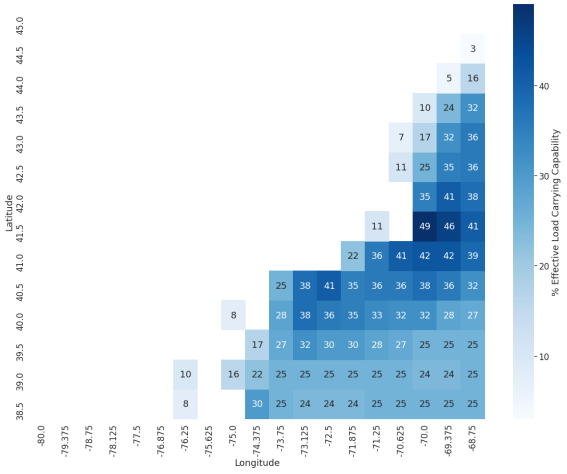

(e) 1000MW offshore wind generator

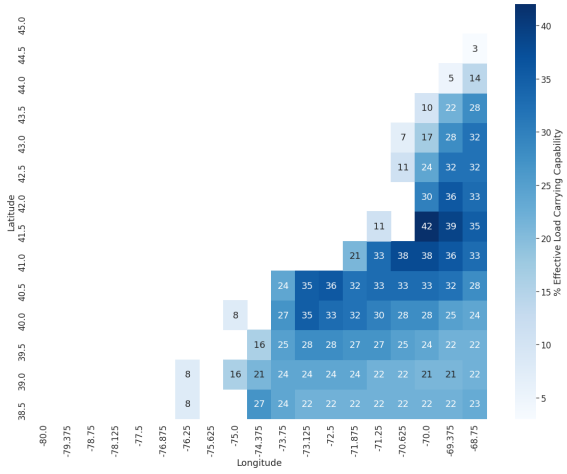

(f) 2000MW offshore wind generator

Figure A.11: Geographical distribution of ELCC values for offshore wind generators over a base fleet representing the High Solar scenario.

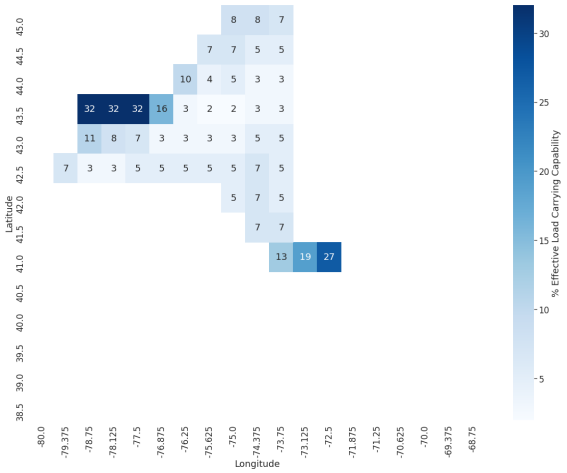

(a) 50MW onshore wind generator

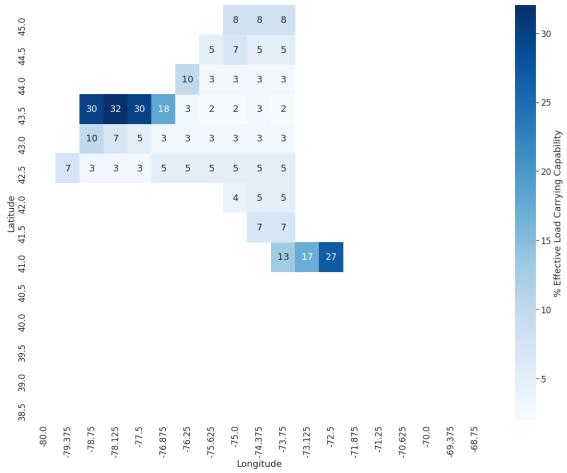

(b) 100MW onshore wind generator

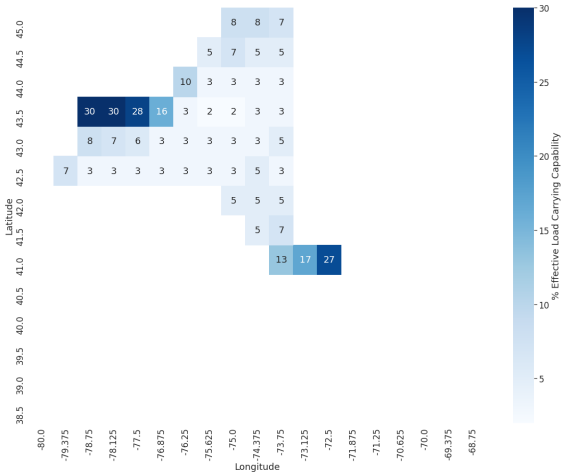

(c) 250MW onshore wind generator

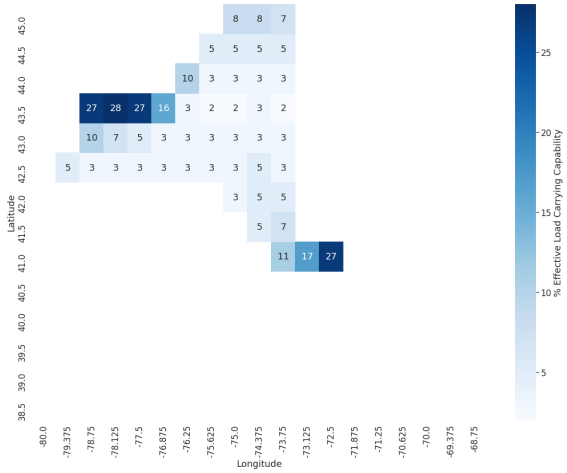

(d) 500MW onshore wind generator

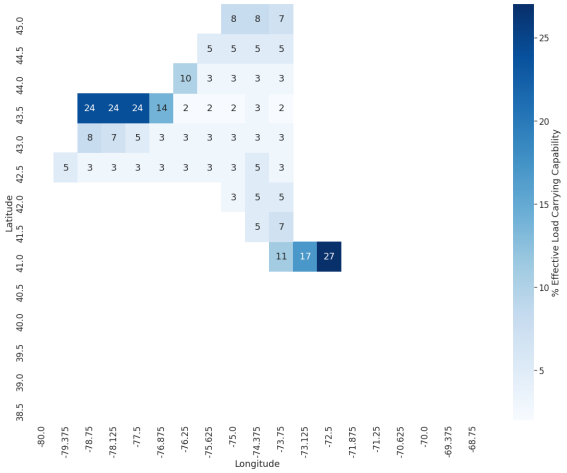

(e) 1000MW onshore wind generator

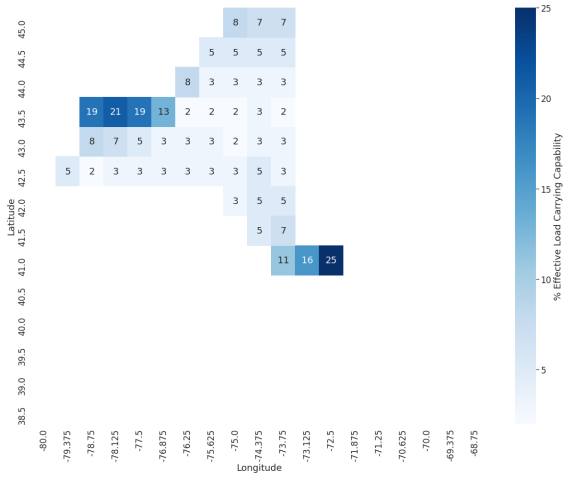

(f) 2000MW onshore wind generator

Figure A.12: Geographical distribution of ELCC values for onshore wind generators over a base fleet representing the High Solar scenario.

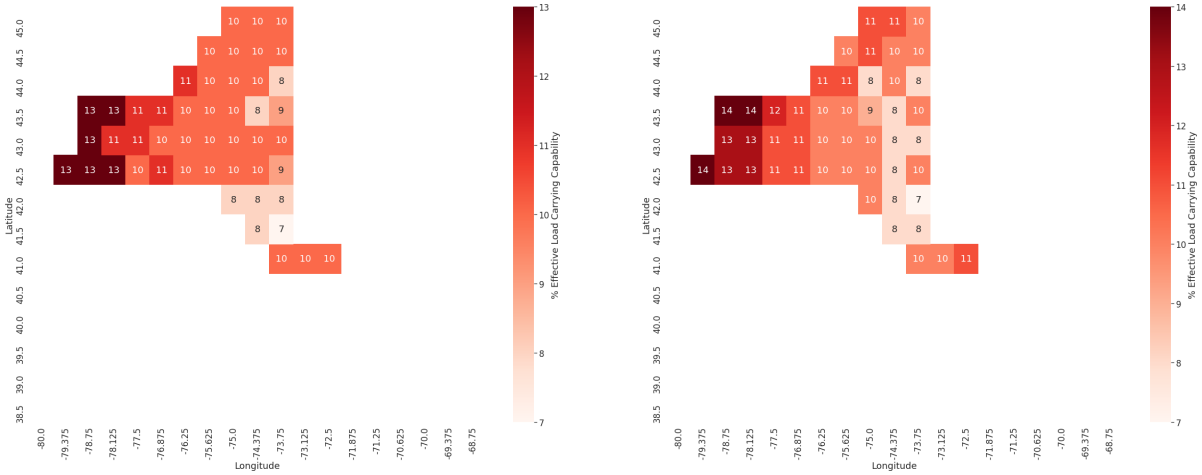

(a) 50MW solar PV generator

(b) 100MW solar PV generator

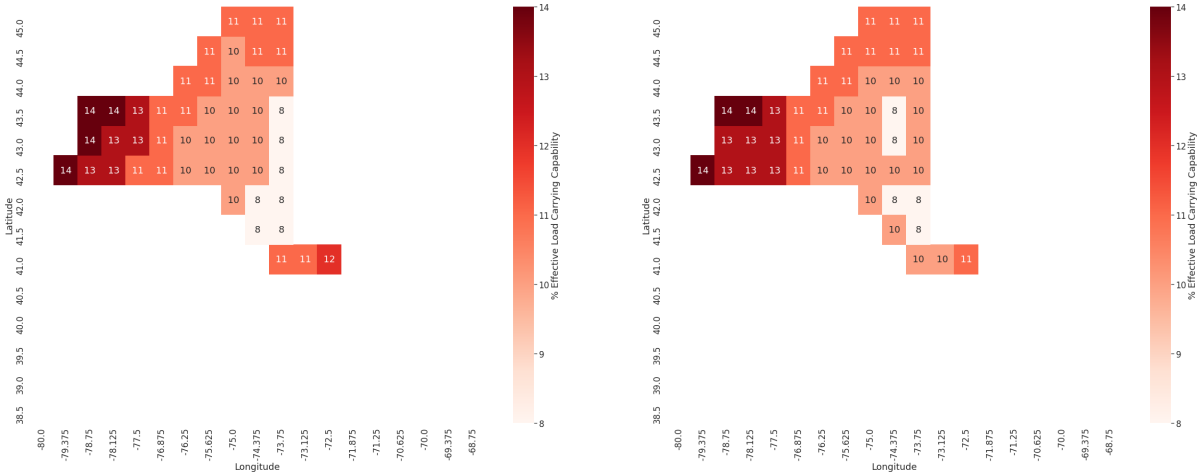

(c) 250MW solar PV generator

(d) 500MW solar PV generator

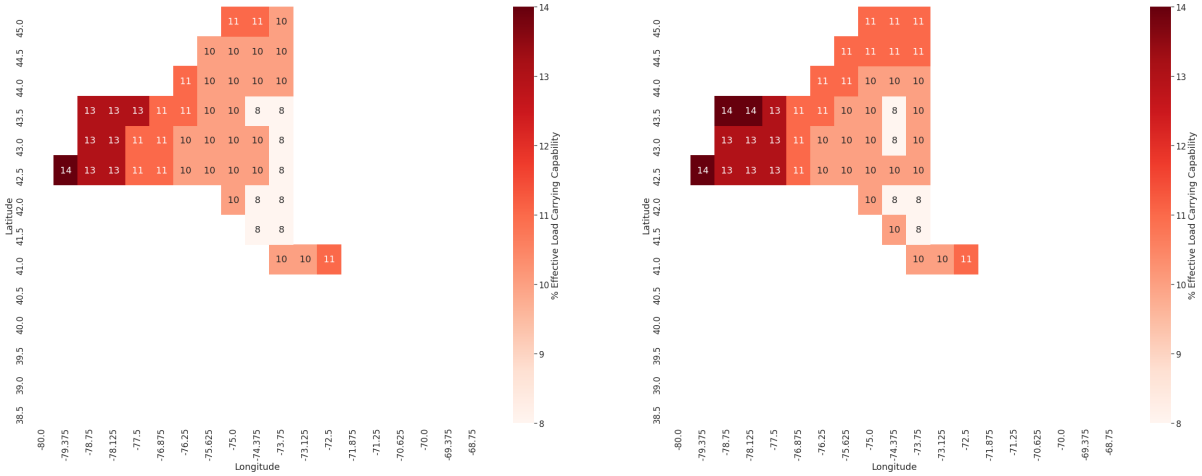

(e) 1000MW solar PV generator

(f) 2000MW solar PV generator

Figure A.13: Geographical distribution of ELCC values for solar generators over a base fleet representing the High Natural Gas scenario.

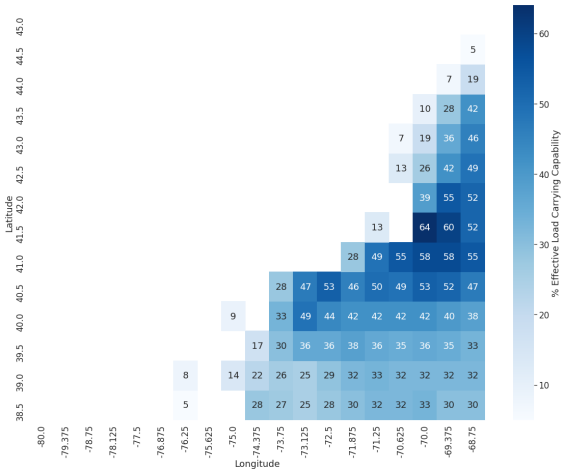

(a) 50MW offshore wind generator

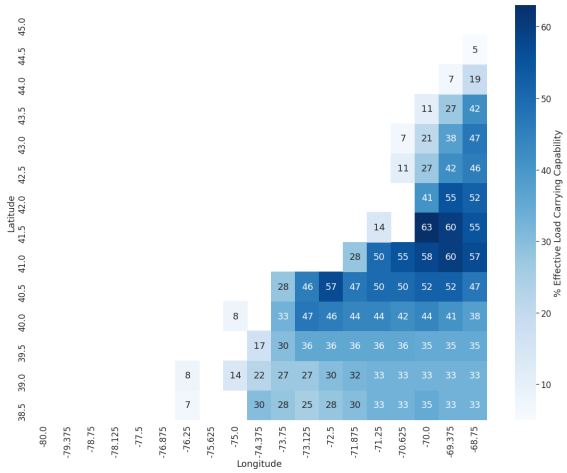

(b) 100MW offshore wind generator

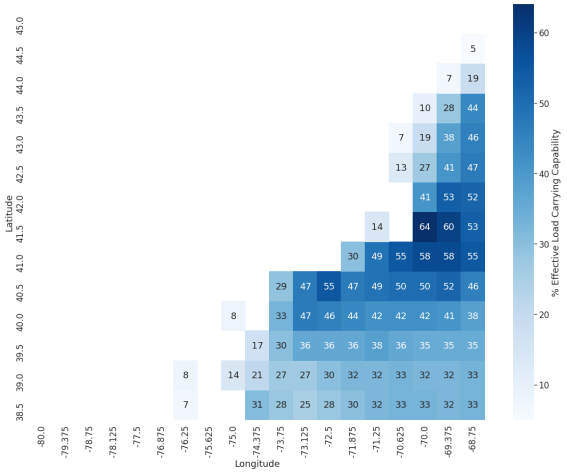

(c) 250MW offshore wind generator

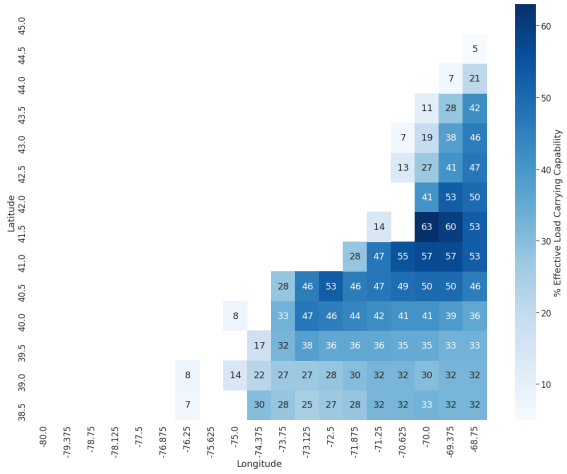

(d) 500MW offshore wind generator

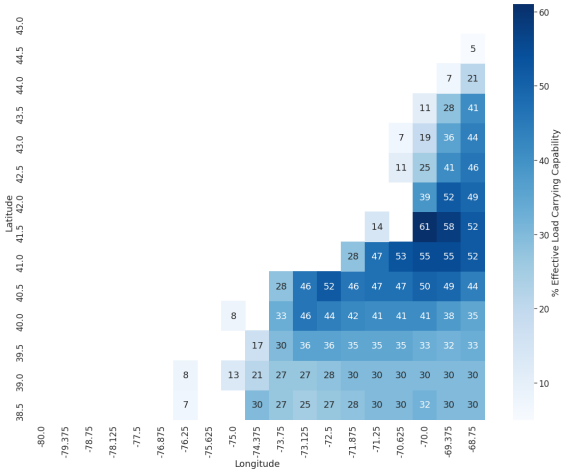

(e) 1000MW offshore wind generator

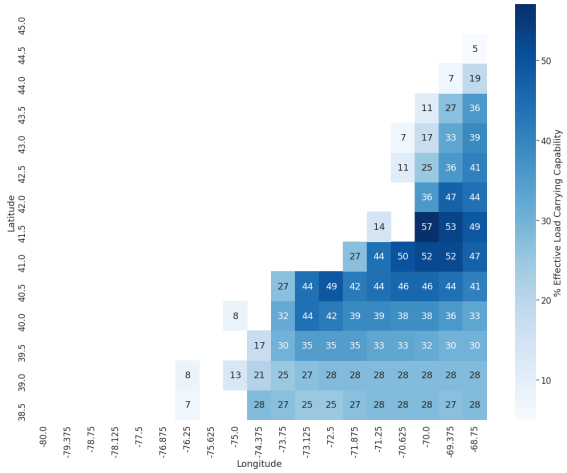

(f) 2000MW offshore wind generator

Figure A.14: Geographical distribution of ELCC values for offshore wind generators over a base fleet representing the High Natural Gas scenario.

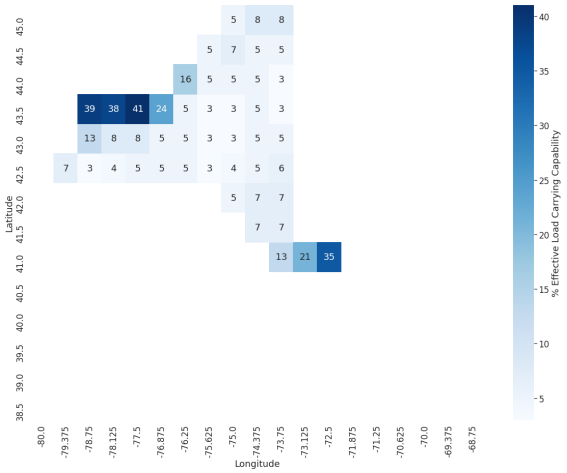

(a) 50MW onshore wind generator

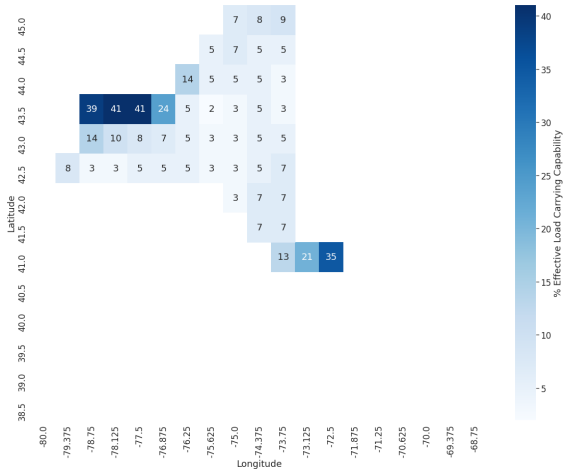

(b) 100MW onshore wind generator

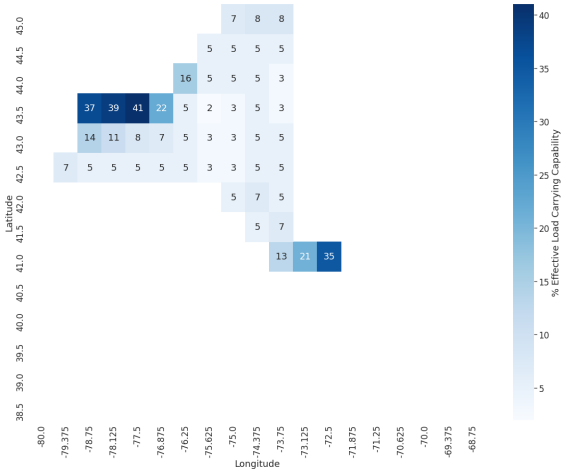

(c) 250MW onshore wind generator

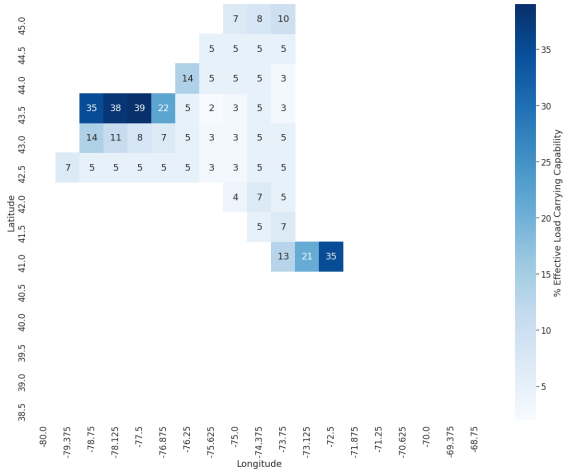

(d) 500MW onshore wind generator

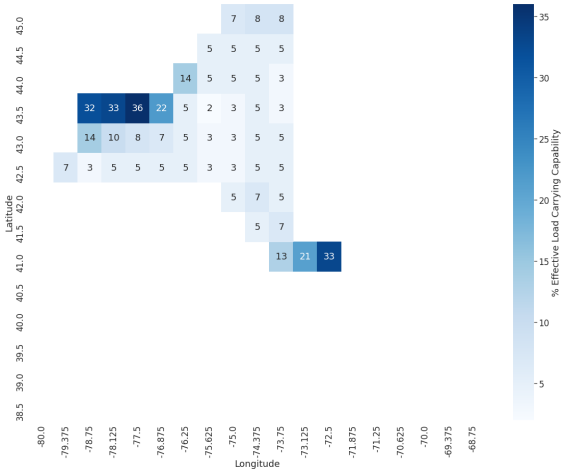

(e) 1000MW onshore wind generator

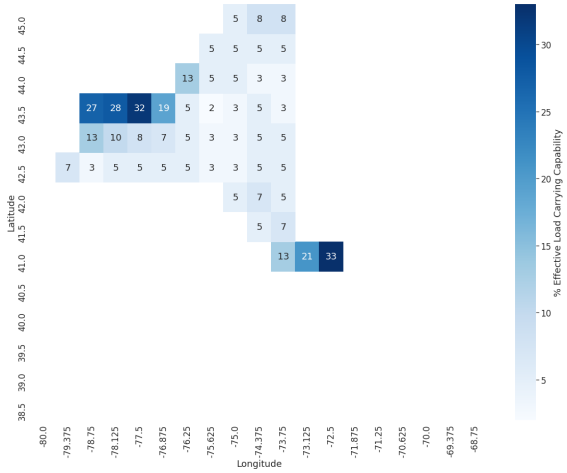

(f) 2000MW onshore wind generator

Figure A.15: Geographical distribution of ELCC values for onshore wind generators over a base fleet representing the High Natural Gas scenario.

Appendix B: Appendix supporting Chapter 3

B.1 Balancing Authority acronyms

The following table denotes Balancing Authority acronyms, their full names, and the state of the largest population center, whose coordinates we used to extract hourly temperature from MERRA database. Note, that some of these BAs are not just utilities, but large Independent System Operators (ISOs) governing multiple states. These 7 ISOs/BAs are:

1. California ISO (CISO), governing the state of CA.

2. New York ISO (NYIS), governing the state of NY.

3. ISO - New England, governing the states of MA, CT, RI, VT, NH, & ME.

4. Electricity Reliability Council of Texas, governing the state of TX.

5. Midcontinent ISO (MISO), governing parts of the states of AR, IL, IN, IA, LA, KY, MI, MN, MS, MO, ND, SD, TX, and WI)

6. Southwest Power Pool (SPP), governing parts of the states of AR, IA, KS, LA, MN, MO, MT, NE, NM, ND, SD, OK, TX, WY, and also provides contract services to parts of AZ, CO, and UT.

7. PJM governing the states of PA, MD, and NJ, and parts of DE, IL, IN, KY, NC, OH, TN, VA, WV, and DC.

Note, in total, North America has 9 ISOs, out of which 7 ISOs participate in managing the electricity requirements of the US, and the other two govern multiple regions in Canada.

Table B.1: Balancing Authorities in the US; their full names and their corresponding acronyms that is used in main paper

Code	Name	State
AEC	PowerSouth Energy Cooperative	AL
AECI	Associated Electric Cooperative, Inc.	MO
AVA	Avista Corporation	WA
AZPS	Arizona Public Service Company	AZ
BANC	Balancing Authority of Northern California	CA
BPAT	Bonneville Power Administration	OR
CHPD	Public Utility District No. 1 of Chelan County	WA
CISO	California Independent System Operator	CA
CPLE	Duke Energy Progress East	NC
CPLW	Duke Energy Progress West	NC
DOPD	PUD No. 1 of Douglas County	WA
DUK	Duke Energy Carolinas	NC
ERCO	Electric Reliability Council of Texas, Inc.	TX
FMPP	Florida Municipal Power Pool	FL
FPC	Duke Energy Florida, Inc.	FL
FPL	Florida Power & Light Co.	FL
GCPD	Public Utility District No. 2 of Grant County, Washington	WA
GVL	Gainesville Regional Utilities	FL
HST	City of Homestead	FL
IID	Imperial Irrigation District	CA
IPCO	Idaho Power Company	ID

ISNE	ISO New England	MA
JEA	JEA	FL
LDWP	Los Angeles Department of Water and Power	CA
LGEE	Louisville Gas and Electric Company and Kentucky Utilities Company	KY
MISO	Midcontinent Independent System Operator, Inc.	IN, IL,
NEVP	Nevada Power Company	NV
NSB	Utilities Commission of New Smyrna Beach	FL
NWMT	NorthWestern Corporation	MT
NYIS	New York Independent System Operator	NY
PACE	PacifiCorp East	OR
PACW	PacifiCorp West	OR
PGE	Portland General Electric Company	OR
PJM	PJM Interconnection, LLC	PA
PNM	Public Service Company of New Mexico	NM
PSCO	Public Service Company of Colorado	CO
PSEI	Puget Sound Energy, Inc.	WA
SC	South Carolina Public Service Authority	SC
SCEG	South Carolina Electric & Gas Company	SC
SCL	Seattle City Light	WA
SOCO	Southern Company Services, Inc. - Trans	GA
SRP	Salt River Project Agricultural Improvement and Power District	AZ
SWPP	Southwest Power Pool	AR
TAL	City of Tallahassee	FL
TEC	Tampa Electric Company	FL
TEPC	Tucson Electric Power	AZ
TIDC	Turlock Irrigation District	CA
TPWR	City of Tacoma, Department of Public Utilities, Light Division	WA

TVA	Tennessee Valley Authority	TN
WACM	Western Area Power Administration - Rocky Mountain Region	CO
WALC	Western Area Power Administration - Desert Southwest Region	AZ
WAUW	Western Area Power Administration - Upper Great Plains West	MT

B.2 Model Validation

The model validation process included testing both Piecewise Linear Regression (PLR) and LSTM model on the validation set while testing several model hyper-parameters for each of the 53 BAs. Our aim was to calibrate both models to achieve best performance on three evaluation metrics described in the main text, i.e., the Root Mean Squared Error (RMSE) value, the adjusted Coefficient of Determination or R^2 value, and the Mean Absolute Percentage Error (MAPE) value, while ensuring that the selected hyper-parameters lead to maximum generalizability in all BAs. The challenge in this technique is to carefully understand the trade-off between choosing the best hyper-parameters for a single BA vs. choosing hyper-parameters that lead to optimal performance of our models for all BAs.

The hyper-parameters that were tuned during this process were the temperature bins in the Piecewise Linear Regression model, which helps in preserving the continuity between break-points of the estimated mathematical function and thus helps in capturing the non-linear relationship between temperature and electricity demand. These bins were determined by plotting the distribution of temperature data to understand how it changed. Different bin sizes were tested to derive a generalized form that is applicable to all BAs. The selected temperature bins were:

- < 0
- 0 - 5
- 5 - 10
- 10 - 15

Hyper-parameter type	Value
Number of stacked layers	2
Learning Rate	0.009
Epochs	2500
Optimizer	Adam
Dropout probability	0.2
Time taken per epoch	143 sec

Table B.2: Optimal Hyper-parameters chosen for the LSTM model architecture

- 15 - 20
- 20 - 30
- 30 - 45
- > 45

On the other hand, for the LSTM network had more number of hyper-parameters involved due to its considerable depth and network width. Several We changed the number of stacked LSTM layers between 2 to 4, and analyzed the performance against the validation set to arrive at the optimal number of stacked LSTM layers, i.e. 2. Furthermore, we also experimented with regularization techniques, such as Dropout (Srivastava et al., 2014), i.e., 'dropping' or ignoring some neurons at random during the training phase. We experimented with dropout values between 0 - 0.5. We also experimented with Stochastic Gradient Descent and Adam optimizers while changing the total number of epochs. Validating our results for the several hyper-parameters using our validation set, we arrived at the optimal set (Table B.2).

B.3 Top 20 demand hours for all Balancing Authorities

For both summer and winter peaking systems, the extent of building capacity reserves for reliability is driven by largest demand hours. In Chapter 3, Figure 3.5, we showed the largest 20 demand hours plotted for the top 8 Balancing Authorities, ranked in their order of amount of electricity consumption.

In Figures B.1, B.2, B.3, and B.4, we show the top twenty demand hours for all other Balancing Authorities (after removing the BAs which did not show a smooth temperature and load relationship; and also resulted in very low validation performance - Table 4.1).

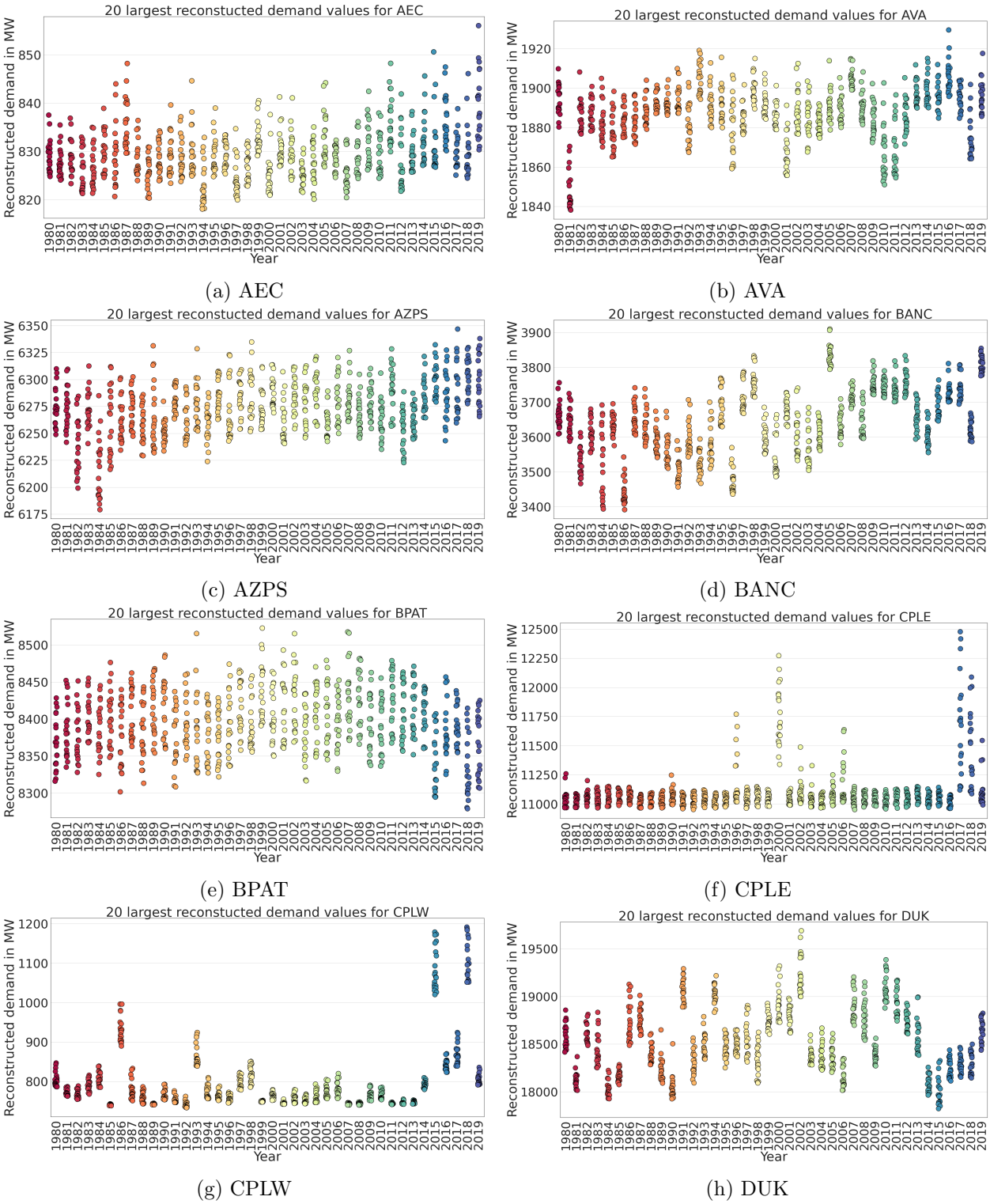

(a) AEC (b) AVA

(c) AZPS (d) BANC

(e) BPAT (f) CPLE

(g) CPLW (h) DUK

Figure B.1: Hourly temperature values corresponding to the reconstructed top 20 demand hours between 1980 - 2019 segregated by months (colored) for BAs of the US.

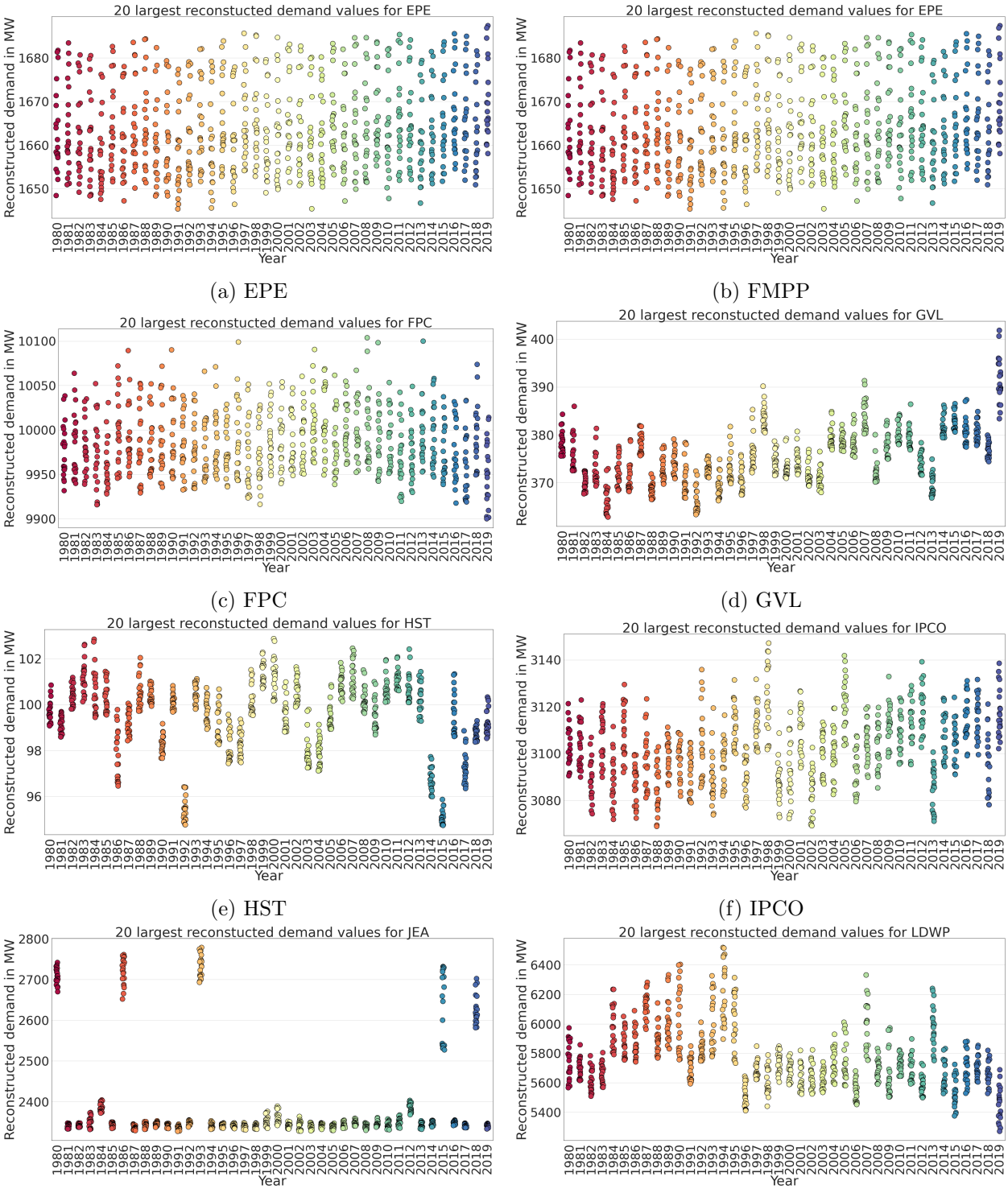

(a) EPE (b) FMPP (c) FPC (d) GVL (e) HST (f) IPCO (g) JEA (h) LDWP

Figure B.2: Hourly demand values corresponding to the reconstructed top 20 demand hours between 1980 - 2019 segregated by months (colored) for BAs of the US.

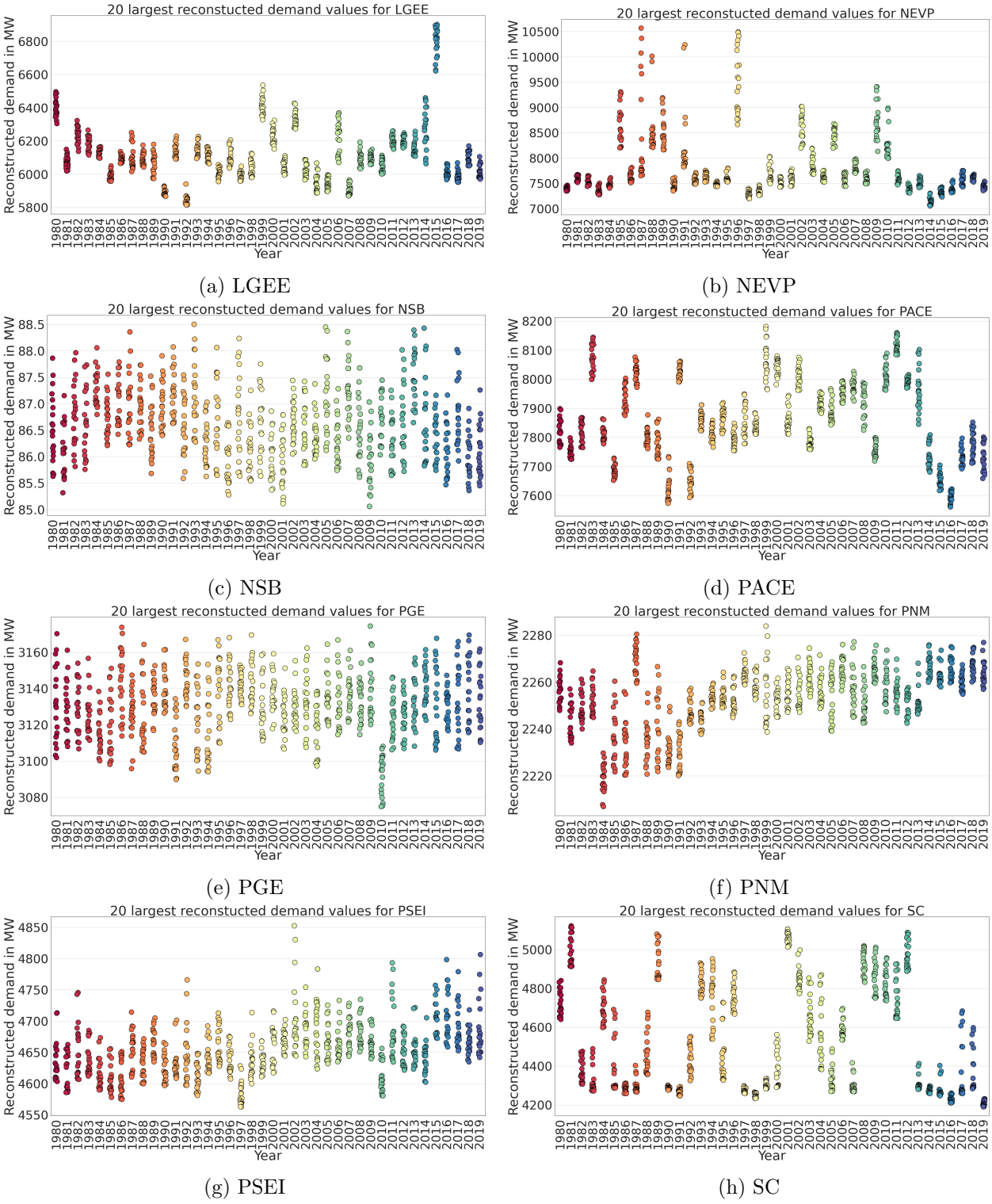

(a) LGEE (b) NEVP (c) NSB (d) PACE (e) PGE (f) PNM (g) PSEI (h) SC

Figure B.3: Hourly top 20 demand hours between 1980 - 2019 for Balancing Authorities (in alphabetical order) of the US.

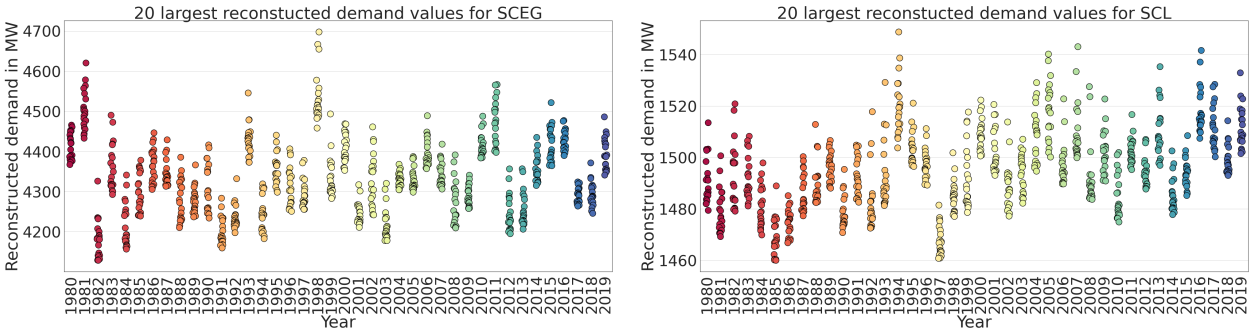

(a) SCEG

(b) SCL

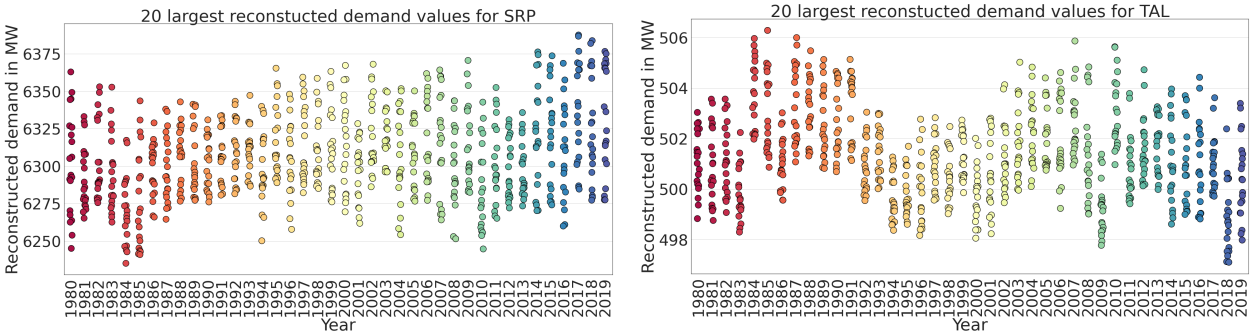

(c) SRP

(d) TAL

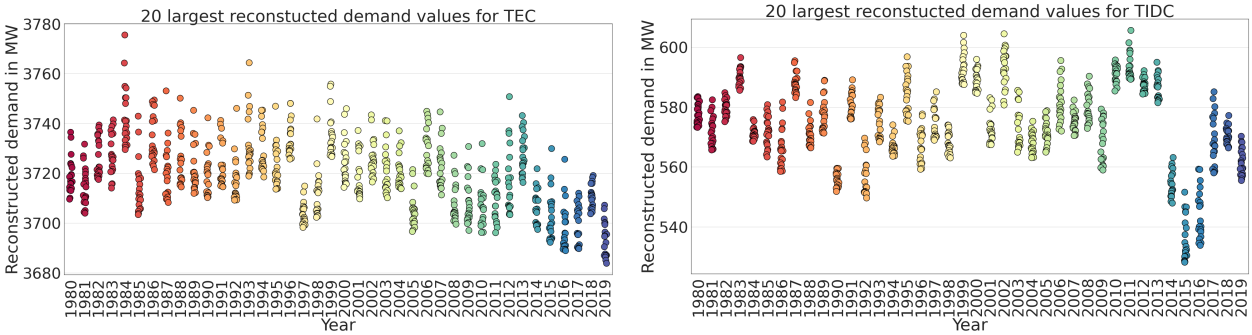

(e) TEC

(f) TIDC

Figure B.4: Hourly top 20 demand hours between 1980 - 2019 of Balancing Authorities of the US.

Appendix C: Appendix supporting Chapter 4

C.1 ELCC Maps for ISO-NE, CAISO, and ERCOT

The geographical distribution of ELCC values of a 100-MW solar, onshore wind, and offshore wind generator added to every grid cell (50km x 60km) within the footprint of Independent System Operator of New England (ISO - NE), California - Independent System Operator (CA- ISO), and Electricity Reliability Council of Texas (ERCOT) have been shown below for each of the 40 years of study (1980 - 2019).

Within each year, the spatial heterogeneity in ELCC values is directly driven by the change in capacity factors of solar and wind resources across the longitudes of the BA, that is if we go farther away from the shore and up north (across latitudes) the wind capacity factors become larger. Solar capacity factors within the footprint of ISO-NE and CAISO remain fairly constant, but for the case of ERCOT, which is larger in size and is also located further south from the other two BAs, the solar irradiance potential increases. The solar capacity factors, which are larger in magnitude in Texas region, also changes by relatively larger amount across grid cells as compared to ISO-NE and CAISO.

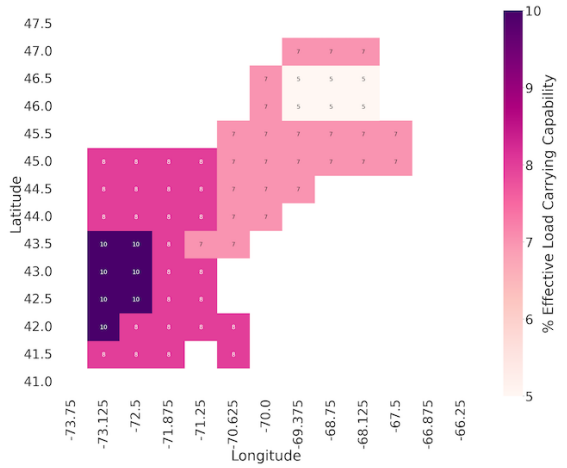

(a) ELCC value of 100-MW solar generator in 1980

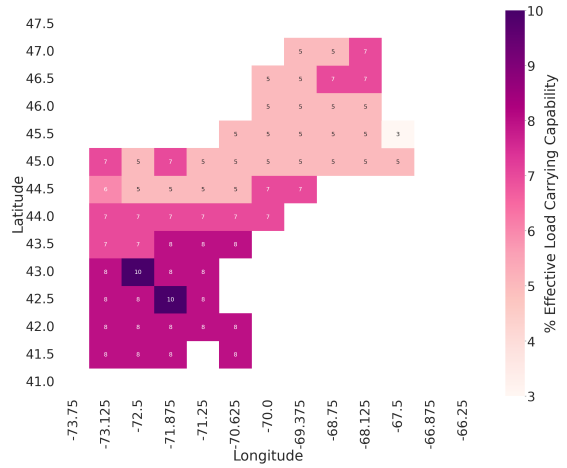

(b) ELCC value of 100-MW solar generator in 1981

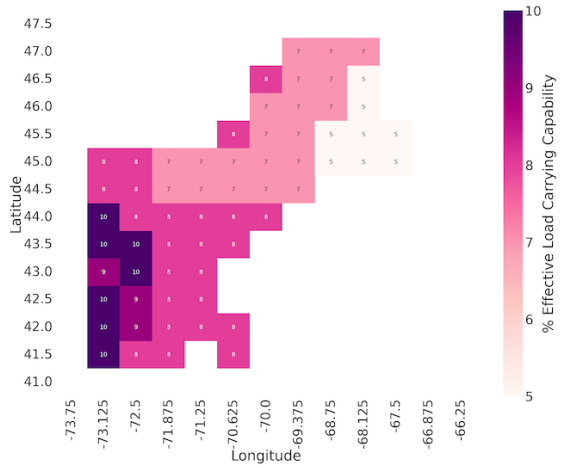

(c) ELCC value of 100-MW solar generator in 1982

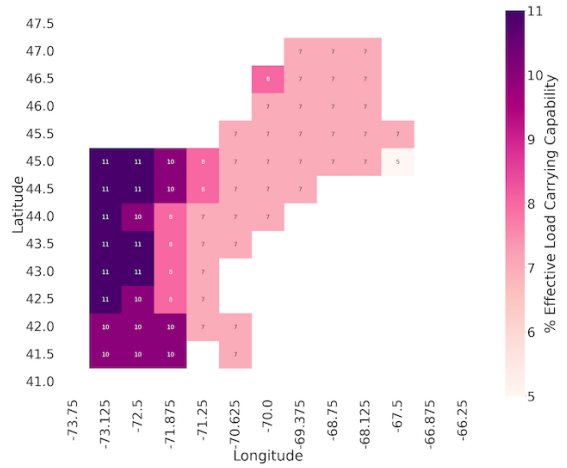

(d) ELCC value of 100-MW solar generator in 1983

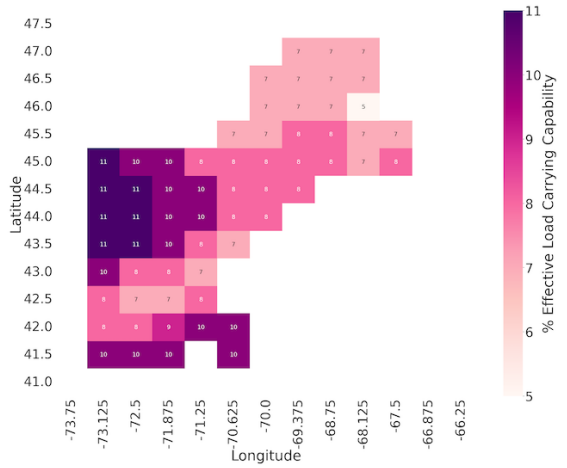

(e) ELCC value of 100-MW solar generator in 1985

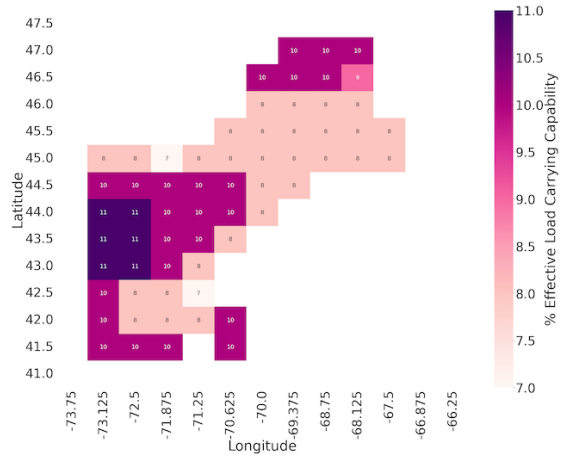

(f) ELCC value of 100-MW solar generator in 1985

Figure C.1: Geographical distribution of ELCC values between 1980 -1985 for a new 100-MW offshore wind generator added to the existing base fleet from 2019 of IS0-New England.

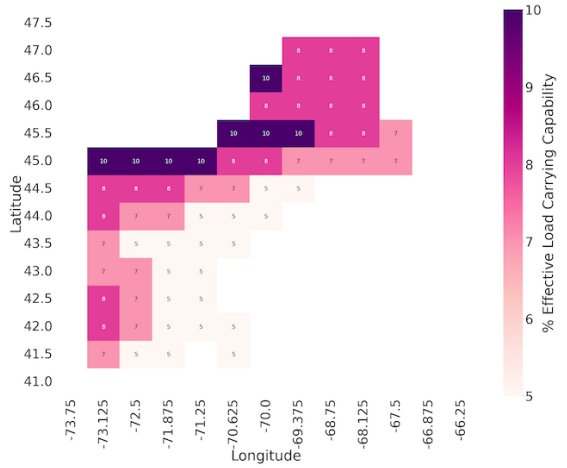

(a) ELCC value of 100-MW solar generator in 1986

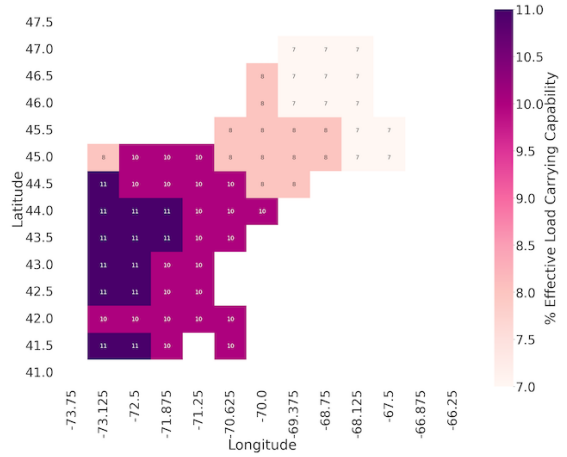

(b) ELCC value of 100-MW solar generator in 1987

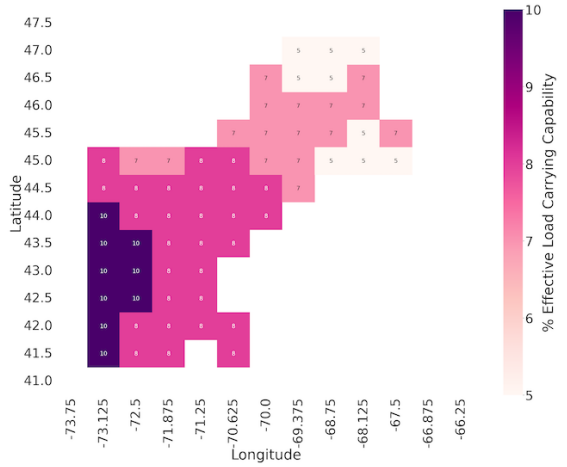

(c) ELCC value of 100-MW solar generator in 1988

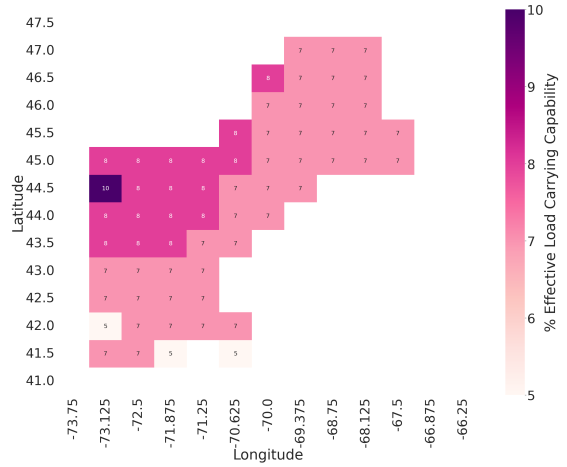

(d) ELCC value of 100-MW solar generator in 1989

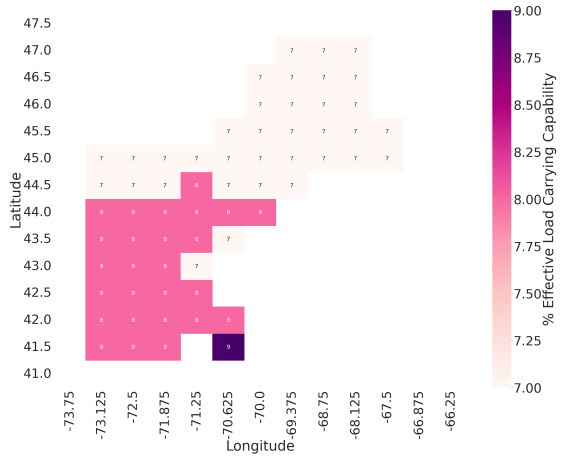

(e) ELCC value of 100-MW solar generator in 1990

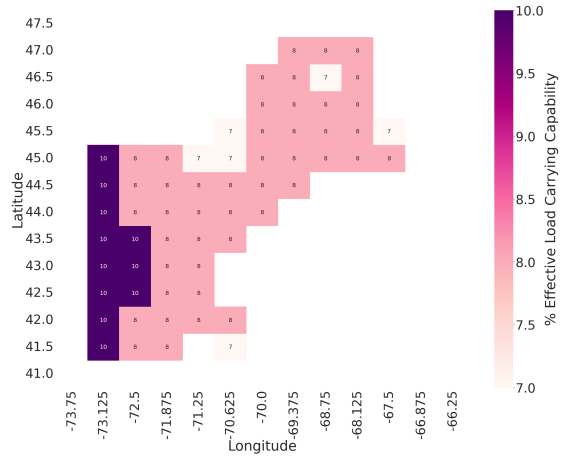

(f) ELCC value of 100-MW solar generator in 1991

Figure C.2: Geographical distribution of ELCC values between 1986 -1991 for a new 100-MW offshore wind generator added to the existing base fleet from 2019 of IS0-New England.

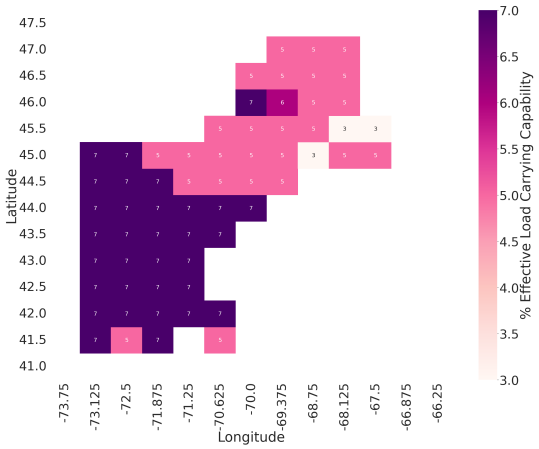

(a) ELCC value of 100-MW solar generator in 1992

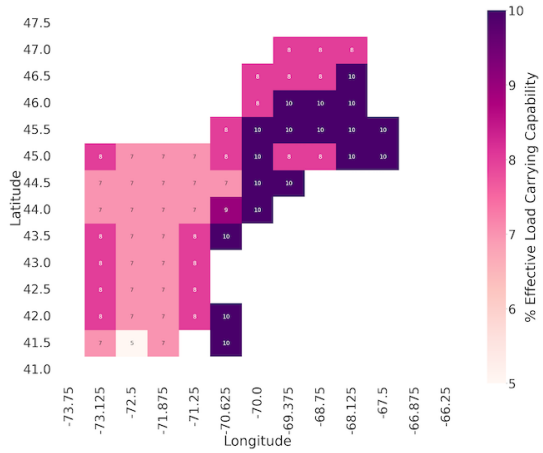

(b) ELCC value of 100-MW solar generator in 1993

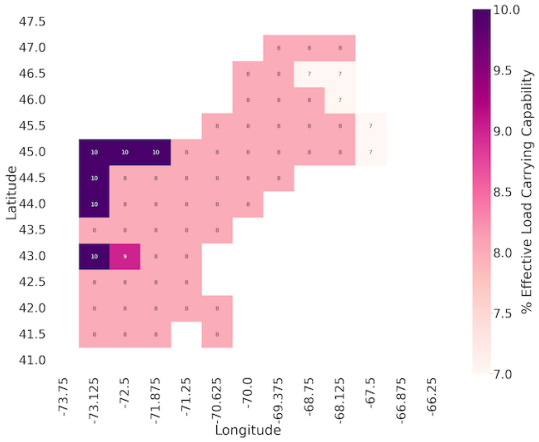

(c) ELCC value of 100-MW solar generator in 1994

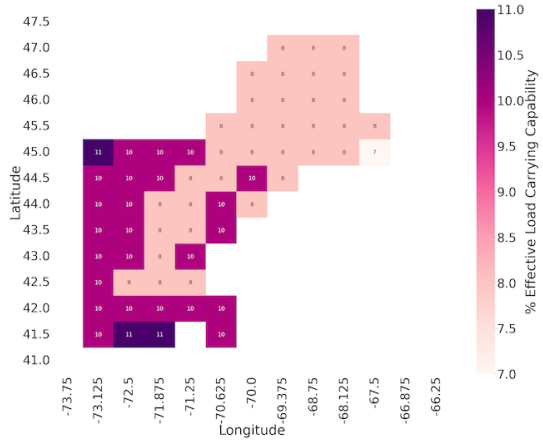

(d) ELCC value of 100-MW solar generator in 1995

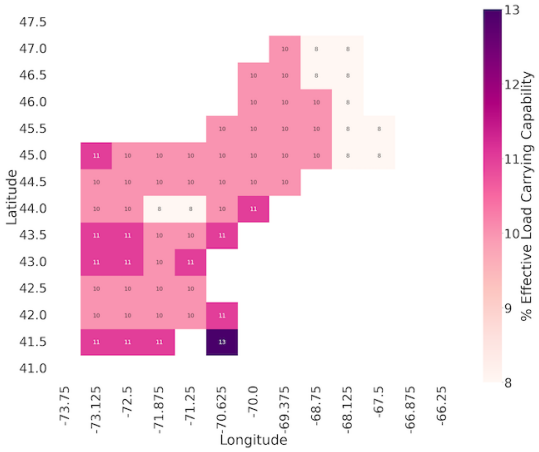

(e) ELCC value of 100-MW solar generator in 1996

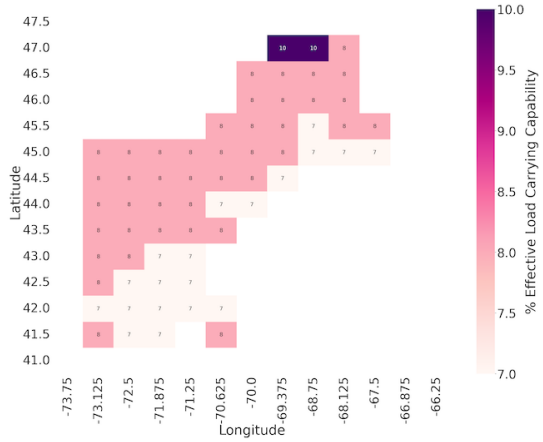

(f) ELCC value of 100-MW solar generator in 1997

Figure C.3: Geographical distribution of ELCC values between 1992 -1997 for a new 100-MW offshore wind generator added to the existing base fleet from 2019 of IS0-New England.

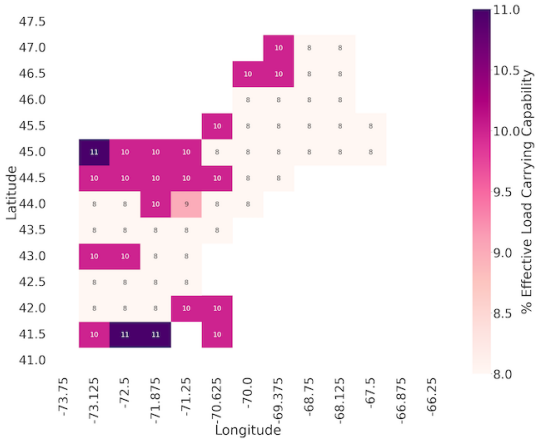

(a) ELCC value of 100-MW solar generator in 1998

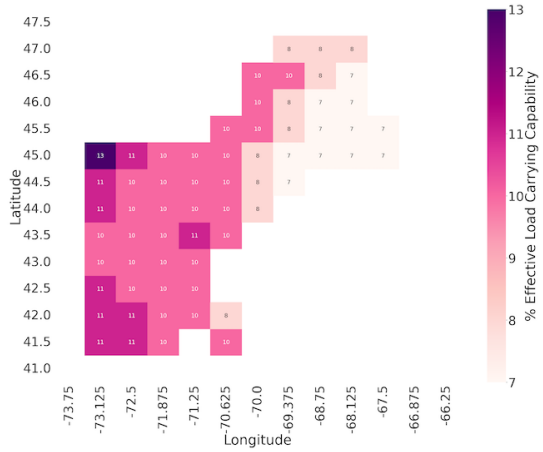

(b) ELCC value of 100-MW solar generator in 1999

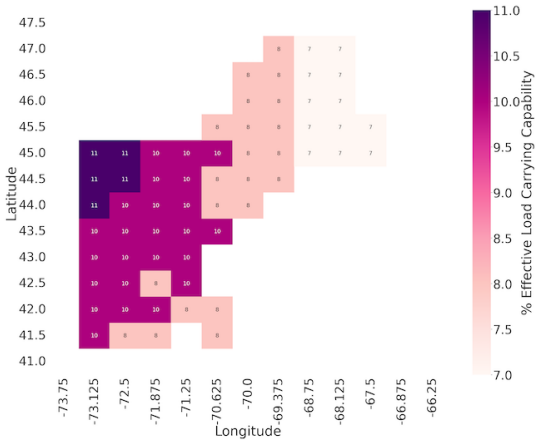

(c) ELCC value of 100-MW solar generator in 2000

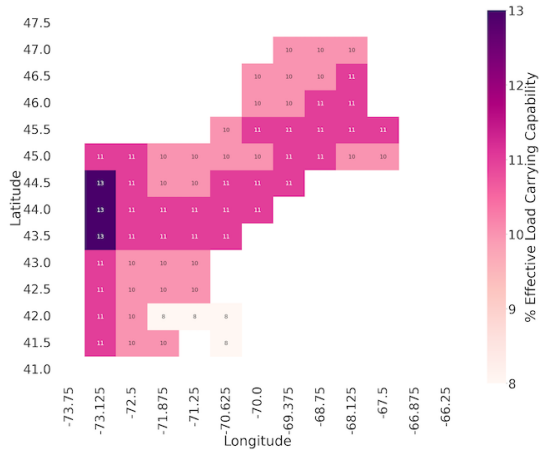

(d) ELCC value of 100-MW solar generator in 2001

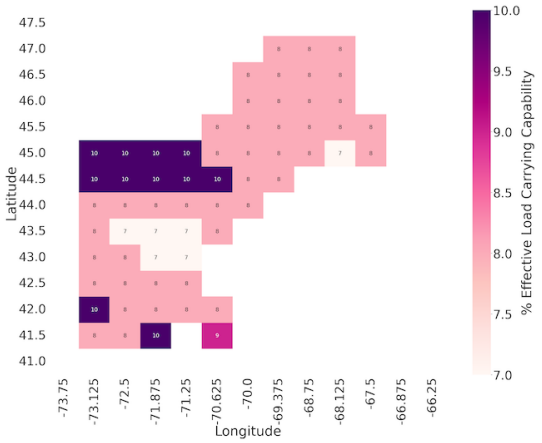

(e) ELCC value of 100-MW solar generator in 2002

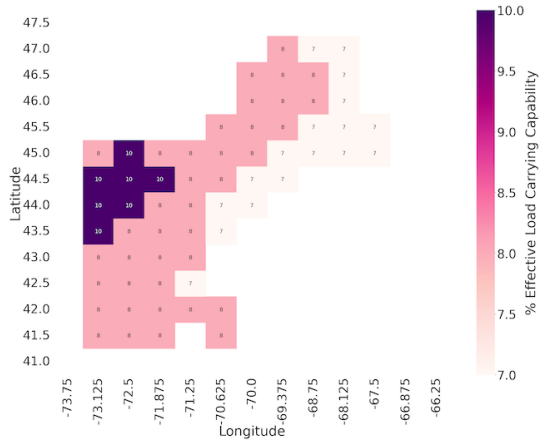

(f) ELCC value of 100-MW solar generator in 2003

Figure C.4: Geographical distribution of ELCC values between 1998 - 2003 for a new 100-MW offshore wind generator added to the existing base fleet from 2019 of IS0-New England.

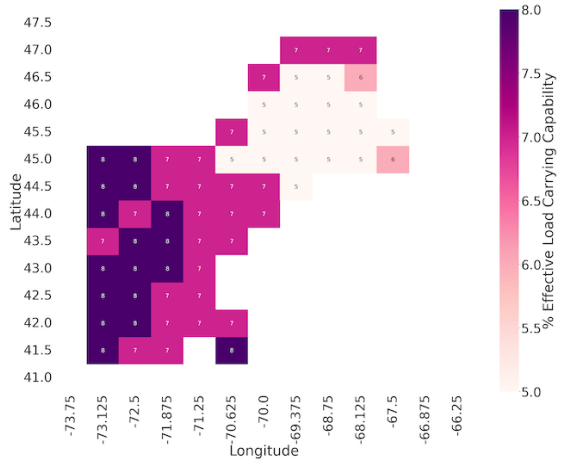

(a) ELCC value of 100-MW solar generator in 2004

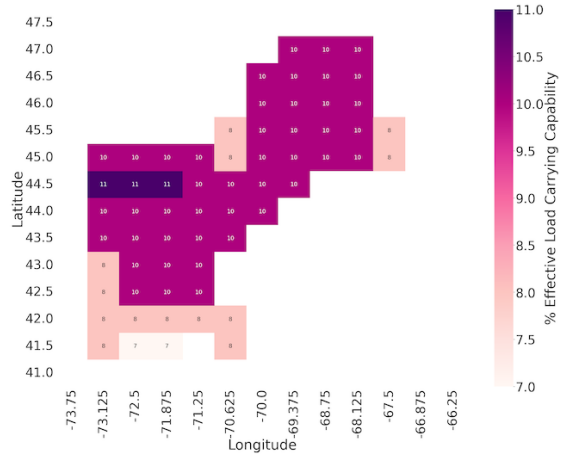

(b) ELCC value of 100-MW solar generator in 2005

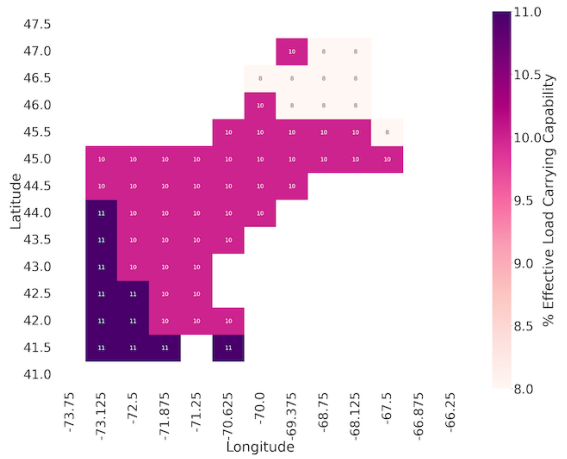

(c) ELCC value of 100-MW solar generator in 2006

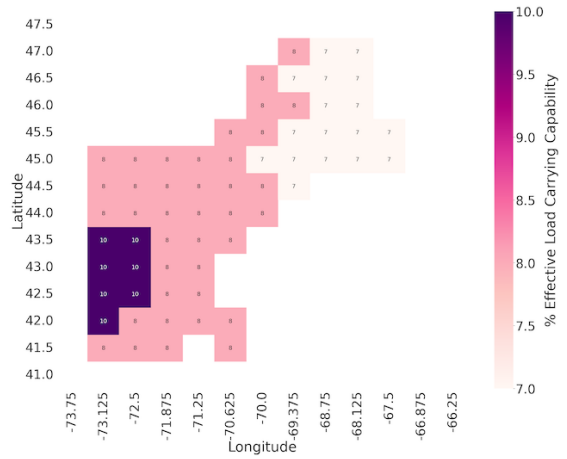

(d) ELCC value of 100-MW solar generator in 2007

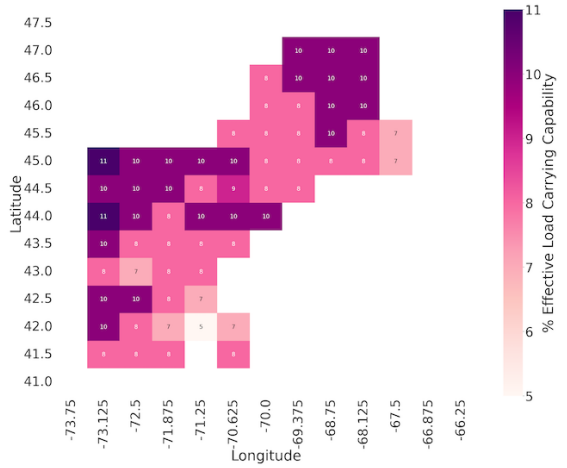

(e) ELCC value of 100-MW solar generator in 2008

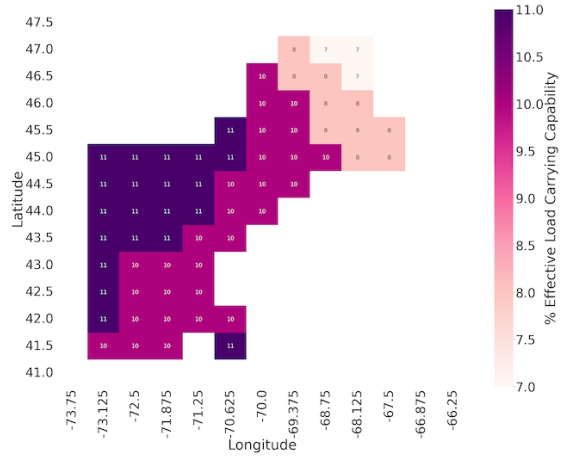

(f) ELCC value of 100-MW solar generator in 2009

Figure C.5: Geographical distribution of ELCC values between 2004 - 2009 for a new 100-MW offshore wind generator added to the existing base fleet from 2019 of IS0-New England.

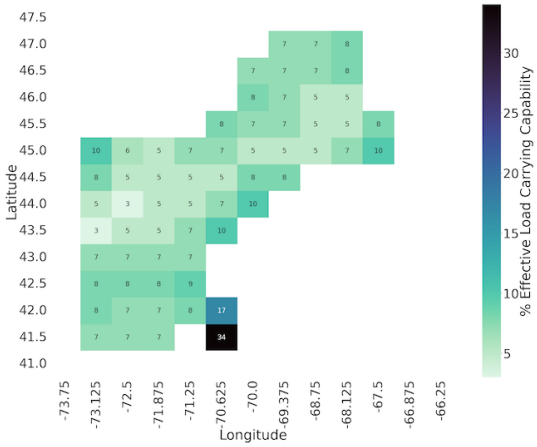

(a) ELCC of 100-MW onshore wind generator, 1980

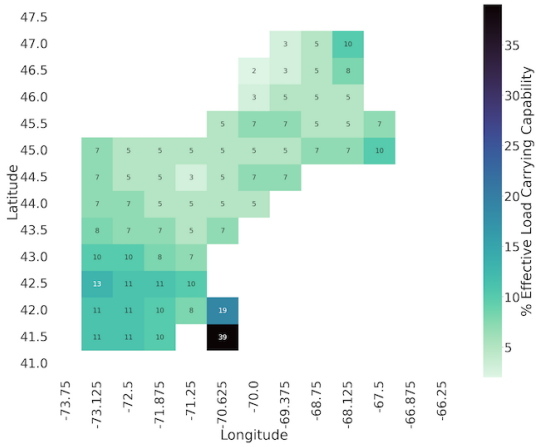

(b) ELCC of 100-MW onshore wind generator, 1981

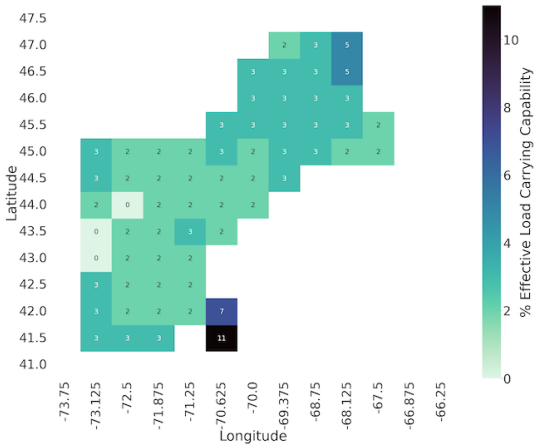

(c) ELCC of 100-MW onshore wind generator, 1982

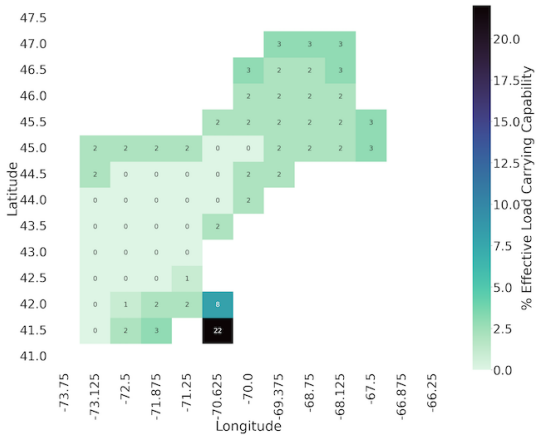

(d) ELCC of 100-MW onshore wind generator, 1983

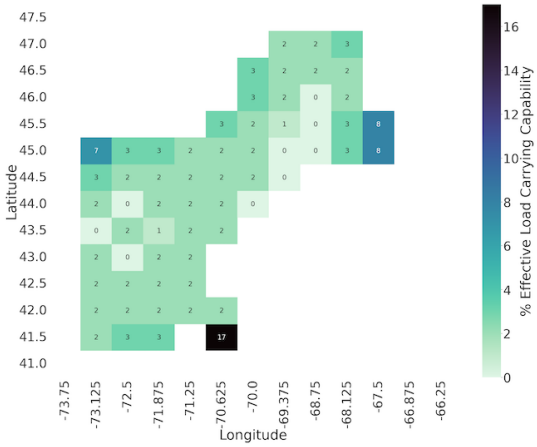

(e) ELCC of 100-MW onshore wind generator, 1984

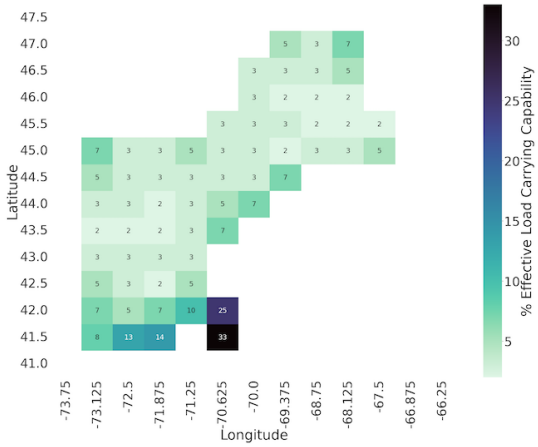

(f) ELCC of 100-MW onshore wind generator, 1985

Figure C.6: Geographical distribution of ELCC values between 1980 -1985 for a new 100-MW onshore wind generator added to the existing base fleet from 2019 of IS0-New England.

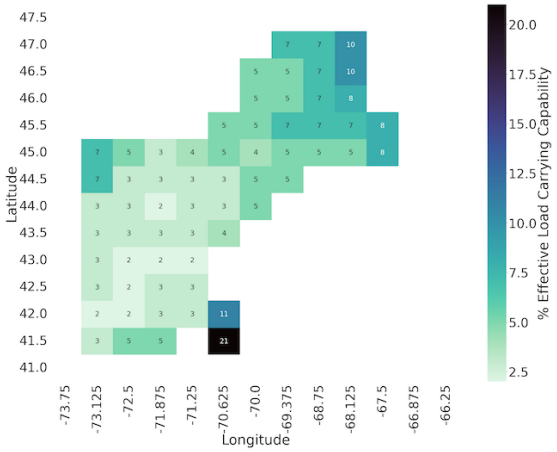

(a) ELCC of 100-MW onshore wind generator, 1986

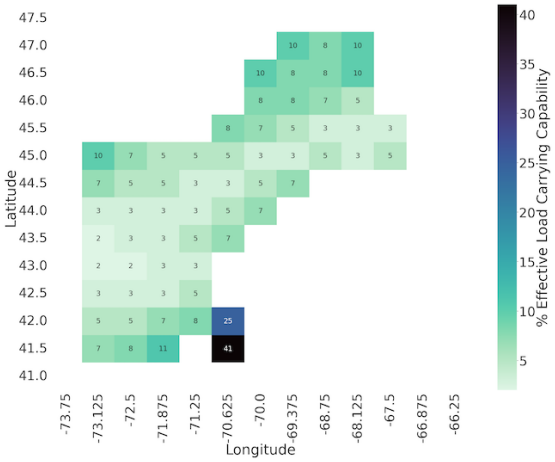

(b) ELCC of 100-MW onshore wind generator, 1987

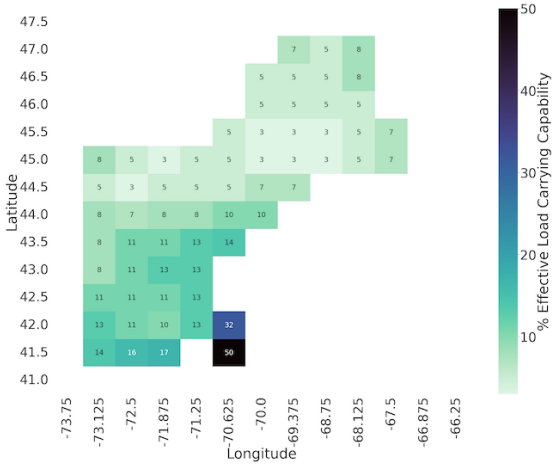

(c) ELCC of 100-MW onshore wind generator, 1988

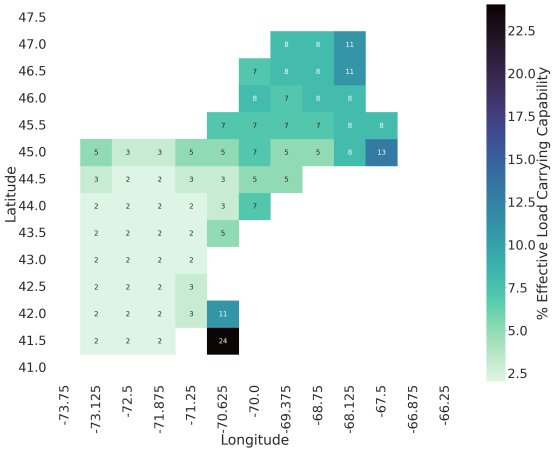

(d) ELCC of 100-MW onshore wind generator, 1989

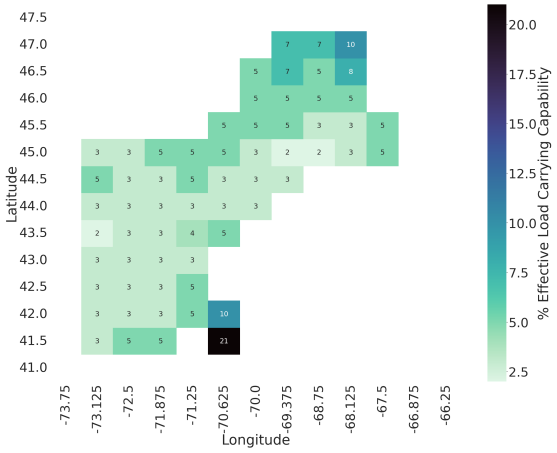

(e) ELCC of 100-MW onshore wind generator, 1990

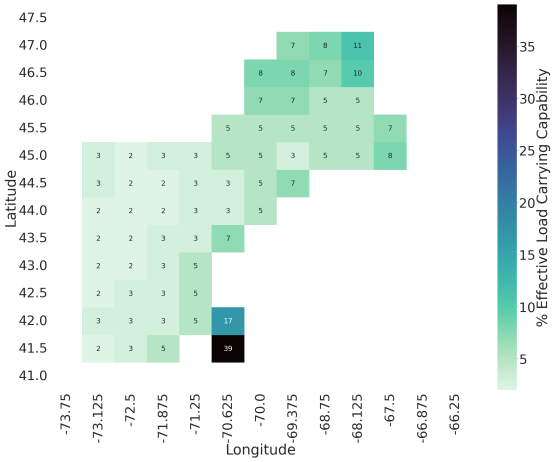

(f) ELCC of 100-MW onshore wind generator, 1991

Figure C.7: Geographical distribution of ELCC values between 1986 -1991 for a new 100-MW onshore wind generator added to the existing base fleet from 2019 of IS0-New England.

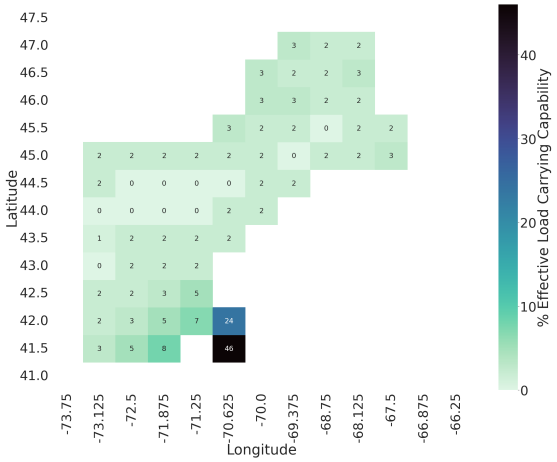

(a) ELCC of 100-MW onshore wind generator, 1992

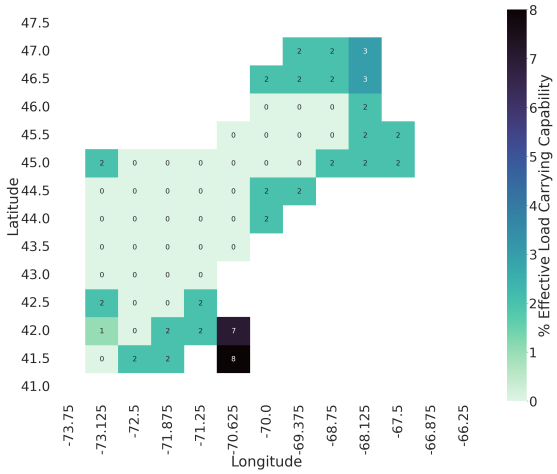

(b) ELCC of 100-MW onshore wind generator, 1993

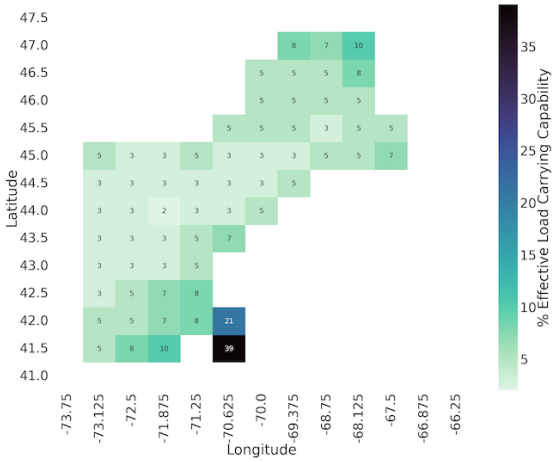

(c) ELCC of 100-MW onshore wind generator, 1994

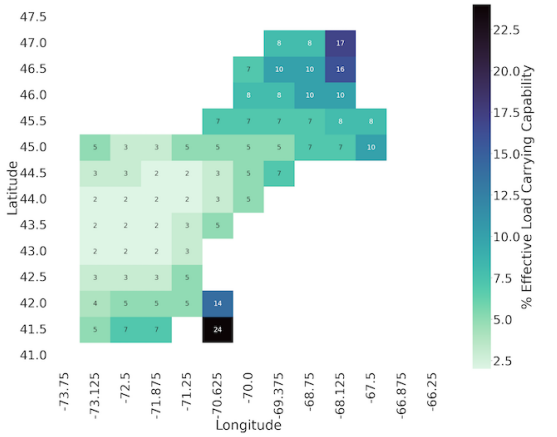

(d) ELCC of 100-MW onshore wind generator, 1995

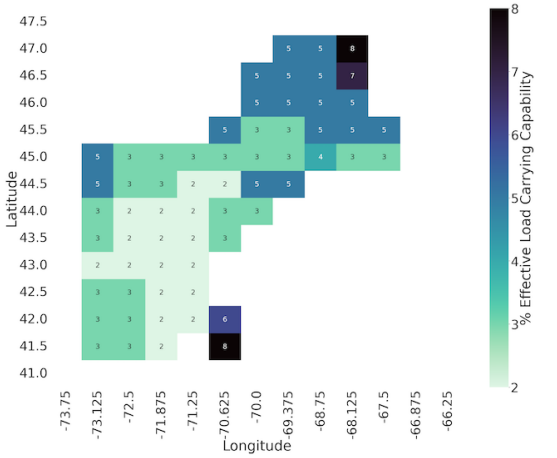

(e) ELCC of 100-MW onshore wind generator, 1996

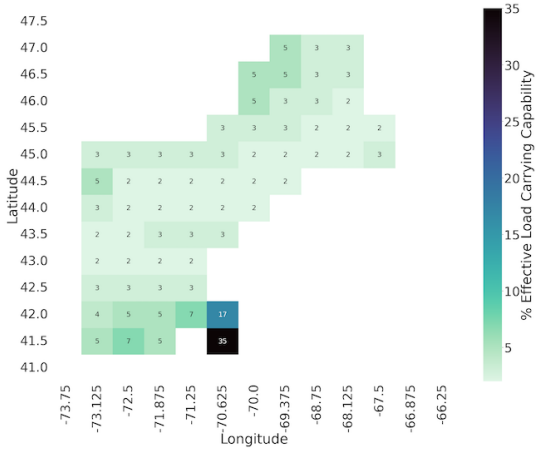

(f) ELCC of 100-MW onshore wind generator, 1997

Figure C.8: Geographical distribution of ELCC values between 1992 -1997 for a new 100-MW onshore wind generator added to the existing base fleet from 2019 of IS0-New England.

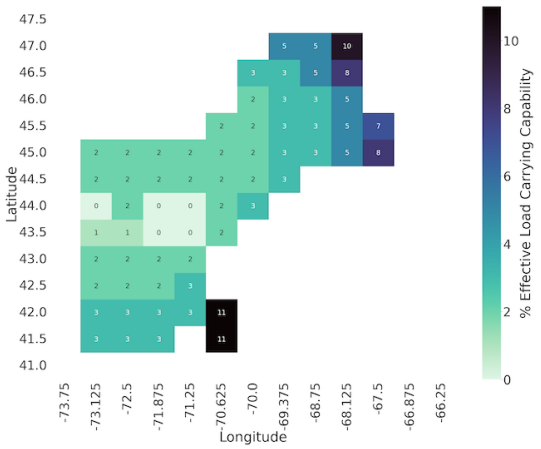

(a) ELCC of 100-MW onshore wind generator, 1998

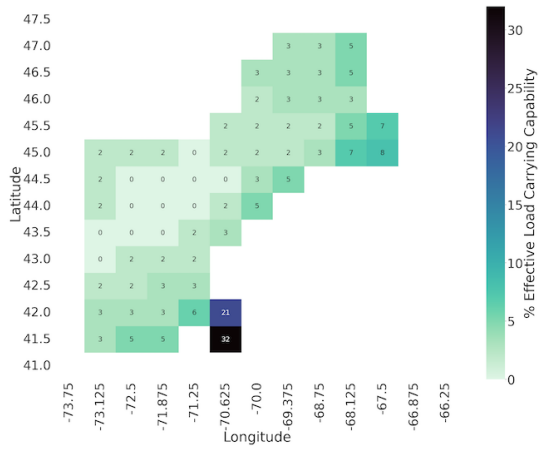

(b) ELCC of 100-MW onshore wind generator, 1999

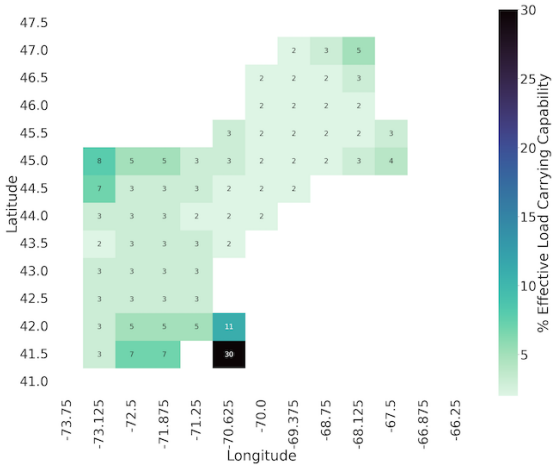

(c) ELCC of 100-MW onshore wind generator, 2000

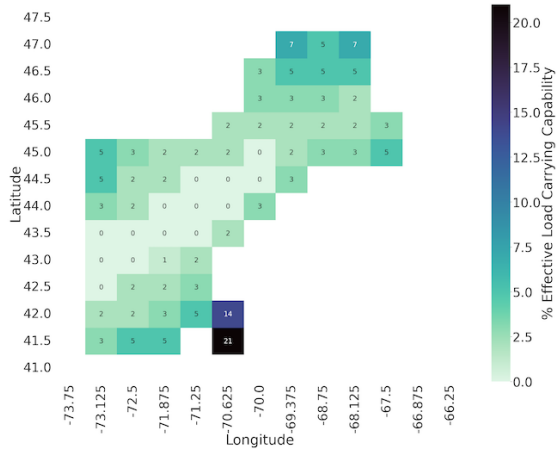

(d) ELCC of 100-MW onshore wind generator, 2001

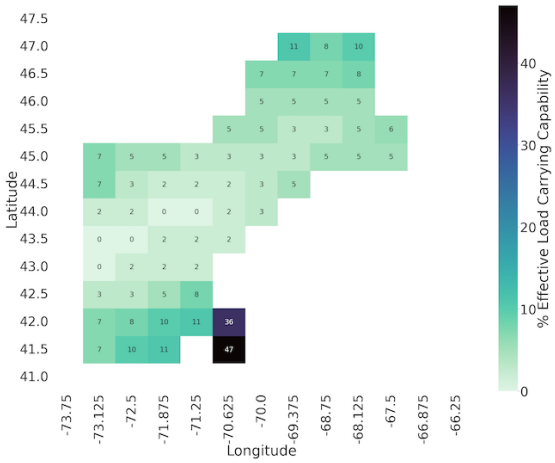

(e) ELCC of 100-MW onshore wind generator, 2002

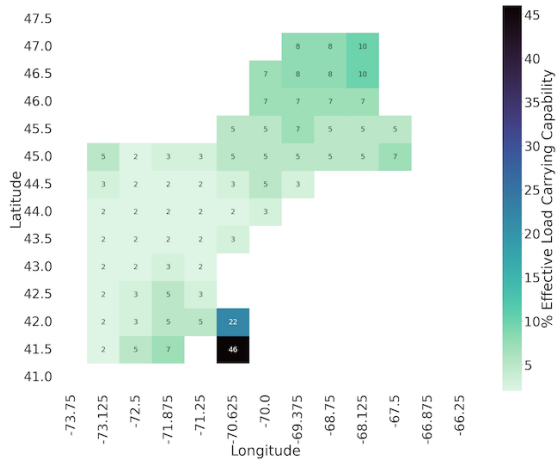

(f) ELCC of 100-MW onshore wind generator, 2003

Figure C.9: Geographical distribution of ELCC values between 1998 - 2003 for a new 100-MW onshore wind generator added to the existing base fleet from 2019 of IS0-New England.

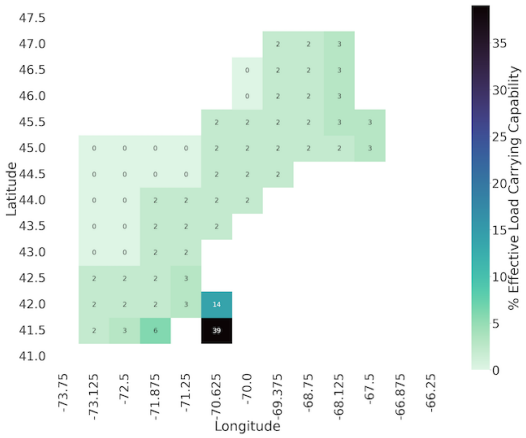

(a) ELCC of 100-MW onshore wind generator, 2004

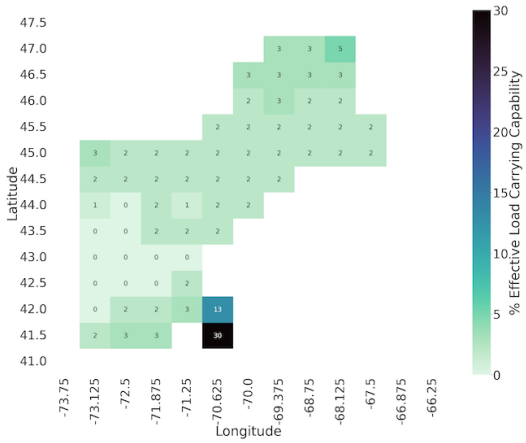

(b) ELCC of 100-MW onshore wind generator, 2005

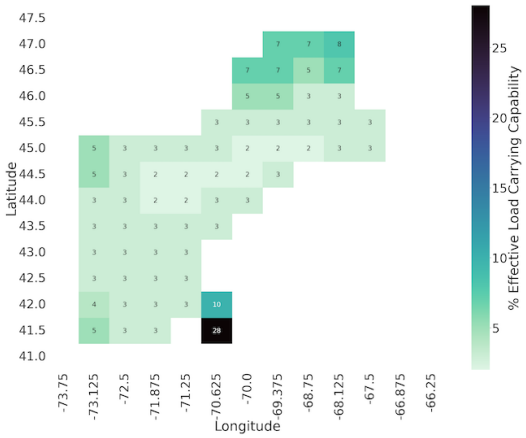

(c) ELCC of 100-MW onshore wind generator, 2006

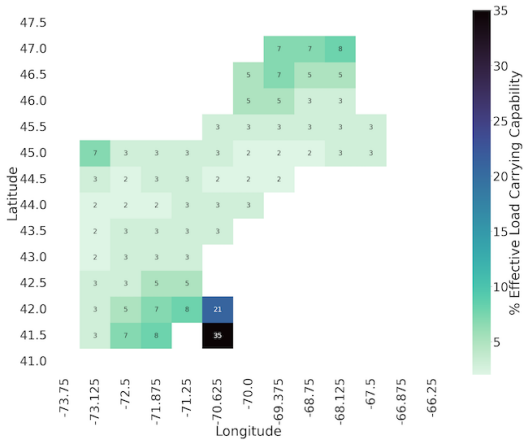

(d) ELCC of 100-MW onshore wind generator, 2007

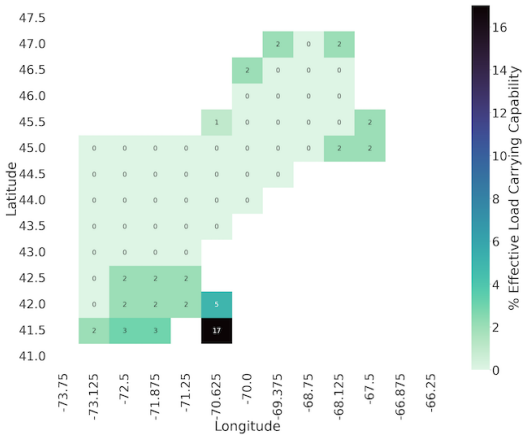

(e) ELCC of 100-MW onshore wind generator, 2008

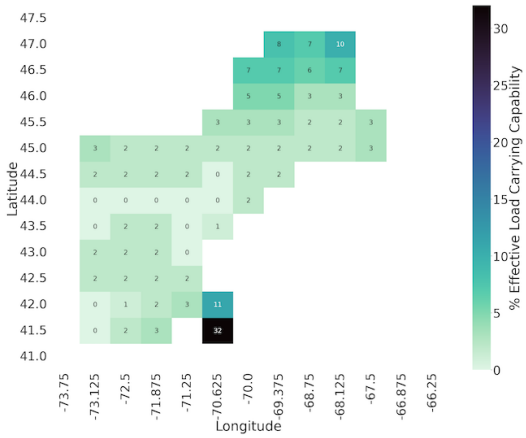

(f) ELCC of 100-MW onshore wind generator, 2009

Figure C.10: ELCC values between 2004-2009 for a new 100-MW onshore wind generator added to the existing base fleet of IS0-New England.

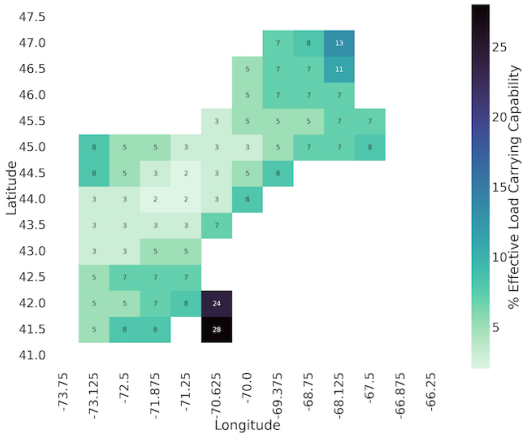

(a) ELCC of 100-MW onshore wind generator, 2010

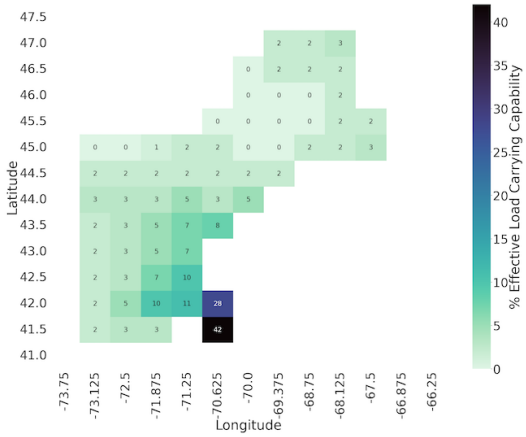

(b) ELCC of 100-MW onshore wind generator, 2011

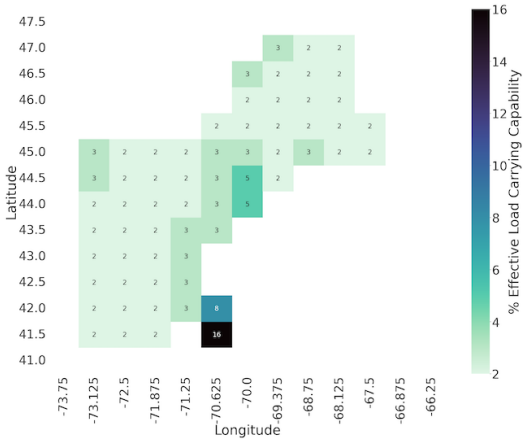

(c) ELCC of 100-MW onshore wind generator, 2012

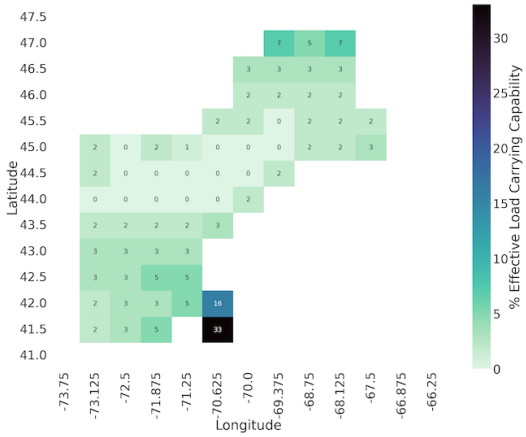

(d) ELCC of 100-MW onshore wind generator, 2013

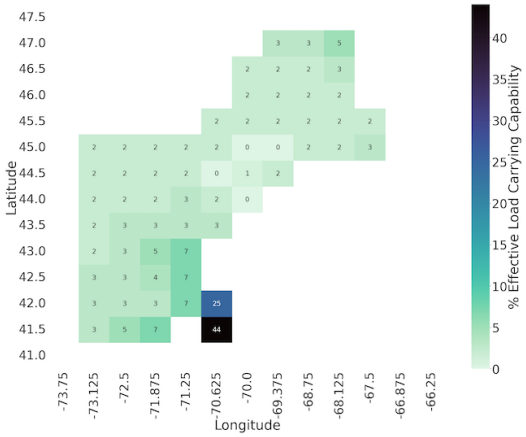

(e) ELCC of 100-MW onshore wind generator, 2014

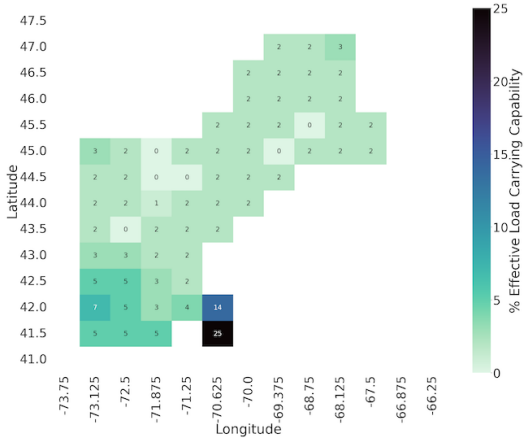

(f) ELCC of 100-MW onshore wind generator, 2015

Figure C.11: ELCC values between 2010 - 2014 for a new 100-MW onshore wind generator added to the existing base fleet from 2019 of ISNE.

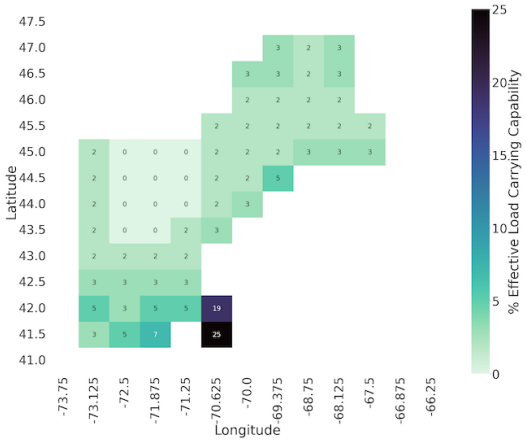

(a) ELCC of 100-MW onshore wind generator, 2016

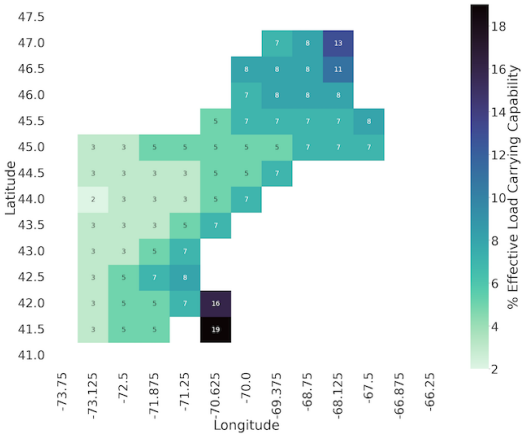

(b) ELCC of 100-MW onshore wind generator, 2017

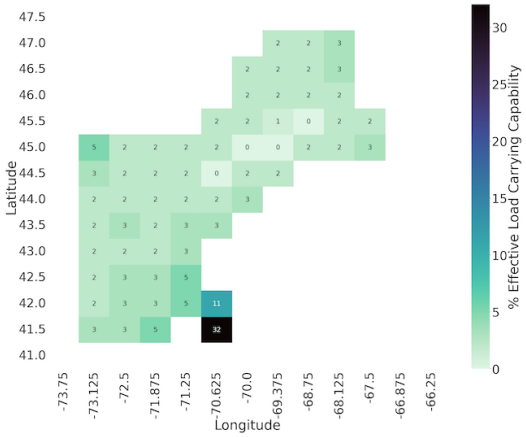

(c) ELCC of 100-MW onshore wind generator, 2018

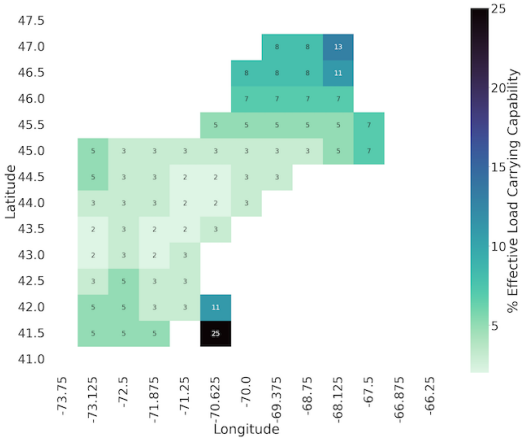

(d) ELCC of 100-MW onshore wind generator, 2019

Figure C.12: Geographical distribution of ELCC values between 2016 - 2019 for a new 100-MW onshore wind generator added to the existing base fleet from 2019 of IS0-New England.

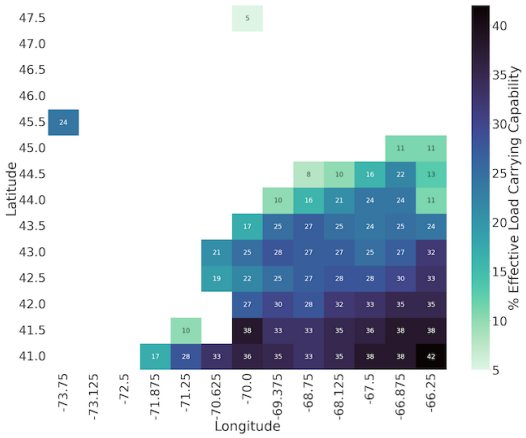

(a) ELCC of 100-MW offshore wind generator, 1980

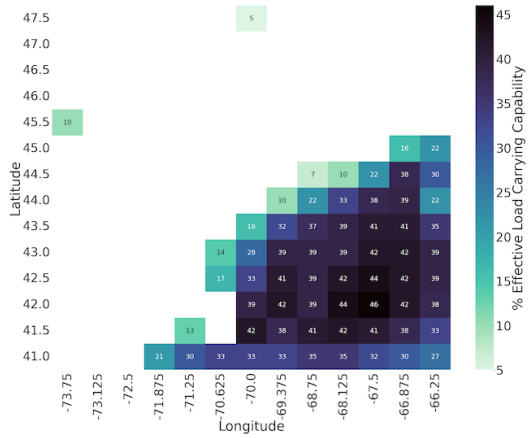

(b) ELCC of 100-MW offshore wind generator, 1981

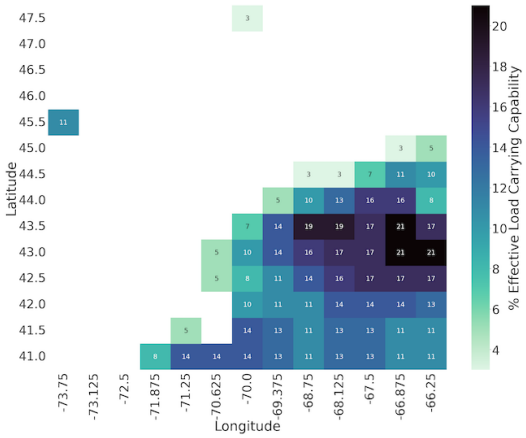

(c) ELCC of 100-MW offshore wind generator, 1982

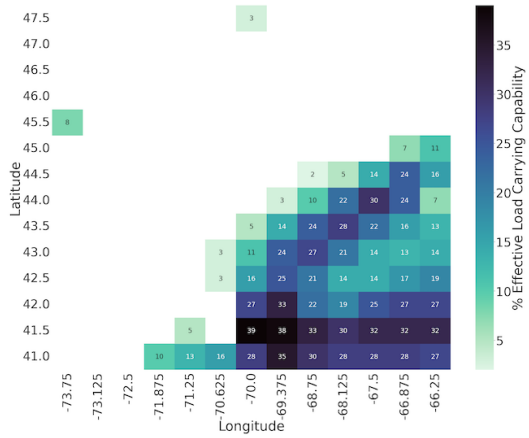

(d) ELCC of 100-MW offshore wind generator, 1983

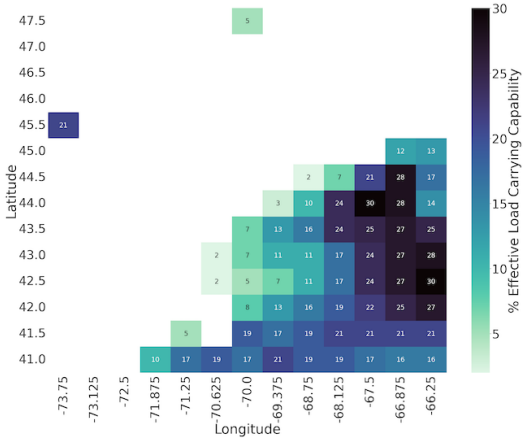

(e) ELCC of 100-MW offshore wind generator, 1984

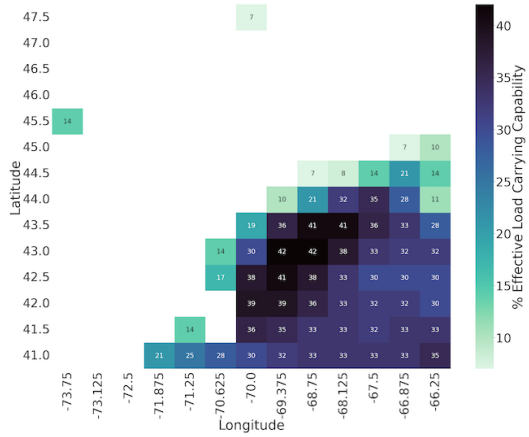

(f) ELCC of 100-MW offshore wind generator, 1985

Figure C.13: Geographical distribution of ELCC values between 1980 -1985 for a new 100-MW offshore wind generator added to the existing base fleet from 2019 of IS0-New England.

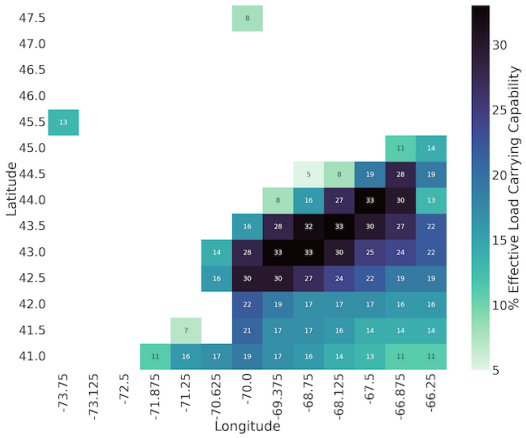

(a) ELCC of 100-MW offshore wind generator, 1986

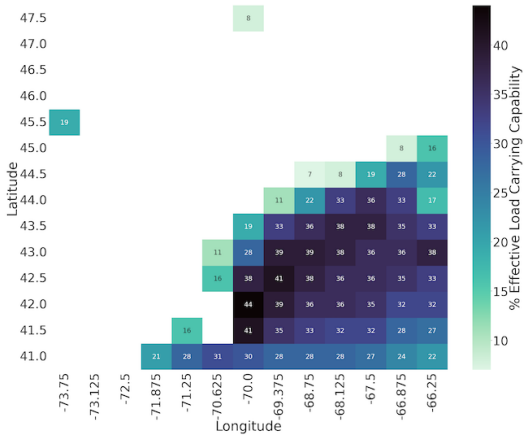

(b) ELCC of 100-MW offshore wind generator, 1987

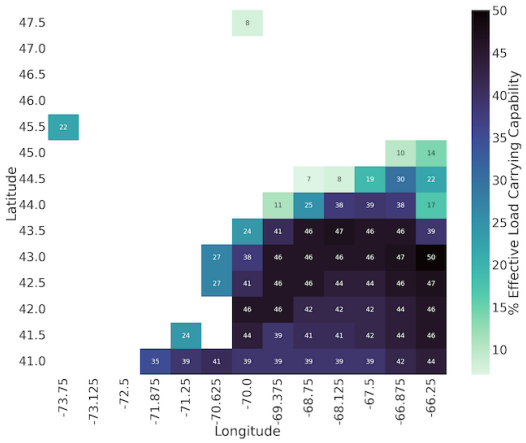

(c) ELCC of 100-MW offshore wind generator, 1988

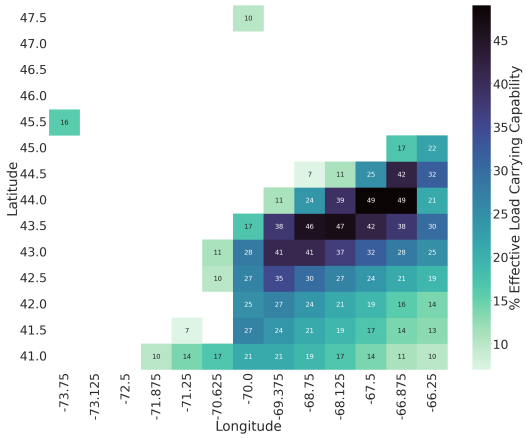

(d) ELCC of 100-MW offshore wind generator, 1989

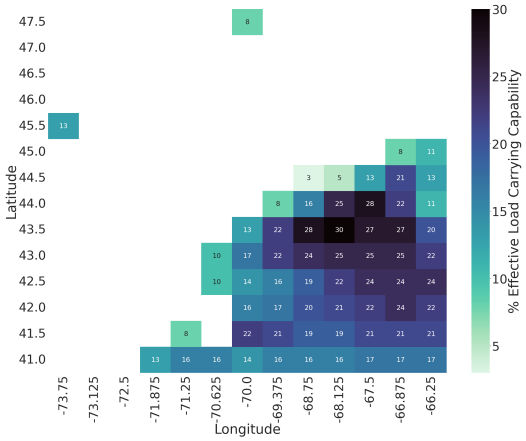

(e) ELCC of 100-MW offshore wind generator, 1990

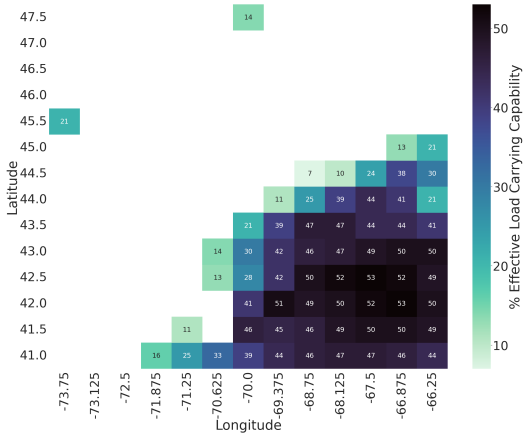

(f) ELCC of 100-MW offshore wind generator, 1991

Figure C.14: Geographical distribution of ELCC values between 1986 -1991 for a new 100-MW offshore wind generator added to the existing base fleet from 2019 of IS0-New England.

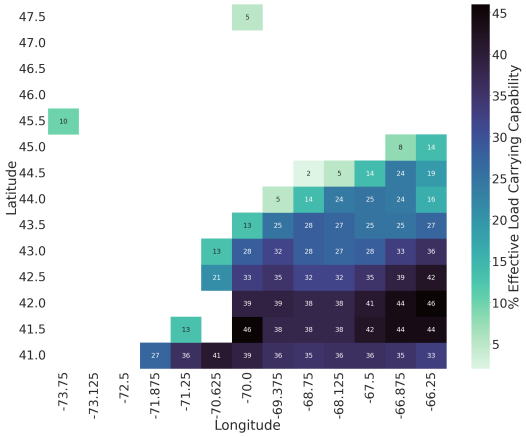

(a) ELCC of 100-MW offshore wind generator, 1992

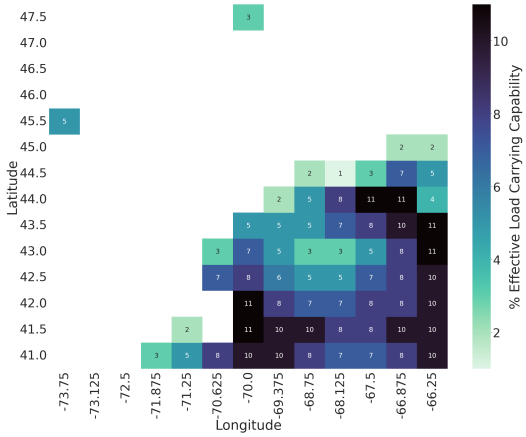

(b) ELCC of 100-MW offshore wind generator, 1993

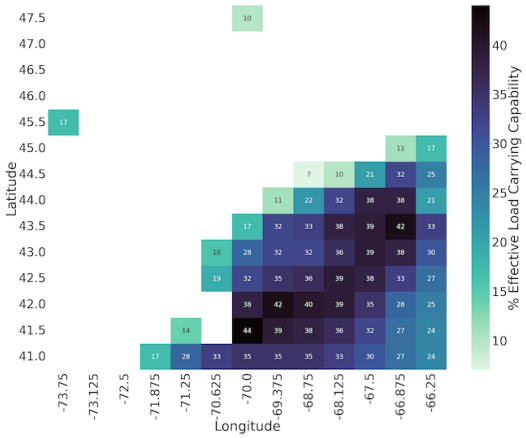

(c) ELCC of 100-MW offshore wind generator, 1994

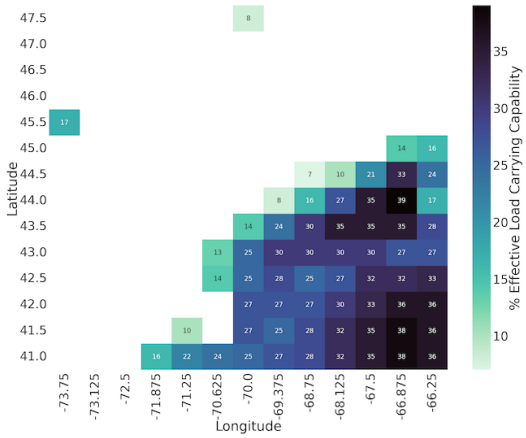

(d) ELCC of 100-MW offshore wind generator, 1995

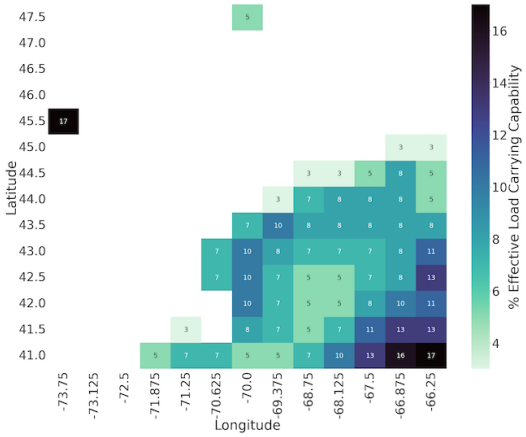

(e) ELCC of 100-MW offshore wind generator, 1996

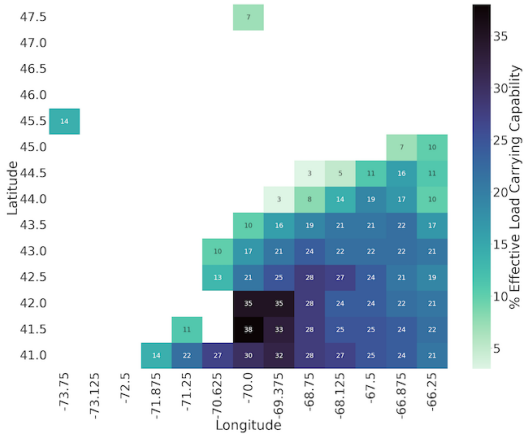

(f) ELCC of 100-MW offshore wind generator, 1997

Figure C.15: Geographical distribution of ELCC values between 1992 -1997 for a new 100-MW offshore wind generator added to the existing base fleet from 2019 of IS0-New England.

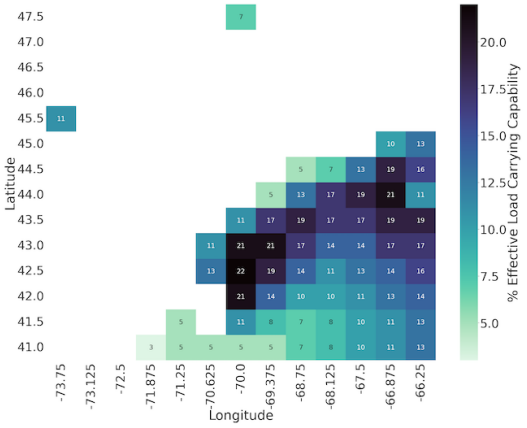

(a) ELCC of 100-MW offshore wind generator, 1998

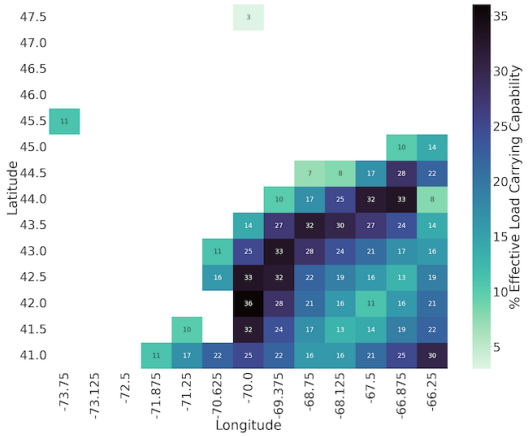

(b) ELCC of 100-MW offshore wind generator, 1999

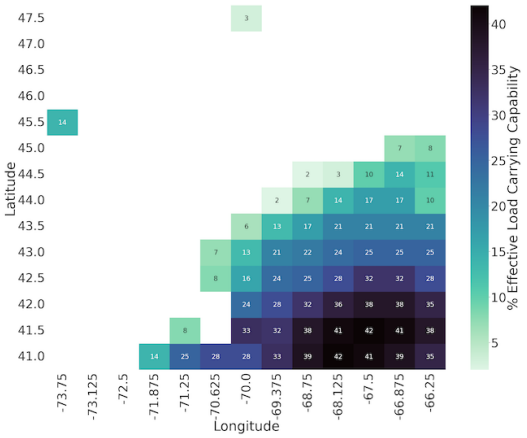

(c) ELCC of 100-MW offshore wind generator, 2000

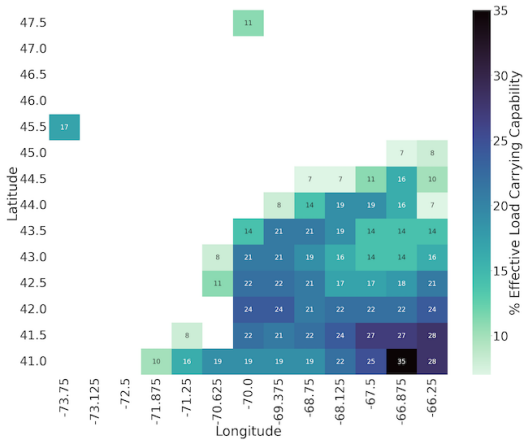

(d) ELCC of 100-MW offshore wind generator, 2001

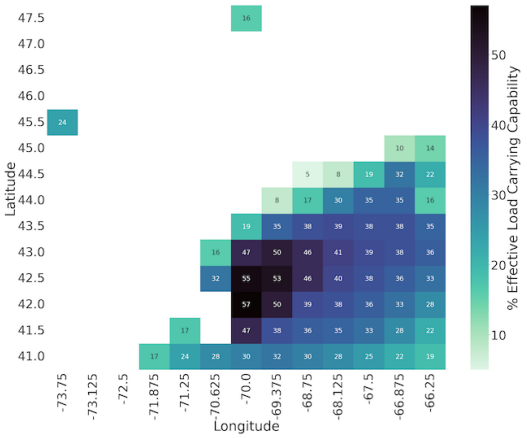

(e) ELCC of 100-MW offshore wind generator, 2002

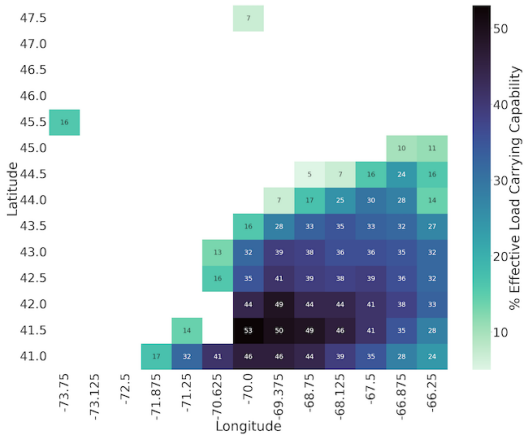

(f) ELCC of 100-MW offshore wind generator, 2003

Figure C.16: Geographical distribution of ELCC values between 1998 - 2003 for a new 100-MW offshore wind generator added to the existing base fleet from 2019 of IS0-New England.

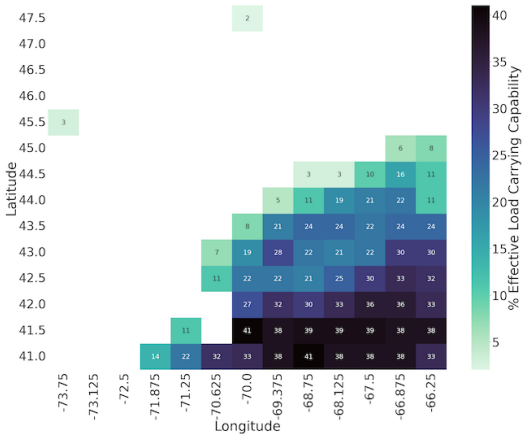

(a) ELCC of 100-MW offshore wind generator, 2004

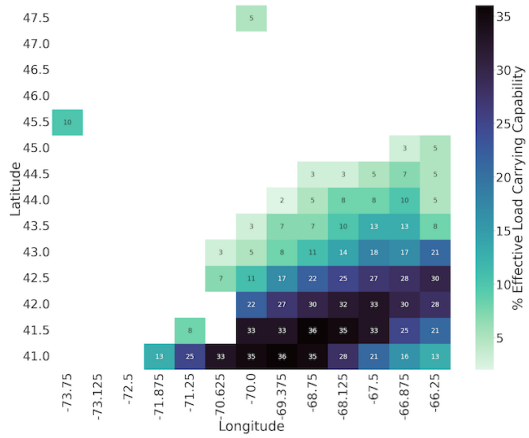

(b) ELCC of 100-MW offshore wind generator, 2005

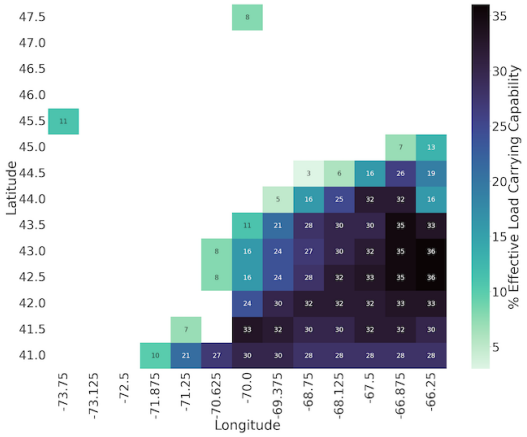

(c) ELCC of 100-MW offshore wind generator, 2006

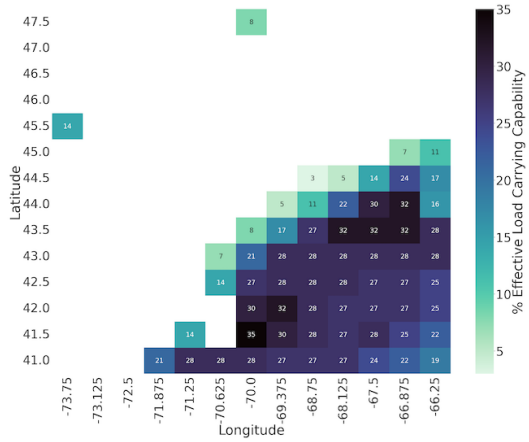

(d) ELCC of 100-MW offshore wind generator, 2007

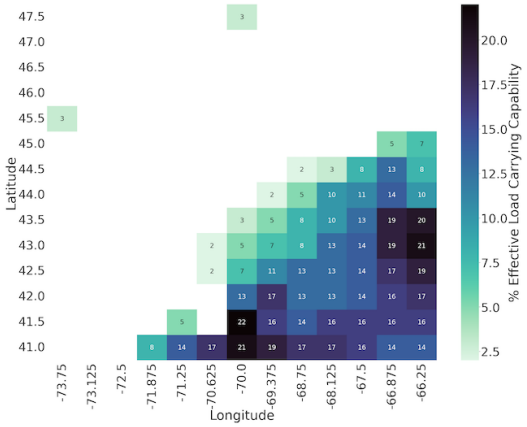

(e) ELCC of 100-MW offshore wind generator, 2008

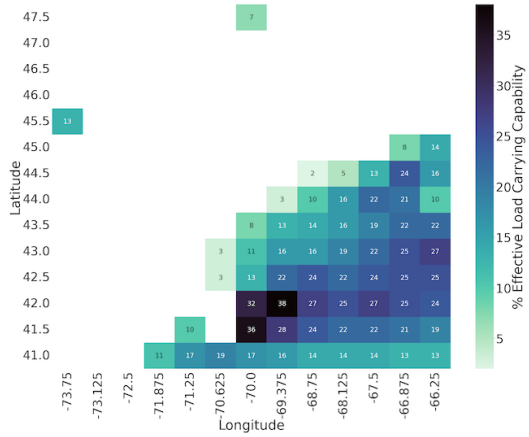

(f) ELCC of 100-MW offshore wind generator, 2009

Figure C.17: Geographical distribution of ELCC values between 2004 - 2009 for a new 100-MW offshore wind generator added to the existing base fleet from 2019 of IS0-New England.

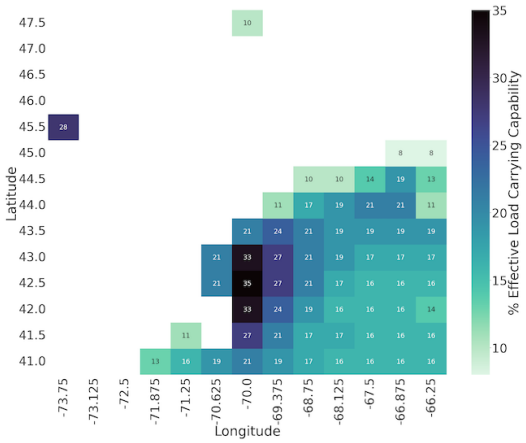

(a) ELCC of 100-MW offshore wind generator, 2010

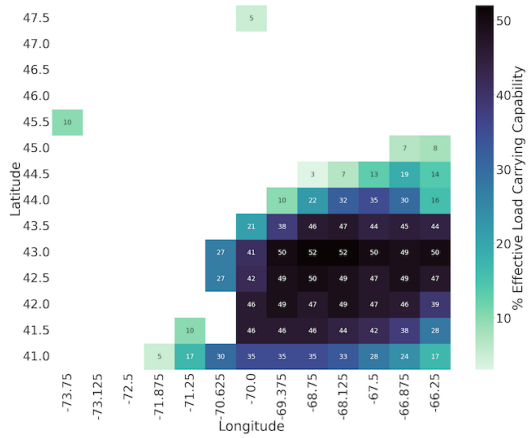

(b) ELCC of 100-MW offshore wind generator, 2011

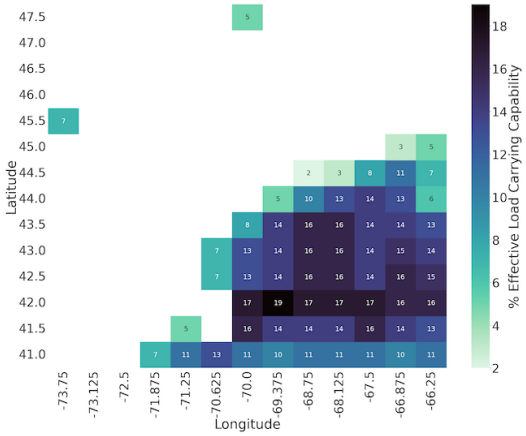

(c) ELCC of 100-MW offshore wind generator, 2012

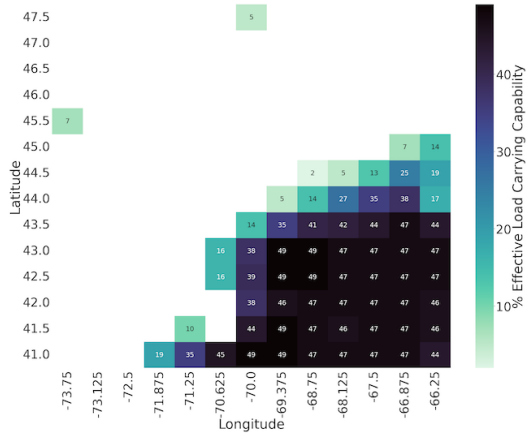

(d) ELCC of 100-MW offshore wind generator, 2013

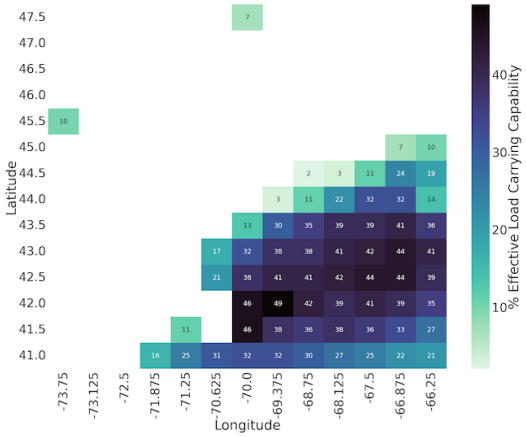

(e) ELCC of 100-MW offshore wind generator, 2014

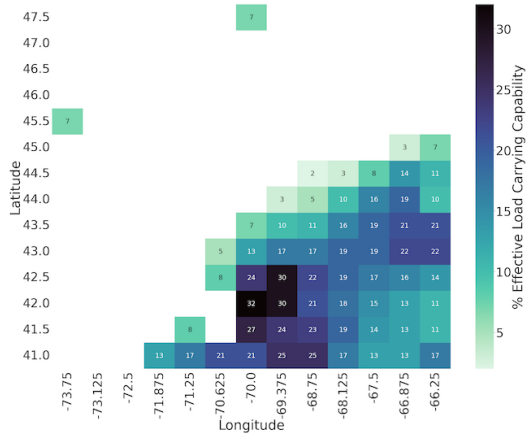

(f) ELCC of 100-MW offshore wind generator, 2015

Figure C.18: Geographical distribution of ELCC values between 2010 - 2014 for a new 100-MW offshore wind generator added to the existing base fleet from 2019 of IS0-New England.

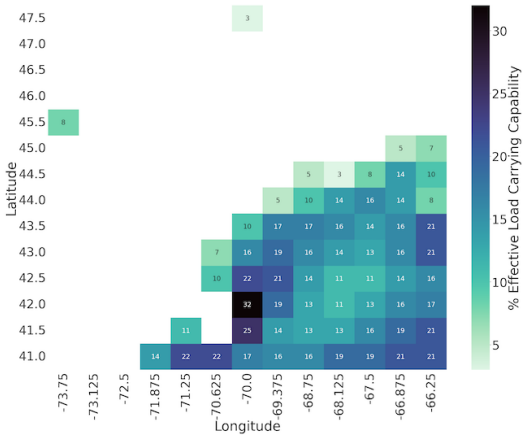

(a) ELCC of 100-MW offshore wind generator, 2016

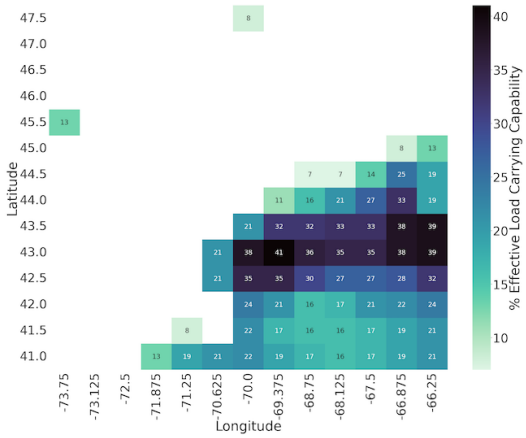

(b) ELCC of 100-MW offshore wind generator, 2017

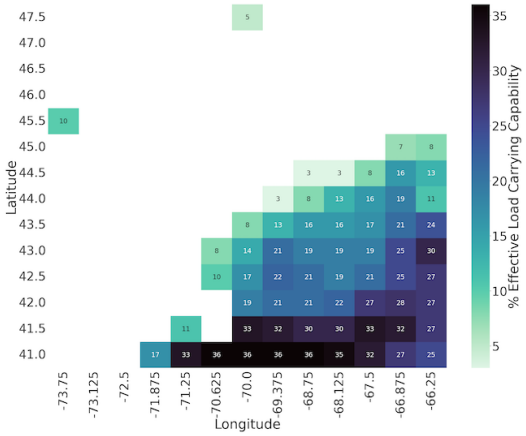

(c) ELCC of 100-MW offshore wind generator, 2018

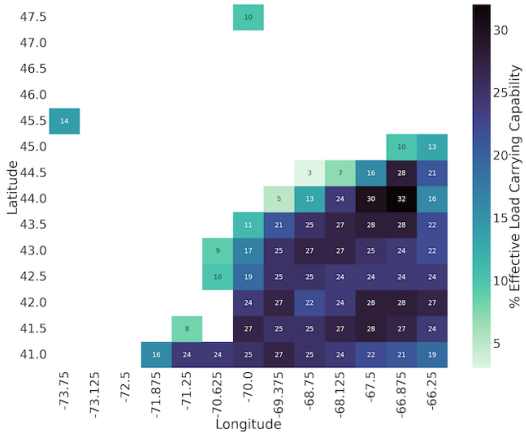

(d) ELCC of 100-MW offshore wind generator, 2019

Figure C.19: Geographical distribution of ELCC values between 2016 - 2019 for a new 100-MW offshore wind generator added to the existing base fleet from 2019 of IS0-New England.

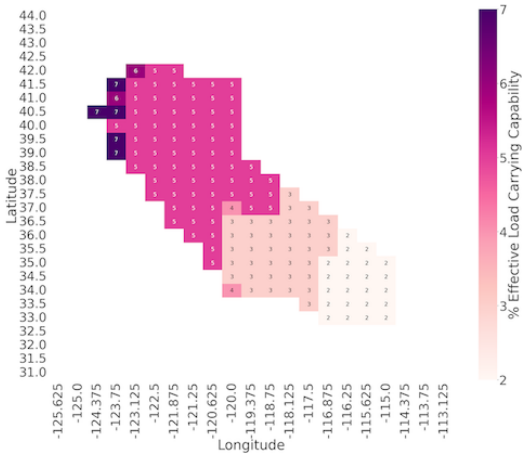

(a) ELCC of 100-MW solar generator, 1980

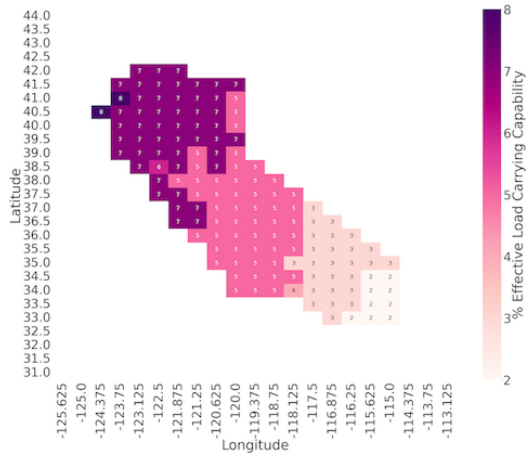

(b) ELCC of 100-MW solar generator, 1981

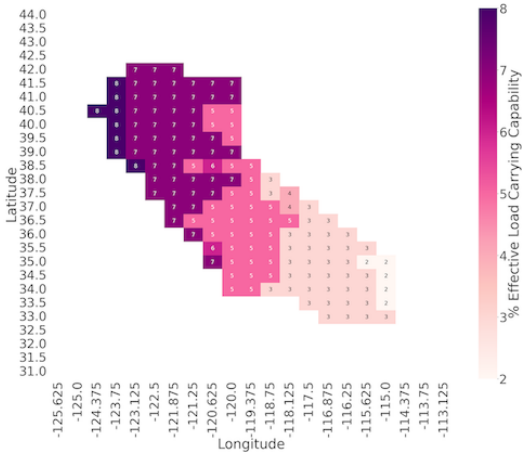

(c) ELCC of 100-MW solar generator, 1982

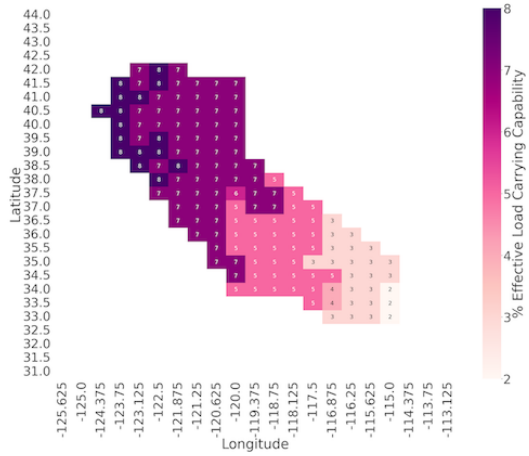

(d) ELCC of 100-MW solar generator, 1983

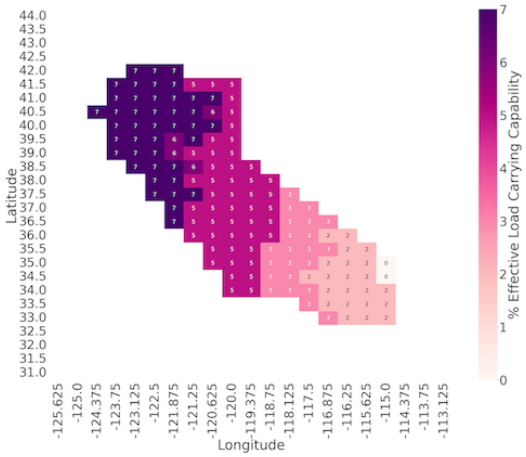

(e) ELCC of 100-MW solar generator, 1984

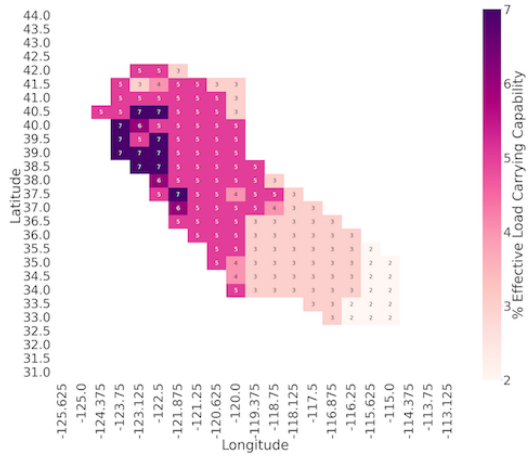

(f) ELCC of 100-MW solar generator, 1985

Figure C.20: Geographical distribution of ELCC values between 1980 -1985 for a new 100-MW solar generator added to the existing base fleet from 2019 of CAISO.

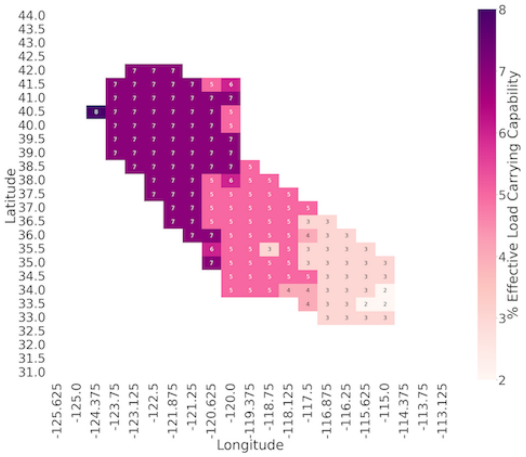

(a) ELCC of 100-MW solar generator, 1986

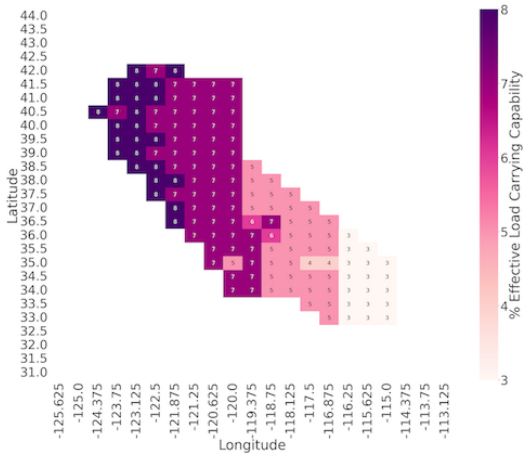

(b) ELCC of 100-MW solar generator,1987

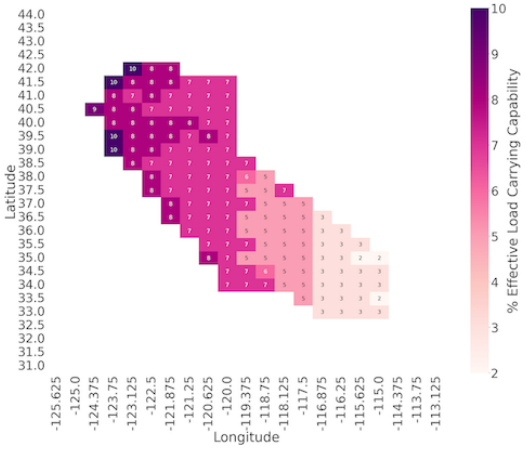

(c) ELCC of 100-MW solar generator, 1988

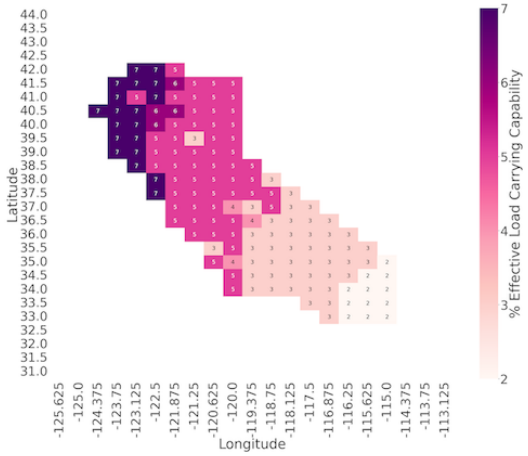

(d) ELCC of 100-MW solar generator, 1989

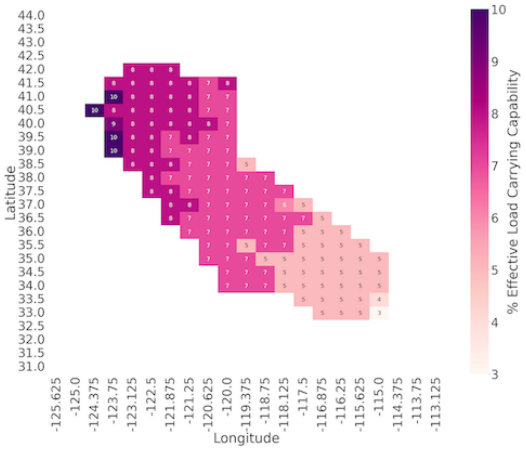

(e) ELCC of 100-MW solar generator, 1990

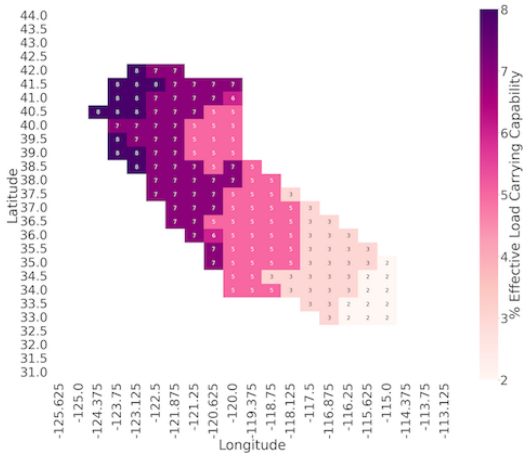

(f) ELCC of 100-MW solar generator, 1991

Figure C.21: Geographical distribution of ELCC values between 1986 -1991 for a new 100-MW solar generator added to the existing base fleet from 2019 of California Independent System Operator.

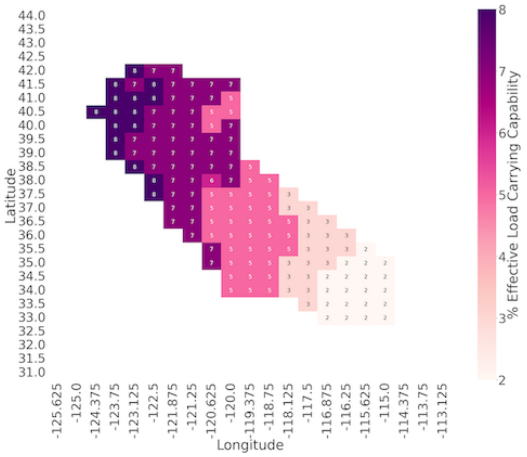

(a) ELCC of 100-MW solar generator, 1992

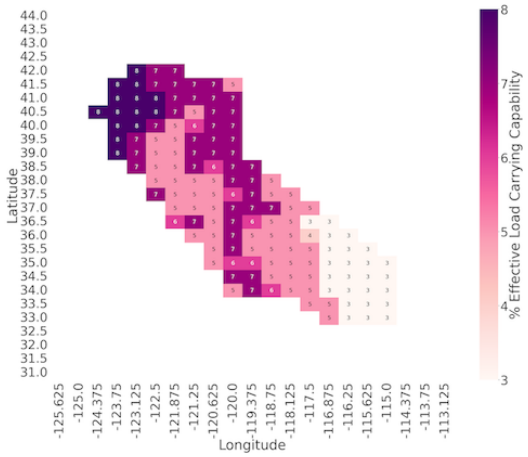

(b) ELCC of 100-MW solar generator, 1993

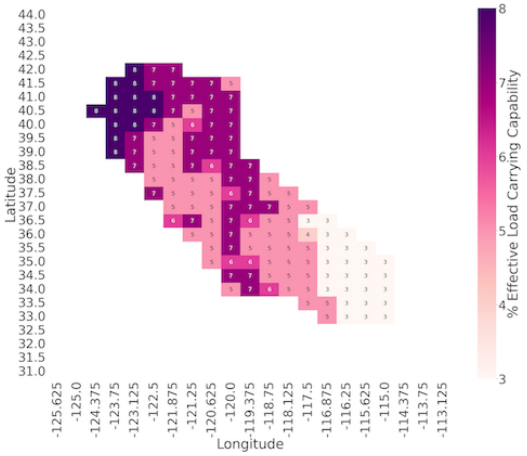

(c) ELCC of 100-MW solar generator, 1994

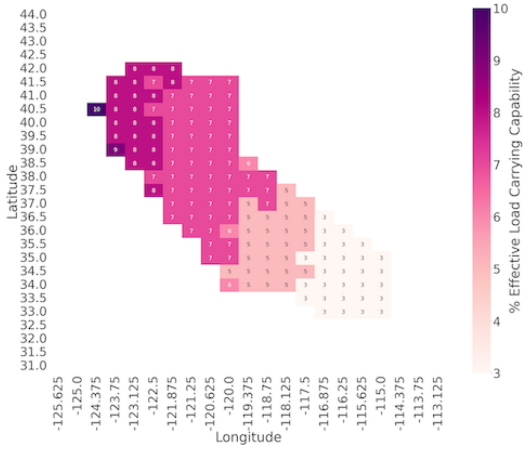

(d) ELCC of 100-MW solar generator, 1995

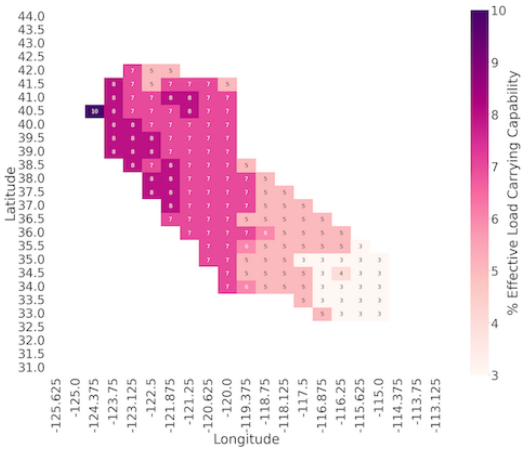

(e) ELCC of 100-MW solar generator, 1996

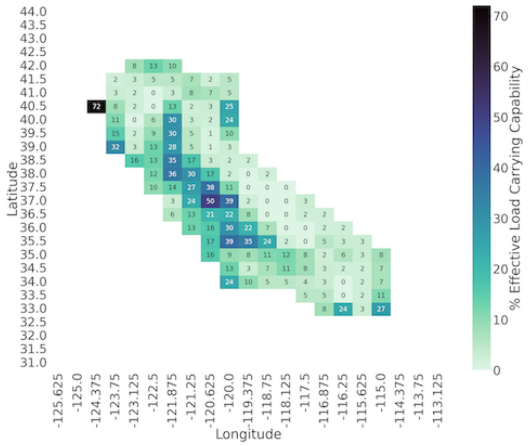

(f) ELCC of 100-MW solar generator, 1997

Figure C.22: Geographical distribution of ELCCs for a new 100-MW solar generator added to the existing base fleet of California Independent System Operator between 1992 -1997.

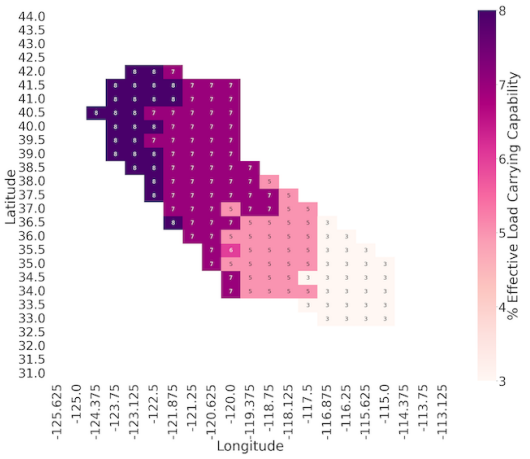

(a) ELCC of 100-MW solar generator, 1998

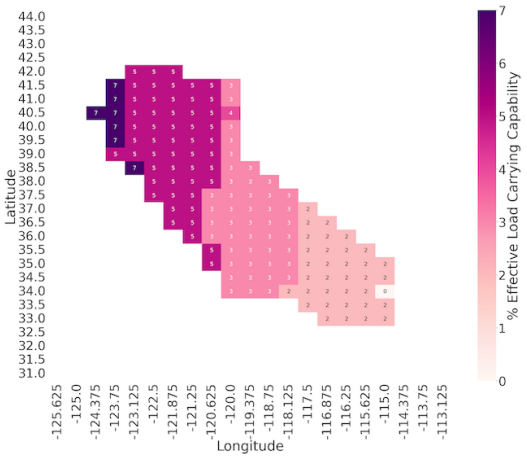

(b) ELCC of 100-MW solar generator, 1999

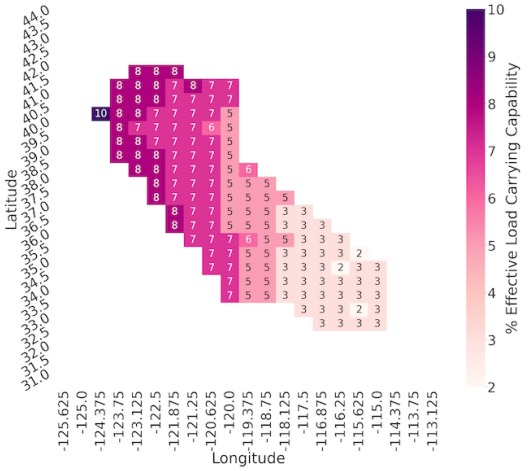

(c) ELCC of 100-MW solar generator, 2000

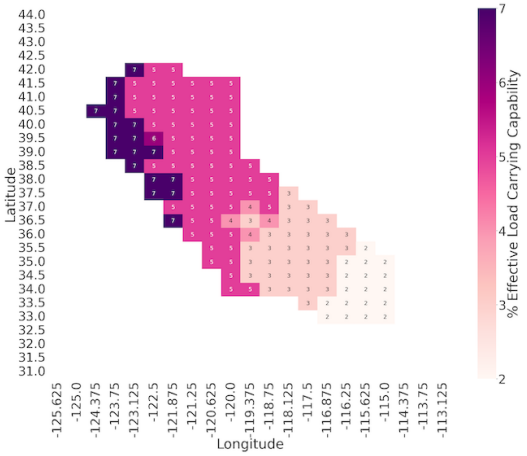

(d) ELCC of 100-MW solar generator, 2001

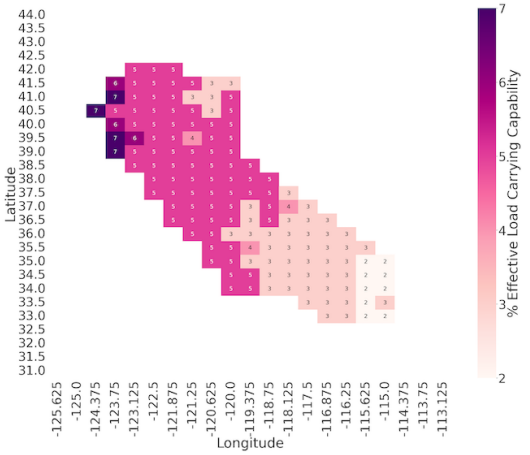

(e) ELCC value of 100-MW solar generator in 2002

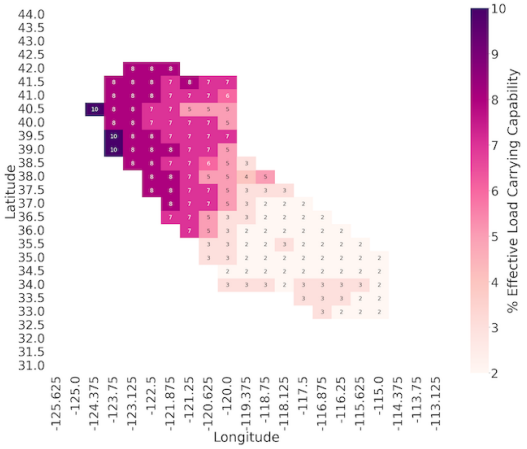

(f) ELCC of 100-MW solar generator, 2003

Figure C.23: Geographical distribution of ELCCs for a new 100-MW solar generator added to the existing base fleet of California Independent System Operator between 1998 - 2003.

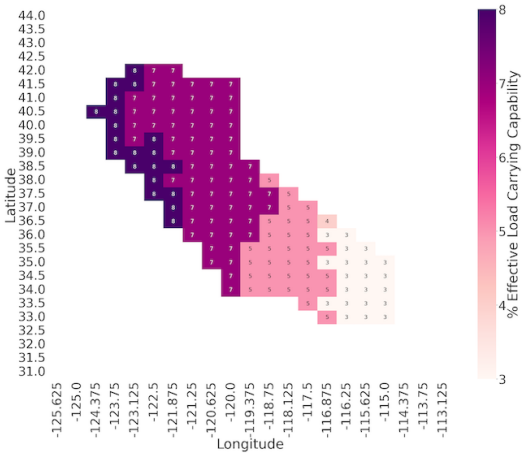

(a) ELCC of 100-MW solar generator, 2004

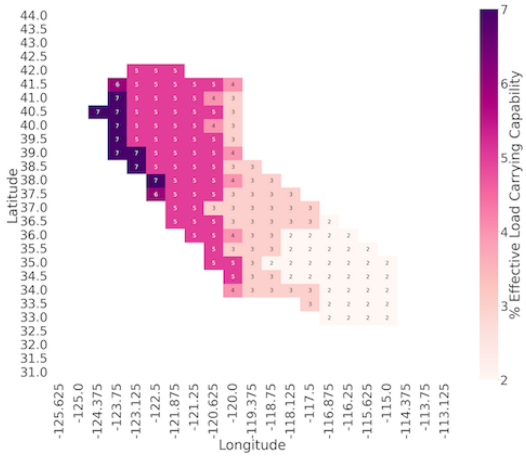

(b) ELCC of 100-MW solar generator, 2005

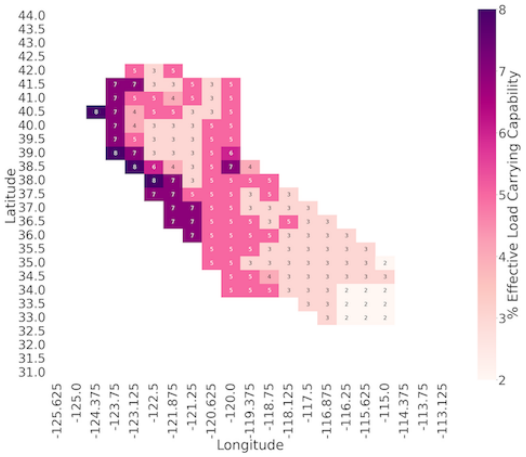

(c) ELCC of 100-MW solar generator, 2006

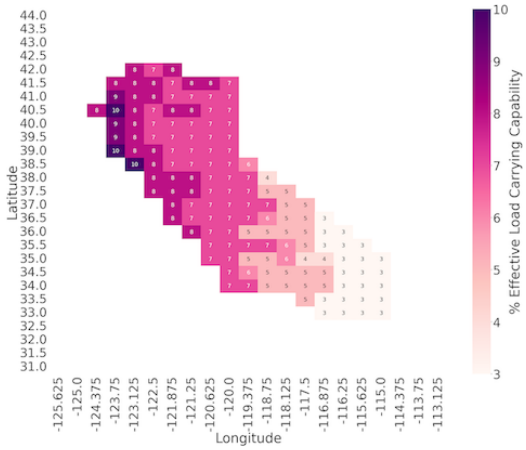

(d) ELCC of 100-MW solar generator, 2007

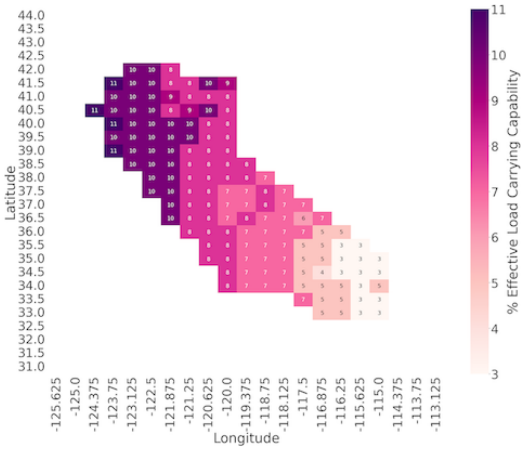

(e) ELCC of 100-MW solar generator, 2008

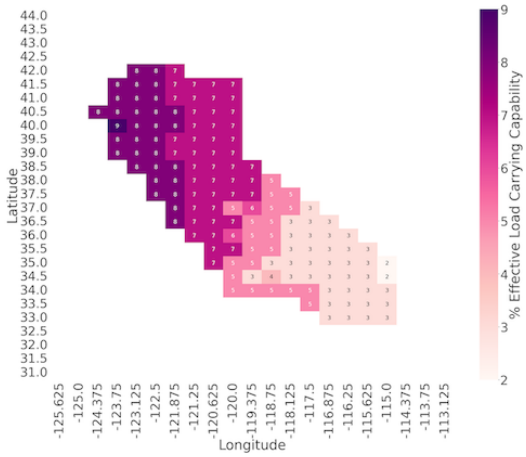

(f) ELCC of 100-MW solar generator, 2009

Figure C.24: Geographical distribution of ELCCs for a new 100-MW solar generator added to the existing base fleet of California Independent System Operator between 2004 - 2009.

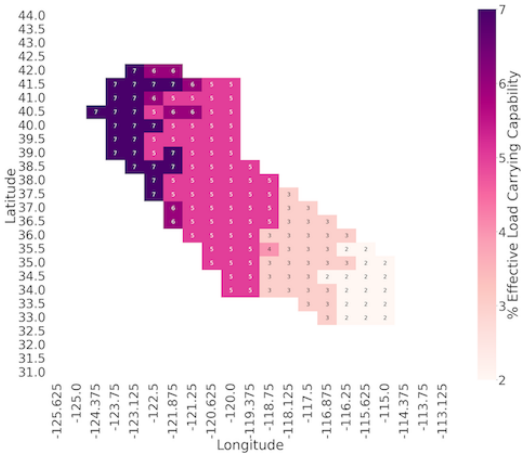

(a) ELCC of 100-MW solar generator, 2010

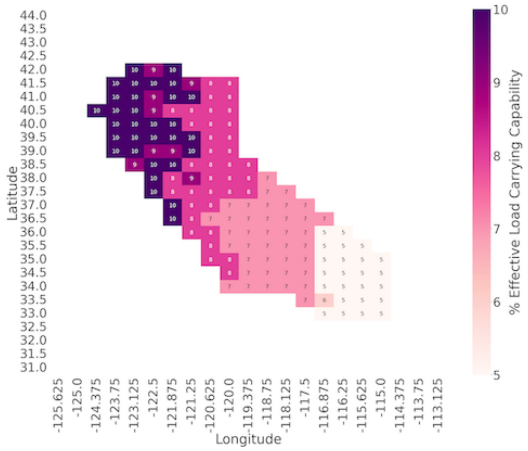

(b) ELCC of 100-MW solar generator, 2011

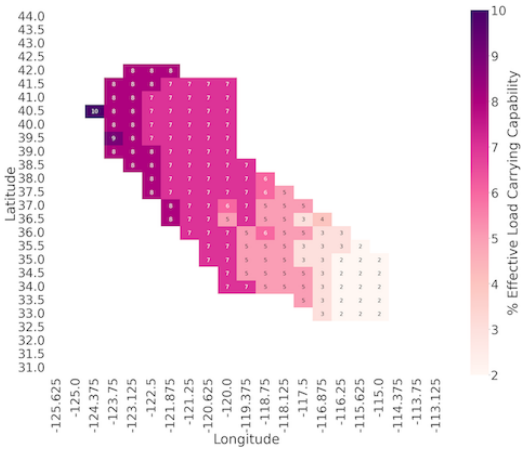

(c) ELCC of 100-MW solar generator, 2012

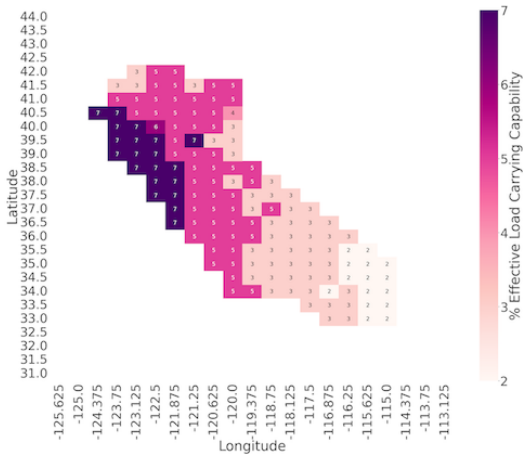

(d) ELCC of 100-MW solar generator, 2013

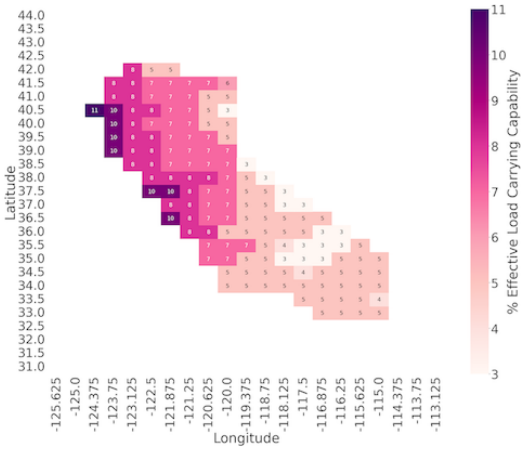

(e) ELCC of 100-MW solar generator, 2014

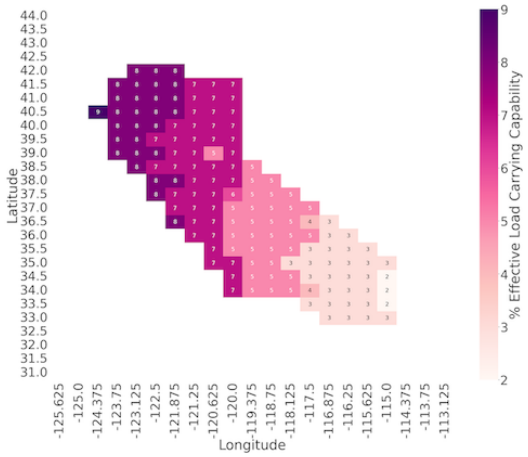

(f) ELCC of 100-MW solar generator, 2015

Figure C.25: Geographical distribution of ELCCs for a new 100-MW solar generator added to the existing base fleet of California Independent System Operator between 2010 - 2015.

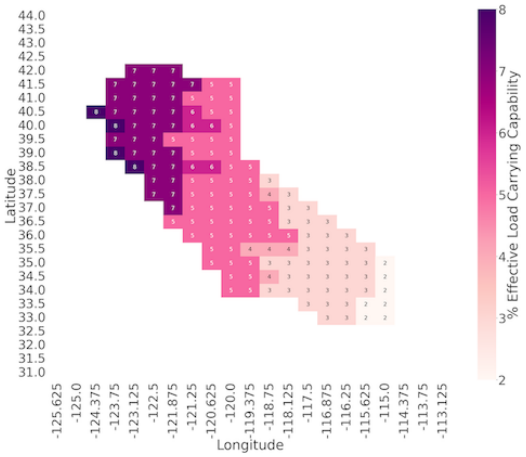

(a) ELCC of 100-MW solar generator, 2016

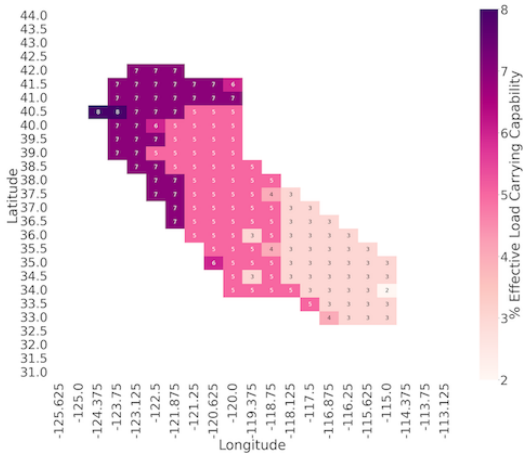

(b) ELCC of 100-MW solar generator, 2017

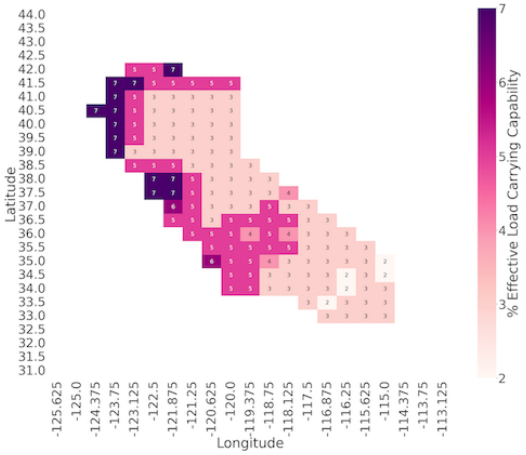

(c) ELCC of 100-MW solar generator, 2018

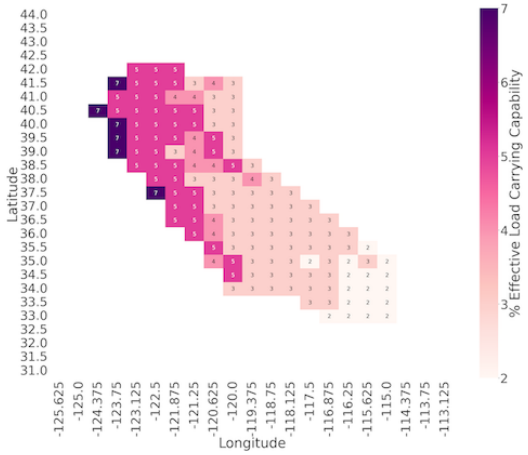

(d) ELCC of 100-MW solar generator, 2019

Figure C.26: Geographical distribution of ELCCs for a new 100-MW solar generator added to the existing base fleet of California Independent System Operator between 2016 - 2019.

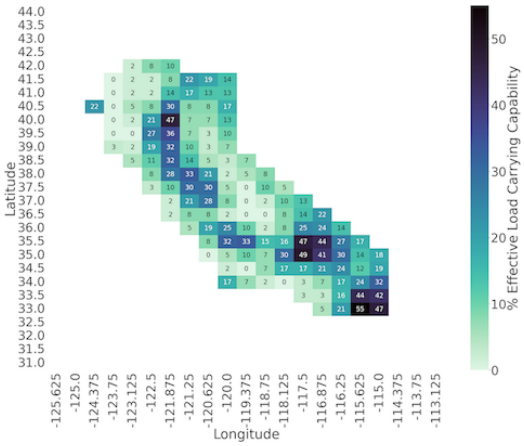

(a) ELCC of 100-MW onshore wind generator, 1980

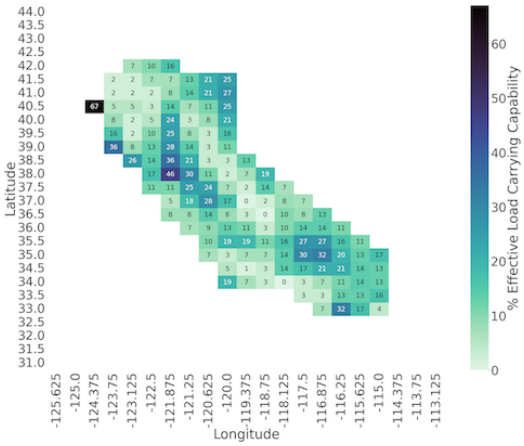

(b) ELCC of 100-MW onshore wind generator, 1981

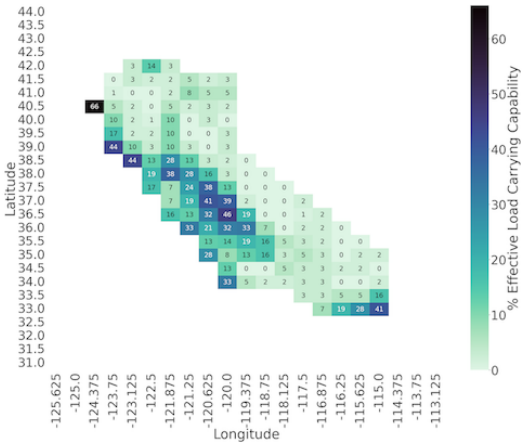

(c) ELCC of 100-MW onshore wind generator, 1982

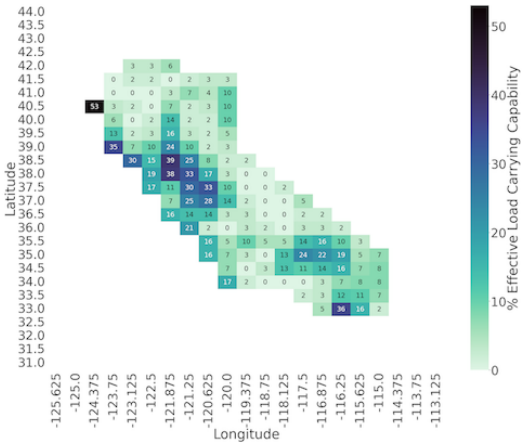

(d) ELCC of 100-MW onshore wind generator, 1983

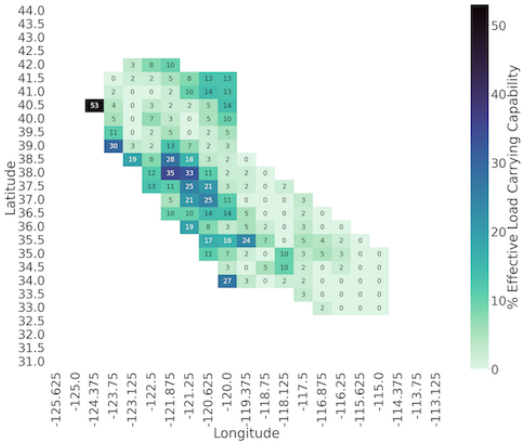

(e) ELCC of 100-MW onshore wind generator, 1984

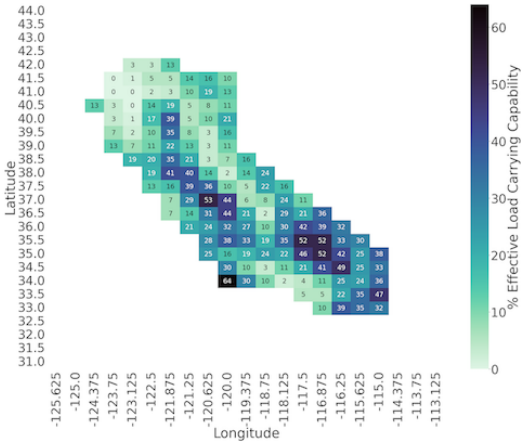

(f) ELCC of 100-MW onshore wind generator, 1985

Figure C.27: Geographical distribution of ELCCs for a new 100-MW onshore wind generator added to the existing base fleet of California Independent System Operator between 1980-1985.

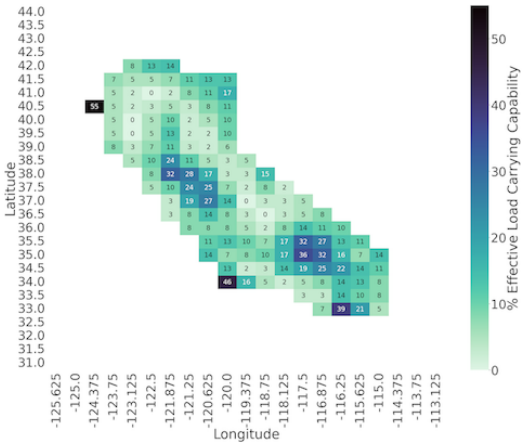

(a) ELCC of 100-MW onshore wind generator, 1986

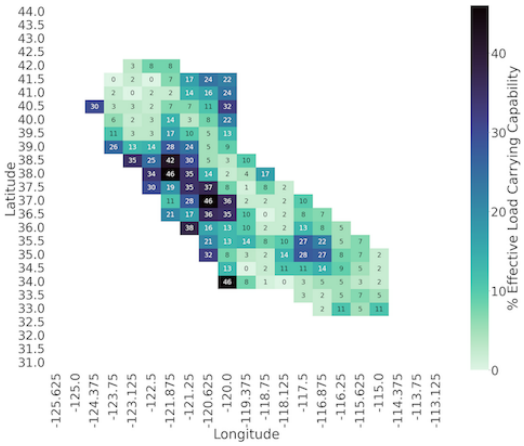

(b) ELCC of 100-MW onshore wind generator, 1987

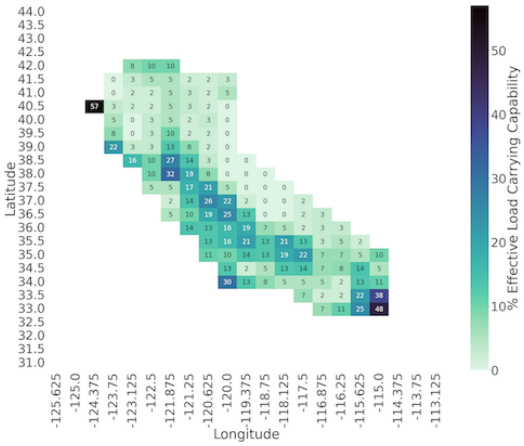

(c) ELCC of 100-MW onshore wind generator, 1988

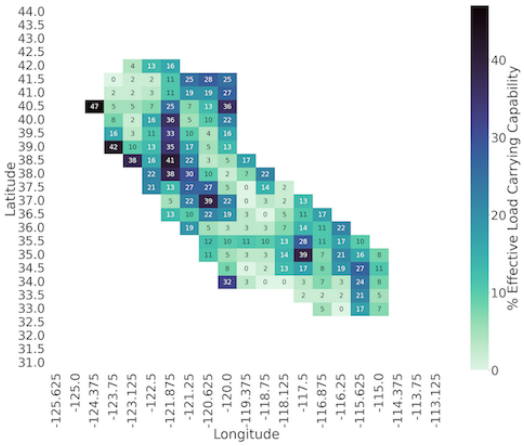

(d) ELCC of 100-MW onshore wind generator, 1989

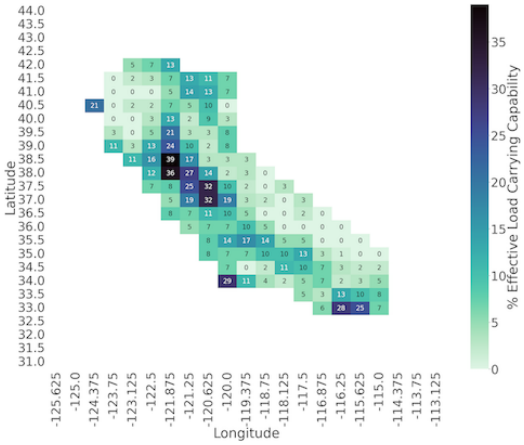

(e) ELCC of 100-MW onshore wind generator, 1990

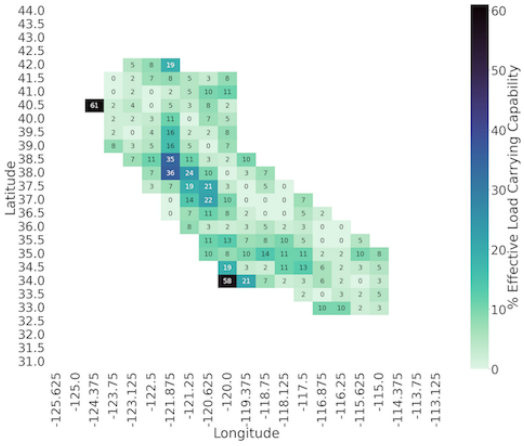

(f) ELCC of 100-MW onshore wind generator, 1991

Figure C.28: Geographical distribution of ELCCs for a new 100-MW onshore wind generator added to the existing base fleet of California Independent System Operator between 1986 -1991.

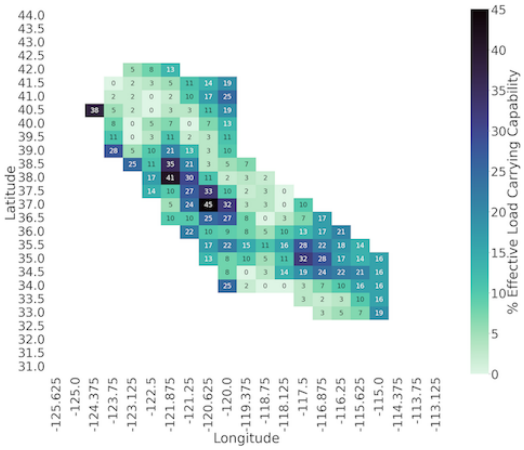

(a) ELCC of 100-MW onshore wind generator, 1992

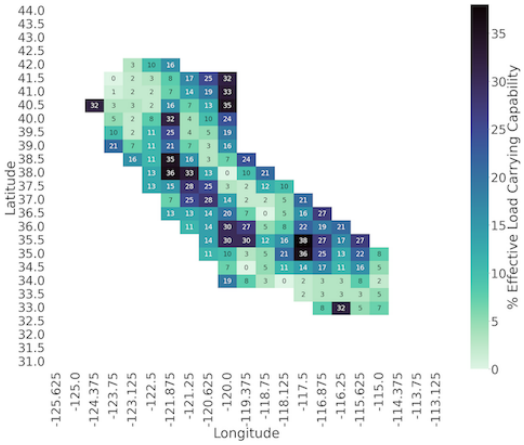

(b) ELCC of 100-MW onshore wind generator, 1993

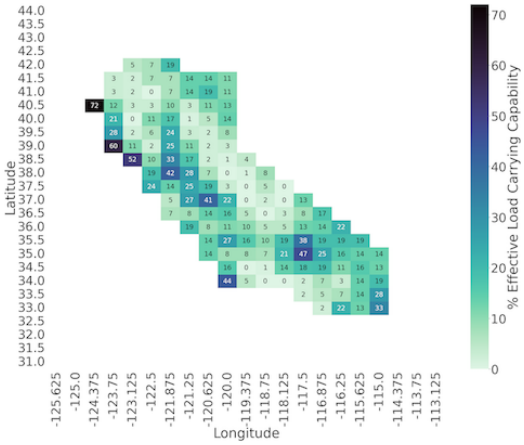

(c) ELCC of 100-MW onshore wind generator, 1994

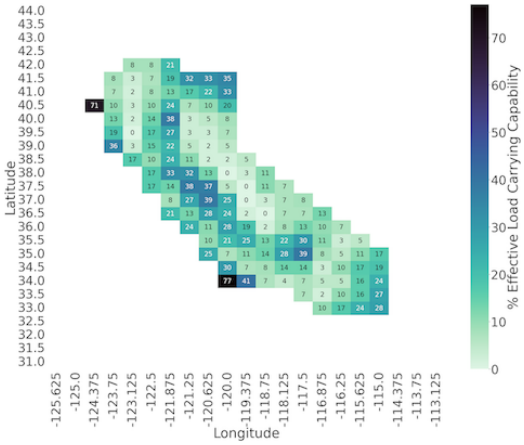

(d) ELCC of 100-MW onshore wind generator, 1995

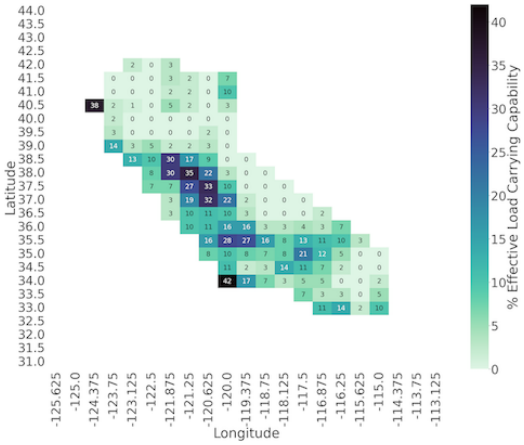

(e) ELCC of 100-MW onshore wind generator, 1996

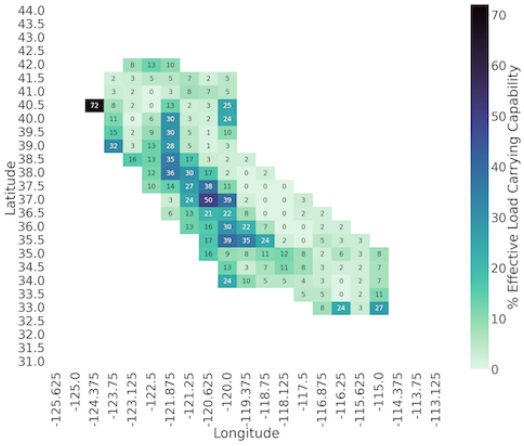

(f) ELCC of 100-MW onshore wind generator, 1997

Figure C.29: Geographical distribution of ELCCs for a new 100-MW onshore wind generator added to the existing base fleet of California Independent System Operator between 1992 -1997.

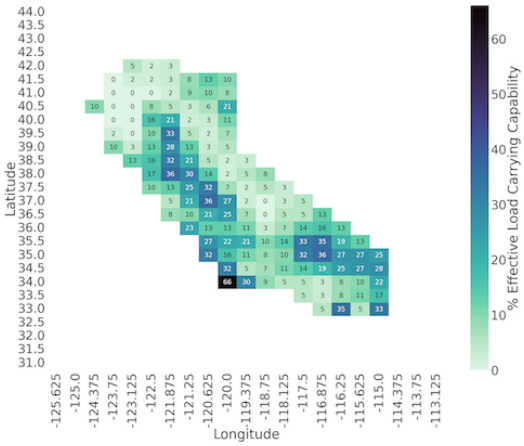

(a) ELCC of 100-MW onshore wind generator, 1998

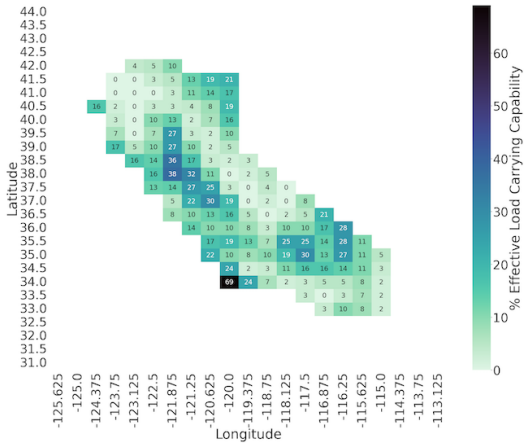

(b) ELCC of 100-MW onshore wind generator, 1999

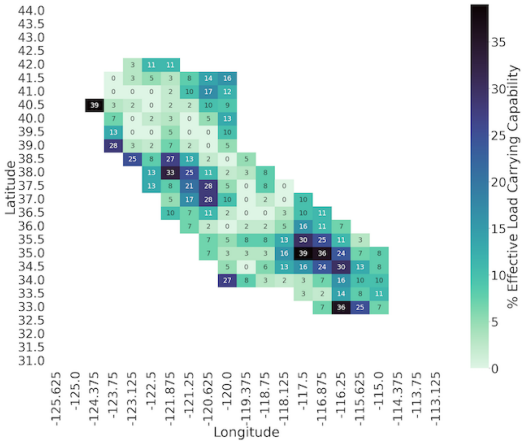

(c) ELCC of 100-MW onshore wind generator, 2000

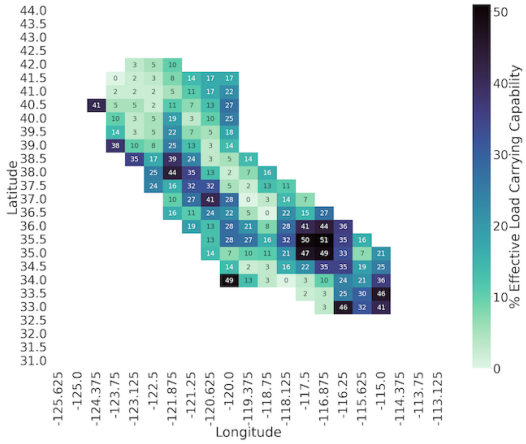

(d) ELCC of 100-MW onshore wind generator, 2001

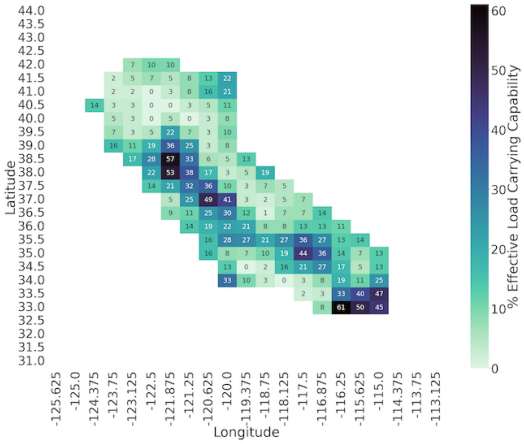

(e) ELCC of 100-MW onshore wind generator, 2002

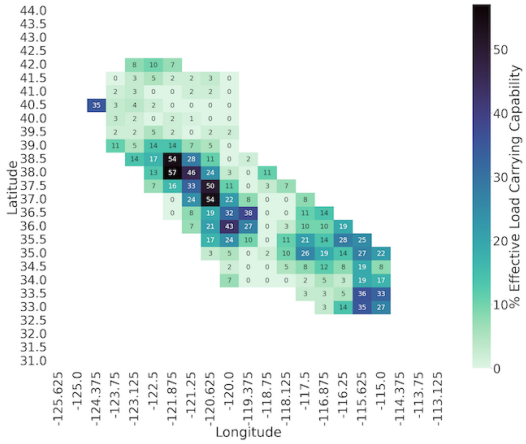

(f) ELCC of 100-MW onshore wind generator, 2003

Figure C.30: Geographical distribution of ELCCs for a new 100-MW onshore wind generator added to the existing base fleet of California Independent System Operator between 1998 - 2003.

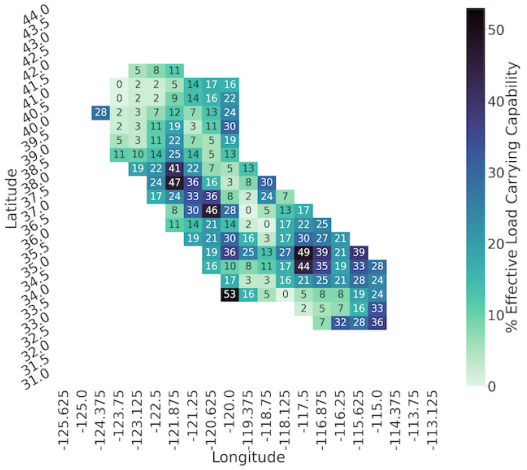

(a) ELCC of 100-MW onshore wind generator, 2004

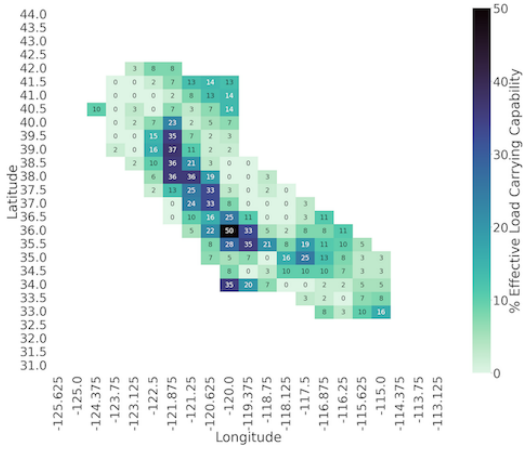

(b) ELCC of 100-MW onshore wind generator, 2005

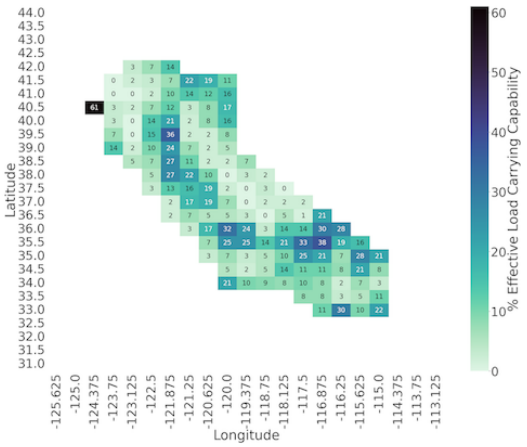

(c) ELCC of 100-MW onshore wind generator, 2006

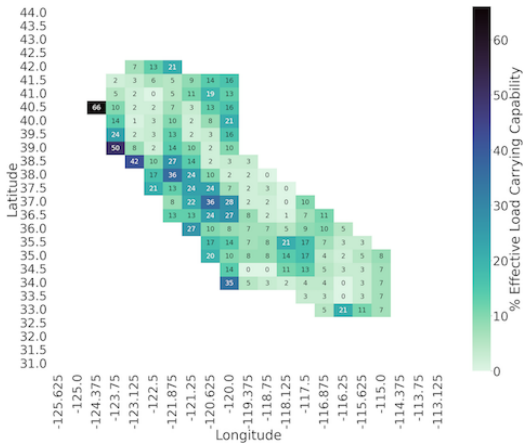

(d) ELCC of 100-MW onshore wind generator, 2007

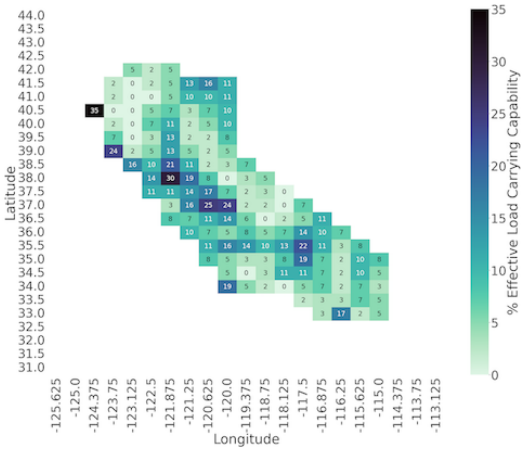

(e) ELCC of 100-MW onshore wind generator, 2008

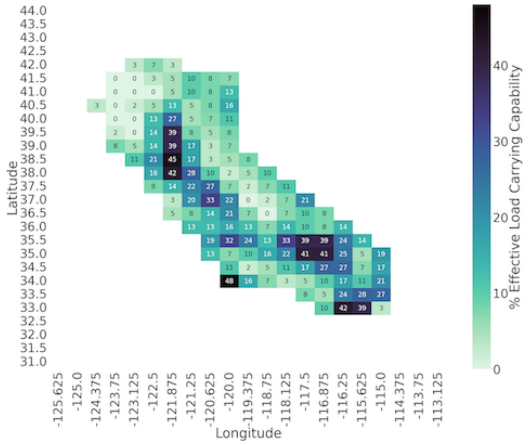

(f) ELCC of 100-MW onshore wind generator, 2009

Figure C.31: Geographical distribution of ELCCs for a new 100-MW solar generator added to the existing base fleet of California Independent System Operator between 2004 - 2009.

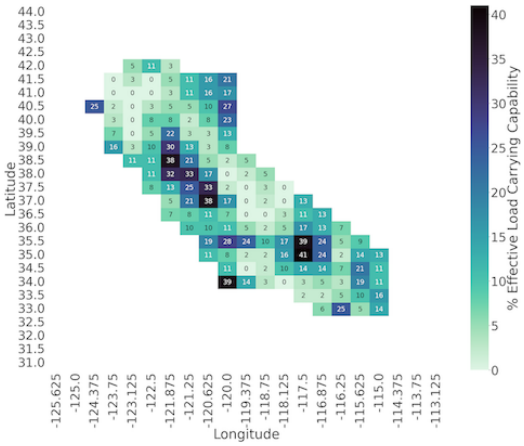

(a) ELCC of 100-MW onshore wind generator, 2010

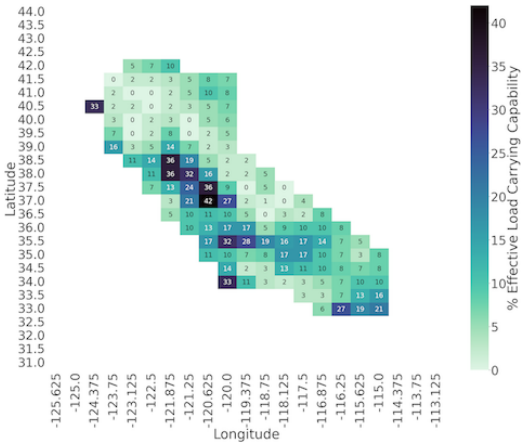

(b) ELCC of 100-MW onshore wind generator, 2011

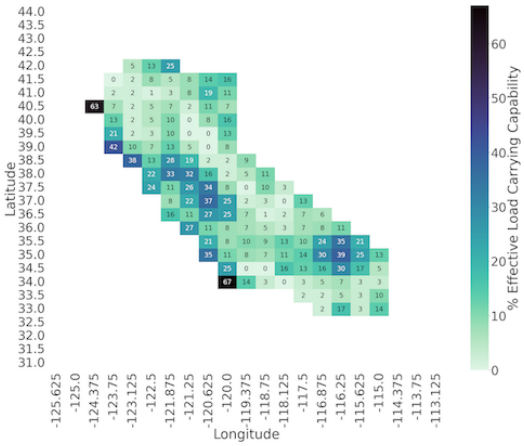

(c) ELCC of 100-MW onshore wind generator, 2012

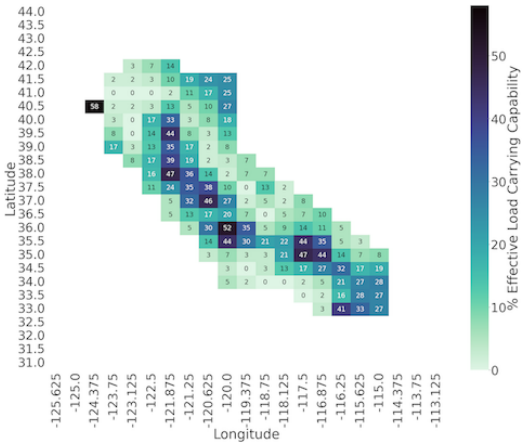

(d) ELCC of 100-MW onshore wind generator, 2013

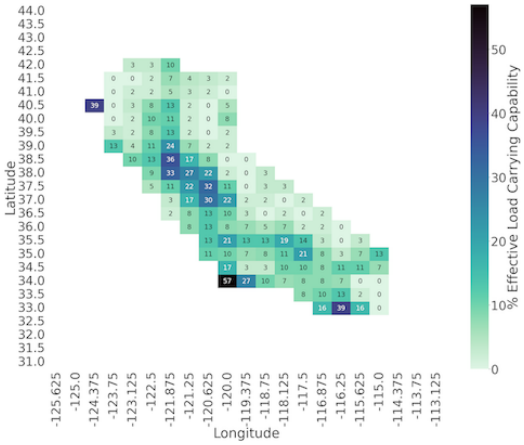

(e) ELCC of 100-MW onshore wind generator, 2014

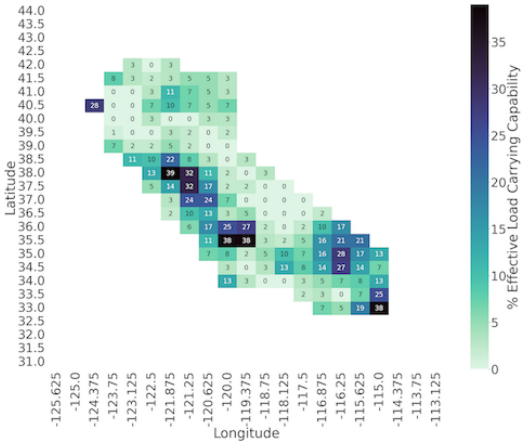

(f) ELCC of 100-MW onshore wind generator, 2015

Figure C.32: Geographical distribution of ELCCs for a new 100-MW onshore wind generator added to the existing base fleet of California Independent System Operator between 2010 - 2015.

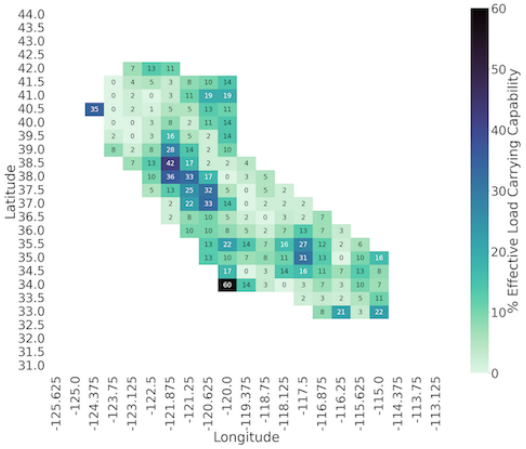

(a) ELCC value of 100-MW onshore wind generator in 2016

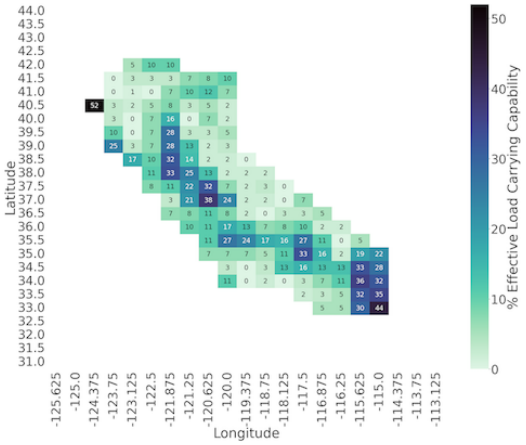

(b) ELCC value of 100-MW solar generator in 2017

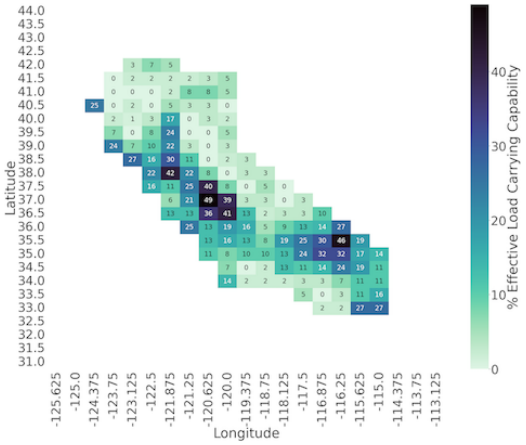

(c) ELCC value of 100-MW onshore wind generator in 2018

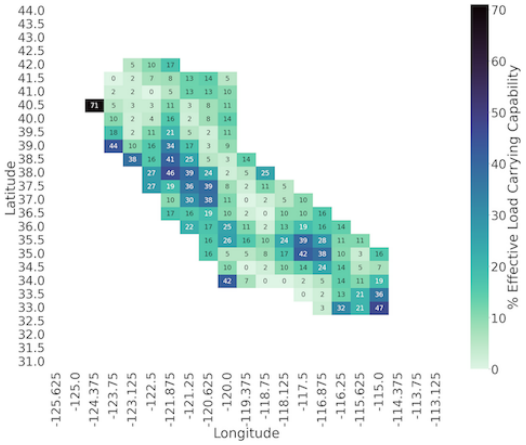

(d) ELCC of 100-MW onshore wind generator, 2019

Figure C.33: Geographical distribution of ELCCs for a new 100-MW onshore generator added to the existing base fleet of California Independent System Operator between 2015 - 2019.

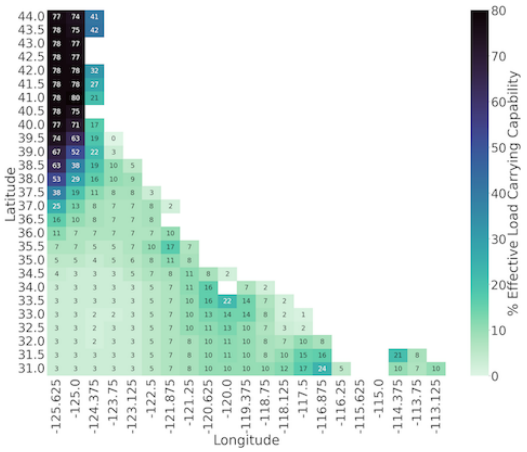

(a) ELCC of 100-MW offshore wind generator, 1980

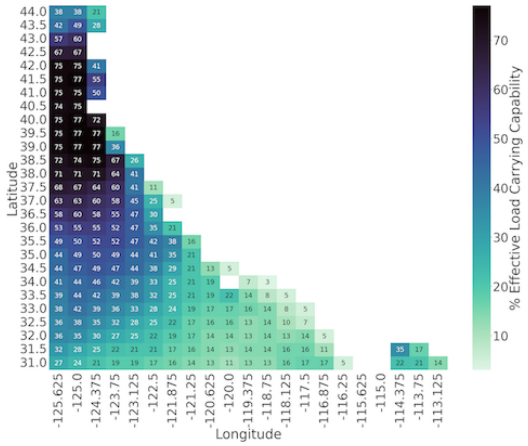

(b) ELCC of 100-MW offshore wind generator, 1981

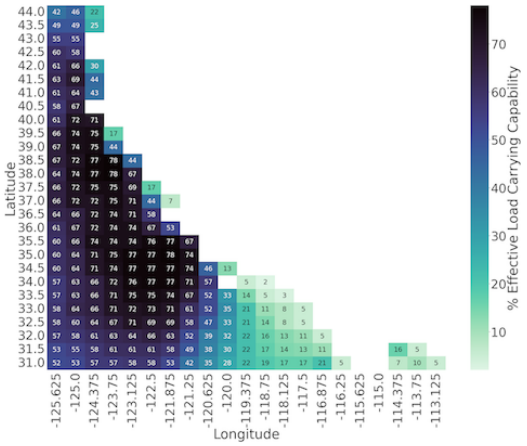

(c) ELCC of 100-MW offshore wind generator, 1982

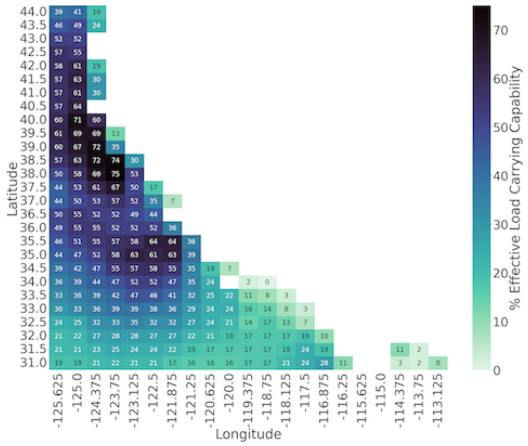

(d) ELCC of 100-MW offshore wind generator, 1983

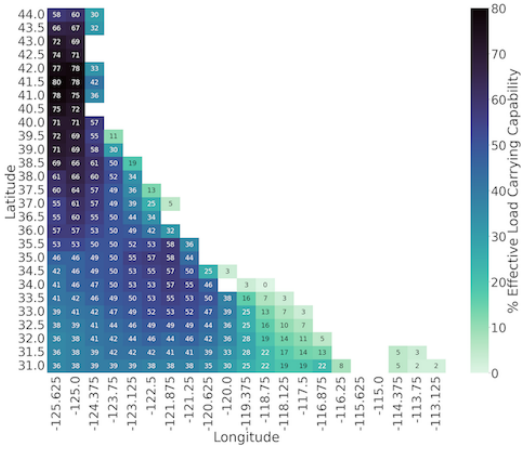

(e) ELCC of 100-MW offshore wind generator, 1984

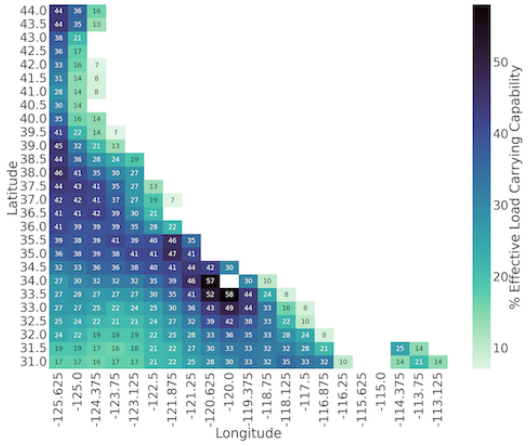

(f) ELCC of 100-MW offshore wind generator, 1985

Figure C.34: Geographical distribution of ELCCs for a new 100-MW offshore wind generator added to the existing base fleet of California Independent System Operator between 1980 -1985.

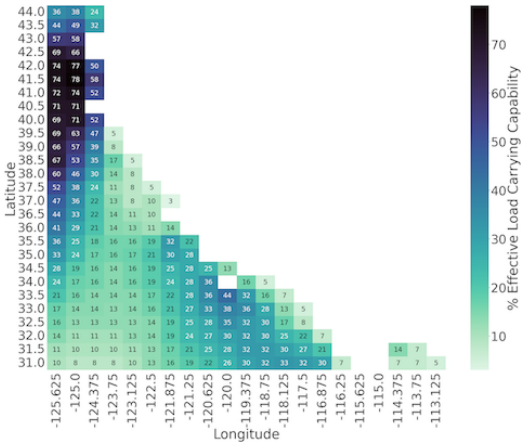

(a) ELCC of 100-MW offshore wind generator, 1986

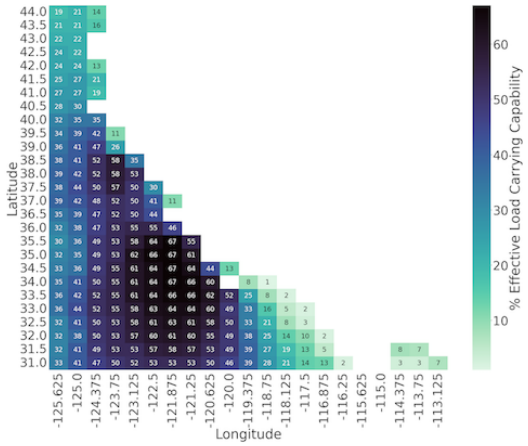

(b) ELCC of 100-MW offshore wind generator, 1987

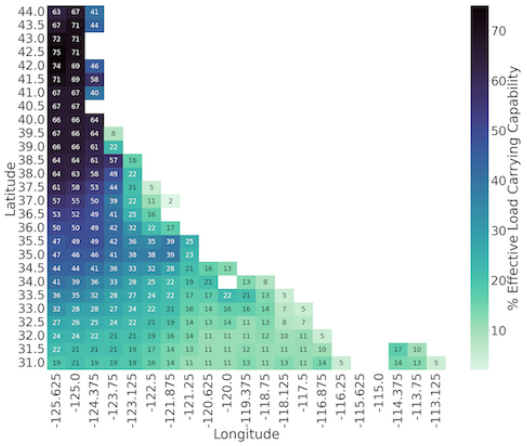

(c) ELCC of 100-MW offshore wind generator, 1988

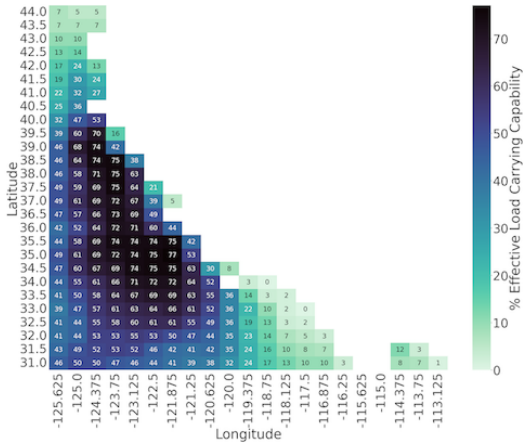

(d) ELCC of 100-MW offshore wind generator, 1989

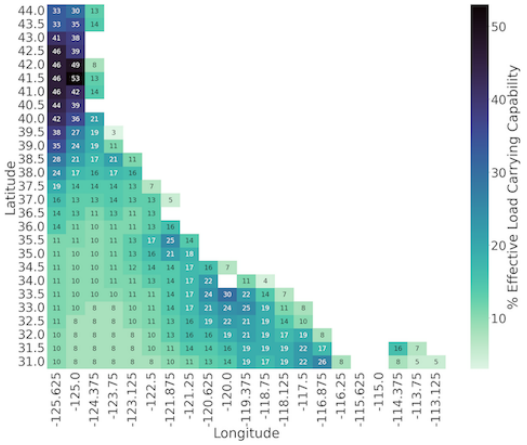

(e) ELCC of 100-MW offshore wind generator, 1990

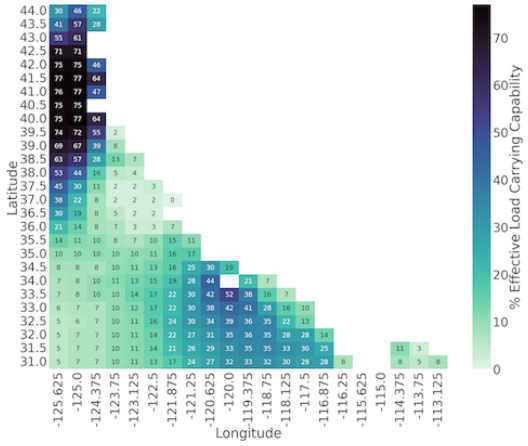

(f) ELCC of 100-MW offshore wind generator, 1991

Figure C.35: Geographical distribution of ELCCs for a new 100-MW offshore wind generator added to the existing base fleet of California Independent System Operator between 1986 -1991.

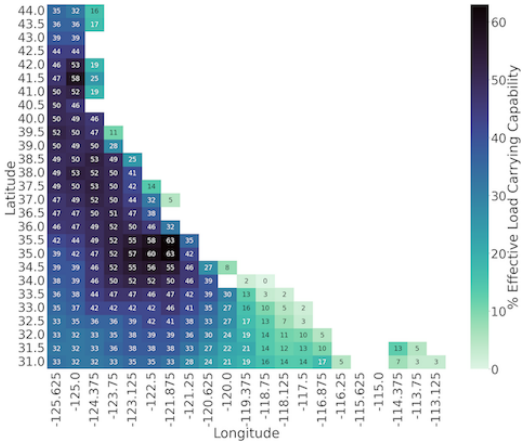

(a) ELCC of 100-MW offshore wind generator, 1992

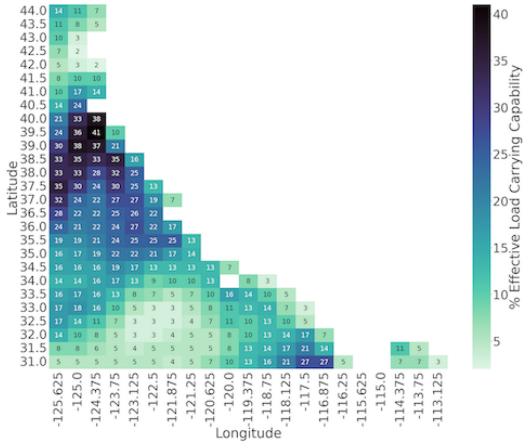

(b) ELCC of 100-MW offshore wind generator, 1993

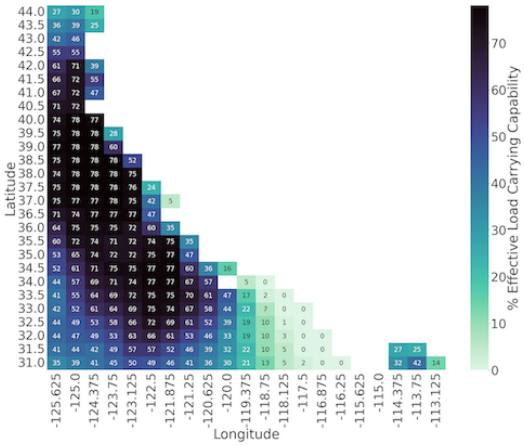

(c) ELCC of 100-MW offshore wind generator, 1994

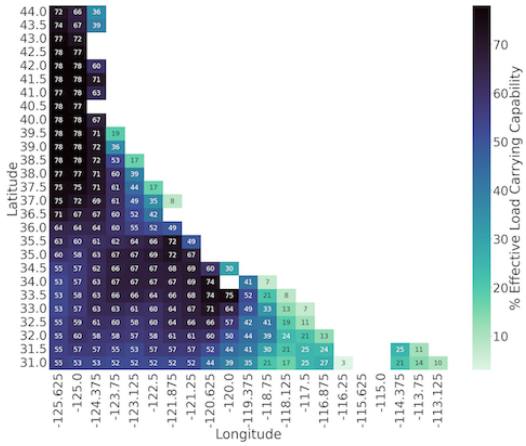

(d) ELCC of 100-MW offshore wind generator, 1995

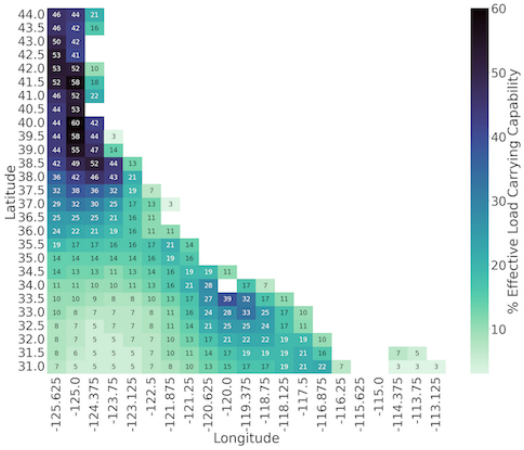

(e) ELCC of 100-MW offshore wind generator, 1996

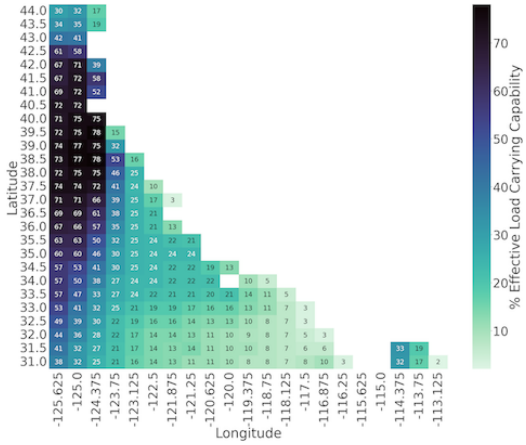

(f) ELCC of 100-MW offshore wind generator, 1997

Figure C.36: Geographical distribution of ELCCs for a new 100-MW offshore wind generator added to the existing base fleet of California Independent System Operator between 1992 - 1997.

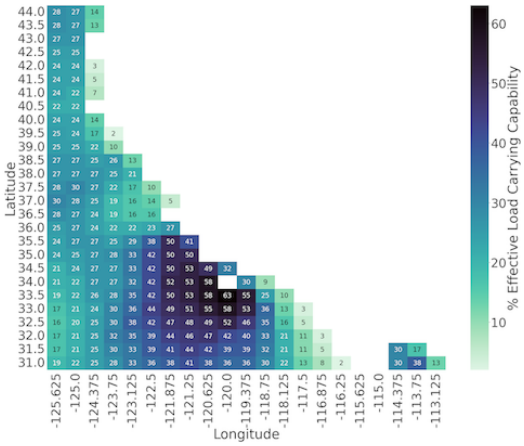

(a) ELCC of 100-MW offshore wind generator, 1998

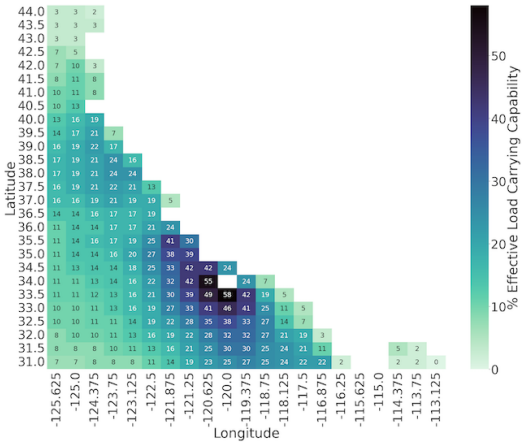

(b) ELCC of 100-MW offshore wind generator, 1999

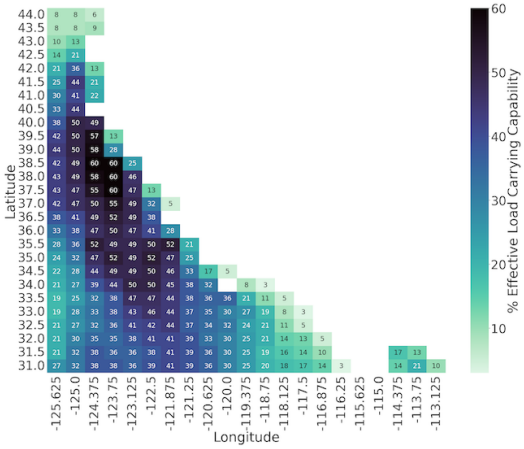

(c) ELCC of 100-MW offshore wind generator, 2000

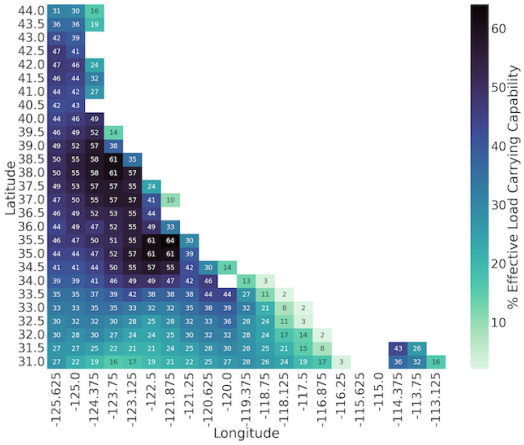

(d) ELCC of 100-MW offshore wind generator, 2001

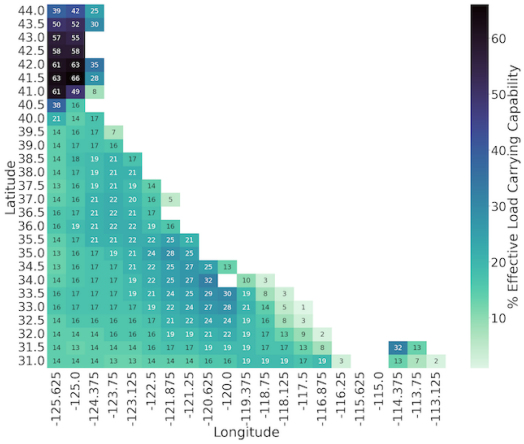

(e) ELCC of 100-MW offshore wind generator, 2002

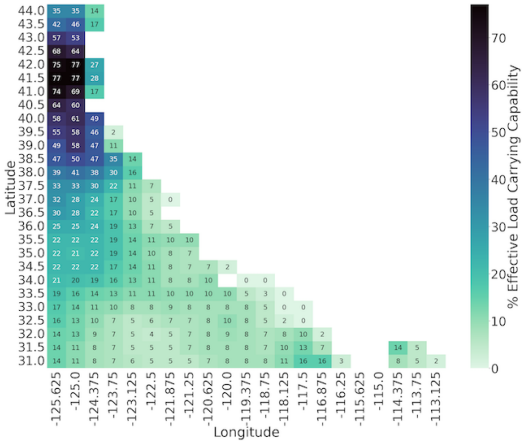

(f) ELCC of 100-MW offshore wind generator, 2003

Figure C.37: Geographical distribution of ELCCs for a new 100-MW offshore wind generator added to the existing base fleet of California Independent System Operator between 1998 - 2003.

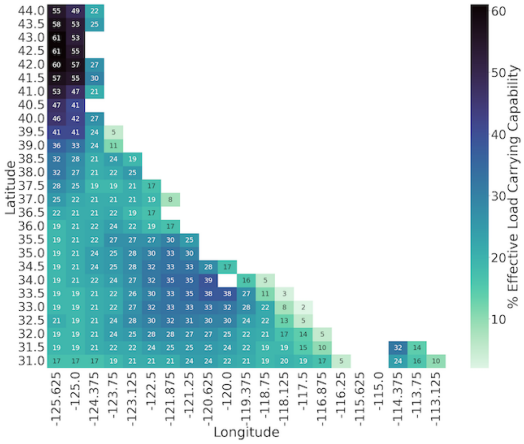

(a) ELCC of 100-MW offshore wind generator, 2004

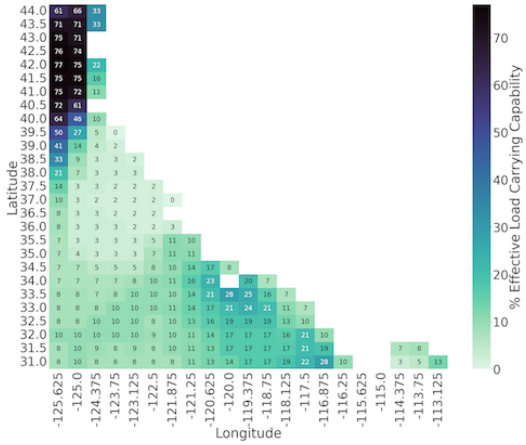

(b) ELCC of 100-MW offshore wind generator, 2005

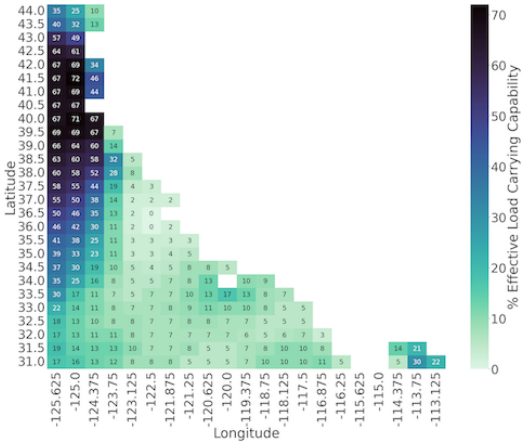

(c) ELCC of 100-MW offshore wind generator, 2006

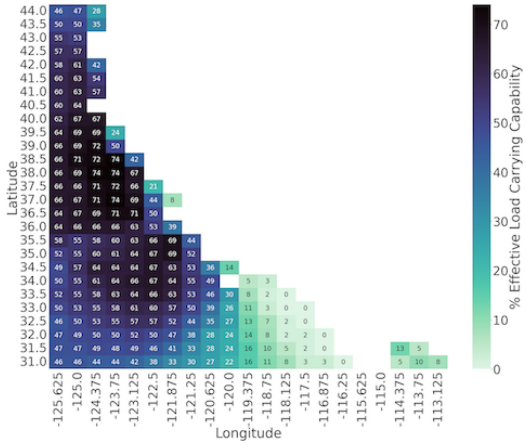

(d) ELCC of 100-MW offshore wind generator, 2007

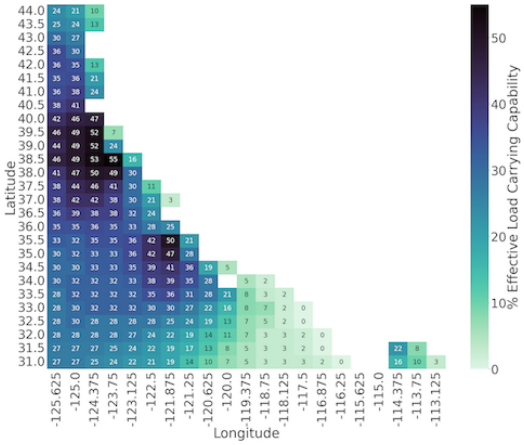

(e) ELCC of 100-MW offshore wind generator, 2008

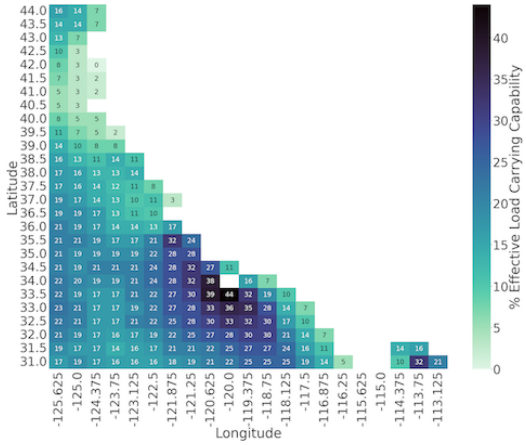

(f) ELCC of 100-MW offshore wind generator, 2009

Figure C.38: Geographical distribution of ELCCs for a new 100-MW offshore wind generator added to the existing base fleet of California Independent System Operator between 2004 - 2009.

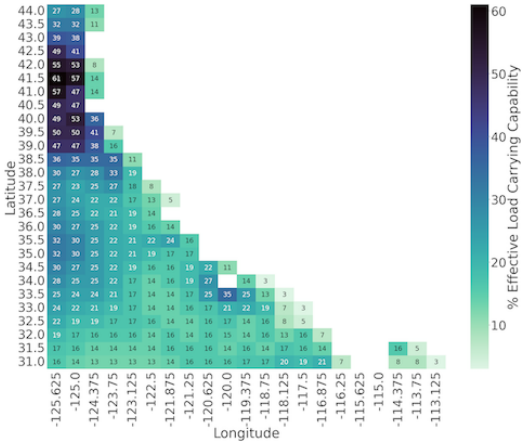

(a) ELCC of 100-MW offshore wind generator, 2010

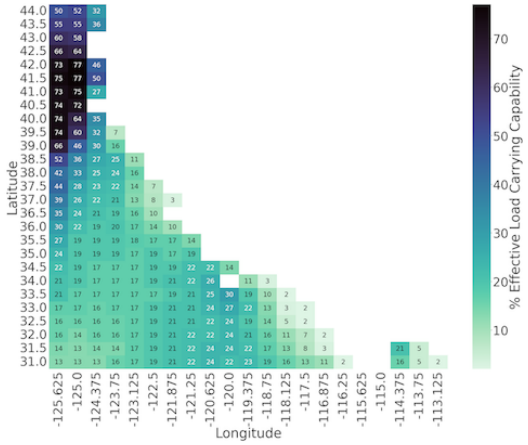

(b) ELCC of 100-MW offshore wind generator, 2011

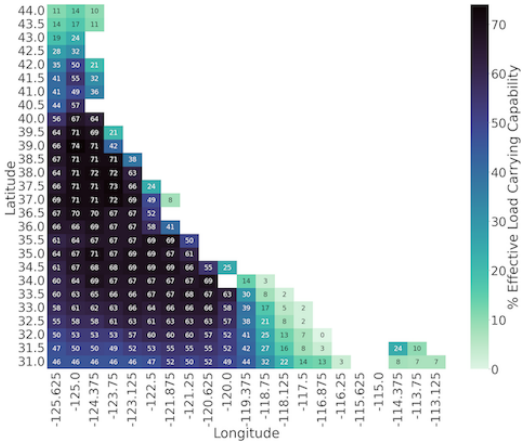

(c) ELCC of 100-MW offshore wind generator, 2012

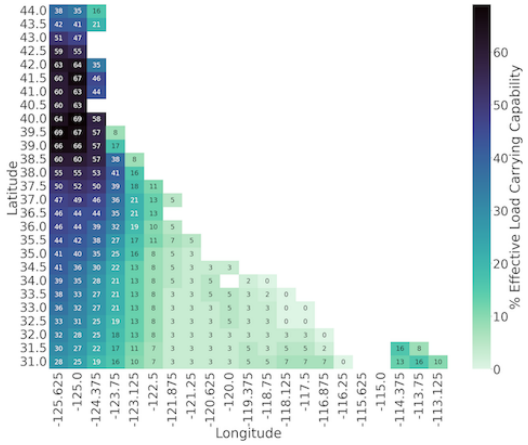

(d) ELCC of 100-MW offshore wind generator, 2013

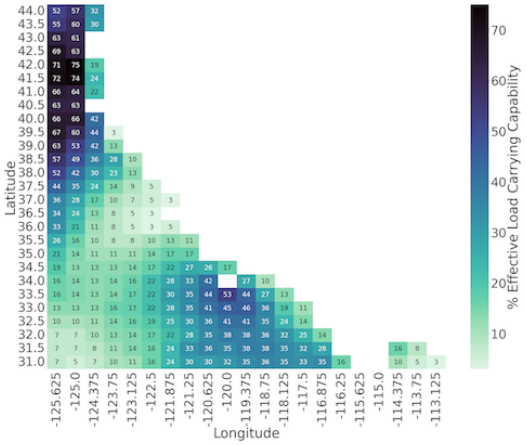

(e) ELCC of 100-MW offshore wind generator, 2014

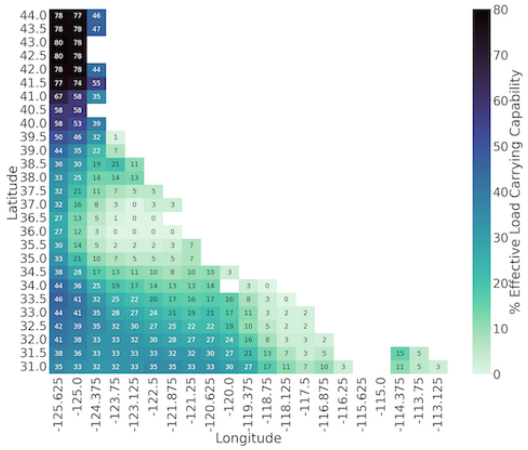

(f) ELCC of 100-MW offshore wind generator, 2015

Figure C.39: Geographical distribution of ELCCs for a new 100-MW offshore wind generator added to the existing base fleet of California Independent System Operator between 2010-2015.

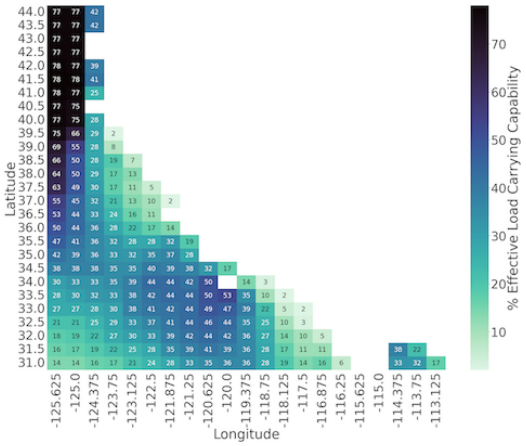

(a) ELCC of 100-MW offshore wind generator, 2016

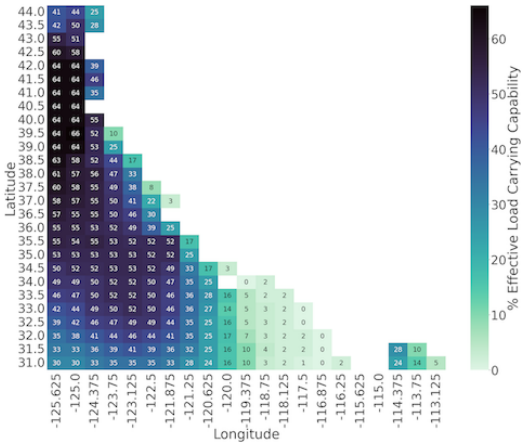

(b) ELCC of 100-MW offshore wind generator, 2017

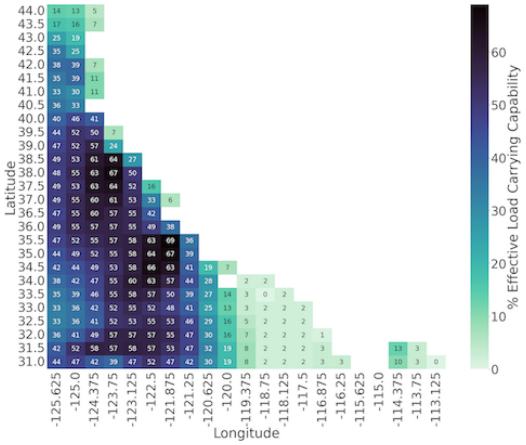

(c) ELCC of 100-MW offshore wind generator, 2018

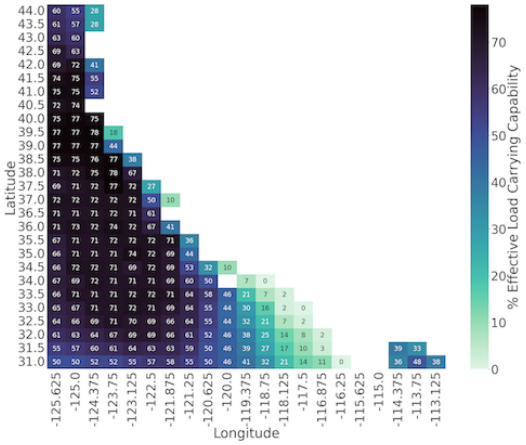

(d) ELCC of 100-MW offshore wind generator, 2019

Figure C.40: Geographical distribution of ELCCs for a new 100-MW offshore wind generator added to the existing base fleet of California Independent System Operator between 2016-2019.

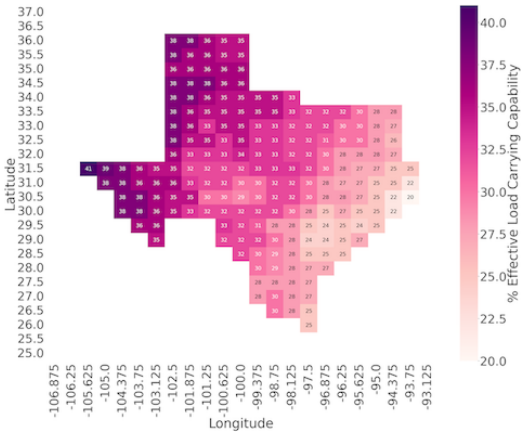

(a) ELCC of 100-MW solar generator, 1980

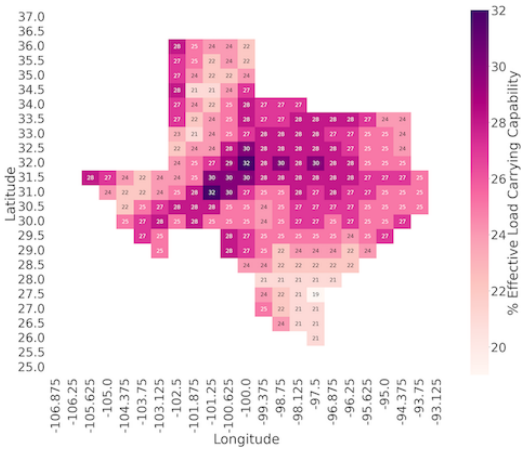

(b) ELCC of 100-MW solar generator, 1981

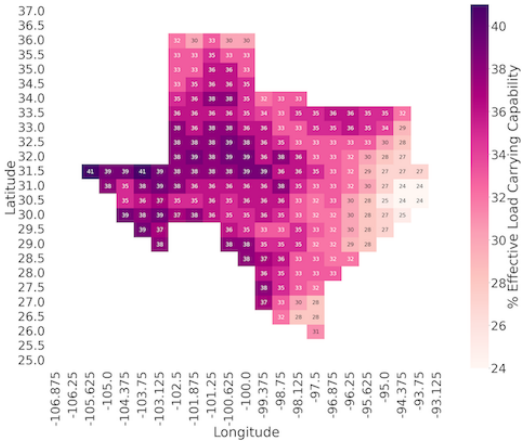

(c) ELCC of 100-MW solar generator, 1982

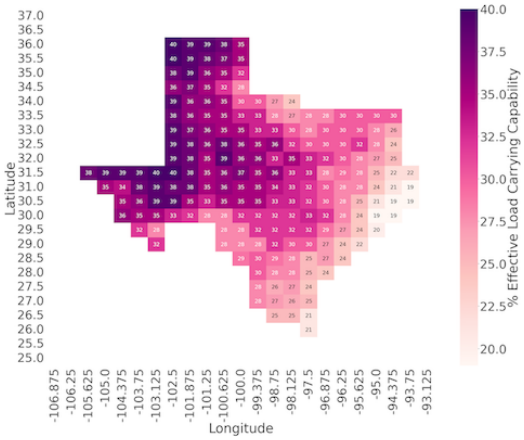

(d) ELCC of 100-MW solar generator, 1983

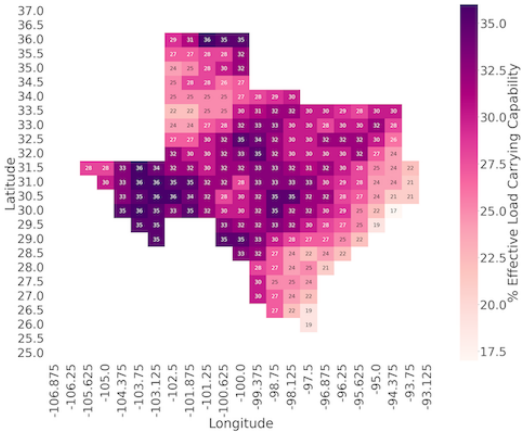

(e) ELCC of 100-MW solar generator, 1984

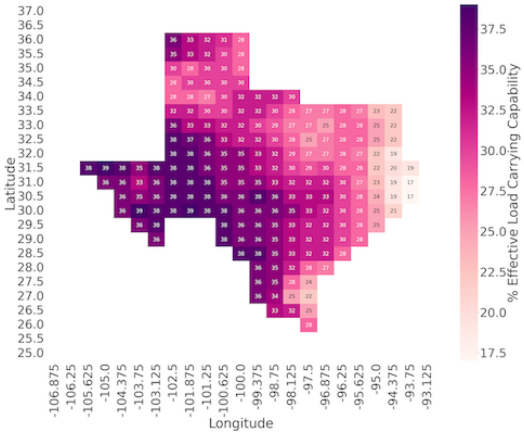

(f) ELCC of 100-MW solar generator, 1985

Figure C.41: Geographical distribution of ELCC values between 1980 -1985 for a new 100-MW solar generator added to the existing base fleet from 2019 of California Independent System Operator.

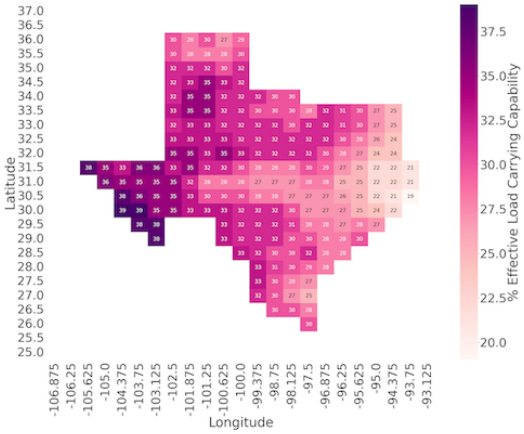

(a) ELCC of 100-MW solar generator, 1986

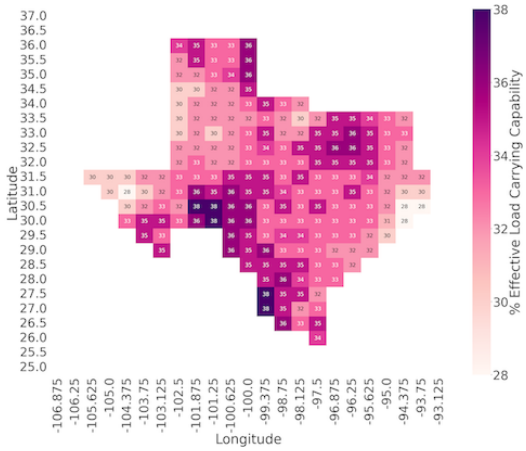

(b) ELCC of 100-MW solar generator,1987

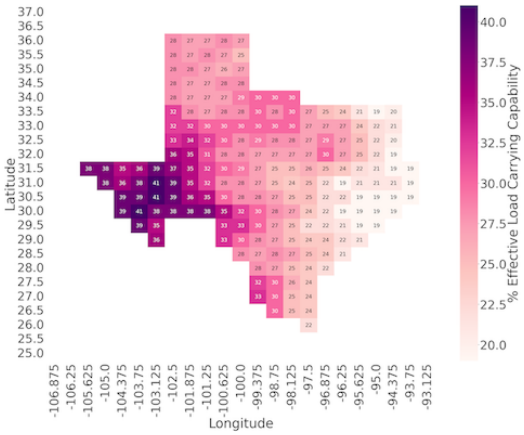

(c) ELCC of 100-MW solar generator, 1988

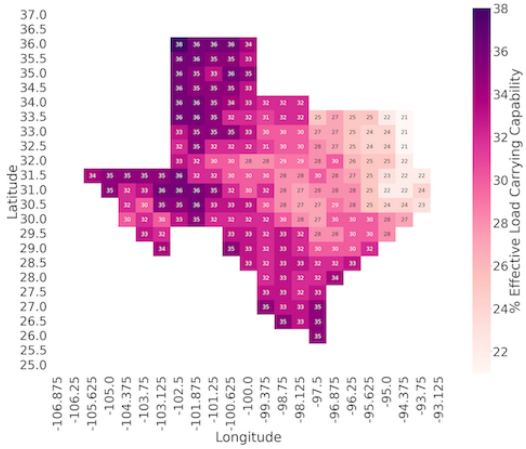

(d) ELCC of 100-MW solar generator, 1989

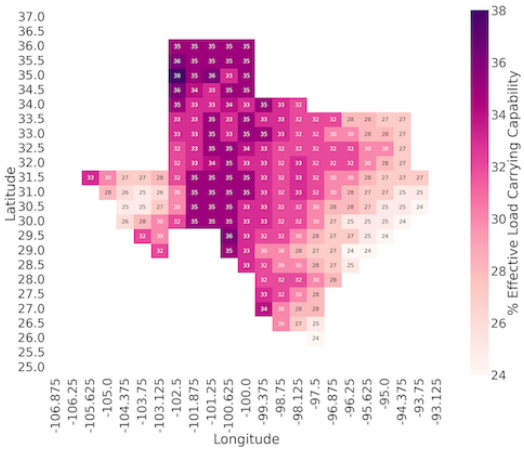

(e) ELCC of 100-MW solar generator, 1990

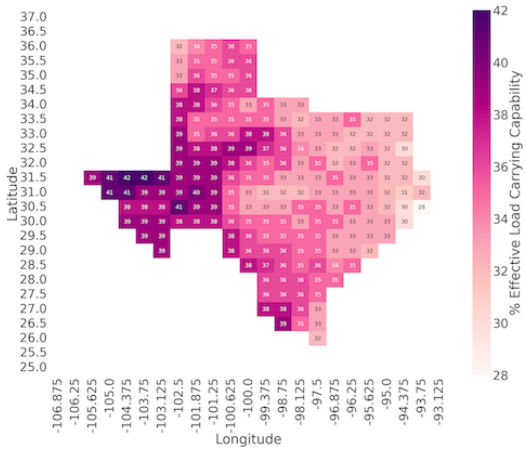

(f) ELCC of 100-MW solar generator, 1991

Figure C.42: Geographical distribution of ELCC values between 1986 -1991 for a new 100-MW solar generator added to the existing base fleet from 2019 of ERCOT.

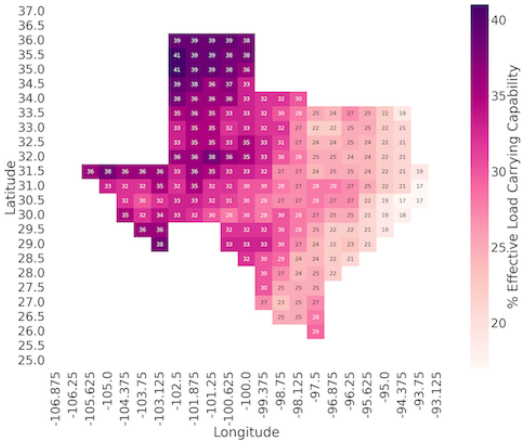

(a) ELCC of 100-MW solar generator, 1992

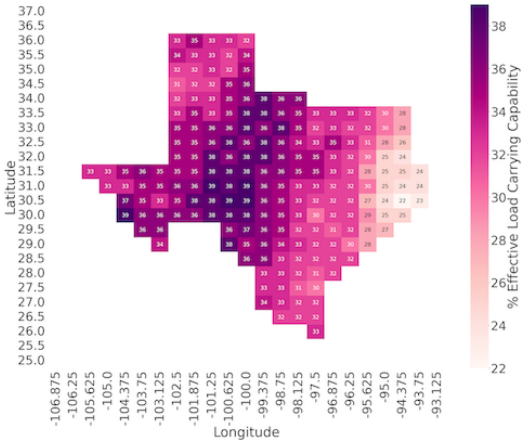

(b) ELCC of 100-MW solar generator, 1993

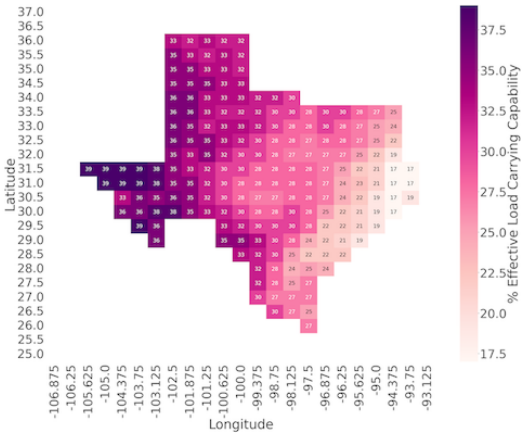

(c) ELCC of 100-MW solar generator, 1994

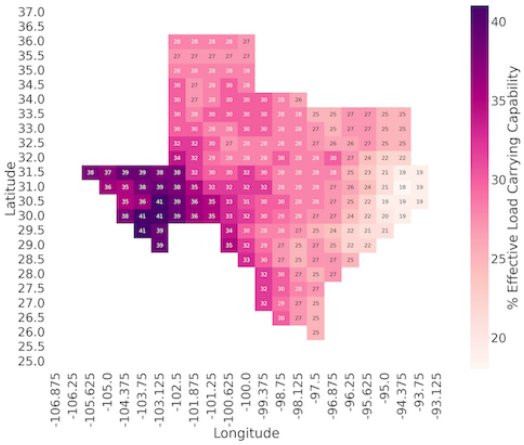

(d) ELCC of 100-MW solar generator, 1995

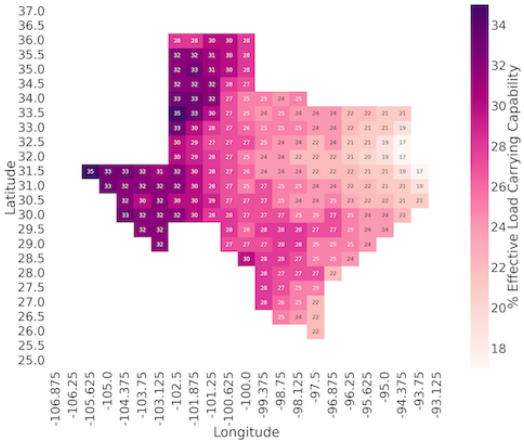

(e) ELCC of 100-MW solar generator, 1996

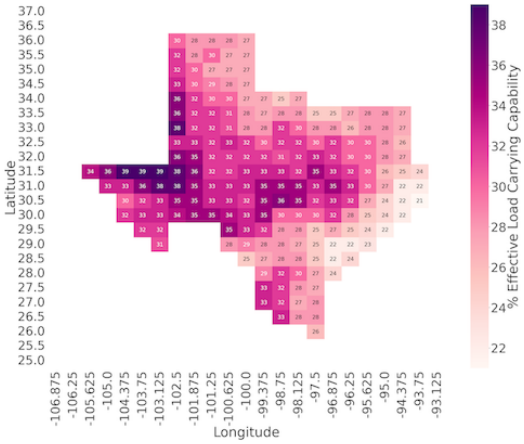

(f) ELCC of 100-MW solar generator, 1997

Figure C.43: Geographical distribution of ELCCs for a new 100-MW solar generator added to the existing base fleet of California Independent System Operator between 1992 -1997.

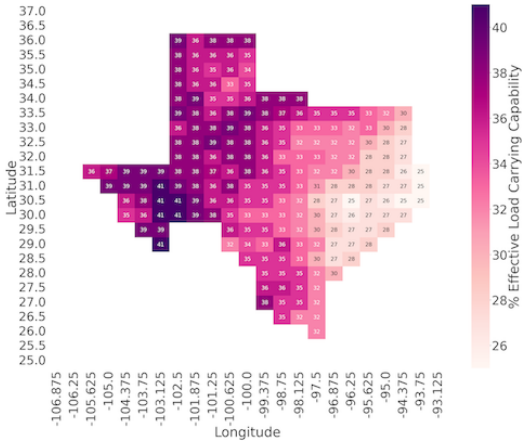

(a) ELCC of 100-MW solar generator, 1998

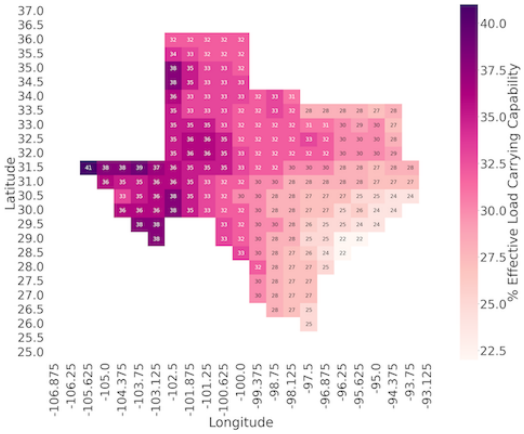

(b) ELCC of 100-MW solar generator, 1999

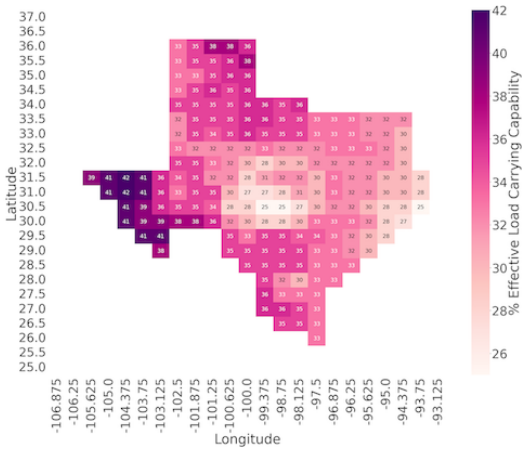

(c) ELCC of 100-MW solar generator, 2000

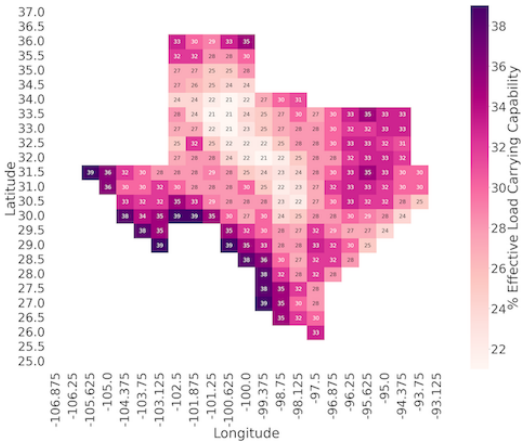

(d) ELCC of 100-MW solar generator, 2001

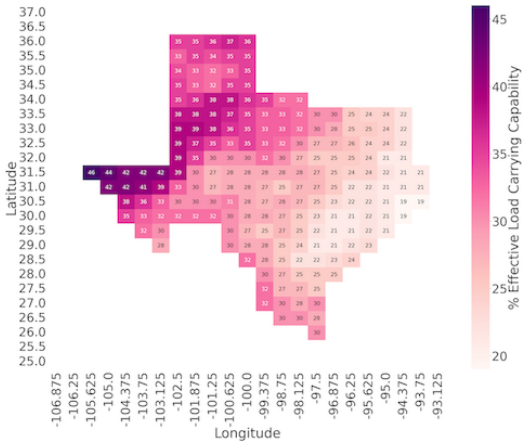

(e) ELCC value of 100-MW solar generator in 2002

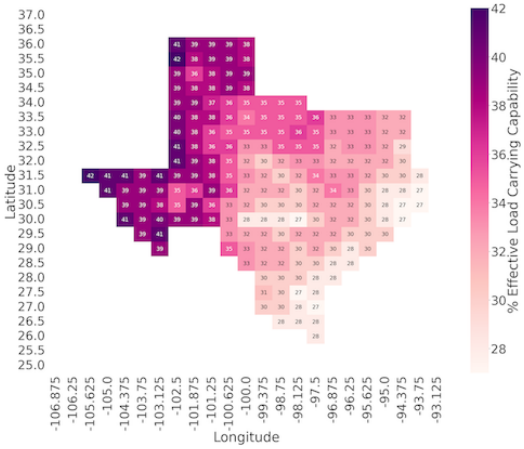

(f) ELCC of 100-MW solar generator, 2003

Figure C.44: Geographical distribution of ELCCs for a new 100-MW solar generator added to the existing base fleet of California Independent System Operator between 1998 - 2003.

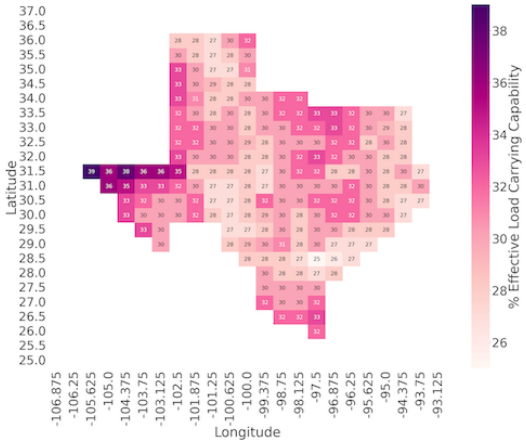

(a) ELCC of 100-MW solar generator, 2004

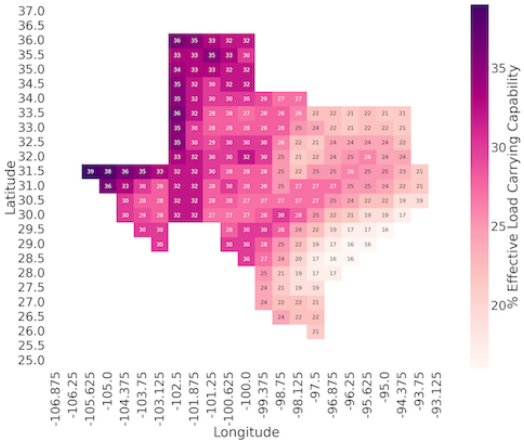

(b) ELCC of 100-MW solar generator, 2005

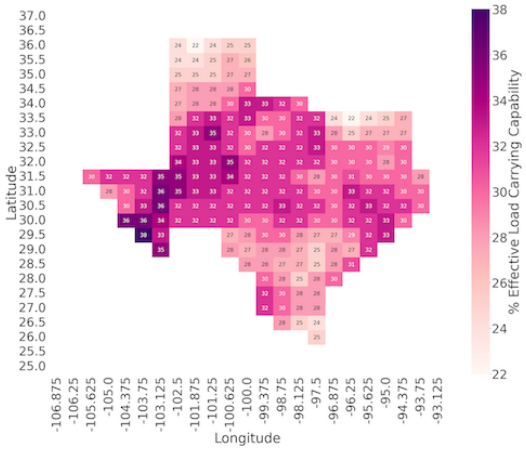

(c) ELCC of 100-MW solar generator, 2006

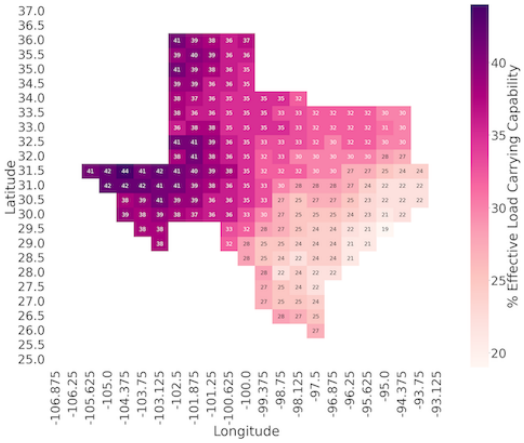

(d) ELCC of 100-MW solar generator, 2007

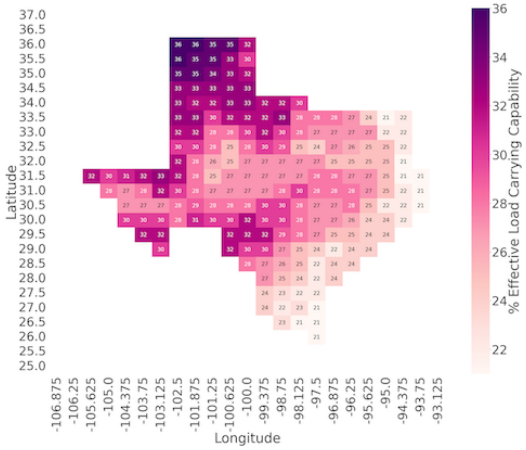

(e) ELCC of 100-MW solar generator, 2008

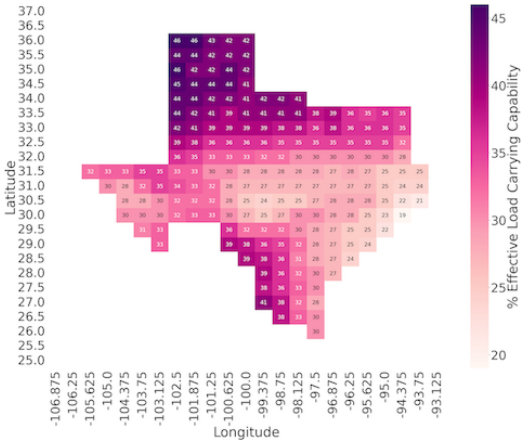

(f) ELCC of 100-MW solar generator, 2009

Figure C.45: Geographical distribution of ELCCs for a new 100-MW solar generator added to the existing base fleet of California Independent System Operator between 2004 - 2009.

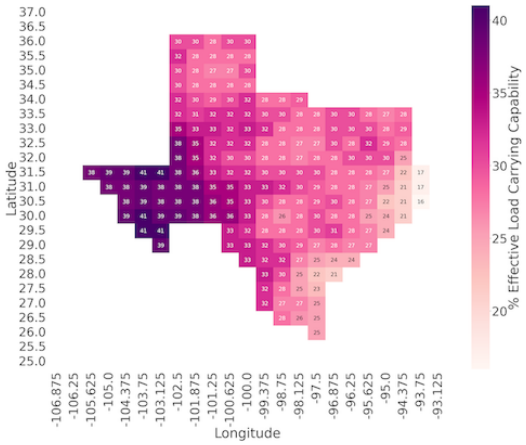

(a) ELCC of 100-MW solar generator, 2010

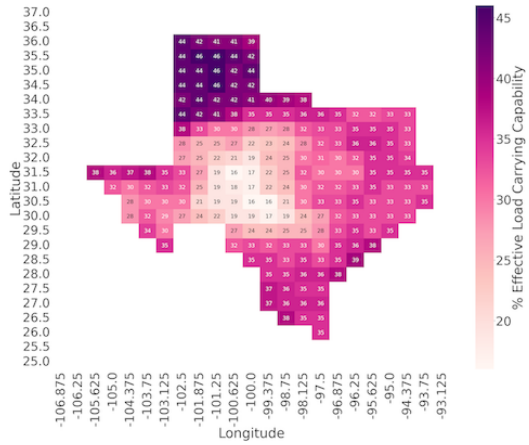

(b) ELCC of 100-MW solar generator, 2011

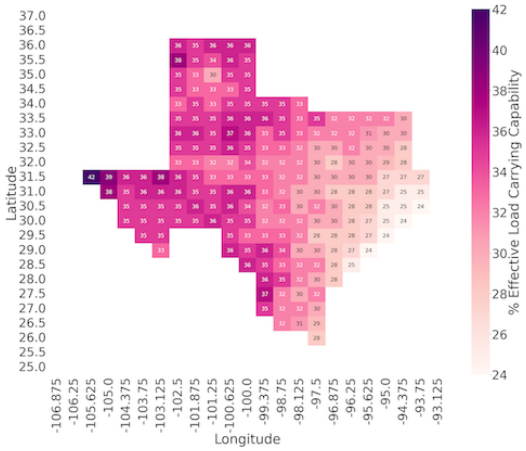

(c) ELCC of 100-MW solar generator, 2012

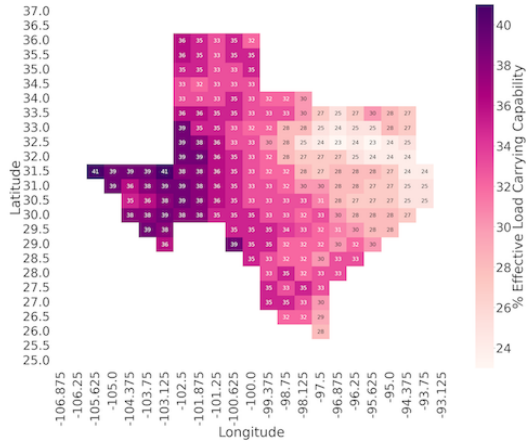

(d) ELCC of 100-MW solar generator, 2013

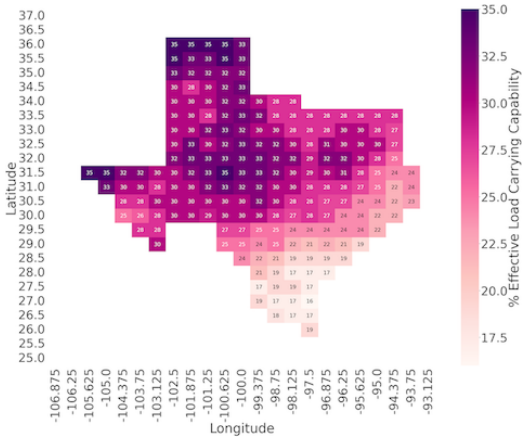

(e) ELCC of 100-MW solar generator, 2014

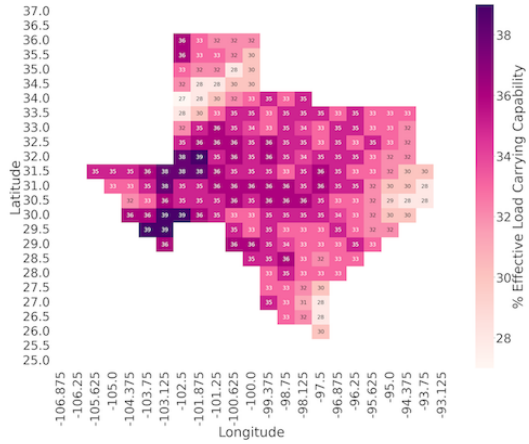

(f) ELCC of 100-MW solar generator, 2015

Figure C.46: Geographical distribution of ELCCs for a new 100-MW solar generator added to the existing base fleet of ERCOT between 2010 - 2015.

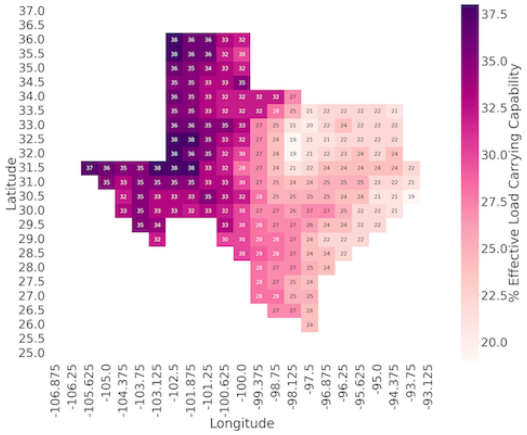

(a) ELCC of 100-MW solar generator, 2016

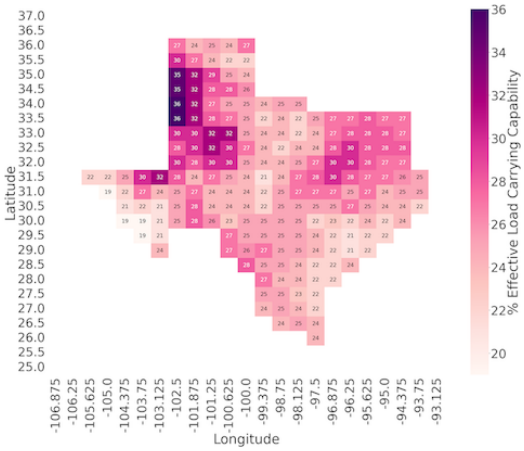

(b) ELCC of 100-MW solar generator, 2017

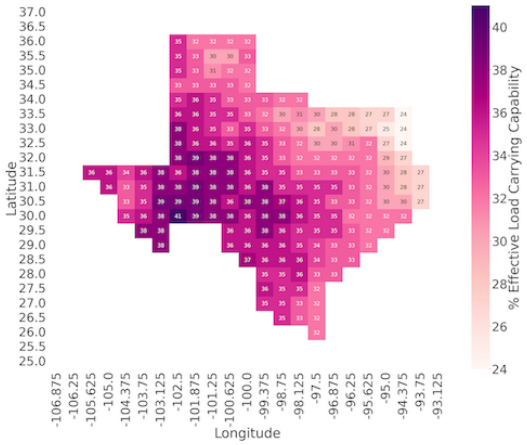

(c) ELCC of 100-MW solar generator, 2018

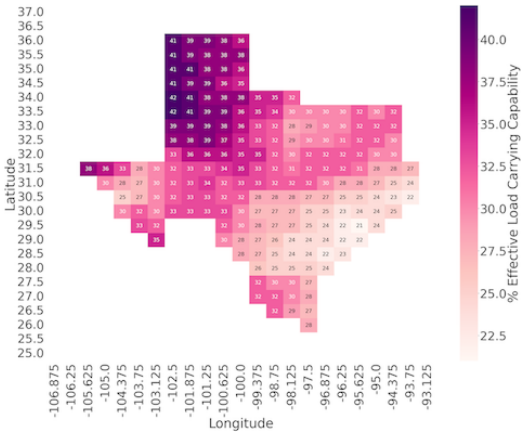

(d) ELCC of 100-MW solar generator, 2019

Figure C.47: Geographical distribution of ELCCs for a new 100-MW solar generator added to the existing base fleet of ERCOT between 2016 - 2019.

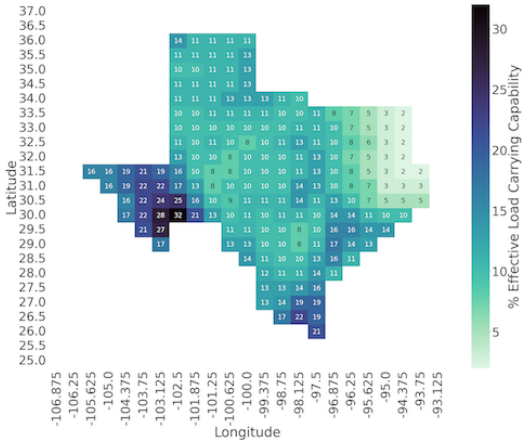

(a) ELCC of 100-MW onshore wind generator, 1980

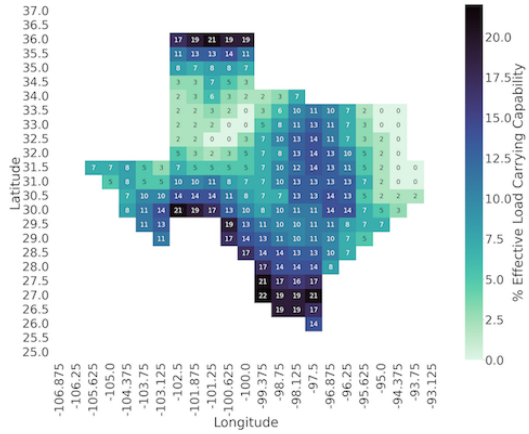

(b) ELCC of 100-MW onshore wind generator, 1981

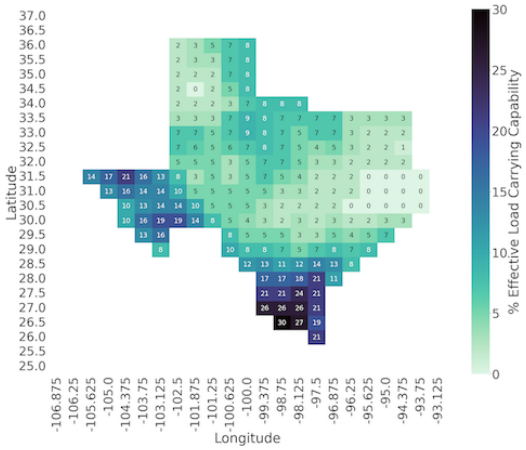

(c) ELCC of 100-MW onshore wind generator, 1982

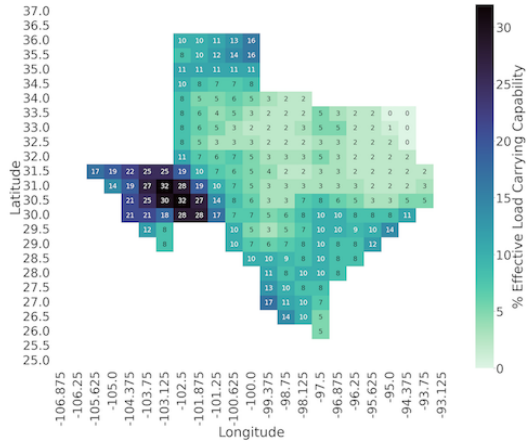

(d) ELCC of 100-MW onshore wind generator, 1983

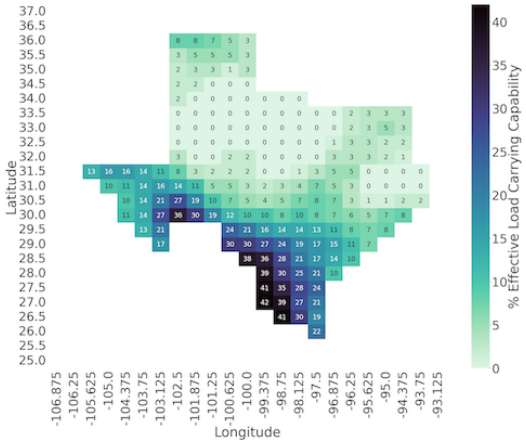

(e) ELCC of 100-MW onshore wind generator, 1984

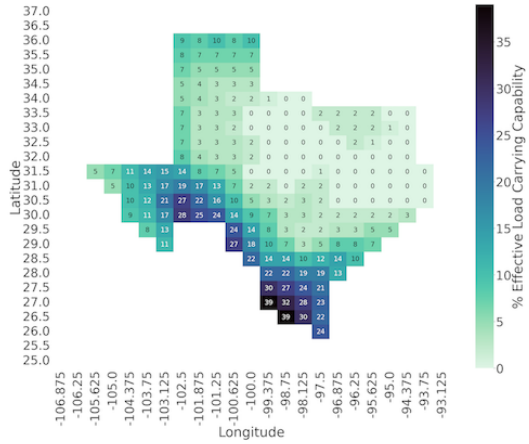

(f) ELCC of 100-MW onshore wind generator, 1985

Figure C.48: Geographical distribution of ELCCs for a new 100-MW onshore wind generator added to the existing base fleet of ERCOT between 1980-1985.

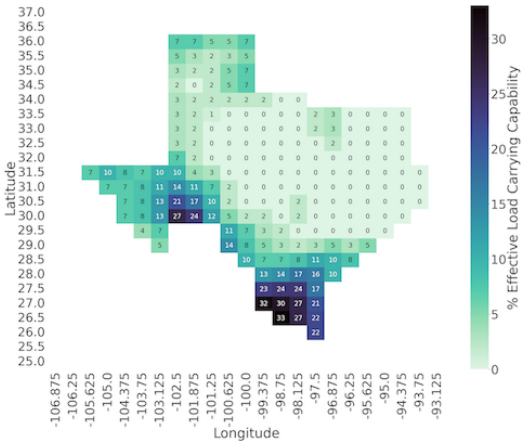

(a) ELCC of 100-MW onshore wind generator, 1986

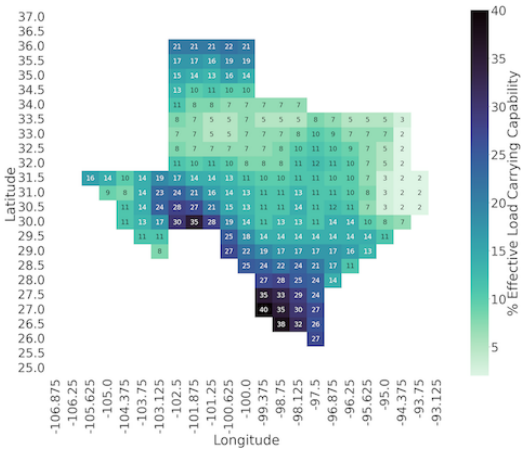

(b) ELCC of 100-MW onshore wind generator, 1987

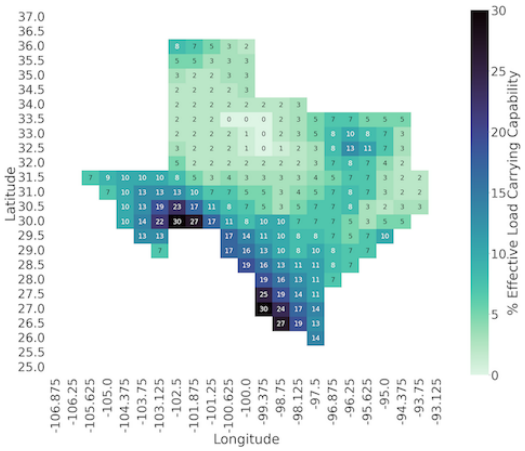

(c) ELCC of 100-MW onshore wind generator, 1988

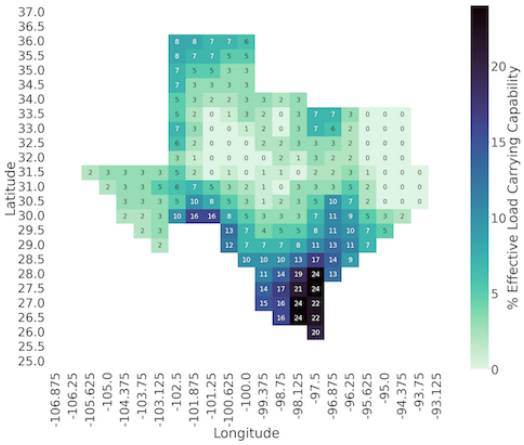

(d) ELCC of 100-MW onshore wind generator, 1989

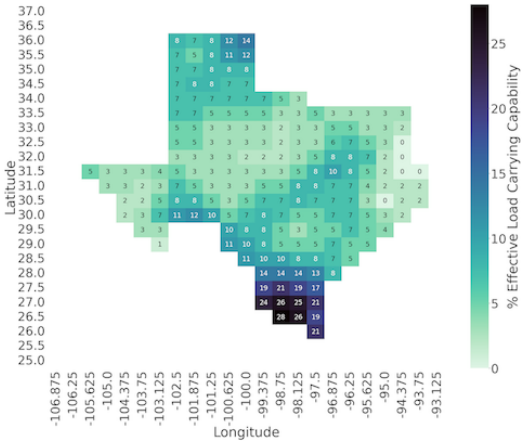

(e) ELCC of 100-MW onshore wind generator, 1990

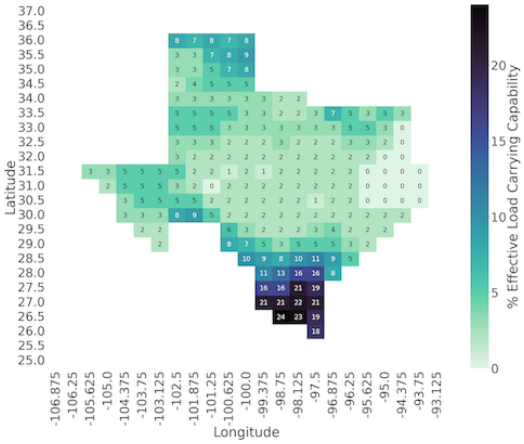

(f) ELCC of 100-MW onshore wind generator, 1991

Figure C.49: Geographical distribution of ELCCs for a new 100-MW onshore wind generator added to the existing base fleet of ERCOT between 1986 -1991.

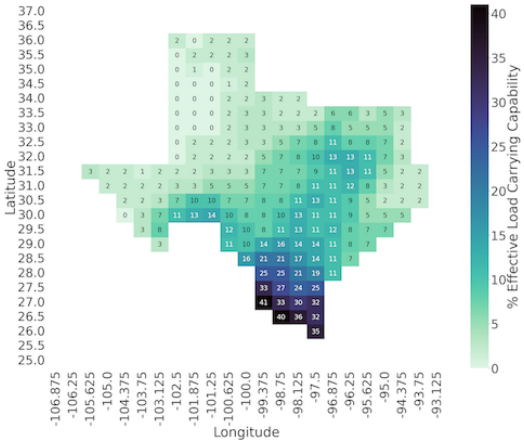

(a) ELCC of 100-MW onshore wind generator, 1992

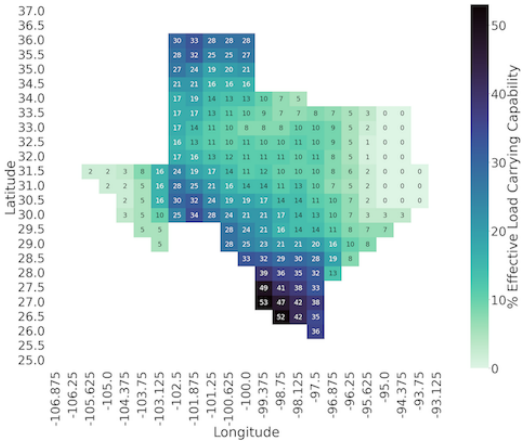

(b) ELCC of 100-MW onshore wind generator, 1993

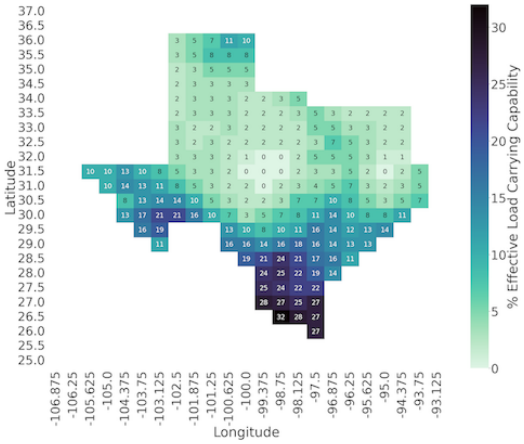

(c) ELCC of 100-MW onshore wind generator, 1994

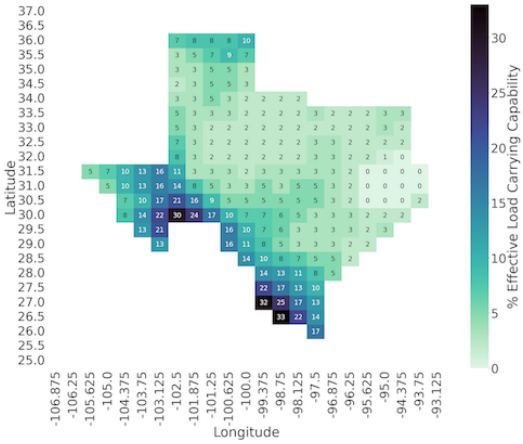

(d) ELCC of 100-MW onshore wind generator, 1995

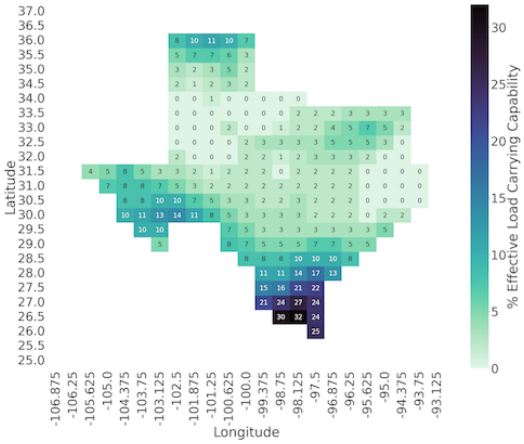

(e) ELCC of 100-MW onshore wind generator, 1996

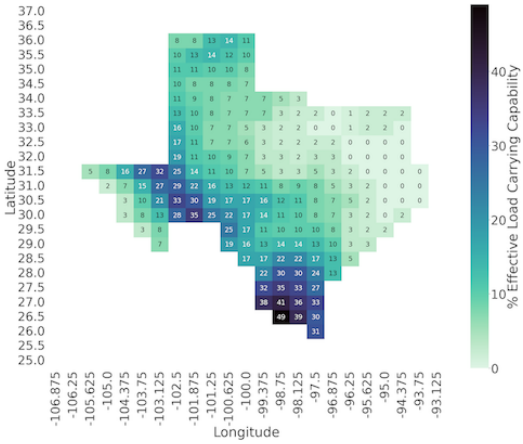

(f) ELCC of 100-MW onshore wind generator, 1997

Figure C.50: Geographical distribution of ELCCs for a new 100-MW onshore wind generator added to the existing base fleet of ERCOT between 1992 -1997.

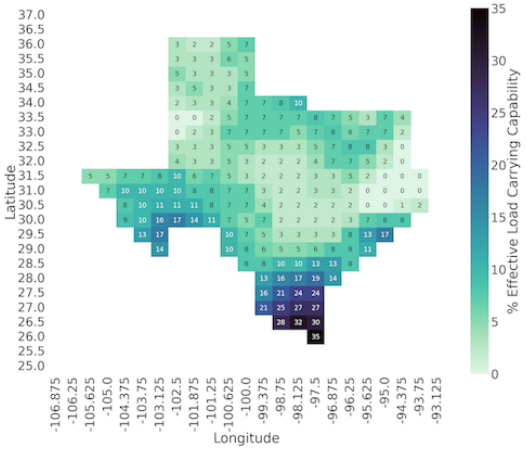

(a) ELCC of 100-MW onshore wind generator, 1998

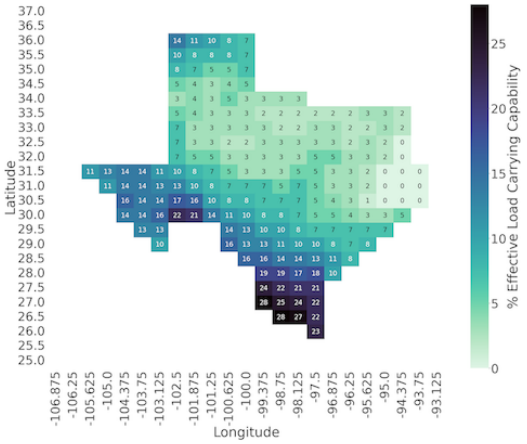

(b) ELCC of 100-MW onshore wind generator, 1999

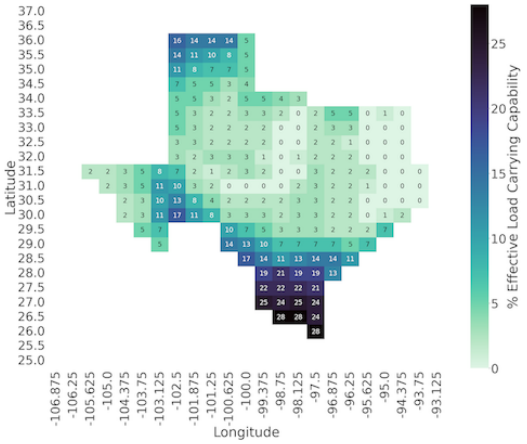

(c) ELCC of 100-MW onshore wind generator, 2000

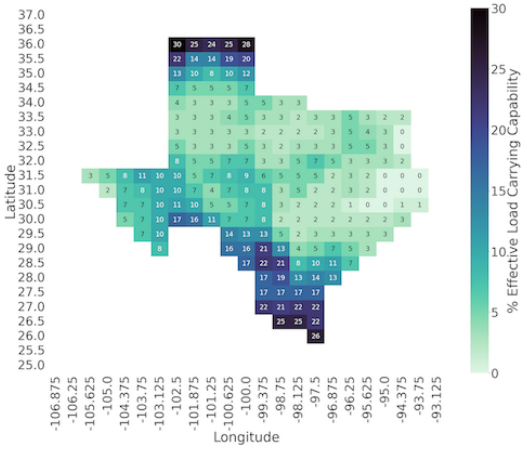

(d) ELCC of 100-MW onshore wind generator, 2001

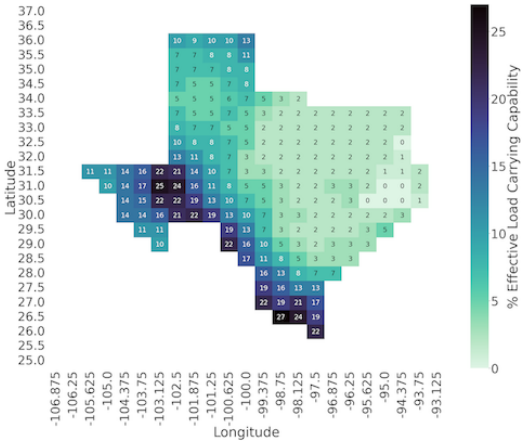

(e) ELCC of 100-MW onshore wind generator, 2002

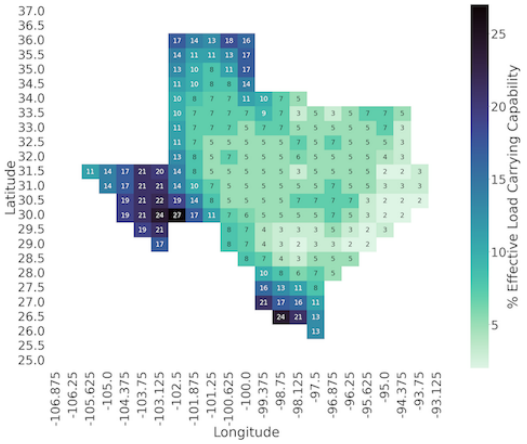

(f) ELCC of 100-MW onshore wind generator, 2003

Figure C.51: Geographical distribution of ELCCs for a new 100-MW onshore wind generator added to the existing base fleet of ERCOT between 1998 - 2003.

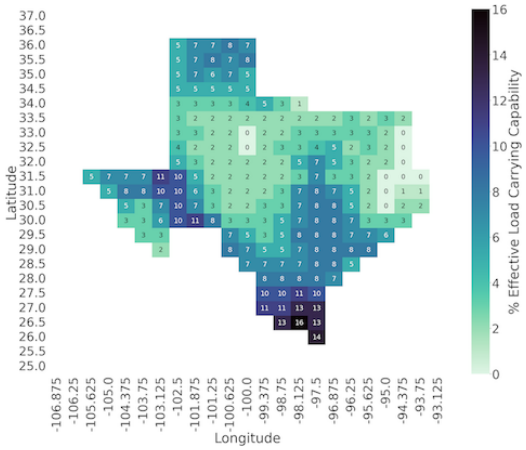

(a) ELCC of 100-MW onshore wind generator, 2004

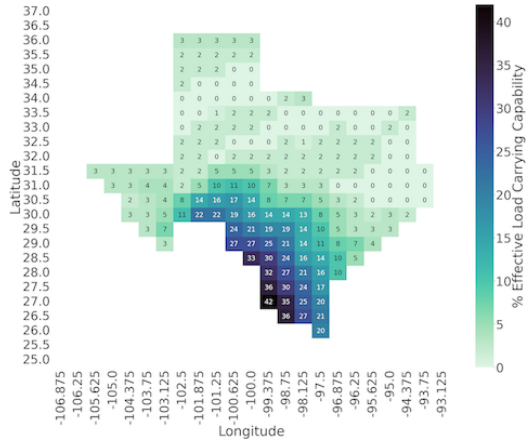

(b) ELCC of 100-MW onshore wind generator, 2005

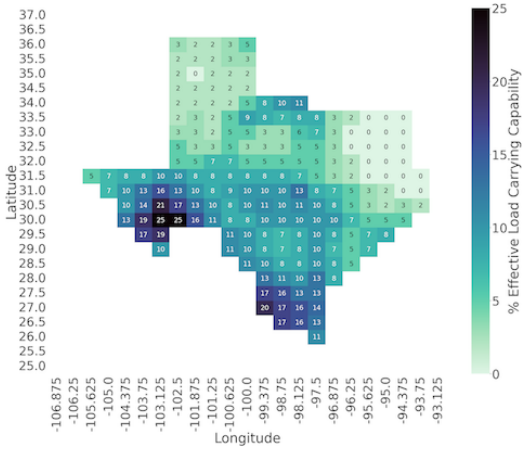

(c) ELCC of 100-MW onshore wind generator, 2006

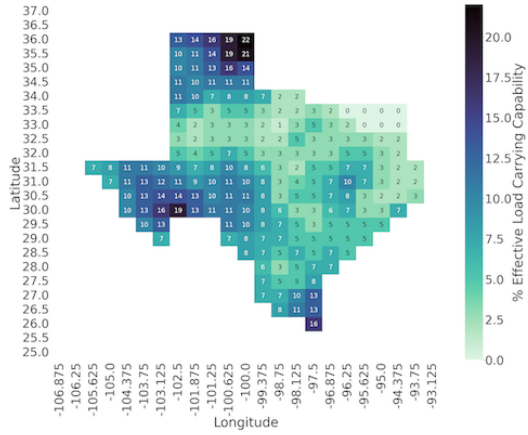

(d) ELCC of 100-MW onshore wind generator, 2007

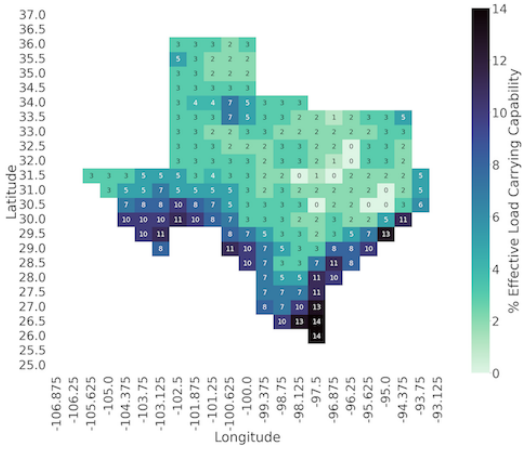

(e) ELCC of 100-MW onshore wind generator, 2008

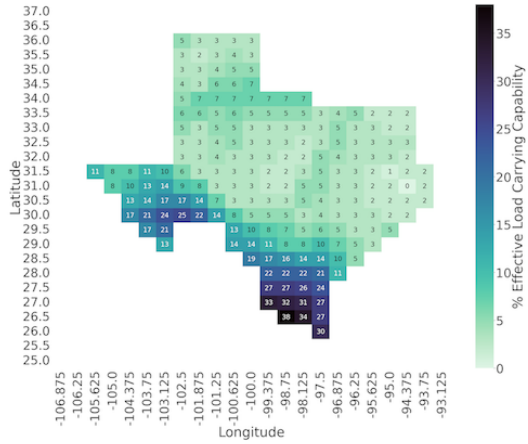

(f) ELCC of 100-MW onshore wind generator, 2009

Figure C.52: Variability of ELCCs between 2004 - 2009 for a new 100-MW onshore wind generator added to the existing base fleet of ERCOT.

References

AEO (2021). URL: https://www.eia.gov/outlooks/aeo/.

Ahmad, Ali (2021). "Increase in frequency of nuclear power outages due to changing climate". In: *Nature Energy* 6.7, pp. 755–762.

Auffhammer, Maximilian, Patrick Baylis, and Catherine H Hausman (2017). "Climate change is projected to have severe impacts on the frequency and intensity of peak electricity demand across the United States". In: *Proceedings of the National Academy of Sciences* 114.8, pp. 1886–1891.

AWEA fact sheet (2019). https://www.google.com/search?q=AWEA+offshore+fact+sheet&oq=AWEA+offshore+fact+sheet&aqs=chrome..69i57j0i22i30j69i65j69i60l2.5106j0j4&sourceid=chrome&ie=UTF-8. (Accessed on 06/09/2021).

Beiter, Philipp C et al. (2020). *The Potential Impact of Offshore Wind Energy on a Future Power System in the US Northeast*. Tech. rep. National Renewable Energy Lab.(NREL), Golden, CO (United States).

Bessec, M. and J. Fouquau (2008). "The non-linear link between electricity consumption and temperature in Europe: A threshold panel approach". In: *Energy Economics* 30.5, pp. 2705–2721. URL: https://doi.org/10.1016/j.eneco.2008.02.003.

Bistline, John ET et al. (2020). "Electric sector impacts of renewable policy coordination: A multi-model study of the North American energy system". In: *Energy Policy* 145, p. 111707.

Blair, Nate et al. (2014). *System advisor model, sam 2014.1. 14: General description*. Tech. rep. National Renewable Energy Lab.(NREL), Golden, CO (United States).

Bloomfield, H. C. et al. (2016). "Quantifying the increasing sensitivity of power systems to climate variability". In: *Environmental Research Letters* 11.12, p. 124025. URL: https://doi.org/10.1088/1748-9326/11/12/124025.

Bloomfield, Hannah, David Brayshaw, and Andrew Charlton-Perez (2020). "ERA5 derived time series of European country-aggregate electricity demand, wind power generation and solar power generation: hourly data from 1979-2019". In:

Bloomfield, Hannah C., D. J. Brayshaw, and A. J. Charlton-Perez (2020). "Characterizing the winter meteorological drivers of the European electricity system using targeted circulation types". In: *Meteorological Applications* 27, p. 1. URL: https://doi.org/10.1002/met.1858.

Bloomfield, HC et al. (2018). "The changing sensitivity of power systems to meteorological drivers: a case study of Great Britain". In: *Environmental Research Letters* 13.5, p. 054028.

Boccard, Nicolas (2009). "Capacity factor of wind power realized values vs. estimates". In: *energy policy* 37.7, pp. 2679–2688.

Bosilovich, MG, R Lucchesi, and M Suarez (2015). "MERRA-2: File specification". In:

Bothwell, Cynthia and Alex Pavlak (2015). "Reliability concerns with ELCC calculations under high wind penetration". In: *2015 IEEE Power & Energy Society General Meeting*. IEEE, pp. 1–5.

Bromley-Dulfano, Isaac, Julian Florez, and Michael T Craig (2021). "Reliability benefits of wide-area renewable energy planning across the Western United States". In: *Renewable Energy* 179, pp. 1487–1499.

Bryce, Richard et al. (2018). "Consequences of neglecting the interannual variability of the solar resource: A case study of photovoltaic power among the Hawaiian Islands". In: *Solar Energy* 167, pp. 61–75.

Bukovsky, Melissa S and Linda O Mearns (2020). "Regional climate change projections from NA-CORDEX and their relation to climate sensitivity". In: *Climatic Change* 162.2, pp. 645–665.

Carreño, Ignacio Losada et al. (2020). "Potential impacts of climate change on wind and solar electricity generation in Texas". In: *Climatic Change* 163.2, pp. 745–766.

Castro, Rui MG and Luís AFM Ferreira (2001). "A comparison between chronological and probabilistic methods to estimate wind power capacity credit". In: *IEEE Transactions on Power Systems* 16.4, pp. 904–909.

Chen, Zexi et al. (2021). "Load Forecasting Based on LSTM Neural Network and Applicable to Loads of "Replacement of Coal with Electricity"". In: *Journal of Electrical Engineering & Technology*, pp. 1–10.

Coker, P. J. et al. (2020). "Interannual weather variability and the challenges for Great Britain's electricity market design". In: *Renewable Energy* 150, pp. 509–522. URL: https://doi.org/10.1016/j.renene.2019.12.082.

Collins, Seán et al. (2018). "Impacts of Inter-annual Wind and Solar Variations on the European Power System". In: *Joule* 2.10, pp. 2076–2090. ISSN: 2542-4351. DOI: https://doi.org/10.1016/j.joule.2018.06.020. URL: https://www.sciencedirect.com/science/article/pii/S254243511830285X.

Council, North American Electricity Reliability (Jan. 2020). *Long-Term Reliability Assessment*. Tech. rep. North American Electricity Reliability Council.

Craig, M et al. (2021). "Climate-Induced Tradeoffs in Planning and Operating Costs of a Regional Electricity System." In: *Environmental Science & Technology*.

Davy, Robert J and Alberto Troccoli (2012). "Interannual variability of solar energy generation in Australia". In: *Solar Energy* 86.12, pp. 3554–3560.

De Felice, Matteo, Andrea Alessandri, and Franco Catalano (2015). "Seasonal climate forecasts for medium-term electricity demand forecasting". In: *Applied Energy* 137, pp. 435–444.

EIA (Mar. 2021). *The United States installed more wind turbine capacity in 2020 than in any other year - Today in Energy - U.S. Energy Information Administration (EIA)*. https://www.eia.gov/todayinenergy/detail.php?id=46976. (Accessed on 10/20/2021).

EIA, US (2015). "Form EIA-860". In: *Visited on* 7.11, p. 2017.

Fedorov, VM (2019). "Analysis of the components of a different physical nature in the interannual variability of the total solar irradiance flux". In: *Solar System Research* 53.5, pp. 376–382.

Fonseca, Francisco Ralston et al. (2019). "Seasonal effects of climate change on intra-day electricity demand patterns". In: *Climatic Change* 154.3, pp. 435–451.

Garrido, Patricio Rocha (2019). *Effective Load Carrying Capability(ELCC) Review*. Tech. rep. Pennsylvania-New Jersey-Maryland Balancing Authority. URL: https://www.pjm.com/-/media/committees-groups/committees/pc/20191017/20191017-item-18-elcc-review.ashx.

HIFLD Control Areas (n.d.). URL: https://hifld-geoplatform.opendata.arcgis.com/datasets/control-areas/explore.

Hochreiter, Sepp and Jürgen Schmidhuber (1997). "Long short-term memory". In: *Neural computation* 9.8, pp. 1735–1780.

Hodge, Tyler (Feb. 2020). *Hourly electricity consumption varies throughout the day and across seasons - Today in Energy - U.S. Energy Information Administration (EIA)*. URL: https://www.eia.gov/todayinenergy/detail.php?id=42915.

Holmgren, Will et al. (Jan. 2021). *pvlib/pvlib-python: v0.8.1*. Version v0.8.1. DOI: 10.5281/zenodo.4417742. URL: https://doi.org/10.5281/zenodo.4417742.

Holmgren, William F, Clifford W Hansen, and Mark A Mikofski (2018). "pvlib python: A python package for modeling solar energy systems". In: *Journal of Open Source Software* 3.29, p. 884.

Hor, Ching-Lai, Simon J Watson, and Shanti Majithia (2005). "Analyzing the impact of weather variables on monthly electricity demand". In: *IEEE transactions on power systems* 20.4, pp. 2078–2085.

Hostick, Donna et al. (2012). *Renewable Electricity Futures Study. Volume 3. End-Use Electricity Demand*. Tech. rep. National Renewable Energy Lab.(NREL), Golden, CO (United States).

Ibanez, Eduardo and Michael Milligan (2014). "Comparing resource adequacy metrics and their influence on capacity value". In: *2014 International Conference on Probabilistic Methods Applied to Power Systems (PMAPS)*. IEEE, pp. 1–6.

IEA (2020). *Renewable Energy*. Tech. rep. International Energy Agency.

IEC 61400 (May 2021). URL: https://en.wikipedia.org/wiki/IEC_61400.

Jung, Christopher, Diana Taubert, and Dirk Schindler (2019). "The temporal variability of global wind energy–Long-term trends and inter-annual variability". In: *Energy Conversion and Management* 188, pp. 462–472.

Keane, Andrew et al. (2010). "Capacity value of wind power". In: *IEEE Transactions on Power Systems* 26.2, pp. 564–572.

Keeley, Sarah (Jan. 2021). *Climate reanalysis*. URL: https://www.ecmwf.int/en/research/climate-reanalysis.

Krakauer, N. Y. and D. S. Cohan (2017). "Interannual Variability and Seasonal Predictability of Wind and Solar Resources". In: *Resources* 6.3, p. 29. URL: https://doi.org/10.3390/resources6030029.

Kramer, Oliver (2016). "Scikit-learn". In: *Machine learning for evolution strategies*. Springer, pp. 45–53.

Kumar, Rohini et al. (2020). "Asymmetrical response of California electricity demand to summer-time temperature variation". In: *Scientific reports* 10.1, pp. 1–9.

Kumler, Andrew et al. (2019). "Inter-annual variability of wind and solar electricity generation and capacity values in Texas". In: *Environmental Research Letters* 14.4, p. 044032.

Li, X. et al. (2010). "Climate and climate variability of the wind power resources in the Great Lakes region of the United States". In: *Journal of Geophysical Research: Atmospheres* 115.D18107, pp. 1–15. URL: https://doi.org/10.1029/2009JD013415.

Lopez, Anthony et al. (2021). "Land use and turbine technology influences on wind potential in the United States". In: *Energy* 223, p. 120044.

Madaeni, Seyed Hossein, Ramteen Sioshansi, and Paul Denholm (2012). "Comparing capacity value estimation techniques for photovoltaic solar power". In: *IEEE Journal of Photovoltaics* 3.1, pp. 407–415.

Maia-Silva, Debora, Rohini Kumar, and Roshanak Nateghi (2020). "The critical role of humidity in modeling summer electricity demand across the United States". In: *Nature communications* 11.1, pp. 1–8.

Martinot, Eric (2016). "Grid integration of renewable energy: flexibility, innovation, and experience". In: *Annual Review of Environment and Resources* 41.

Maxwell, Eugene L (1987). "A quasi-physical model for converting hourly global horizontal to direct normal insolation". In: *Unknow*.

McVicar, Tim R et al. (2012). "Global review and synthesis of trends in observed terrestrial near-surface wind speeds: Implications for evaporation". In: *Journal of Hydrology* 416, pp. 182–205.

Megan Cleveland, Laura Shields (2021). URL: https://www.ncsl.org/research/energy/renewable-portfolio-standards.aspx.

MERRA-2 (2020). URL: https://gmao.gsfc.nasa.gov/reanalysis/MERRA-2/.

Mohsin, Mohamad Farhan Mohamad, Abdul Razak Hamdan, and Azuraliza Abu Bakar (2013). "The effect of normalization for real value negative selection algorithm". In: *International Multi-Conference on Artificial Intelligence Technology*. Springer, pp. 194–205.

Murphy, Sinnott, Fallaw Sowell, and Jay Apt (2019). "A time-dependent model of generator failures and recoveries captures correlated events and quantifies temperature dependence". In: *Applied Energy* 253, p. 113513.

NERC (July 2019). *Probabilistic Adequacy and Measures*. URL: https://www.nerc.com/comm/PC/Probabilistic%20Assessment%20Working%20Group%20PAWG%20Relat/Probabilistic%20Adequacy%20and%20Measures%20Report.pdf.

New England, Independent System Operator of (Oct. 2019). *NESCOE 2019 Economic Study*. Tech. rep. ISO-NE. URL: https://www.iso-ne.com/static-assets/documents/2020/02/a6_nescoe_2019_Econ_8000.pdf.

NREL (2016). *Maintaining Reliability of Power Systems*. Tech. rep. National Renewable Energy Laboratory. URL: https://www.energy.gov/sites/prod/files/2017/01/f34/Maintaining%5C%20Reliability%5C%20in%5C%20the%5C%20Modern%5C%20Power%5C%20System.pdf.

Pryor, S. C., T. J. Shepherd, and R. J. Barthelmie (2018). "Interannual variability of wind climates and wind turbine annual energy production". In: *Wind Energy Science* 3, pp. 651–665. URL: https://doi.org/10.5194/wes-3-651-2018.

Reanalysis Data (n.d.). URL: https://www.ncdc.noaa.gov/data-access/model-data/model-datasets/reanalysis.

Rinaldi, K. Z. et al. (2021). "Wind and Solar Resource Droughts in California Highlight the Benefits of Long-Term Storage and Integration with the Western Interconnect". In: *Environmental*

Science Technology 55, pp. 6214–6226. URL: https://doi.org/10.1021/acs.est.0c07848.

Ruggles, Tyler H and Ken Caldeira (2022). "Wind and solar generation may reduce the inter-annual variability of peak residual load in certain electricity systems". In: *Applied Energy* 305, p. 117773.

Ruggles, Tyler H. and David J. Farnham (Oct. 2020). *EIA Cleaned Hourly Electricity Demand Data*. Version v1.3. DOI: 10.5281/zenodo.4116342. URL: https://doi.org/10.5281/zenodo.4116342.

Ruijven, Bas J van, Enrica De Cian, and Ian Sue Wing (2019). "Amplification of future energy demand growth due to climate change". In: *Nature communications* 10.1, pp. 1–12.

Shaner, M. R. et al. (2018). "Geophysical constraints on the reliability of solar and wind power in the United States". In: *Energy Environmental Science* 11, pp. 914–925. URL: https://doi.org/10.1039/C7EE03029K.

Slusarewicz, Joanna H and Daniel S Cohan (2018). "Assessing solar and wind complementarity in Texas". In: *Renewables: Wind, Water, and Solar* 5.1, pp. 1–13.

Sorkun, Murat Cihan, ÖZLEM DURMAZ İNCEL, and Christophe Paoli (2020). "Time series forecasting on multivariate solar radiation data using deep learning (LSTM)". In: *Turkish Journal of Electrical Engineering & Computer Sciences* 28.1, pp. 211–223.

Srivastava, Nitish et al. (2014). "Dropout: A Simple Way to Prevent Neural Networks from Overfitting". In: *Journal of Machine Learning Research* 15.56, pp. 1929–1958. URL: http://jmlr.org/papers/v15/srivastava14a.html.

System Advisor Model (2020). URL: https://sam.nrel.gov/.

Thornton, H. E., B. J. Hoskins, and A. A. Scaife (2016). "The role of temperature in the variability and extremes of electricity and gas demand in Great Britain". In: *Environmental Research Letters* 11.114015, pp. 1–13. URL: https://doi.org/10.1088/1748-9326/11/11/114015.

Valor, Enric, Vicente Meneu, and Vicente Caselles (2001). "Daily air temperature and electricity load in Spain". In: *Journal of applied Meteorology* 40.8, pp. 1413–1421.

Waheeb, Waddah and Rozaida Ghazali (2020). "A novel error-output recurrent neural network model for time series forecasting". In: *Neural Computing and Applications* 32.13, pp. 9621–9647.

Wu, Jian et al. (2018). “Changes in terrestrial near-surface wind speed and their possible causes: an overview”. In: *Climate dynamics* 51.5, pp. 2039–2078.

Yalew, Seleshi G et al. (2020). “Impacts of climate change on energy systems in global and regional scenarios”. In: *Nature Energy* 5.10, pp. 794–802.

Zeng, Zhenzhong et al. (2019). “A reversal in global terrestrial stilling and its implications for wind energy production”. In: *Nature Climate Change* 9.12, pp. 979–985.

Zeyringer, Marianne et al. (2018). “Designing low-carbon power systems for Great Britain in 2050 that are robust to the spatiotemporal and inter-annual variability of weather”. In: *Nature Energy* 3.5, pp. 395–403.